The University Of Sheffield.

The identification of proteins involved in a novel mitotic DNA damage checkpoint.

Rachel Jane Gatenby

A thesis submitted in partial fulfilment of the requirements for the degree of Doctor of Philosophy.

The University of Sheffield
Faculty of Medicine, Dentistry and Health
Department of Oncology and Metabolism

October 2021

Declaration

I, the author, confirm that the Thesis is my own work. I am aware of the University's Guidance on the Use of Unfair Means (www.sheffield.ac.uk/ssid/unfair-means). This work has not been previously been presented for an award at this, or any other, university.

Acknowledgements

Firstly, I would like to thank my primary supervisor Dr Ruth Thompson for her help and support throughout my PhD. This project has not been straightforward in any sense, but I am grateful for all your ideas and persistence to make this work achievable. I would also like to thank Professor Mark Dickman and Dr Caroline Evans for all their help and extensive expertise during all the mass spectroscopy work conducted in this thesis. Additionally, I would like to thank Dr Helen Bryant and Dr Spencer Collis for all their advice.

I must give credit to the students that I supervised; Priya Lata, Alex Breitwieser and Afzaal Tufail for the work they have contributed towards the project. Further thanks to my lovely and excellent colleagues from the Collis, Bryant and Thompson labs; Tim, Pat, Dan, Katie, Xin, Tom, Leona, Aurelie, Ola, Connor, Polly and Steven. I wish them all the best for the future. With special mention to Katie for all her wisdom and help throughout my PhD, I would not have been able to do it without her. Another special mention to Pat for her help with all my bacteria, DNA and protein needs. Extra special mentions to the amazing Priya, Emma, Callum and Dan, for their lasting friendship, constant support and ability to make the tough days bearable. Without them the PhD would have been much less enjoyable. I look forward to watching them excel in anything they choose to do. Plus, an extra, extra special thanks to Priya for encouraging me to take time to do non-science things; quizzes, pancake dinners and getting free stuff, I appreciated every moment. Thank you for being persistent.

As ever, I would like to thank my family, specifically my parents for their everlasting love and encouragement in everything I do, despite not always fully understanding what that is. I must also give special thanks to my siblings, Nicola and James for putting up with me and all my phone calls for company whilst on the microscope. I would also like to thank Stephen's parents for all their love and support too. Additionally, I want to dedicate my thesis to my Grandad and Auntie Tracy, who are sadly no longer here to see me complete my PhD, but I know would have been so proud.

Finally, I want to thank my partner Stephen for everything. You have been there every day to share the highs and the lows but have always encouraged me to continue. You have helped in any way you could, and I hope you have at least learnt something interesting from all the presentations you have endured. Thank you, I couldn’t have done it without you.

Abstract

Common cancer treatments, such as radiotherapy, primarily involve the induction of DNA damage. Like healthy cells, the cancer cells rely on the highly conserved DNA damage response (DDR) checkpoints for survival, leading to therapeutic resistance. There are established DDR checkpoints in each interphase stage of the cell cycle, which impede the cell cycle until the damage has been sufficiently repaired. However, there is limited evidence of a specific DDR checkpoint in mitosis. The spindle assembly checkpoint (SAC) is a protective mechanism that regulates mitotic spindle attachment to the centromere, regulating metaphase-anaphase transition. There is emerging evidence to suggest crosstalk between the DDR and SAC pathways in damaged conditions. I have consistently observed a delay in mitotic transit time following the induction of DNA damage by various agents including irradiation, chemotherapeutics and H_2O_2. Overall, this indicates the existence of a mitotic DNA damage checkpoint (MDDC), which may contribute to treatment resistance. This thesis aims to identify proteins involved and begin to establish a pathway for this novel checkpoint. Firstly, an examination into the antioxidant enzyme superoxide dismutase 1 (SOD1), which was highlighted in a preliminary siRNA DNA damage screen of potential proteins involved in the checkpoint. I observed the MDDC was dependent on SOD1 and revealed SOD1 regulates phosphatase PP2A activity to activate the MDDC. Furthermore, a role of SOD1 in DNA damage repair was also identified. Then a mass spectrometry screen was performed to reveal novel interactors of SAC protein BubR1, identifying the non-sense mediated decay (NMD) factor, Upstream frameshift 1's (UPF1) involvement in the MDDC. Overall, an initial pathway for the MDDC has been established and future direction determined, which will provide potential drug targets to reduce therapeutic resistance of cancer cells to conventional treatments.

Table of contents

List of figures

List of tables

Abbreviations

• OH	Hydroxyl radical
53BP1	p53 binding protein 1
8-oxodG	8-oxo-7,8-dihydro-2′-deoxyguanosine
9-1-1 complex	Rad9-Rad1-Hus1
ABC	Ammonium bicarbonate
ACN	Acetonitrile
AGC	Automatic gain control
ALS	Amyotrophic lateral sclerosis
AP	Affinity purification
APC/C	Anaphase-promoting complex/cyclosome
APS	Ammonium persulfate
ATCC	American Type Culture Collection
ATM	Ataxia-telangiectasia mutated
ATR	ATM- and Rad3-related
ATRIP	ATR interacting protein
BER	Base excision repair
BRCA1	Breast cancer type 1 susceptibility protein
BSA	Bovine serum albumin
BSA-Tx	BSA-Triton-X
Bub	Budding uninhibited by benzimidazole
BubR1	Budding uninhibited by benzimidazole-related 1
C	Cysteine
C-Mad2	Closed-Mad2
$CaCl_2$	Calcium chloride
CAT	Catalase
Cdc20	Cell division cycle 20
CDC25	Cell division control protein 25
Cdh1	Cdc20 homolog 1
CDK	Cyclin dependent kinase
cDNA	Complementary DNA
Chk	Checkpoint kinase
$CLR4^{Cdt2}$	Cullin-RING 4
CM-H2DCFDA	Chloromethyl-2',7'-dichlorodihydrofluorescein diacetate
CoA	Coenzyme A
DAPI	4′,6-Diamidino-2-phenylindole dihydrochloride
DDB1	DNA damage-binding protein 1
ddH_2O	Deionised water
DDR	DNA damage response
DMEM	Dulbecco’s Modified Eagle’s Medium

DMF	Dimethylformamide
DMSO	Dimethyl sulfoxide
DNA-PK	DNA-dependent protein kinase
dNTPs	Deoxyribonucleotides
Dox	Doxycycline
DSB	Double strand break
DSBR	Double strand break repair
DTT	Dithiothreitol
ECL	Enhanced chemiluminescence
EDTA	Ethylenediaminetetraacetic acid
EdU	5'Ethynyl-2'-deoxyuridine
EGTA	Ethylene glycol tetraacetic acid
ESI	Electrospray ionisation
FACs	Fluorescence-activated cell sorting
FCS	Foetal calf serum
Fe	Iron
G85R	Glycine to arginine mutation at position 85
G93A	Glycine to alanine mutation at position 93
GAPDH	Glyceraldehyde 3-phosphate dehydrogenase
GFP	Green fluorescent protein
GPx	Glutathione peroxidase
GSH	Reduced glutathione
GSK3β	Glycogen synthase kinase 3β
H2AX	H2A histone family, member X
H_2O_2	Hydrogen peroxide
HCL	Hydrochloric acid
HPLC	High phase liquid chromatography
HR	Homologous recombination
HRP	Horse radish peroxidase
ICL	Interstrand crosslinks
IF	Immunofluorescence
IMS	Industrial methylated spirit
IP	Immunoprecipitation
IR	Ionising radiation/ irradiation
KCL	Potassium chloride
Keap1	Kelch-like ECH-associated protein 1
KNL1	kinetochore scaffold 1
KPRP	Keratinocyte proline-rich protein
LB	Luria broth base
Mad	Mitotic arrest deficient
MCAK	Mitotic centromere-associated kinesin
MCC	Mitotic checkpoint complex
MDC1	Mediator of DNA damage checkpoint 1

MDDC	Mitotic DNA damage checkpoint
MELT	Methionine-glutamic acid-leucine-threonine
$MgCl_2$	Magnesium chloride
MGMT	O^6-methylguanine DNA methyltransferase
$MgSO_4$	Magnesium Sulphate
MiDAS	Mitotic DNA repair synthesis
MMR	Mismatch repair
mMRN	Mitotic MRN complex
MPS1	Monopolar spindle 1
MRE11	Mitotic recombination 11
MRN complex	MRE11-Rad50-NBS1
mRNA	Messenger RNA
MS	Mass spectroscopy
MTH1	Human MutT Homolog 1
MycGFP-BubR1	Myc and green fluorescent protein (GFP) tagged BubR1 protein
NAC	N-acetyl-L-cysteine
NaCl	Sodium chloride
NaOH	Sodium hydroxide
NBS1	Nijmegen breakage syndrome 1
NER	Nucleotide excision repair
NIR	Near-infrared
NHEJ	Non-homologous end joining
NMD	Non-sense mediated decay
NRF2	Nuclear factor erythoid-2 related factor 2
NSCLC	Non-small cell lung cancer
O-Mad2	Open-Mad2
$O_2^{\bullet-}$	Superoxide anion
OA	Okadaic acid
OD	Optical density
OGG1	8-oxoguanine glycosylase
PARP1	Poly (ADP-ribose) polymerase 1
PBS	Phosphate buffered saline
PBS-Tx	PBS-Triton-X
PCR	Polymerase chain reaction
PEG	Polyethylene glycol
PFA	Paraformaldehyde
pH3	Phosphorylated histone 3
PI	Propidium iodide
Plk1	Polo-like kinase 1
PP1	Protein phosphatase 1
PP2A	Protein phosphatase 2A
PP2A-C	PP2A catalytic domain

Prx1	Peroxiredoxin 1
PSP	Protein serine-threonine phosphatases
PTC	Premature termination codons
PTP	Protein tyrosine phosphatase
QE	Q-Extractive HF
RIPA	Radioimmunoprecipitation assay
RNA	Ribonucleic acid
RNF8	RING-finger protein 8
ROS	Reactive oxygen species
RPA	Replication factor A
RPM	Revolutions per minute
RT-qPCR	Reverse transcription-quantitative polymerase chain reaction
S	Serine
S60,99A	Serine to alanine mutation at positions 60 and 99
S99A	Serine to alanine mutation at position 99
SAC	Spindle assembly checkpoint
Scc1	Sister chromatid cohesion protein 1
SD	Standard deviation
SDM	Site-directed mutagenesis
SDS	Sodium dodecyl sulfate
SDS-PAGE	SDS-polyacrylamide gel electrophoresis
SEM	Standard error of the mean
SFM	Serum free media
shRNA	Short hairpin RNA
siRNA	Short interfering RNA
SOD	Superoxide dismutase
SSB	Single Strand Break
SSBR	Single strand break repair
ssDNA	Single stranded DNA
T	Threonine
TAE	Tris-acetate-EDTA
TAE	Tris-acetate-EDTA
TBS	Tris-buffered saline
TBS-T	TBS-Tween
TEMED	Tetramethylethylenediamine
TFA	Trifluoroacetic acid
Tm	Melting temperature
TMZ	Temozolomide
TOPBP1	DNA topoisomerase II binding protein 1
Ub	Ubiquitination
UPF1	Upstream frameshift 1
UTR	Untranslated region
UV	Ultraviolet

WB	Western blotting
WT	Wildtype
XRCC1	X-ray repair cross-complementing protein 1
Y	Tyrosine
β-TrCP-SCF	β-Transducin repeat containing E3 ubiquitin protein ligase-Skp, Cullin, F-box containing complex
ΔCt	delta Ct value
ΔΔCt	delta delta Ct value

Chapter 1: Introduction.

1.1 DNA Damage Response.

1.1.1 DNA damage.

All cells frequently experience significant amounts of DNA damage, through constant exposure to endogenous factors, such as the generation of reactive oxygen species during cellular respiration and exogenous factors, such as environmental ultraviolet (UV) light (Jackson and Bartek, 2009). There are numerous types of DNA damage that can occur, examples include base alterations, interstrand crosslinks (ICL), single strand breaks (SSB) and double strand breaks (DSBs) (Hosoya and Miyagawa, 2014). DSBs are also formed when the DNA possesses two proximal SSBs or during DNA replication an unrepaired SSB is encountered. This lesion is the most deleterious and toxic to the cell due to a greater difficulty to repair compared to other lesions (Jackson and Bartek, 2009). The repair of these lesions allows the cell to continue without any negative effects. However, if the damage is not fully and correctly repaired, genetic aberrations and mutations will occur and induce cell death or promote tumorigenesis (Jackson and Bartek, 2009; Hosoya and Miyagawa, 2014).

Cells have evolved a series of interlinking signalling cascades (checkpoints) throughout the interphase cell cycle (G1, S and G2), which are collectively termed the DNA damage response (DDR), to overcome the frequent DNA damage experienced and ensure genomic stability. Each DDR checkpoint relies on the rigorous and timely co-ordination of a vast protein network, to first detect the damage via sensory proteins, then indicate the presence of damage to signal transducer proteins, which then activate the appropriate effector proteins to pause the cell cycle, promote DNA repair and determine cellular fate (Schmitt *et al.*, 2007; Jackson and Bartek, 2009).

1.1.2 Sensors of DNA damage.

The immediate action of the DDR involves damage recognition, which is achieved by the sensory protein complexes; the mitotic recombination 11 (MRE11)-Rad50-nijmegen breakage syndrome 1 (NBS1) (MRN) complex (Hosoya and Miyagawa, 2014) and the Rad9-Rad1-Hus1 (9-1-1) complex (Parrilla-Castellar, Arlander and

Karnitz, 2004). The MRN complex responds to DSBs and activates the key signal transducer ataxia-telangiectasia mutated (ATM) (Uziel *et al.*, 2003). Whereas the 9-1-1 complex contributes to the activation of the signal transducer ATM- and Rad3-related (ATR), in response to multiple lesions which generate single stranded DNA (ssDNA) such as SSBs and replication stress (Zou and Elledge, 2003; Hosoya and Miyagawa, 2014). In the presence of ssDNA, the DNA is coated with replication factor A (RPA) which allows ATR interacting protein (ATRIP) to associate with DNA contributing to ATR activation, as typically ATR exists within a complex with ATRIP (Zou and Elledge, 2003). Then DNA topoisomerase II binding protein 1 (TOPBP1) acts as a linker protein, as it interacts with the ATRIP-ATR complex and the Rad9 component of the 9-1-1 complex to facilitate the complete activation of ATR (Delacroix *et al.*, 2007).

1.1.3 Signal transducers of DNA damage.

ATM and ATR are large serine (S)/threonine (T) kinases that respond to different types of damage to facilitate the activation of the appropriate effector proteins (Munk *et al.*, 2017). The main and well-established targets of ATM and ATR are H2A histone family member X (H2AX) and checkpoint kinase (Chk) 2 and Chk1 respectively (Jackson and Bartek, 2009). The mediator protein H2AX is activated via phosphorylation at S139 by ATM and ATR resulting in γH2AX, a biomarker for DSBs (Rogakou *et al.*, 1998; Jackson and Bartek, 2009). The γH2AX protein then disperses 1-2 mega-bases along the DNA strand, termed a focus (a collection of proteins) (Rogakou *et al.*, 1999), to recruit other factors involved in the DDR checkpoints and repair mechanisms, as well as modifying the chromatin structure for protein conjugation at the damage site (Jackson and Bartek, 2009).

1.1.4 DDR checkpoints.

1.1.4.1 G1 checkpoint.

ATM activates the G1 checkpoint after DNA damage (DSBs) has occurred. This involves the ATM-mediated activation of H2AX (S139) and Chk2 (T68), which then stimulates many corresponding proteins (Ahn *et al.*, 2000; Jackson and Bartek, 2009). The transcription factor and tumour suppressor protein, p53 is activated by ATM and Chk2 **(Figure 1.1)** via phosphorylation on S15 and S20 respectively (Hirao *et al.*, 2000). These phosphorylation sites protect p53 from MDM2-mediated proteasome

degradation, hence p53 accumulates intracellularly (Unger *et al.*, 1999). p53 is vital for G1 checkpoint functionality, as it relocates into the nucleus and actuates transcription of a variety of downstream gene targets, contributing towards cell cycle arrest and potentially apoptosis (Hyun and Jang, 2015; Shaltiel *et al.*, 2015). One important checkpoint target of p53 is p21, due to the increase of p53 the intracellular concentration of p21 increases respectively (Neganova *et al.*, 2011; Shaltiel *et al.*, 2015). p21 inhibits the activity of the cyclin dependent kinase (CDK) 2/cyclin E and CDK4/cyclin D complexes **(Figure 1.1)** (He *et al.*, 2005), arresting the cell cycle at G1. This is supported by the inhibitory phosphorylation of CDK2 at T14/ tyrosine (Y) 15 residues (Hughes *et al.*, 2013). ATM and Chk2 also stimulate the prompt proteolytic inactivation and degradation of cell division control protein 25 (CDC25) A **(Figure 1.1)**, a phosphatase that removes the T14/Y15 inhibitory phosphorylations on CDK2 (Falck *et al.*, 2001). ATM is also involved in cyclin D proteolysis, via glycogen synthase kinase 3β (GSK3β) phosphorylation to further prevent entry into S phase (Pontano *et al.*, 2008). These actions contribute to the overall inhibition of the cell cycle at G1.

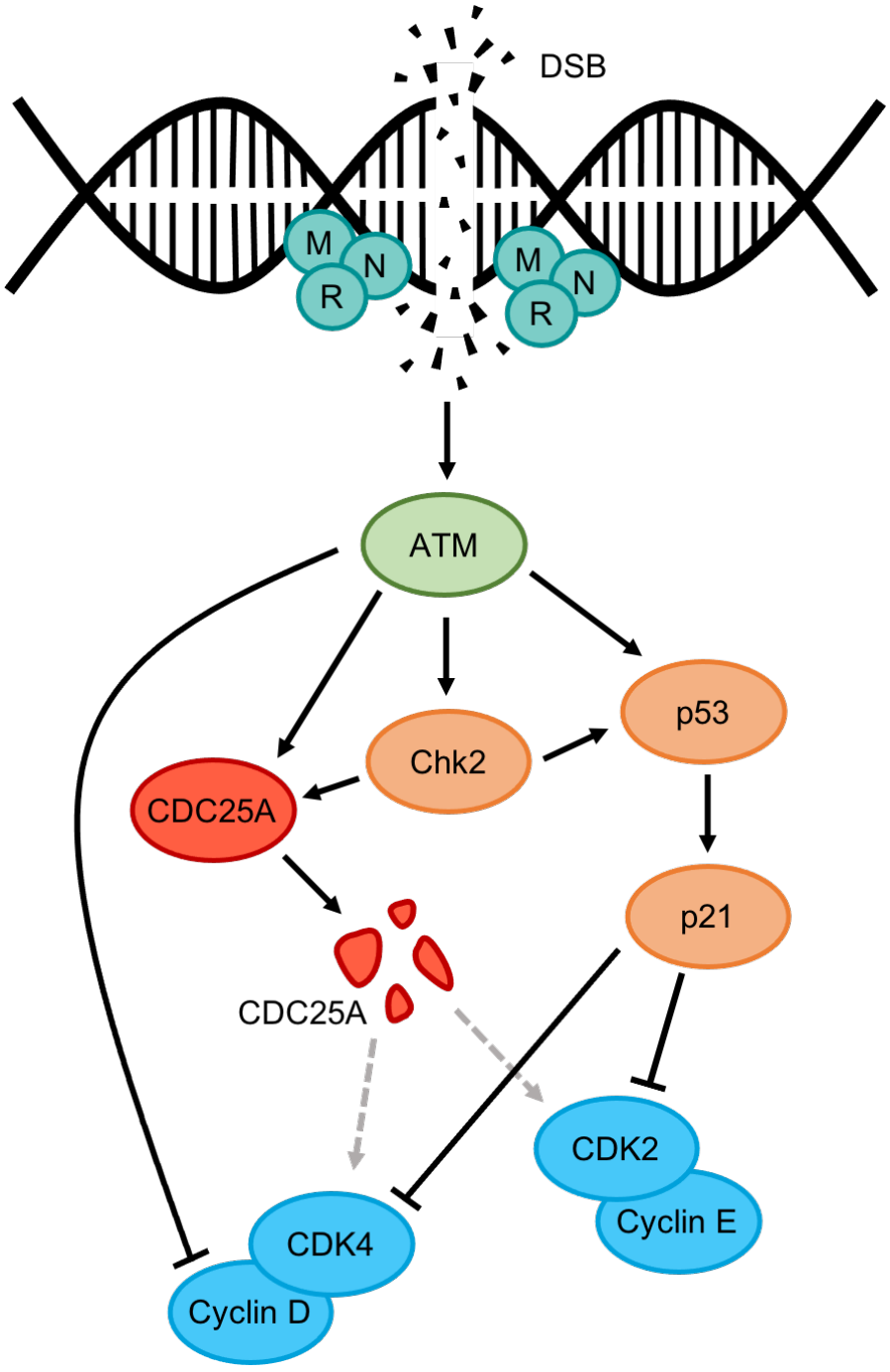

Figure 1.1: An overview of the G1 checkpoint.

ATM is activated in response to DNA double strand breaks (DSBs) leading to Chk2 activation. ATM and Chk2 then promote p53 for p21 expression. These factors then contribute to the inhibition of CDC25A and CDK2/cyclin E and CDK4/cyclin D, arresting the cell cycle in G1.

1.1.4.2 Intra-S checkpoint.

SSBs and replication fork collapse activate the intra-S checkpoint, via the presence of ssDNA which recruits RPA and subsequently activates ATR kinase (Zou and Elledge, 2003; Hosoya and Miyagawa, 2014). ATR then activates factors such as Chk1 (phosphorylation at S317 and S345) (Zhao and Piwnica-Worms, 2001) and p53 (Tibbetts *et al.*, 1999). Chk1 also targets the CDC25A for inhibition and degradation **(Figure 1.2)**, via the phosphorylation of various serine residues (123, 178, 278 and 292) (Sørensen *et al.*, 2003). In turn, the removal of T14/Y15 phosphorylation events on CDK2 is disabled, leading to cell cycle arrest. Chk1 also activates Wee1 kinase via S549 phosphorylation, which facilitates 14-3-3 binding for protein stabilisation (O'Connell *et al.*, 1997; Lee, Kumagai and Dunphy, 2001). This kinase performs similar roles to p21 in the G1 checkpoint **(Figure 1.2).** Wee1 maintains the inhibitory phosphorylation on CDK2, opposing CDC25A activity (Watanabe, Broome and Hunter, 1995). Overall, the cell is paused in S phase.

Furthermore, the lesions experienced may progress to DSBs (Jackson and Bartek, 2009), resulting in the activation of MRN, ATM and Chk2 during the intra-S checkpoint **(Figure 1.2)** As a result, p53 is further activated in S phase, but p21 is targeted for proteolytic degradation by the E3 ligase Cullin-RING 4 $(CLR4)^{Cdt2}$ (Abbas *et al.*, 2008) and via ATR mediated activation of GSK3β (Lee *et al.*, 2007) **(Figure 1.2)**. p21 levels must be eradicated during S phase, as p21 is capable of reactivating DNA replication which would cause further damage to the cell (Kim, Starostina and Kipreos, 2008).

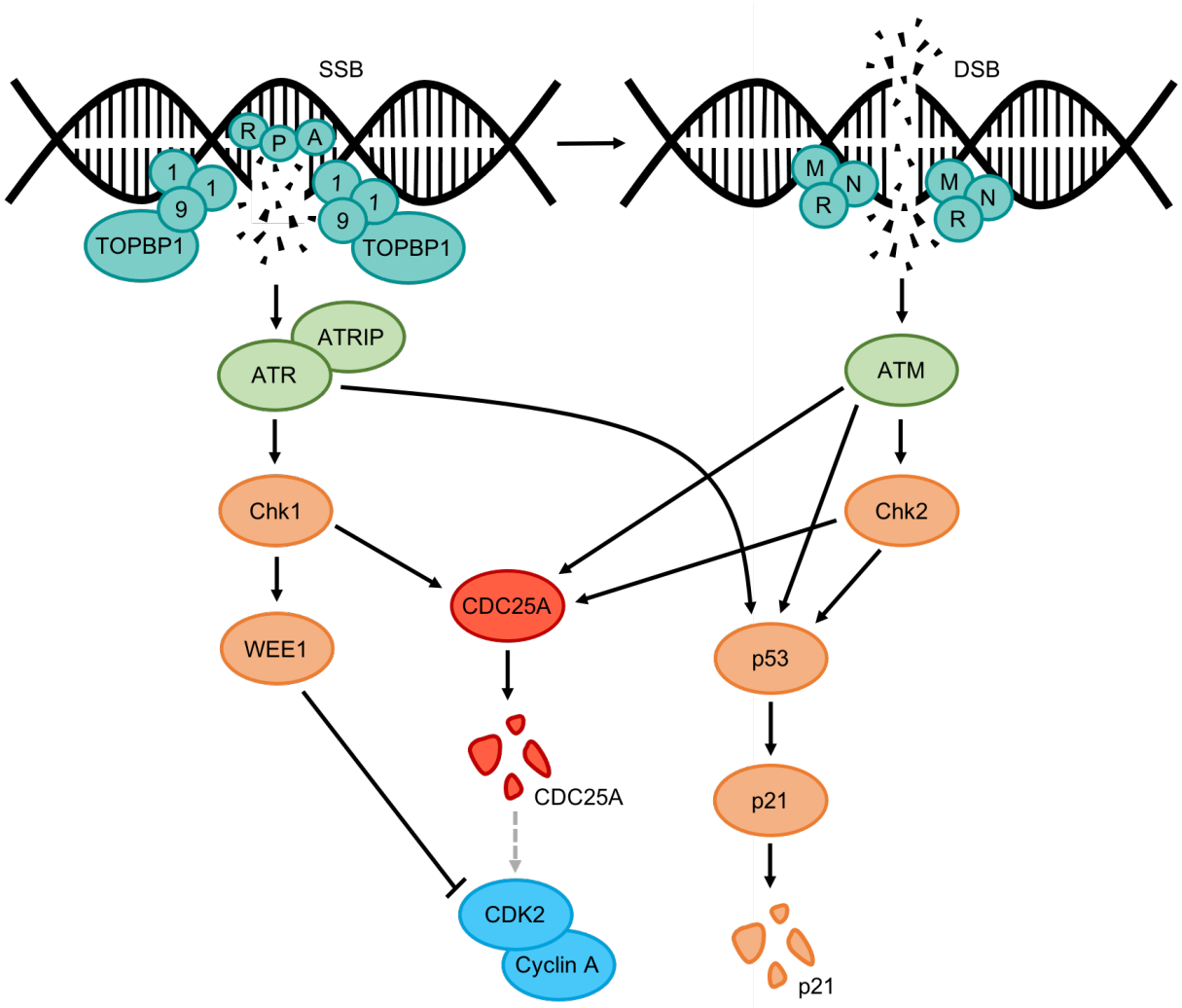

Figure 1.2: A summary of the intra-S checkpoint.

ATM and ATR are activated due to DNA single strand breaks (SSBs), replication stress and double strand breaks (DSBs), stopping the cell cycle in the S phase. Chk2 activates p21 via p53, but p21 promotes replication so is degraded. Whereas ATM, Chk2 and Chk1 inhibit CDC25A and Chk1 also activates Wee1 kinase, contributing to the inhibition of CDK2/cyclin A.

1.1.4.3 G2 checkpoint.

The G2 checkpoint is equipped to respond to a range of DNA damage (SSBs, replication stress and DSBs) inflicted during this cell cycle phase or unrepaired during G1 and S phase, hence both ATM/Chk2 and ATR/Chk1 pathways are functional during this checkpoint **(Figure 1.3)** (Bucher and Britten, 2008). Chk1 and Chk2 kinases target the CDC25 family (A/B/C) of phosphatases **(Figure 1.3)**. CDC25A (Falck *et al.*, 2001;

Sørensen *et al.*, 2003) and CDC25C (Peng *et al.*, 1997; Matsuoka, Huang and Elledge, 1998) are phosphorylated at numerous serine residues by both kinases. Whereas CDC25B endures several inactivating phosphorylations by Chk1 (Giles, Forrest and Gabrielli, 2003). The inhibition of these phosphatases is facilitated by 14-3-3 binding and results in CDC25 retention in the cytosol for degradation (Peng *et al.*, 1997; Giles, Forrest and Gabrielli, 2003). Overall, contributing to CDK1/cyclin B inactivation and the inhibition of the cell cycle in G2.

Furthermore, Chk2 activates p53, leading to p21 expression contributing towards the overall inactivation of CDK1/cyclin B **(Figure 1.3)** and cell cycle arrest (Bunz *et al.*, 1998). In addition to p53, Wee1 kinase activity is utilised in this checkpoint via Chk1 mediated activation, to ensure CDK1 inactivity and enhance cell cycle arrest **(Figure 1.3)** (O'Connell *et al.*, 1997).

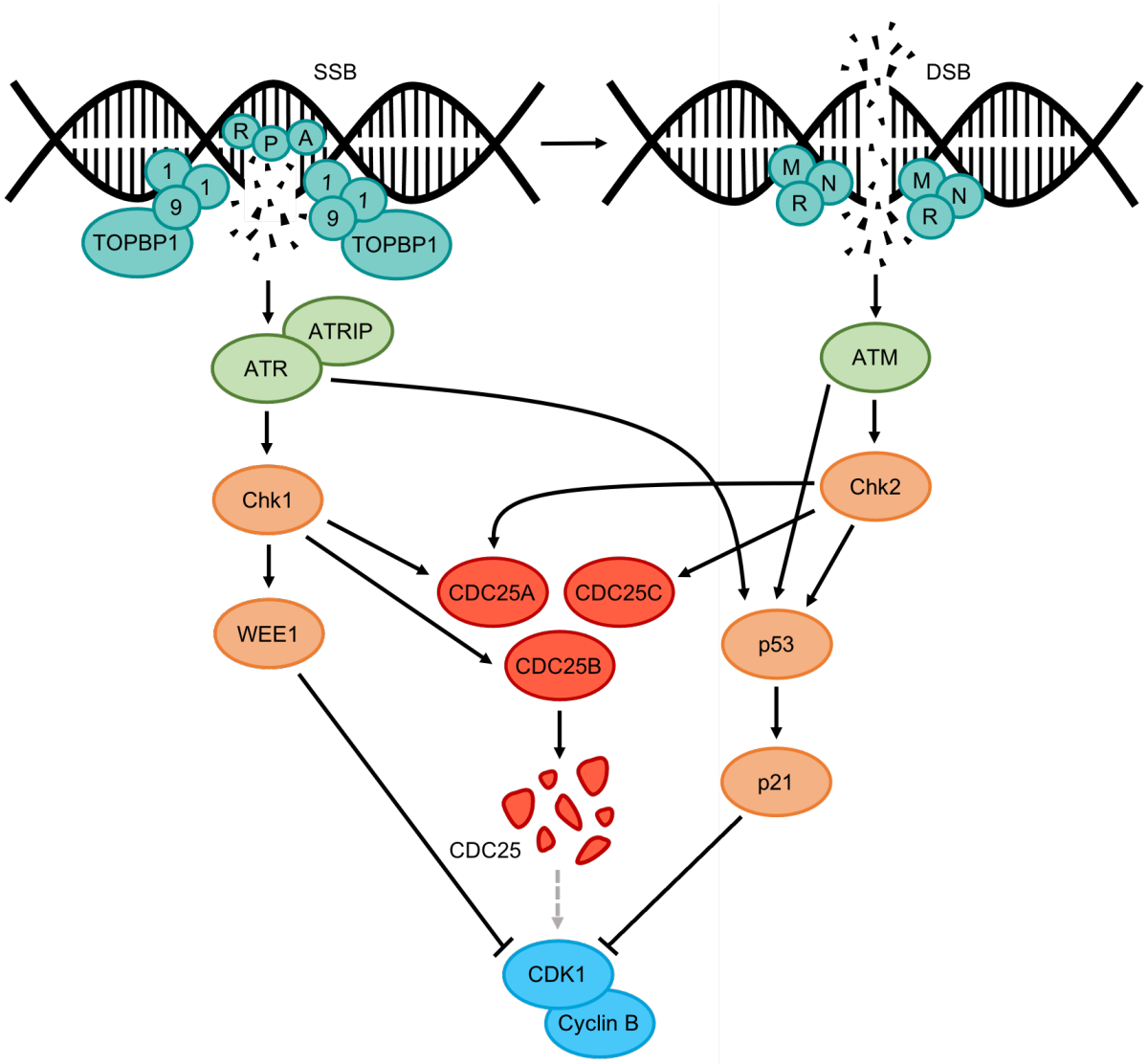

Figure 1.3: An overview of the G2 checkpoint.

This checkpoint involves the activation of both ATM and ATR in response to a variety of DNA damage such as replication stress and double strand breaks (DSBs). Chk1 and Chk2 both act to inhibit the CDK1/cyclin B directly via inhibition of the CDC25 family and indirectly via Wee1 kinase and p21, arresting the cell cycle in G2.

1.1.4.4 The role of MDC1 in the intra-S and G2 checkpoint functionality.

Mediator of DNA damage checkpoint 1 (MDC1) is a key factor during the activation of the intra-S and G2 checkpoints in response to DSBs. Firstly, MDC1 is involved in a positive feedback loop with ATM and γH2AX for the enrichment of damage signalling intensity (Lou *et al.*, 2006). Following initial ATM activation in response to DNA damage, ATM activates H2AX and MDC1 via phosphorylation events which induce the

formation of γH2AX foci and MDC1 oligomerisation and accumulation at the damage site (Luo, Yuan and Lou, 2011). MDC1 binds to γH2AX and then to ATM at the damage site, resulting in the enhanced activation, accumulation and signalling of ATM. This includes the further stimulation of H2AX and MDC1, as well as the recruitment of other DDR proteins and repair factors such as the MRN complex, BRCA1 and p53 binding protein 1 (53BP1) (Lou *et al.*, 2006). MDC1 also possesses the ability to amplify ATR signalling, via phosphorylated MDC1 binding to TOPBP1 to regulate the ATR-mediated activation of Chk1 at S345 (Wang, Gong and Chen, 2011).

In addition to contributing to the intra-S and G2 checkpoint functionality, MDC1 also has a role in determining cell fate in response to DNA damage. MDC1 interacts with the activated form of Chk2 (T68 phosphorylation by ATM), which allows MDC1 to mediate the phosphorylation of p53 at S20 by Chk2, ensuring checkpoint signalling and activation of apoptosis (Lou *et al.*, 2003).

1.1.4.5 Mitotic checkpoint.

Currently, it is accepted that there is no mitotic DDR checkpoint and DNA repair is largely inhibited during this phase of the cell cycle, due to the impracticality of changes to the condensed chromatin for repair and the increased susceptibility to telomere fusion (Giunta, Belotserkovskaya and Jackson, 2010; Orthwein *et al.*, 2014). Although, non-homologous end joining (NHEJ) is thought to be the only feasible repair mechanism in mitosis due to the condensed state of the chromatin (Godinez *et al.*, 2020). However, the extension to mitosis required to conduct repair could result in deleterious chromosomal translocations, telomere fusions and aneuploidy (Hayashi *et al.*, 2012; Benada *et al.*, 2015). Therefore, following damage encountered in mitosis, it is thought the DDR and subsequent repair is only fully activated once the cell progresses into G1 (Giunta, Belotserkovskaya and Jackson, 2010). However, there is increasing evidence to support the existence of a DNA damage response in mitosis, and preliminary data from the Thompson laboratory has shown that cells which progress through to mitosis with unrepaired DNA damage exhibit delayed mitotic transit. Furthermore, DNA repair has also been shown to occur in mitosis (Godinez *et al.*, 2020).

1.1.5 DNA repair mechanisms.

The cell features different repair mechanisms for specific types of DNA damage, including base excision repair (BER), nucleotide excision repair (NER), mismatch repair (MMR), single strand break repair (SSBR) and double strand break repair (DSBR). BER, NER and MMR typically respond to specific types of damage and errors within the DNA, rather than physical breaks experienced for SSBR and DSBR. Although, SSBs may occur during the removal of the damaged base/nucleotide within the DNA, which may also develop into DSBs, resulting in SSBR or DSBR (Schipler and Iliakis, 2013; Erasimus *et al.*, 2016).

BER, NER and MMR all feature a similar premise of repair but function via different mechanisms. BER responds to lesions inflicted to the DNA bases by damage such as oxidation and involves the removal and replacement of the base through utilising the opposite DNA strand (David, O'Shea and Kundu, 2007). NER responds to bulky DNA adducts caused by exogenous factors such as UV radiation and chemotherapeutics, which distort the DNA helix structure (Chatterjee and Walker, 2017). During this repair mechanism, the lesion is excised along with additional surrounding nucleotides to form ssDNA, allowing the assembly of repair complexes for subsequent replacement of the damaged nucleotide. Then MMR detects the incorporation of incorrect nucleotides during DNA replication or base modification by alkylating chemotherapeutic agents, stimulating the removal and degradation of the incorrect nucleotide and resynthesis of the lesion. (Hoeijmakers, 2001).

SSBR responds to SSBs caused by endogenous and exogenous damage or during the intermediate steps of other repair mechanisms. This involves the detection of the damage lesion by poly (ADP-ribose) polymerase 1 (PARP1), which then recruits X-ray cross-complementing protein 1 (XRCC1) forming a scaffold for the accumulation of proteins involved in downstream SSBR, other repair pathways and the DDR. SSBR is regarded as a sub-pathway of BER as there is considerable consolidation between the pathways. (Abbotts and Wilson, 2017).

DSBR can utilise two different repair mechanisms: NHEJ and homologous recombination (HR). DSBs activate the ATM axis of the DDR, which involves the downstream activation of NHEJ or HR repair. NHEJ involves the direct ligation of the

broken DNA ends together, via the recruitment and co-ordinated actions of factors such as DNA- protein kinase (DNA-PK), 53BP1, XRCC4 and DNA ligase 4 (Chatterjee and Walker, 2017). This repair mechanism is suitable for any cell cycle phase as it is not dependent on the structure of the DNA (Jackson and Bartek, 2009). HR involves the generation of ssDNA via strand invasion by the MRN complex, which leads to RPA binding and recruitment of other factors such as RAD51, breast cancer type 1 susceptibility protein (BRCA1) and BRCA2, to facilitate DNA strand exchange with the sister chromatid for repair (Hoeijmakers, 2001; Krajewska *et al.*, 2015). As this repair mechanism requires a sister chromatid, it is thought that HR is dominant during S and G2 phases as DNA replication had occurred (Hoeijmakers, 2001). In addition to DSBs, HR also responds to ICL and replication fork collapse (Jackson and Bartek, 2009).

Overall, these repair mechanisms protect the cell from adverse effects on the genome, ensuring stability and cell survival.

1.2 The spindle assembly checkpoint.

1.2.1 Mitotic cell division.

Mitosis is the process by which a somatic cell divides producing two daughter cells with identical genetic material. This cell cycle phase can be further divided into prophase, prometaphase, metaphase, anaphase, and telophase. Mitosis is strictly controlled by phosphorylation and dephosphorylation events which are regulated by kinases and opposing phosphatases (Burgess *et al.*, 2017). This ensures the exact protein and subsequent pathway are activated or inactivated at the correct point for the overall accurate completion of cell division.

During prophase, the interphase chromatin condenses into a highly packed spatial arrangement, termed chromosomes **(Figure 1.4)**. The centrosomes move to the opposing cellular poles rapidly producing short and dynamic microtubules **(Figure 1.4)**. Prometaphase primarily involves the breakdown of the nuclear envelope, allowing the accessibility of the chromosomes for the initiation of the attachment of the microtubules **(Figure 1.4)**. This leads to metaphase, where the completion of chromosome attachment takes place, resulting in the recognisable characteristic of chromosome

alignment at the cell equator **(Figure 1.4)**. This highly important process is regulated by the spindle assembly checkpoint to ensure genomic integrity (explained in detail in **1.2.2**). During anaphase **(Figure 1.4)**, the centromeres are cleaved, and the chromatids move to the opposing poles of the cell (anaphase A). Following this, the poles move further apart in preparation for cell division (anaphase B). Finally, the chromosomes decondense and the nuclear envelope is re-established during telophase **(Figure 1.4)**. Cytokinesis initiates the division of the cell, which is completed through the cleavage of the remaining cytoplasmic bridge or midbody by abscission. (Walczak, Cai and Khodjakov, 2010).

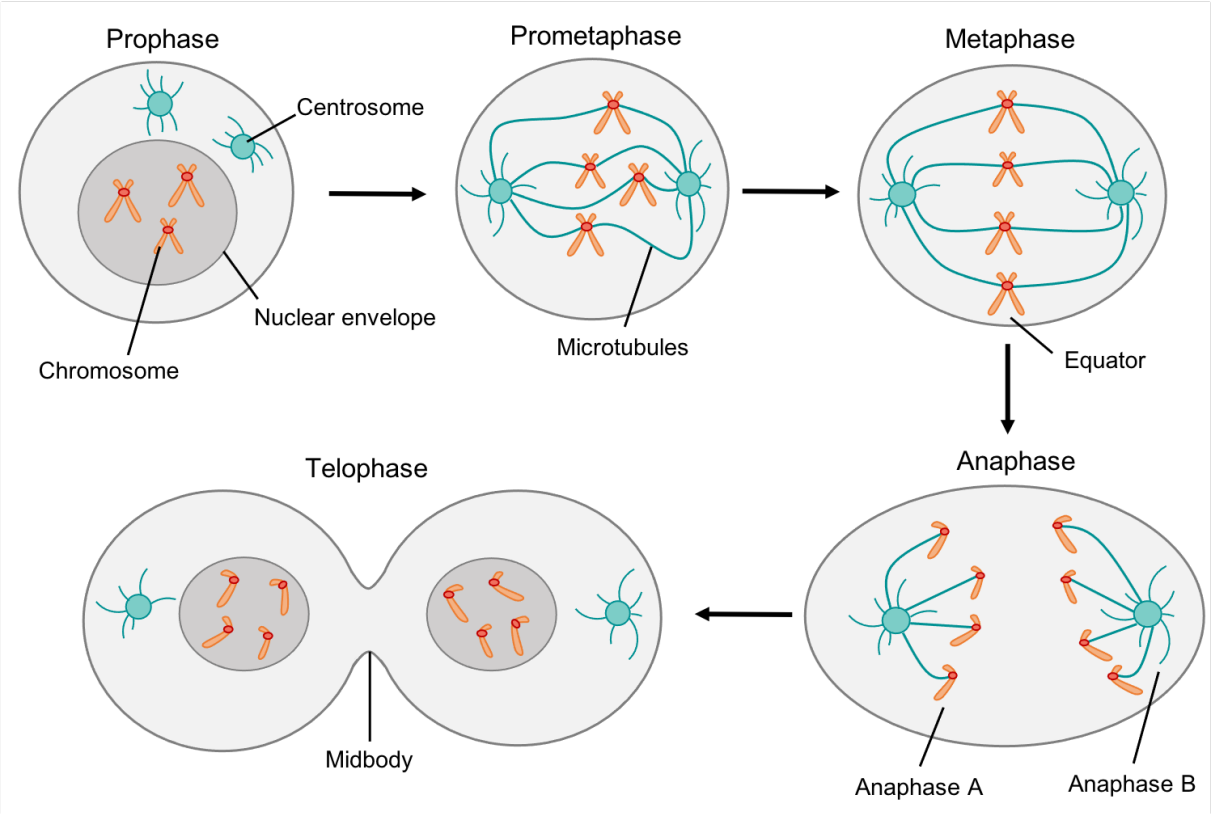

Figure 1.4: A summary of mitosis.

The key characteristics of each phase are illustrated (prophase, prometaphase, metaphase, anaphase (anaphase A and B) and telophase) (Adapted with permission of Nature Reviews from Walczak, Cai and Khodjakov, 2010).

1.2.2 What is the spindle assembly checkpoint?

In mitosis, metaphase-anaphase transition is regulated by the spindle assembly checkpoint (SAC). The SAC is constantly active surveying chromosome-microtubule

attachment and preventing progression into anaphase until successful attachment has been achieved to disable the checkpoint. (Farr and Cohen-Fix, 1999). More specifically, a large tiered multi-protein complex termed kinetochore, assembles at the centromere and provides a platform for microtubule attachment (Foley and Kapoor, 2012). The kinetochore is also where numerous SAC signalling proteins accumulate to mediate the attachment and prevent anaphase (Musacchio and Salmon, 2007). In summary, this checkpoint is vital for ensuring successful segregation of the chromatids, preventing aneuploidy which is a contributing factor to oncogenesis (Musacchio and Salmon, 2007).

1.2.3 The mitotic checkpoint complex and APC/C inhibition.

The SAC prevents anaphase through the inhibition of the ubiquitin ligase anaphase-promoting complex/cyclosome (APC/C), which stimulates metaphase-anaphase transition and mitotic exit, through targeting specific regulatory mitotic proteins for degradation. The SAC specifically targets cell division cycle 20 (Cdc20), an activating substrate of APC/C via the mitotic checkpoint complex (MCC), which consists of budding uninhibited by benzimidazole (Bub)-related 1 (BubR1), Bub3, mitotic arrest deficient (Mad) 2 and Cdc20 (Musacchio and Salmon, 2007).

The formation of the MCC complex is initiated by the SAC kinase monopolar spindle 1 (MPS1), via the phosphorylation of the methionine-glutamic acid-leucine-threonine (MELT) repeat motifs of the exterior kinetochore subunit, kinetochore scaffold 1 (KNL1) **(Figure 1.5A)**, resulting in the recruitment of Bub1-Bub3 and BubR1-Bub3 complexes (Yamagishi *et al.*, 2012; Primorac *et al.*, 2013; Overlack *et al.*, 2015). Bub3 of the Bub1-Bub3 complex binds to the phosphorylated T of the MELT motifs (Primorac *et al.*, 2013), then Bub1 acts as a platform for MCC formation via associating with BubR1 of the BubR1-Bub3 complex **(Figure 1.5B)** (Overlack *et al.*, 2015). BubR1 then recruits Cdc20 to the kinetochore facilitating Mad2 binding (Lischetti *et al.*, 2014). Mad2 first requires conformational activation to bind to Cdc20, described by the Mad2 template model established by De Antoni *et al.* (2005). This involves Mad1 acting as a receptor for Mad2 binding at the kinetochore **(Figure 1.5B)**, producing a complex containing a closed (C)-Mad2 confirmation (Mad1-C-Mad2 complex) (De Antoni *et al.*, 2005). This complex, along with MPS1 (Hewitt *et al.*, 2010), then recruits open (O)-Mad2 which

binds to Cdc20, resulting in Cdc20-C-Mad2 (De Antoni *et al.*, 2005) and the completion of the MCC formation **(Figure 1.5C)**.

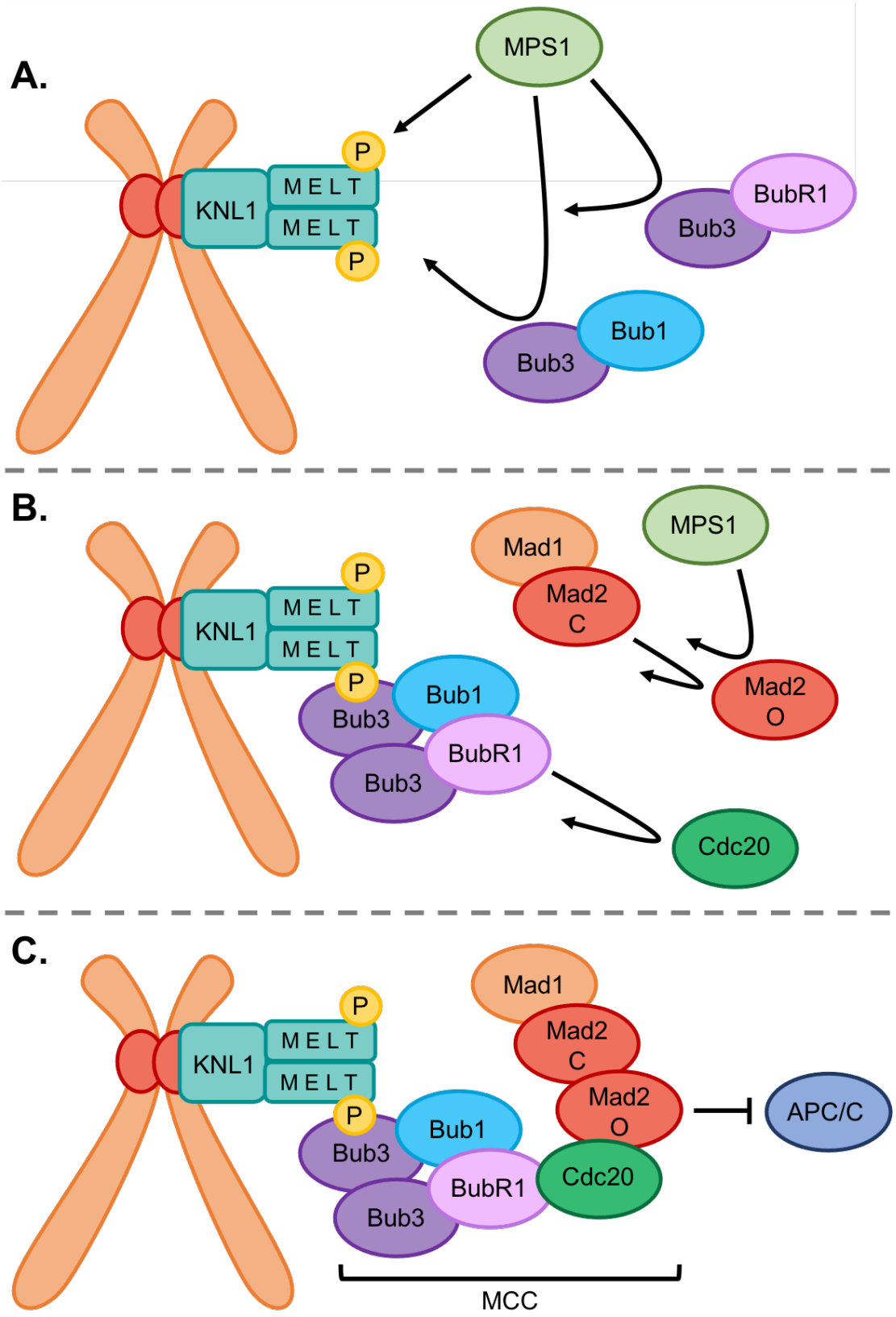

Figure 1.5: The mechanism of MCC assembly for APC/C inhibition during the SAC.
Legend on next page.

Figure 1.5: The mechanism of MCC assembly and APC/C inhibition during the SAC. **A.** MSP1 phosphorylates the MELT motifs of the kinetochore protein KNL1, resulting in the recruitment of BubR1-Bub3 and Bub1-Bub3. **B.** Bub3 (Bub1-Bub3) binds to the kinetochore, BubR1-Bub3 binds to Bub1 and BubR1 recruits Cdc20. Mad1-Closed (C)-Mad2 locates at the kinetochore and along with MSP1, recruits open (O)-Mad2. **C.** Active Mad2 binds to Cdc20 and the MCC is formed at the kinetochore, inhibiting APC/C.

In addition to Cdc20 sequestration by Mad2, the MCC specifically BubR1, possesses further mechanisms to inhibit APC/C. Firstly, it was determined that BubR1 acted as a pseudosubstrate for APC/C to prevent actual substrate binding, in yeast (Burton and Solomon, 2007) and mammalian cells (Lara-Gonzalez *et al.*, 2011). Furthermore, in the event of SAC re-activation following initial satisfaction, the MCC (BubR1) is unable to displace substrates from APC/C (Lara-Gonzalez *et al.*, 2011) and as Mad2 and APC/C bind to the same region of Cdc20 (Izawa and Pines, 2012), a more rapid mechanism of anaphase inhibition is required. In response to this, it was found that BubR1 interacts with a second Cdc20 protein which has already bound to APC/C, inhibiting Cdc20 and APC/C activity (Izawa and Pines, 2015). Another alternative and potentially less potent mechanism of Cdc20 inhibition involves CDK1 phosphorylation of Cdc20, which promotes Mad2 association (D'Angiolella *et al.*, 2003) and prevents APC/C binding (Yudkovsky *et al.*, 2000; D'Angiolella *et al.*, 2003). Overall, all Cdc20 inhibitory mechanisms contribute to APC/C inactivity, preventing chromatid segregation and mitotic exit, until the SAC is satisfied through proper microtubule attachment to the kinetochores at the centromere (Musacchio and Salmon, 2007).

1.2.4 Phosphoregulation of the SAC.

Phosphorylation events during mitosis are key for efficient and successful cell division. Master regulatory kinases such as Aurora A, Aurora B, polo-like kinase 1 (Plk1) and CDK1 and phosphatases such as protein phosphatase 1 (PP1) and PP2A, are vital for each stage of mitosis, including mitotic entry, centrosome separation, nuclear envelope breakdown, kinetochore-microtubule attachment and mitotic exit (Burgess *et al.*, 2017). Aurora B, Plk1 and PP2A also play major roles in the control of the SAC.

Aurora B promotes SAC functionality, via stimulating the recruitment of MPS1 (Saurin *et al.*, 2011), BubR1 and Mad2 to the kinetochore (Ditchfield *et al.*, 2003). This kinase responds to incorrect kinetochore-microtubule attachment, as in addition to SAC activation, Aurora B also stimulates microtubule depolymerisation factor mitotic centromere-associated kinesin (MCAK), allowing for correct reattachment (Lan *et al.*, 2004). Then Plk1 interacts with Bub1 to phosphorylate MPS1 and the MELT motifs directly, to stimulate the MCC (Ikeda and Tanaka, 2017). Plk1-Bub1 also targets Cdc20 to inactivate APC/C, in addition to and in support of MCC activity (Jia, Li and Yu, 2016). Therefore, Plk1 promotes SAC functionality. Furthermore, Plk1 hyperphosphorylates BubR1 to promote kinetochore-microtubule stability and mitotic progression (Elowe *et al.*, 2007).

Phosphatase activity in mitosis is required to counter kinase overactivity and reduce certain signalling to enable cell cycle progression. PP2A is a major S/T phosphatase in mitosis and is composed of three subunits, A; the scaffold, B; the regulatory subunit, which determines substrate specificity and C; the catalytic domain (Raman and Pervaiz, 2019). The B56 subunit of PP2A has been implicated in many aspects of mitosis, such as antagonising Aurora B and Plk1 activity at the kinetochores (Foley, Maldonado and Kapoor, 2011). More specifically, PP2A-B56 binds to BubR1 following hyperphosphorylation by Plk1, to oppose Aurora B destabilisation activity at the kinetochores, to ensure effective kinetochore-microtubule attachment (Suijkerbuijk *et al.*, 2012). The PP2A-B56-BubR1 interaction also dephosphorylates the KNL1 MELT motifs, opposing MPS1 activity for SAC silencing and mitotic progression (Espert *et al.*, 2014).

1.2.5 SAC satisfaction and mitotic exit.

When all microtubules are correctly attached to the chromatids, the SAC is fulfilled leading to MPS1 dissociation from the kinetochore (Jelluma *et al.*, 2010), PP2A-B56-BubR1 dephosphorylation of the KNL1 MELT motifs and subsequent Bub3 dissociation from the kinetochore (Espert *et al.*, 2014). Mad1-Mad2 also disconnects from the kinetochore (Buffin *et al.*, 2005) and releases Cdc20 for APC/C activation. In addition to SAC inhibition of Cdc20, the CDK1 phosphorylated and inactivated Cdc20 is dephosphorylated by PP2A-B56-BubR1 (Hein *et al.*, 2021). Cdc20 activity stimulates

APC/C leading to the polyubiquitination of various targets for degradation, including the cell cycle inhibitors securin and cyclin B **(Figure 1.6)** (Musacchio and Salmon, 2007). Securin impedes chromatid segregation via direct inhibition of separase protease activity (Hornig *et al.*, 2002), which maintains the integrity of cohesin between the sister chromatids. Following APC/C-Cdc20-mediated degradation of securin, separase is active to cleave the sister chromatid cohesion protein 1 (Scc1) component of cohesin, enabling chromatid separation and anaphase **(Figure 1.6)** (Uhlmann *et al.*, 2000). Then the APC/C-Cdc20-mediated degradation of cyclin B inhibits CDK1 activity enabling anaphase, mitotic progression and exit **(Figure 1.6)** (Castro *et al.*, 2005). PP2A-B56 also inactivates CDK1 via the dephosphorylation and inhibition of CDC25C, preventing the removal of the inhibitory T14/Y15 phosphorylation of CDK1, promoting mitotic progression and exit (Forester *et al.*, 2007).

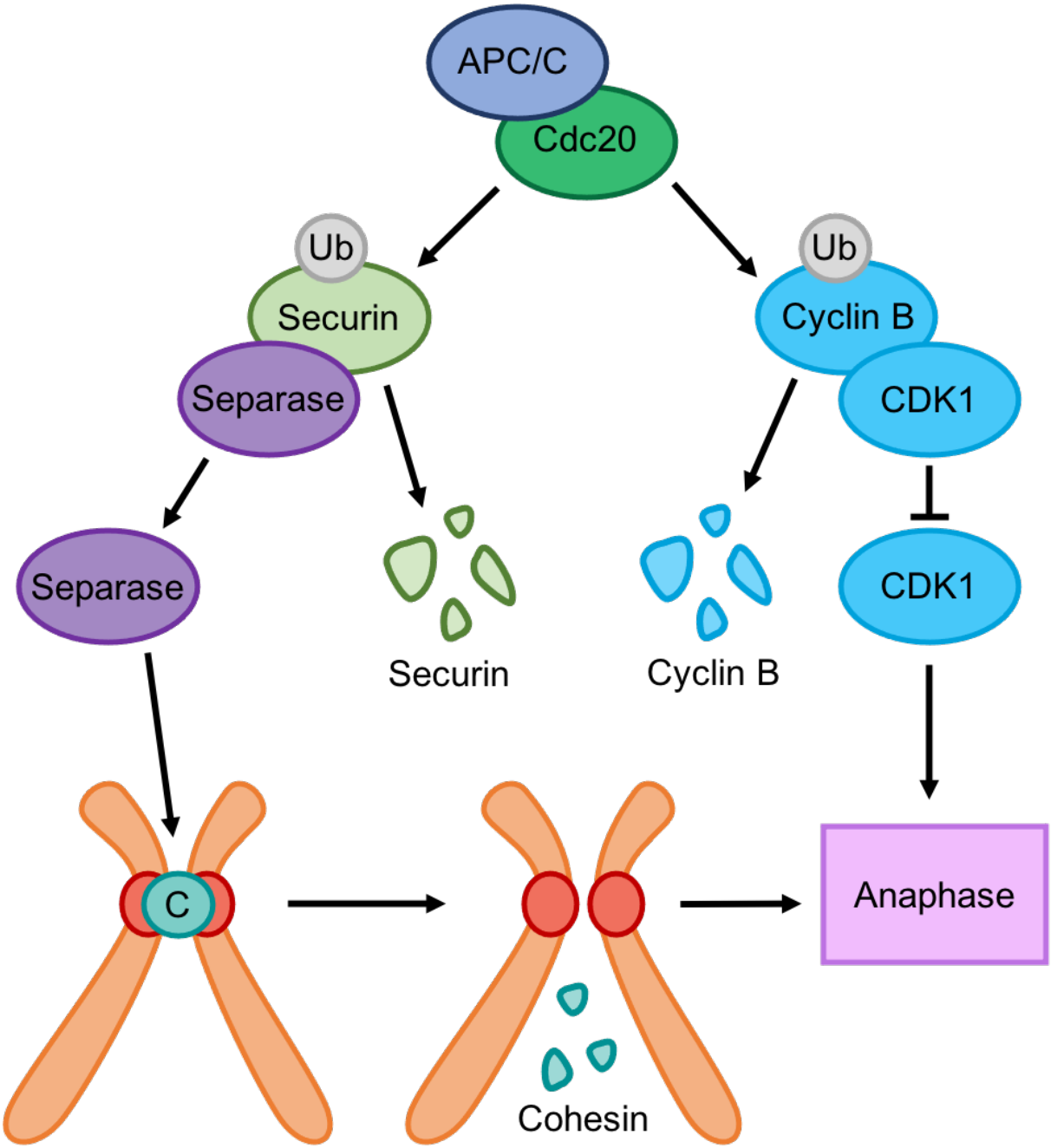

Figure 1.6: The actions following APC/C activation.

When the SAC is satisfied, Cdc20 is released and activates APC/C ubiquitination (Ub) activity leading to securin degradation and separase stimulation. Separase breaks down cohesin (C) between the sister chromatids, allowing separation and progression into anaphase. Cyclin B is also degraded leading to CDK1 inactivity, progression into anaphase and subsequent mitotic exit.

Furthermore, Cdc20 homolog 1 (Cdh1) is a subsequent activator of APC/C, which is phosphorylated by CDK1 preventing APC/C binding. Following APC/C-Cdc20-

mediated degradation of cyclin B and inactivation of CDK1, Cdh1 is dephosphorylated and binds to APC/C. This complex then facilitates mitotic exit by promoting the degradation of factors such as Cdc20, cyclin B, Aurora A and Plk1. (Castro *et al.*, 2005).

1.3 DDR and SAC crosstalk.

The DDR and SAC are two vital cellular mechanisms, that are considered to function independently. Yet there is accumulating evidence to suggest crosstalk between the pathways during mitosis, in the absence and presence of DNA damage in numerous organisms, including humans (reviewed in Thompson, Gatenby and Sidi, 2019). This indicates the existence of a DDR in mitosis, which is currently considered to be impractical and inhibited during this cell cycle phase.

1.3.1 DDR inhibition in mitosis.

As mentioned in section **1.1.8**, it is thought that the DDR is inhibited in mitosis. When DNA damage such as DSBs occur, it is currently recognised that the MRN, ATM, H2AX and MDC1 are activated **(Figure 1.7)**, like in the interphase checkpoints (Giunta, Belotserkovskaya and Jackson, 2010). In interphase, ATM activated MDC1 recruits the E3 ligase RING-finger protein 8 (RNF8) to the DSB site (Kolas *et al.*, 2007), which poly-ubiquitinates H2A and H2AX histones (Mailand *et al.*, 2007) and recruits another E3 ligase, RNF168, to amplify the ubiquitination marks on the chromatin (Doil *et al.*, 2009), leading to the recruitment of NHEJ and HR repair factors 53BP1 and BRCA1 respectively (Kolas *et al.*, 2007; Mailand *et al.*, 2007; Doil *et al.*, 2009). However, the RNF dependent events following MDC1 activation are repressed in mitosis (Giunta, Belotserkovskaya and Jackson, 2010).

The mitotic kinases, CDK1 and Plk1 negatively regulate the DNA repair in mitosis **(Figure 1.7)** (van Vugt *et al.*, 2010). Firstly, CDK1 phosphorylates RNF8 leading to inactivity and inhibition of subsequent downstream DNA repair pathways (Orthwein *et al.*, 2014). Then CDK1 and Plk1 target 53BP1 and XRCC4, preventing NHEJ repair (van Vugt *et al.*, 2010; Orthwein *et al.*, 2014; Terasawa, Shinohara and Shinohara, 2014). Additionally, Plk1 further phosphorylates 53BP1, providing a platform for Plk1

binding and inhibition of Chk2 at multiple sites, preventing the NHEJ pathway **(Figure 1.7)** The suppression of Chk2 is enhanced by the lessened ability of ATM to activate the kinase during mitosis **(Figure 1.7)** (van Vugt *et al.*, 2010).

Finally, Plk1 acts to inhibit the ATR-Chk1 axis. ATR activation of Chk1 requires the adaptor protein claspin, which Plk1 targets for degradation by β-Transducin repeat containing E3 ubiquitin protein ligase- Skp, Cullin, F-box containing complex (β-TrCP-SCF) **(Figure 1.7)** (Mamely *et al.*, 2006). This degradation of claspin results in Chk1 suppression, inhibiting the DDR.

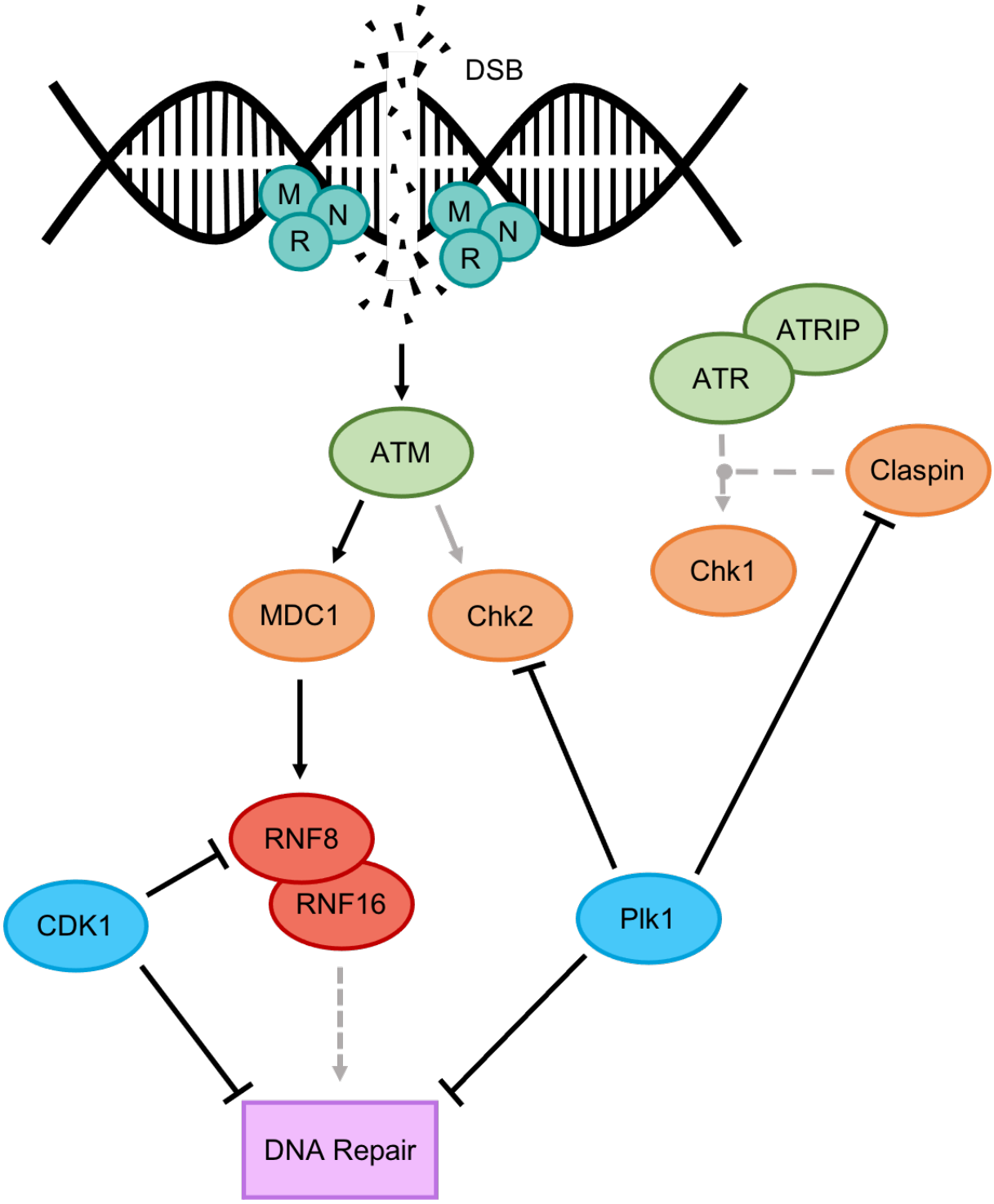

Figure 1.7: A simplified summary of the DDR during mitosis.

The presence of double strand breaks (DSBs) in mitosis stimulates ATM activity, leading to the activation of MDC1 and the reduced activation (grey arrow) of Chk2. MDC1 then activates RNF8 and RNF168 for subsequent DNA repair. CDK1 inhibits RNF8 and DNA repair factors directly and indirectly via RNF8 (grey dashed arrow). Plk1 also inhibits DNA repair, Chk2 and the intermediate activator of Chk1, claspin. In summary, the DDR and repair are inhibited in mitosis.

1.3.2 Evidence in support of a mitotic DNA damage checkpoint.

There is substantial evidence in support of a mitotic DNA damage checkpoint, which responds to damage both induced directly to mitotic cells and indirectly via damage induced to interphase cells that progress into mitosis due to impairment of interphase DDR checkpoints (reviewed in Thompson, Gatenby and Sidi, 2019). Evidence includes, mitotic cells exhibiting a prolonged transit time and even conducting DNA repair following DNA damage. In addition to many studies identifying a relationship between numerous DDR (ATM, MDC1 and Chk1) and SAC proteins (BubR1 and Plk1) during both pathways, highlighting the capability of a mitotic response to DNA damage. Furthermore, preliminary data collected in the Thompson laboratory supports the crosstalk between the pathways and the existence of a DDR checkpoint in mitosis. However, there remains controversy regarding the existence of the checkpoint, as well as the dispute of the specific role of some proteins potentially involved in the mitotic response to DNA damage. Hence the DDR signalling pathway in mitosis has not yet been defined.

1.3.2.1 Cells arrest in mitosis following DNA damage.

DNA damage has been extensively shown to arrest cells in mitosis. Firstly, in yeast, the homologues of ATM (Tel1) and ATR (Mec1) were found to arrest the cell in metaphase via the utilisation of SAC proteins Mad1, Mad2, Mad3 (BubR1), Bub1 and Bub3, following treatment with a replication stress inducing agent. It was deduced that the SAC-mediated APC/C-Cdc20 inhibition and subsequent securin maintenance caused the mitotic arrest, independent of the kinetochore-microtubule attachment status. (Kim and Burke, 2008). DNA damage induced mitotic arrest has also been demonstrated in human cells. Osteosarcoma U2OS cells blocked in mitosis with nocodazole were exposed to various DNA damaging treatments and upon release from nocodazole, the majority of cells remained in mitosis for at least 8 hours-post damage in an ATM dependent manner, compared to the untreated condition (Smits *et al.*, 2000). Similarly, following DNA damage induction in p53-deficient HeLa and HCT116 (cervical and colorectal cancer respectively) cell lines, mitotic arrest in metaphase via SAC activation was exhibited for up to 10 hours, prior to cell death in mitosis (Nitta *et al.*, 2004). Furthermore, in numerous cell lines it was deduced that the SAC arrested cells in metaphase for prolonged periods, following exposure to various

DNA damage inducing agents, but independent of ATM activity (Mikhailov, Cole and Rieder, 2002). Finally, indirect mitotic DNA damage, achieved by the impairment of the interphase DDR checkpoints by administration of a Chk1 inhibitor before ionising radiation (IR) treatment, was found to prolong mitotic progression (Thompson *et al.*, 2015), indicating DNA damage induced mitotic arrest. Overall, it can be confirmed that DNA damage induces mitotic arrest/extended mitotic transit, typically at metaphase, supporting the existence of a DDR checkpoint in mitosis. Although there is uncertainty and dispute regarding how the arrest occurs.

1.3.2.2 Cells are capable of DNA repair during mitosis.

As previously described in section **1.3.1**, the DNA repair pathways such as NHEJ and HR are inhibited in mitosis. However, it has been described that upon DSB induction during mitosis, NHEJ can occur to a lesser degree than interphase cells, to partially repair the damage. The limited level of NHEJ in mitosis was proposed to be due to XRCC4 inhibitory phosphorylation by CDK1 and Plk1. Although it was considered that NHEJ is activated to bridge the DSB ends, to allow progression into G1 for repair completion (Terasawa, Shinohara and Shinohara, 2014). More recently, Godinez *et al.* (2020) have shown that NHEJ and HR are activated in mitosis, following near-infrared (NIR) laser micro-irradiation induced DSBs, SSBs and base crosslinking. In mitosis, all NHEJ factors assembled at the damage sites indicating repair. Whereas only the upstream HR factors accumulated at damage sites, leading to the extension of HR into G1. NHEJ factors were also retained in G1. (Godinez *et al.*, 2020). Therefore, DSB repair can be conducted in mitosis, primarily via the NHEJ pathway and repair can also be completed in G1. Mitotic cells also exhibit a mechanism to overcome replication stress, termed mitotic DNA repair synthesis (MiDAS), which is initiated in prophase to enable completion of DNA synthesis before chromatin condensation for overall genome protection (Minocherhomji *et al.*, 2015). Recently it has been described that Plk1 phosphorylation of RAD51 promotes MiDAS, following replication stress or incomplete replication. It was also determined that the inhibition of MiDAS or RAD51 delayed anaphase via SAC activation, due to the presence of DNA damage (Wassing *et al.*, 2021).

1.3.2.3 ATM and ATR mediation of the SAC.

ATM and ATR are considered key in the relationship between the DDR and SAC pathways. These upstream DDR proteins have been found to activate downstream DDR and SAC proteins in undamaged mitotic cells and in response to DNA damage. Firstly, during unperturbed mitosis, ATM was found to be activated by the phosphorylation of S1403 by Aurora B, which is considered the main mitotic activator of ATM (Yang *et al.*, 2011). ATM then regulates mitotic progression through targeting the activation of Bub1 (Yang *et al.*, 2011), Mad1 and subsequently Mad2 (Yang *et al.*, 2014), contributing to the MCC formation and SAC activity. Furthermore, ATM has been shown to activate H2AX and MDC1 at the kinetochores, where MDC1 then regulates the recruitment of Mad2 and Cdc20 (Eliezer *et al.*, 2014). It has also been observed that ATM activates Chk2 (T68) during mitosis in the absence of damage (Yang *et al.*, 2011), leading to Chk2 activation of BRCA1 at S988, which regulates normal SAC functioning (Stolz *et al.*, 2010). Additionally, in the undamaged mitotic cells, ATM and ATR activate Chk1, which then promotes Aurora B and BubR1, regulating SAC activity (Zachos *et al.*, 2007). The participation of DDR proteins in normal SAC functioning demonstrates the existence of crosstalk between the pathways and facilitates the idea that the activities of these DDR proteins during normal mitosis could also be easily activated in response to DNA damage.

DNA damage following replication stress activated ATM (Tel1) and ATR (Mec1) during mitosis in yeast cells, which then arrested the cell in metaphase via the utilisation of the MCC proteins Mad1, Mad2, BubR1 (Mad3), Bub1 and Bub3 to activate the SAC independently of the kinetochore-microtubule attachment (Kim and Burke, 2008). Yet the involvement of ATM is disputed in higher organisms, as similarly to yeast cells the SAC was activated upon exposure to various DNA damage inducing agents leading to mitotic arrest but did not require ATM activity in mouse oocytes (Lane *et al.*, 2017) and numerous human cell lines (Mikhailov, Cole and Rieder, 2002). Although ATM has been found to target specific SAC proteins following DNA damage in human cells. Upon exposure to irradiation (IR), ATM activates Bub1 at the same phosphorylation site targeted for mitotic functioning in undamaged cells, where Bub1 was found to be an integral factor in the response to DNA damage (Yang *et al.*, 2012). This highlights a phosphorylation site that may be key for a mitotic DDR. Moreover, ATM was also

shown to induce mitotic arrest in response to DNA damage via the inhibition of Plk1 (Smits *et al.*, 2000), yet further work is required to determine how this is achieved.

1.3.2.4 Involvement of MDC1 in metaphase-anaphase transition.

MDC1 is another important DDR protein found to contribute to mitotic progression via the SAC. Yet the exact role MDC1 possesses in mitosis is unclear. Firstly, MDC1 has been found to bind to APC/C in unperturbed cells. Interestingly, after induction of DSBs via IR treatment, the MDC1-APC/C interaction was enriched in a dose dependent manner (Coster *et al.*, 2007). The exact role of this interaction was not determined in this study but may provide a mechanism of DDR mediated mitotic arrest following DNA damage. Expanding on the findings of Coster *et al.* (2007), another study confirmed the association of MDC1 and APC/C and further identified an interaction between MDC1 and Cdc20, concluding MDC1 regulates Cdc20 activation of APC/C in unperturbed cells (Townsend *et al.*, 2009). Therefore, it was deduced that MDC1 regulates normal metaphase-anaphase transition through APC/C activation. In addition to this research, Li *et al.* (2017) found that MDC1 stimulates prometaphase-metaphase transition, but through Plk1 mediated activation of MDC1 at the kinetochores, ensuring chromosome stability (Z. Li *et al.*, 2017). Then there is also evidence to support a role of MDC1 in the stimulation of SAC activity and APC/C inhibition. A study by Eliezer *et al.* (2014), determined MDC1 is activated at the kinetochores through ATM and γH2AX and recruits Cdc20 and Mad2 to the kinetochores, promoting SAC activity in undamaged cells. Overall, MDC1 may possess multiple roles which influence metaphase-anaphase transition.

Finally, another role of MDC1 in mitosis following DNA damage has been identified. As more recently in response to DSBs experienced in mitosis, MDC1 accumulates at the damage site and recruits TOPBP1, which forms filamentous structures between MDC1 foci, to connect the breaks for chromosome segregation and ensure subsequent repair in G1 (Leimbacher *et al.*, 2019). Overall, the role of MDC1 in mitosis requires further investigation, yet highlights a potential involvement within the mitotic response to DNA damage.

1.3.2.5 Chk1 induces mitotic arrest following DNA damage.

Chk1 has also been implicated in crosstalk with SAC proteins primarily in damaged cells. In yeast, it was observed that following the induction of replication stress there was the presence of recurring DNA damage in mitosis, leading to the activation of Chk1, which then stimulates the SAC and metaphase arrest via Mad2 (Collura *et al.*, 2005). In support of this, an association of Chk1 and Mad2 was confirmed in both undamaged and damaged human cells, which contributed to both the DDR and SAC (Chilà *et al.*, 2013). Furthermore, in *Drosophila*, Chk1 responded to chromosomal breaks to induce metaphase arrest. BubR1 was shown to work synergistically with Chk1 for metaphase arrest following higher doses of damage, due to impairment of the kinetochore (Royou, Macias and Sullivan, 2005). Then in mammalian cells, the inhibition of Chk1 in combination with IR treatment was found to prolong mitotic progression (Thompson *et al.*, 2015), indicating a DNA damage induced mitotic arrest. To mention, Chk1 has been implicated in mitotic functioning in undamaged cells, via activating Plk1 and its subsequent downstream activity (Adam *et al.*, 2018), which may be important during mitotic DNA damage.

1.3.2.6 BubR1 responds to DNA damage.

Many studies have determined BubR1 as a prominent factor for the SAC-mediated response to DNA damage. This protein was found to be hyperphosphorylated (Choi and Lee, 2008) and accumulate at the kinetochores after damage, hence contributing to SAC-mediated mitotic arrest (Nitta *et al.*, 2004; Royou, Macias and Sullivan, 2005; Choi and Lee, 2008). It was deduced that the mitotic arrest was abrogated following BubR1 depletion (Nitta *et al.*, 2004), supporting a key role of this SAC protein in the mitotic response to DNA damage. Furthermore, in *Drosophila* BubR1 along with Plk1 and Aurora B was found to accumulate at DSBs and form a tether structure between the ends, to ensure segregation and overall protection of the cell from the damage encountered. It was also proposed that BubR1 enrichment at the damage site may facilitate DNA repair. (Royou *et al.*, 2010). More recently, BubR1 overexpression has been associated with promoting NHEJ via binding to ATM following IR treatment (Komura *et al.*, 2021). However, Komura *et al.* (2021) determined this as a mechanism of cancer cell resistance to IR. Despite this, these findings indicate that BubR1 is capable of contributing to DNA repair. Furthermore, it has been identified that BubR1

induced mitotic arrest potentially through an interaction with DDR protein PARP1 at the kinetochores. In the same study, BubR1 deficient cells exhibited impaired mitotic arrest and a decrease in PARP1, γH2AX, p53 and p21 levels after DSBs induction. (Fang *et al.*, 2006). Thus, further indicating that the DDR pathway in mitosis requires BubR1 functionality. To summarise, it can be deduced that BubR1 may act as an upstream DDR signalling protein in mitosis, mediating the SAC and DDR response to DNA damage and initiating repair. BubR1 provides a promising basis for further experimental testing into the mitotic DDR pathway.

1.3.2.7 Other proteins involved in DDR and SAC crosstalk.

Numerous other DDR and mitotic proteins have been shown to exhibit crosstalk. Recently, a novel role for the MRN complex has been identified in mitosis, which involves Plk1 activation of MRN and MMAP to form the mitotic MRN complex (mMRN), which in turn enables Plk1-mediated microtubule deconstruction and chromosome segregation in unstressed conditions (Xu *et al.*, 2018). Moreover, Plk1 has been found to phosphorylate and bind to BRCA2, to promote the hyperphosphorylation of BubR1 for PP2A-B56 binding, ensuring proper kinetochore-microtubule attachment (Ehlen *et al.*, 2020). In response to mitotic DNA damage, it is thought Plk1 is inhibited by the phosphatase PP2A. A study by Jang *et al.* (2007) proposed that upon DNA damage induced in early mitosis (prometaphase), PP2A dephosphorylates and inactivates Plk1, leading to the suppression of mitotic transit and reversal back into G2 (Jang *et al.*, 2007). Expanding on the study by Jang *et al*. (2007), it was deduced that mitotic DNA damage activated the ATM DDR pathway and inhibited PP2A negative regulators, enabling PP2A inhibition of Plk1, resulting in entry into interphase without proper segregation and cytokinesis (mitotic slippage) (Kim, Hyun and Jang, 2019). Despite these studies theorising that cells exit mitosis abruptly without completing cell division following the exposure to DNA damage, it can be deduced that PP2A may influence DDR checkpoint recovery in mitosis.

Securin has also become a known site of conversion between the DNA damage and SAC pathways, as the ATM pathway has been shown to phosphorylate securin following DNA damage, suggesting a mechanism for a DNA damage checkpoint arrest in mitosis (Cohen-Fix and Koshland, 1997). Then ATM has also been found to inhibit

securin degradation via stimulation of the SAC following DNA damage (Kim and Burke, 2008). Whereas Chk1 has been found to directly phosphorylate securin, preventing APC/C-mediated degradation and promoting the DDR (Wang *et al.*, 2001). These studies were conducted in yeast yet provide a good experimental basis for an investigation into human cells.

In summary, there is substantial evidence to suggest that DNA damage present in mitotic cells may cause metaphase arrest via numerous DDR and mitotic proteins contributing to the SAC and even initiating DNA repair.

1.4 Cellular redox homeostasis.

Reactive oxygen species (ROS) are by-products generated during normal oxygen metabolism. In turn, ROS contributes to numerous cellular processes such as cell division and the immune response (Kumari *et al.*, 2018). The balance between the production of ROS and its clearance by antioxidants (redox homeostasis) within the cell must be regulated to avoid detrimental consequences. If this balance is not maintained or there is an accumulation of ROS through endogenous or exogenous factors, the cell experiences oxidative stress. This causes the oxidation of important biological structures such as lipids, proteins and DNA, resulting in damage. (Pizzino *et al.*, 2017). The cell is equipped with mechanisms to avoid and repair this damage, yet excess ROS may cause the cell to undergo apoptosis or contribute to the development of pathologies such as cancer, cardiovascular and neurodegenerative diseases (Snezhkina *et al.*, 2019).

1.4.1 Types of ROS and its regulation.

The term ROS encompasses different oxygen and hydroxyl molecules such as the superoxide anion ($O_2^{\bullet-}$), hydroxyl radical ($^{\bullet}OH$) and hydrogen peroxide (H_2O_2). $O_2^{\bullet-}$ and $^{\bullet}OH$ free radicals are very short-lived due to the presence of an unpaired electron; 10^{-6} seconds and 10^{-10} seconds respectively. Whereas H_2O_2 has no unpaired electrons and is more intracellularly stable (Kumari *et al.*, 2018). $O_2^{\bullet-}$ and H_2O_2 are moderately reactive and both can be converted into the highly reactive and damaging $^{\bullet}OH$, in addition to $O_2^{\bullet-}$ also producing H_2O_2 **(Figure 1.8)**. $O_2^{\bullet-}$ is primarily generated via

aerobic respiration through oxidative phosphorylation, which is then converted to H_2O_2 **(Figure 1.8)**. (Harris and Denicola, 2020). To regulate the intracellular ROS concentration to prevent oxidative damage and ensure redox homeostasis, there are different protective antioxidant-dependent mechanisms to process and detoxify ROS (Aprioku, 2013).

Antioxidants are reducing agents which detoxify ROS by donating electrons to the radicals, resulting in their own oxidation. This can be achieved through enzymatic or non-enzymatic mechanisms. (Aprioku, 2013). Enzymatic mechanisms of ROS clearance involve multi-step reactions and are often complemented by co-factor molecules. $O_2^{\bullet-}$ is dismutated to H_2O_2 by the superoxide dismutase (SOD) family of antioxidant metalloenzymes **(Figure 1.8)**. $O_2^{\bullet-}$ is unable to diffuse across cellular membranes due to its anionic charge (Harris and Denicola, 2020), so there are specific SOD isoforms (SOD1/2/3) situated in $O_2^{\bullet-}$ abundant sub-cellular environments (Wang *et al.*, 2018). As $O_2^{\bullet-}$ can be responsible for the generation of other types of ROS (H_2O_2 and $^{\bullet}OH$), the SOD enzymes are highly efficient in the dismutation of $O_2^{\bullet-}$ ($\sim 2 \times 10^9$ $Mol^{-1} \cdot sec^{-1}$) (Forman and Fridovich, 1973). The most abundant SOD enzyme is SOD1, which contains a zinc/copper catalytic site (Che *et al.*, 2016) and is localised throughout the cytoplasm (Slot *et al.*, 1986), mitochondrial intermembrane space (Sturtz *et al.*, 2001) and the nucleus (Slot *et al.*, 1986; Tsang *et al.*, 2014). Then SOD2 features manganese metal ions (Che *et al.*, 2016) and is only located in the mitochondrial matrix (Slot *et al.*, 1986). Finally, SOD3 also has a zinc/copper catalytic site (Che *et al.*, 2016), but functions within the extracellular matrix (Marklund, Holme and Hellner, 1982). Ultimately, SOD enzymes are well distributed to protect the cell from $O_2^{\bullet-}$ radical damage.

Considering the stability and longer half-life of H_2O_2, this radical can diffuse across membranes increasing oxidation of primarily proteins, distal from its source. Optimum levels of 1-10 nM are beneficial for H_2O_2 involvement in cell signalling pathways. However, if the cellular concentration is greater than 100 nM there becomes a ROS-antioxidant imbalance, leading to oxidative stress. (Harris and Denicola, 2020). The antioxidant enzyme catalase (CAT) detoxifies H_2O_2 into H_2O (Aebi, 1984) through interaction with the tetrameric haem *b* enzymatic site **(Figure 1.8)** (Glorieux *et al.*, 2015). CAT activity is mainly associated with the peroxisomes due to its large

production of H_2O_2 (Glorieux *et al.*, 2015), but has also been identified in the cytoplasm in human fibroblasts (Wanders *et al.*, 1987). Additionally, the family of glutathione peroxidase (GPx) selenoenzymes are also involved in the conversion of H_2O_2 to H_2O (Rotruck *et al.*, 1973) **(Figure 1.8)**. The active site of GPx features a selenocysteine residue (Rotruck *et al.*, 1973), which reacts with H_2O_2 using a non-enzyme antioxidant co-factor, glutathione in its reduced state (GSH) (Bhowmick and Mugesh, 2015). Both the selenocysteine residue and glutathione are regulated by other factors to return these molecules to their active state, allowing for further ROS metabolism.

Highly reactive $^{\bullet}OH$ radicals are derived from $O_2^{\bullet-}$ and H_2O_2 through the Haber-Weiss/ Fenton reactions **(Figure 1.8)**. These reactions require a metal catalyst, such as iron (Fe) ions for redox functionality. (Winterbourn, 1995). $^{\bullet}OH$ radicals react non-specifically and rapidly with most important biological molecules, resulting in detrimental effects to the cell (Aprioku, 2013). The conversion of $O_2^{\bullet-}$ and H_2O_2 to $^{\bullet}OH$ is the main mechanism these ROS molecules induce damage (Harris and Denicola, 2020). Furthermore, cells lack a direct enzymatic response to process $^{\bullet}OH$ radicals, so consequently relies on other antioxidants to eliminate $O_2^{\bullet-}$ and H_2O_2, to overall prevent $^{\bullet}OH$ production. However, it has been found that GSH can react with $^{\bullet}OH$, ultimately ceasing radical activity (Sjoberg, Eriksen and Revesz, 1982; Fiser *et al.*, 2013).

A.

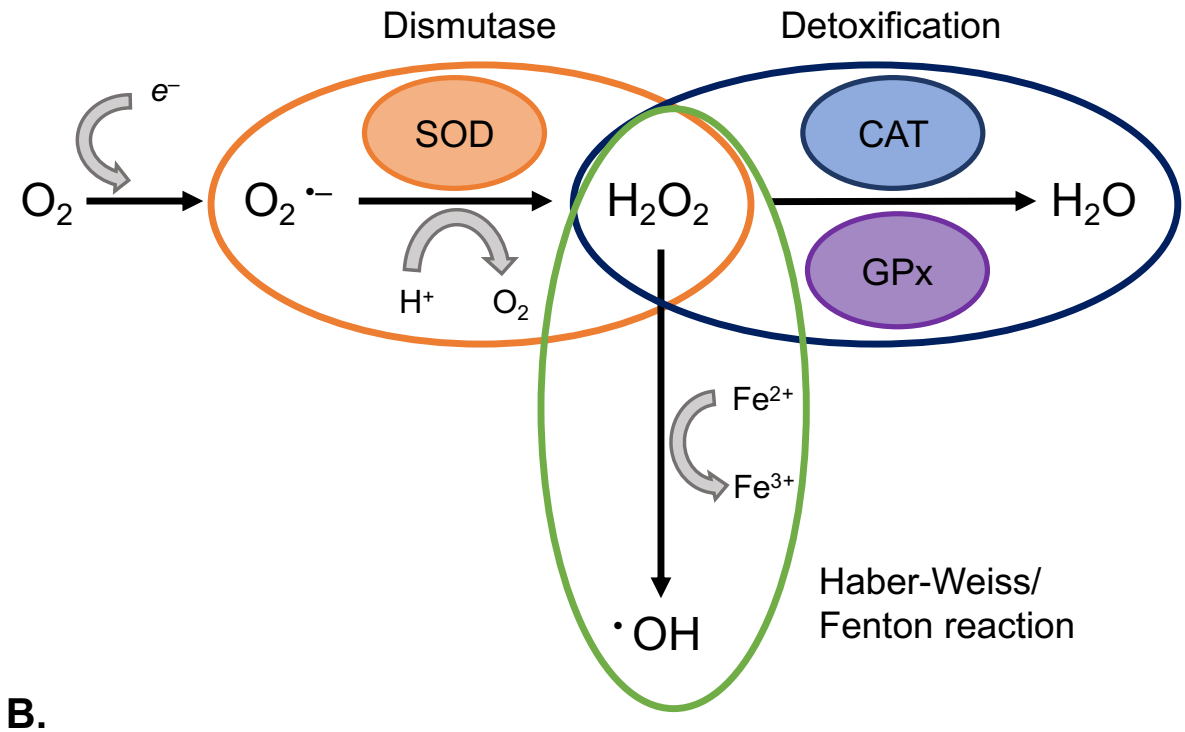

B.

Dismutase by SOD:

$$2O_2^{\bullet-} + 2H^+ \longrightarrow H_2O_2 + O_2$$

Detoxification of H_2O_2:

Detoxification by catalase

$$2H_2O_2 \longrightarrow 2H_2O + O_2$$

Detoxification by glutathione peroxidase

$$H_2O_2 + 2GSH \longrightarrow GSSG + 2H_2O$$

Haber-Weiss/Fenton reaction

$$O_2^{\bullet-} + H_2O_2 \longrightarrow {}^{\bullet}OH + OH^- + O_2$$

Figure 1.8: The generation of ROS and its regulation.

Legend on next page.

Figure 1.8: The generation of ROS and its regulation.

A. A schematic overview of the production of superoxide anions ($O_2^{\bullet-}$), hydrogen peroxide (H_2O_2) and hydroxyl radical ($^{\bullet}OH$). $O_2^{\bullet-}$ is produced from oxygen metabolism and is dismutated by SOD antioxidant enzymes into H_2O_2. H_2O_2 is detoxified by catalase (CAT) or glutathione peroxidase (GPx) into H_2O. $^{\bullet}OH$ radicals are produced by H_2O_2 and $O_2^{\bullet-}$ through the Haber-Weiss/Fenton reactions, which require metal catalysts such as iron (Fe) ions (Wang *et al.*, 2018). Adapted with permission from (Wang *et al.*, 2018). **B.** The net reactions for production/processing of $O_2^{\bullet-}$, H_2O_2 and $^{\bullet}OH$. The dismutation of $O_2^{\bullet-}$ by SOD enzyme into H_2O_2 and O_2 (McCord and Fridovich, 1969). The detoxification of H_2O_2 into H_2O by catalase and glutathione peroxidase. The glutathione peroxidase requires non-enzyme glutathione in a reduced state (GSH) for the reaction, producing oxidized glutathione (GSSG) (Bhowmick and Mugesh, 2015). The generation of $^{\bullet}OH$ from $O_2^{\bullet-}$ and H_2O_2 via the Haber-Weiss/Fenton reactions (Sharma et al., 2012).

Exogenous or naturally occurring non-enzyme antioxidants such as vitamins A (retinoic acid), C (ascorbic acid), E (α-tocopherol) and glutathione, are either lipid- or water-soluble enabling localisation throughout the cell (Aprioku, 2013; Moussa, Judeh and Ahmed, 2020). These molecules quench ROS through direct interaction producing less reactive products or aid in the activity of enzymatic antioxidant reactions.

1.4.2 Oxidative stress.

An imbalance between ROS production and clearance which results in ROS accumulation and in turn damages numerous biological molecules is termed oxidative stress. Similar to the DDR signalling cascades, cells have a signalling response to recognise and combat redox impairment, to prevent oxidative damage. Nuclear factor erythoid-2 related factor 2 (NRF2) is a transcription factor that provides the initial response to oxidative stress. In unstressed conditions, NRF2 is maintained at low levels in the cytoplasm through an interaction with kelch-like ECH-associated protein 1 (Keap1) (Itoh *et al.*, 1999), which induces NRF2 proteasomal degradation (Kobayashi *et al.*, 2004). When ROS levels accumulate, the NRF2-Keap1 interaction is disrupted due to the inactivating oxidation of Keap1 cysteine residues by ROS (Itoh *et al.*, 1999; Yamamoto *et al.*, 2008). NRF2 is then able to translocate to the nucleus (Itoh *et al.*, 1999) and heterodimerise with small Maf proteins for the transactivation of genes exhibiting antioxidant response elements in the promotor regions (Itoh *et al.*,

1997). These genes include those involved in ROS detoxification such as those in the glutathione system (Thimmulappa *et al.*, 2002). It has also been described that the transcriptional activity of NRF2 extends to genes involved in other cellular pathways independent of ROS activity, such as DNA damage repair through the regulation of the RAD51 gene family responsible for HR repair (Jayakumar, Pal and Sandur, 2015).

ROS-induced damage of biomolecules (lipids, proteins and DNA) frequently occurs at low levels under normal physiological conditions but is enhanced when oxidative stress is experienced. One consequence is lipid peroxidation of the cell membrane or lipoproteins due to excess $^{\bullet}OH$ radicals, resulting in large scale damage as lipid peroxidation induces a lipid radical chain reaction. Consequently, mutagenicity and cell death occur. (Pizzino *et al.*, 2017). ROS can also affect both protein structure and activity via reversible and irreversible modifications of protein side chains leading to a range of consequences. The most frequently occurring reversible modifications include the oxidation of cysteine or methionine residues which can alter the protein structure affecting function, including loss or gain of activity (enzymatic) and protein-protein interactions. This is how redox is capable of mediating numerous signalling pathways under normal physiological conditions (Reichmann, Voth and Jakob, 2018). Irreversible protein modifications include carbonylation (generation of reactive aldehydes and ketones through the oxidation of lysine, arginine and proline residues), over-oxidation of cysteine and methionine residues, di-tyrosine formation (cross-linkage of tyrosine residues), tryptophan oxidation and protein-protein cross-linking (Stadtman and Levine, 2000; Reichmann, Voth and Jakob, 2018). These in turn cause the loss of function via protein unfolding, protein aggregation and cell death. However, to protect the cell, damaged proteins are targeted for proteasomal degradation. (Reichmann, Voth and Jakob, 2018). Irreversible protein modifications are associated with the development of several pathologies, such as Parkinson's (Alam *et al.*, 1997) and Alzheimer's disease (Hensley *et al.*, 1994; Smith *et al.*, 1998).

Finally, DNA base lesions generated through reactions with radicals can cause a range of damage including, intrastrand crosslinks, DNA-protein crosslinks, mismatched bases, replication fork collapse, SSBs and DSBs (Davalli *et al.*, 2018). Thus, resulting in the activation of the appropriate DDR repair pathways. A well-characterised biomarker of oxidative damage of DNA involves the formation of 8-oxo-7,8-dihydro-2′-

deoxyguanosine (8-oxodG) adducts via the reaction of radicals with guanine bases (Kasai, 1997). These lesions cause replication and transcriptional errors which leads to the production of aberrant proteins and potential mutagenicity (David, O'Shea and Kundu, 2007). BER initiated by 8-oxoguanine glycosylase (OGG1) responds to 8-oxodG lesions (Lu, Nash and Verdine, 1997).

Overall, these lesions are prevented via antioxidant clearance of ROS, further enhanced by NRF2 signalling or the damage encountered is responded to by other cellular defence mechanisms, such as DNA repair pathways, to ultimately protect the cell against oxidative stress.

1.4.3 Redox participation in signalling pathways.

ROS are known to influence cell-signalling pathways such as the immune and inflammation response, cell proliferation, cell cycle and oxidative stress response, as well as the ubiquitin-proteasomal pathway. This is achieved through the short-term activation or inactivation of various proteins via reversible oxidation, which includes important regulatory kinases and phosphatases. (Zhang *et al.*, 2016). More importantly, ROS have also been reported to impact DDR and mitotic signalling.

1.4.3.1 The interplay between the DDR pathway and redox regulation.

ROS can influence the activity of DDR proteins via reversible oxidation in healthy and malignant cells. Plus, oxidative stress results in damage to DNA and proteins, thus activating the DDR pathway and negatively influencing DDR protein activity. Then DNA damage inducing agents may also generate ROS as a by-product. Therefore, both the DDR and oxidative stress signalling pathways overlap to protect the cell against malignancy and death. (Davalli *et al.*, 2018).

Numerous DDR proteins are oxidised at redox sensitive cysteine residues, suggesting that these proteins may be regulated by ROS during healthy cell signalling and oxidative stress. More specifically, ATM has been observed to be oxidised at cysteine 2991, forming a disulphide bridge that restricts MRN binding, thus its DDR role. Yet the oxidation is required for ATM activation by oxidative stress. Following treatment with both DNA damage and ROS inducing IR, it was proposed that the immediate

consequence would be the induction of ROS and oxidative activation of ATM. Following the short-lived ROS events and detoxification, ATM is then reduced and capable of binding to MRN to initiate the long-term DDR in response to the DNA damage caused directly by IR and indirectly by oxidative stress. (Guo, Deshpande and Paull, 2010). This is supported in a study by Bakkenist and Kastan (2003), as pan-nuclear phosphorylation of ATM was demonstrated 5 minutes post-IR treatment, compared to the ATM foci co-localised with γH2AX 1 hour post-IR treatment, suggesting distinct roles of ATM (Bakkenist and Kastan, 2003). Therefore, ATM possesses alternative activatory mechanisms for oxidative stress and DNA damage. Although the role of ATM in response to oxidative stress is currently unknown.

Alternatively, other DDR proteins are inactivated by oxidation. Firstly, p53 possesses a cysteine rich protein core, where many of the cysteine residues reside within highly conserved domains (Delphin *et al.*, 1994). It has been observed that the oxidation of p53 cysteine residues prevents p53 DNA binding activity (Delphin *et al.*, 1994), via the formation of a disulfide bond, reversibly disrupting the protein structure (Sun *et al.*, 2003). Therefore, attenuating p53 transcription factor activity of downstream DDR, cell cycle and apoptotic proteins. Then CDC25B (Sohn and Rudolph, 2003) and CDC25C have been reported to be susceptible to reversible oxidation by H_2O_2 leading to inactivation, via the formation of an intramolecular disulfide bridge at the active site (Savitsky and Finkel, 2002; Sohn and Rudolph, 2003). This additional inhibitory mechanism of both CDC25 proteins is likely to be more rapid than phospho-degradation stimulated by DDR proteins. Hence will aid in the inhibition of the cell cycle following DNA damage induced by oxidative stress and/or DNA damage, to ensure repair and avoid detrimental consequences.

NRF2 has been identified to respond to DNA damage independently of its antioxidant functions, in both *in vitro* (Jayakumar, Pal and Sandur, 2015; Sun *et al.*, 2020) and in vivo lung cancer models (Sun *et al.*, 2020). Following the induction of DSBs via IR treatment in the presence of ROS scavenging agents, NRF2 proteins levels increased intracellularly and NRF2 was observed to accumulate at the DNA lesions with ATR. It was found that NRF2 activated ATR, stimulating the subsequent ATR mediated DDR pathway, imposing G2 cell cycle arrest for repair and cancer cell protection. (Sun *et al.*, 2020). Furthermore, NRF2 transcriptionally regulates HR proteins such as RAD51

(Jayakumar, Pal and Sandur, 2015) and BRCA1 (Wang *et al.*, 2013), influencing the efficiency of the HR repair pathway. Additionally, DDR proteins also regulate NRF2. First BRCA1 has been identified to transcriptionally regulate NRF2 in response to oxidative stress, as well as numerous other antioxidant genes such as GPx3 and SOD1 (Bae *et al.*, 2004). As NRF2 and BRCA1 seemingly regulate the transcription of each other, the existence of a positive feedback loop between NRF2 and BRCA1 can be proposed in the defence against oxidative stress and DNA damage. Additionally, PARP1 was found to act as a coactivator of NRF2 transcriptional activity by enhancing the interaction between NRF2, Maf proteins and the antioxidant response elements in promotor regions (Wu *et al.*, 2014). Finally, following low levels of oxidative stress p21 functioned independently of its DDR role and was observed to compete with Keap1 for NRF2 binding, which protected NRF2 from degradation and promoted its transcriptional activity (Villeneuve *et al.*, 2009). In addition to protein oxidation, NRF2 is highlighted as an important factor that overlaps the DDR and oxidative stress pathways.

Independently of SOD1's enzymatic role in the regulation of redox homeostasis, this enzyme has also been reported to re-localise to the nucleus after treatment with ROS inducing agent, H_2O_2 in yeast (Tsang *et al.*, 2014) and human cells (Bordoni *et al.*, 2019; X. Li, Qiu, *et al.*, 2019). It was proposed that ATM mediated the activation of SOD1 translocation in response to oxidative stress (Tsang *et al.*, 2014; Bordoni *et al.*, 2019). The resulting nuclear SOD1 initiated gene expression of redox and DNA damage related proteins (Tsang *et al.*, 2014; X. Li, Qiu, *et al.*, 2019). Overall, the literature demonstrates multiple links between the DNA damage and oxidative stress cellular defence pathways in response to both stimuli.

1.4.3.2 Redox regulation of mitosis.

ROS levels have been quantified throughout the cell cycle and were found to be highest during mitosis, which correlated with an elevation in cysteine oxidisation of proteins (Patterson *et al.*, 2019). It is becoming more recognised that the redox system participates in various processes during mitotic entry, progression and exit, typically through ROS mediation of mitotic phosphatases and kinases. Therefore, cellular redox is an influential factor in mitosis.

The antioxidant enzyme, peroxiredoxin 1 (Prx1) has been identified to colocalise with the pericentriolar scaffold of the centrosomes during late prophase-metaphase. It was proposed that Prx1 protects the centrosomal phosphatases from local H_2O_2, the activity of this antioxidant enzyme influences mitotic entry and progression. During early mitosis CDK1-cyclin B phosphorylate and inactivate Prx1, which allows H_2O_2 to inactivate mitotic phosphatases like Cdc14B through reversible cysteine oxidation, preventing early APC/C activation. As mitosis progresses Prx1 is dephosphorylated by PP1 and PP2A to detoxify H_2O_2, leading to Cdc14B reactivation enabling APC/C activation for mitotic exit. (Lim *et al.*, 2015). Furthermore, the centrosomal levels of cyclin B, Plk1 and Aurora A were found to be regulated by H_2O_2 (Lim *et al.*, 2015). Additionally, the phosphatase PP2A has also been reported to be targeted for inactivation by H_2O_2 (Rao and Clayton, 2002), specifically via cysteine oxidation of the catalytical C domain (Foley *et al.*, 2007). Oxidative regulation of PP2A has been shown to impact mitosis, as following the administration of exogenous H_2O_2, cells were observed to have abnormal nuclei in a dose dependent manner. It was determined that this was due to H_2O_2 inactivation of PP2A, which activates factors involved in the reassembly of the nuclear envelope during mitotic exit. (Ahn *et al.*, 2019).

Oxidative stress has also been found to impact SAC functionality. Firstly, it was determined following the administration of H_2O_2 (180-360 μM), SAC arrested cells were able to bypass the checkpoint and exit mitosis via mitotic slippage. This was caused by the reduction of Mad2 binding to Cdc20 via the reintroduction of CDK1 inhibitory phosphorylation, leading to APC/C activation and the stimulation of proteasomal degradation of cyclin B and securin, promoting premature mitotic exit (D'Angiolella, Santarpia and Grieco, 2007). The inhibition of CDK1 may be due to the oxidative inactivation of CDC25C, which is known to target CDK1 for the removal of inhibitory phosphorylations (Savitsky and Finkel, 2002). However, it has also been demonstrated that the APC/C catalytic subunit APC11 is targeted for cysteine oxidation by H_2O_2, impairing ubiquitination activity and subsequent degradation of securin and cyclin B, resulting in a delay in mitotic transit (Chang *et al.*, 2004). This effect was prominently observed at the higher concentrations of H_2O_2 (0.5-1 mM) (Chang *et al.*, 2004), which was supported by D'Angiolella *et al.* (2007) findings, as in this study at higher concentrations of H_2O_2 (over 500 μM) the degradation of cyclin B and securin was no longer observed (D'Angiolella, Santarpia and Grieco, 2007). Furthermore, ROS agents

have also been found to impair Aurora A activity via hyperphosphorylation, which disrupted spindle assembly inducing SAC-mediated mitotic arrest (Wang *et al.*, 2017). In addition to this, Aurora A kinase activity has been found to be regulated by a series of oxidative modifications. Firstly, Coenzyme A (CoA) interacts with Aurora A to form a disulfide adduct in proximity to the Aurora A activatory domain. This has been proposed to inhibit (Tsuchiya *et al.*, 2020) or in contrast, activate (Lim *et al.*, 2020) Aurora A kinase activity. Following the formation of the CoA disulfide adduct, oxidation of complementary cysteine residues within two Aurora A monomers occurs to form a disulfide dimer, which promotes a conformation for activation via phosphorylation (Lim *et al.*, 2020). It has been demonstrated that oxidising agents such as H_2O_2, significantly enhance the phosphorylation of Aurora A (Wang *et al.*, 2017; Tsuchiya *et al.*, 2020), but this is indicative of an inhibitory manner (Wang *et al.*, 2017). In support of this, inactivity of Aurora A by H_2O_2 has been found to occur in a dose dependent manner (Byrne *et al.*, 2020). Therefore, it can be deduced that Aurora A is regulated by redox but requires a multi-step oxidative mechanism to enable phospho-inactivation.

Alternatively, prolonged mitotic transit independent of the SAC has been observed following oxidative stress. It was demonstrated in yeast cells blocked in mitosis with nocodazole, that upon release from nocodazole and exposure to H_2O_2, the majority of cells remained in mitosis in a concentration dependent manner. The same effect was observed using a temperature inactivating APC/C mutant, suggesting the delay in mitosis observed was not due to SAC activity (Atalay *et al.*, 2017). Although this should be verified in human cells.

Interestingly, in the presence of oxidative stress, the p53 pathway is activated and downregulates BubR1 activity to prevent aneuploidy in human non-cancer cells (Ikawa-Yoshida *et al.*, 2013). In turn, this may impair SAC functionality. However, it has been found that oxidative factors inactivate p53 (Delphin *et al.*, 1994). This may identify an oxidative stress-mediated mechanism of tumorigenesis, as the impairment of p53 leads to BubR1 accumulation and stimulation of polyploidy, which can lead to aneuploidy (Ikawa-Yoshida *et al.*, 2013). Importantly this demonstrates a link between the DDR, mitosis and oxidative stress pathways in cancer.

1.5 Cancer and the impact of the DDR, mitotic and oxidative stress pathways.

1.5.1 Cancer.

There are over 200 types of cancer, the most commonly diagnosed are breast, prostate, lung and bowel which contributed to over half (53 %) of new cases (CRUK, 2017). Cancer is the second leading cause of death worldwide, with an estimated 10 million deaths in 2020 (World Health Organisation, 2021). The main treatment modalities include surgery, radiotherapy and chemotherapy, which contribute to a 50 % survival rate of greater than 10 years (CRUK, 2011). The mechanism of action for radio- and chemotherapeutics involve the induction of DNA damage, leading to tumour cell death. Radiotherapy such as IR, can cause large scale amounts of damage directly (International Atomic Energy Agency, 2010) and indirectly via the radiolysis of water to produce $^{\bullet}OH$ radicals (Schipler and Iliakis, 2013). Overall damage encountered from a 1-2 Gray dose of IR can result in approximately over 1000 DNA base damages, ~ 1000 SSBs and ~ 40 DSBs (International Atomic Energy Agency, 2010). Whereas chemotherapeutics generate damage based on the mechanism of action of the reagent, which can be advantageous against certain cancer types. For example, the DNA alkylating agent temozolomide (TMZ) is commonly used for the treatment of glioblastoma. TMZ induces various methylation lesions on DNA bases, such as the most toxic, O^6-methylguanine, which is removed by the repair protein O^6-methylguanine DNA methyltransferase (MGMT) (Erasimus *et al.*, 2016). In ~ 40 % of glioblastoma tumours, the *MGMT* gene is epigenetically repressed (Esteller *et al.*, 1999), indicating tumour sensitivity to TMZ treatment, resulting in cytotoxic unrepaired DNA lesions and an overall positive patient outcome (Hegi *et al.*, 2009). Furthermore, the O^6-methylguanine lesion can directly and indirectly via lack of repair, induce further DNA damage such as SSBs and DSBs (Erasimus *et al.*, 2016).

Radio- and chemotherapeutics are often used in combination to enhance effectiveness and patient survival. However, the reoccurrence of cancer is typically due to resistance of the tumour to current treatment methods. Hence, the development of new treatments is a constant aim within cancer research to improve patient survival. DDR, oxidative stress and mitotic proteins are being investigated as targets for the generation of new anti-cancer therapeutics.

1.5.2 The DDR pathway involvement in tumorigenesis.

The impairment of DDR and repair pathways are involved in many aspects of cancer such as tumorigenesis and treatment resistance, typically caused by the induction and enrichment of genomic instability (the generation of mutations), one of the hallmarks of cancer (Hanahan and Weinberg, 2011). A well-known example involves the breast cancer susceptibility genes, *BRCA1* and *BRCA2*. Germline mutations of *BRCA1* and *BRCA2* have been found to increase the risk of developing breast cancer to 55-72 % and 45-69 % respectively (National Cancer Institute, 2020). The BRCA proteins regulate HR repair which would be impaired in mutated cells, leading to enhanced levels of DNA damage, genomic instability and tumour progression. Additionally, the accumulation of DNA damage is associated with the development of sporadic cancers, possibly caused by repeated exposure to carcinogens. Furthermore, it is particularly favourable for the cancer cells to have enhanced genomic instability via disrupted DDR and repair pathways, as the excessive DNA damage causes further mutations such as oncogene activation and tumour suppressor gene inactivation. (Ciccia and Elledge, 2010).

Therefore, the integrity of the DDR pathway is vital for the cellular defence against cancer. Although this pathway is exploited through the induction of DNA damage for tumour cell death in cancer anti-therapies. However, the tumour cells can utilise the DDR and repair pathways for survival in response to current treatments, highlighting the DDR proteins as an attractive target to enhance the effectiveness of DNA damaging anti-cancer therapeutics. Some examples include ATM (ClinicalTrials.gov, 2021a), PARP1 (ClinicalTrials.gov, 2021b), Chk1 and Chk2 (Lee *et al.*, 2018) inhibitors and these agents are being coupled with the standard radio- and chemotherapies, to enhance tumour cell death and therapeutic value (ClinicalTrials.gov, 2021a, 2021b).

1.5.3 Mitotic proteins expression in cancer.

The mitotic SAC proteins also protect against genomic instability and mitotic dysregulation has been linked to tumorigenesis via excessive cell proliferation. However, gene mutations of these proteins are rare (Yuan *et al.*, 2006), as this process is vital for cell proliferation and survival. Alternatively, the overexpression of numerous SAC proteins has been reported in multiple cancer types. The upregulation of Cdc20

was shown in oral squamous cell carcinoma cell lines and primary head and neck tumours. This positively correlated with the key cancer characteristic of aneuploidy, potentially through the premature activation of APC/C and anaphase (Mondal *et al.*, 2007). The SAC genes *MAD1L1*, *MAD2L1*, *MAD2L2*, *BUB1*, *BUB1B*, *BUB3* and *CDC20* have also been found to be overexpressed in the majority of breast cancer cell lines and high-grade breast cancer tumours (Yuan *et al.*, 2006). Importantly, BubR1 protein levels were increased in ~ 77 % of high-grade breast tumours (Yuan *et al.*, 2006), indicative as a predictive and prognostic biomarker (Yuan *et al.*, 2006; Maciejczyk *et al.*, 2013). Similarly, the overexpression of *BUB1* (84 %), *BUB1B* (68 %) and *BUB3* (79 %) genes were found in primary gastric carcinomas tissue samples, which was associated with an increase in cell proliferation (Grabsch *et al.*, 2003). The overexpression of the MCC proteins in tumour cells indicates a compensatory mechanism for the increase in cancer cell proliferation. Furthermore, increased SAC activity has been observed in platinum-based chemo-resistant cancers (Nagaraj *et al.*, 2018; Moens *et al.*, 2021). More specifically, BubR1 overexpression in chemo-radioresistant bladder cancer has been shown to enhance mutagenicity by accelerating NHEJ (Komura *et al.*, 2021).

Additionally, mitotic kinases are upregulated in numerous cancer types. Examples include Aurora A is overexpressed in hepatocellular carcinomas (Jeng *et al.*, 2004) and breast cancer (Nadler *et al.*, 2008), and Plk1 in non-small cell lung cancer (NSCLC) (Wang *et al.*, 2012) and colorectal tumours (Han *et al.*, 2012). Furthermore, Aurora A (Moens *et al.*, 2021) and Plk1 (Nagaraj *et al.*, 2018) expression was reported to be vital for tumour growth and survival of carboplatin resistant triple-negative breast cancer and cisplatin-resistant ovarian cancer respectively (Nagaraj *et al.*, 2018; Moens *et al.*, 2021). Therefore, inhibitors for these kinases have been investigated, Alisertib (Ren *et al.*, 2015; Falchook *et al.*, 2018) and Volasertib (Awada *et al.*, 2015) inhibit Aurora A and Plk1 respectively, resulting in apoptosis and ultimately inhibiting tumour cell proliferation (Ren *et al.*, 2015) and reducing tumour size (Awada *et al.*, 2015; Falchook *et al.*, 2018). These inhibitors have been combined with other anti-cancer treatments to enhance effectiveness and sensitivity, yielding an enhanced therapeutic value (Awada *et al.*, 2015; Falchook *et al.*, 2018).

1.5.4 Oxidative stress involvement in cancer.

Firstly, oxidative stress can cause cancer through the damage generated by the high ROS levels, such as gene mutations from oxidative DNA damage. Cancer cells typically exhibit higher intracellular ROS levels compared to healthy cells, due to an increased cellular metabolism during oncogenesis. The increased ROS concentration has been implicated in oncogene activation, tumour suppressor gene inactivation, enhanced cell proliferation and angiogenesis. (Kumari *et al.*, 2018). Furthermore, it is known the treatment of cancer with radio- (Riley, 1994) and chemotherapeutics (He *et al.*, 2018) induce ROS resulting in apoptosis (Perillo *et al.*, 2020). The upregulation of antioxidants and oxidative stress proteins has been found in cancer cells, providing a mechanism of cell survival and treatment resistance (Kumari *et al.*, 2018).

NRF2 has been found to be overexpressed in NSCLC, as well as the reduction of Keap1, leading to unregulated and enhanced activity of NRF2 (Solis *et al.*, 2010). This causes resistance to platinum-based chemotherapeutics (Solis *et al.*, 2010) and IR treatments (Sun *et al.*, 2020), which was proposed to be due to the role of NRF2 in the DDR, allowing for DNA repair and cancer cell survival (Jayakumar, Pal and Sandur, 2015; Sun *et al.*, 2020). Therefore, NRF2 possesses therapeutic value and the administration of NRF2 inhibitors has successfully sensitised cancer cells to anti-cancer IR treatment (Lee *et al.*, 2012; Jayakumar, Pal and Sandur, 2015; Sun *et al.*, 2020).

Antioxidant enzyme SOD1 has also been reported to be upregulated in numerous cancer types such as NSCLC (Liu *et al.*, 2020), breast cancer (Papa *et al.*, 2014) and nasopharyngeal carcinoma (Li *et al.*, 2018), contributing to poor patient outcome (Li *et al.*, 2018; Liu *et al.*, 2020). Overall it is vastly recognised that SOD1 promotes tumour proliferation and metastasis (Somwar *et al.*, 2011; X. Li, Chen, *et al.*, 2019; Li *et al.*, 2020; Liu *et al.*, 2020). However, there are multiple mechanisms reported to how SOD1 encourages tumorigenesis. Examples include the upregulation of SOD1 increases H_2O_2 intracellular levels, which are known to regulate cell growth pathways via oxidation (X. Li, Chen, *et al.*, 2019), and SOD1 promotes cancer growth and progression via its increased expression in fibroblasts located in the tumour microenvironment (Li *et al.*, 2020). The numerous mechanisms of SOD1 in tumorigenesis indicates this enzyme to be an attractive target for the development of

anti-cancer therapeutics. SOD1 inhibitors have been developed and have successfully demonstrated an increase in tumour cell death in numerous cancer types (Somwar *et al.*, 2011; Sajesh *et al.*, 2013; Glasauer *et al.*, 2014; X. Li, Chen, *et al.*, 2019; Liu *et al.*, 2020) and some inhibitors have progressed into clinical trials but with varied results (Lin *et al.*, 2013). Understanding the roles of SOD1 in tumour progression is required to develop more effective inhibitors.

In summary, inhibitors targeting these pathways in combination with current treatments are yielding beneficial results in the laboratory and clinic. However, the mitotic DDR pathway may provide a mechanism of resistance to these combination treatments. The dispute of existence and lack of understanding into this mitotic pathway identifies a limitation in the development of anti-cancer therapy. It is important to establish and reveal the pathway involved in the mitotic response to DNA damage, to identify targets for inhibition to prevent tumour cell evasion from the current combination therapy, contributing to the further enhancement of patient survival and reduction in resistance.

1.6 My research.

1.6.1 Preliminary data.

Preliminary analysis conducted in the Thompson laboratory (University of Sheffield) identified that cells that progress into mitosis following IR treatment with unrepaired DNA damage exhibited an extended mitotic transit time compared to untreated cells **(Figure 1.9A)**. This supports the existence of DNA damage induced mitotic arrest via a DDR response, which the Thompson laboratory have termed the mitotic DNA damage checkpoint (MDDC). Furthermore, the mitotic arrest observed was dependent on the presence of the mitotic effector, BubR1 **(Figure 1.9A)**. To establish how BubR1 is involved in the MDDC, a screen of the BubR1 interactome following DNA damage was conducted in this thesis **(Chapter 4)**. In addition to BubR1, the Thompson laboratory then investigated other factors responsible for the MDDC via a high throughput fluorescence microscopy screen **(Figure 1.9B)**. This involved the quantification of mitotic cells following the siRNA knockdown of DNA damage proteins in the presence of DNA damage. The significant reduction of mitotic cells identified an initial list of potential proteins required for the MDDC. This list was refined further in a

secondary screen (data not shown), which analysed mitotic transit time following the knockdown of each protein. This allowed for the elimination of proteins that caused cell cycle arrest in interphase and disabled entry into mitosis. Overall, the final list of proteins potentially involved in the MDDC was generated. Amongst these was the antioxidant enzyme SOD1, which has been shown to be activated by DDR proteins to stimulate the transcription of redox and DNA damage related proteins (Tsang *et al.*, 2014; Bordoni *et al.*, 2019; X. Li, Qiu, *et al.*, 2019). However, SOD1 has not yet been implicated in mitosis. Taken together, this highlights SOD1 as an interesting target to investigate in this thesis **(Chapter 3)**. In summary, this research will identify proteins involved in the MDDC.

Finally, the presence of a DNA damage response in mitosis may provide a mechanism of tumour cell resistance to current anti-cancer therapeutics, which target the interphase checkpoints in addition to DNA damage induction. This thesis aims to contribute to the knowledge of how cells respond to damage in mitosis through the identification of proteins involved in the MDDC.

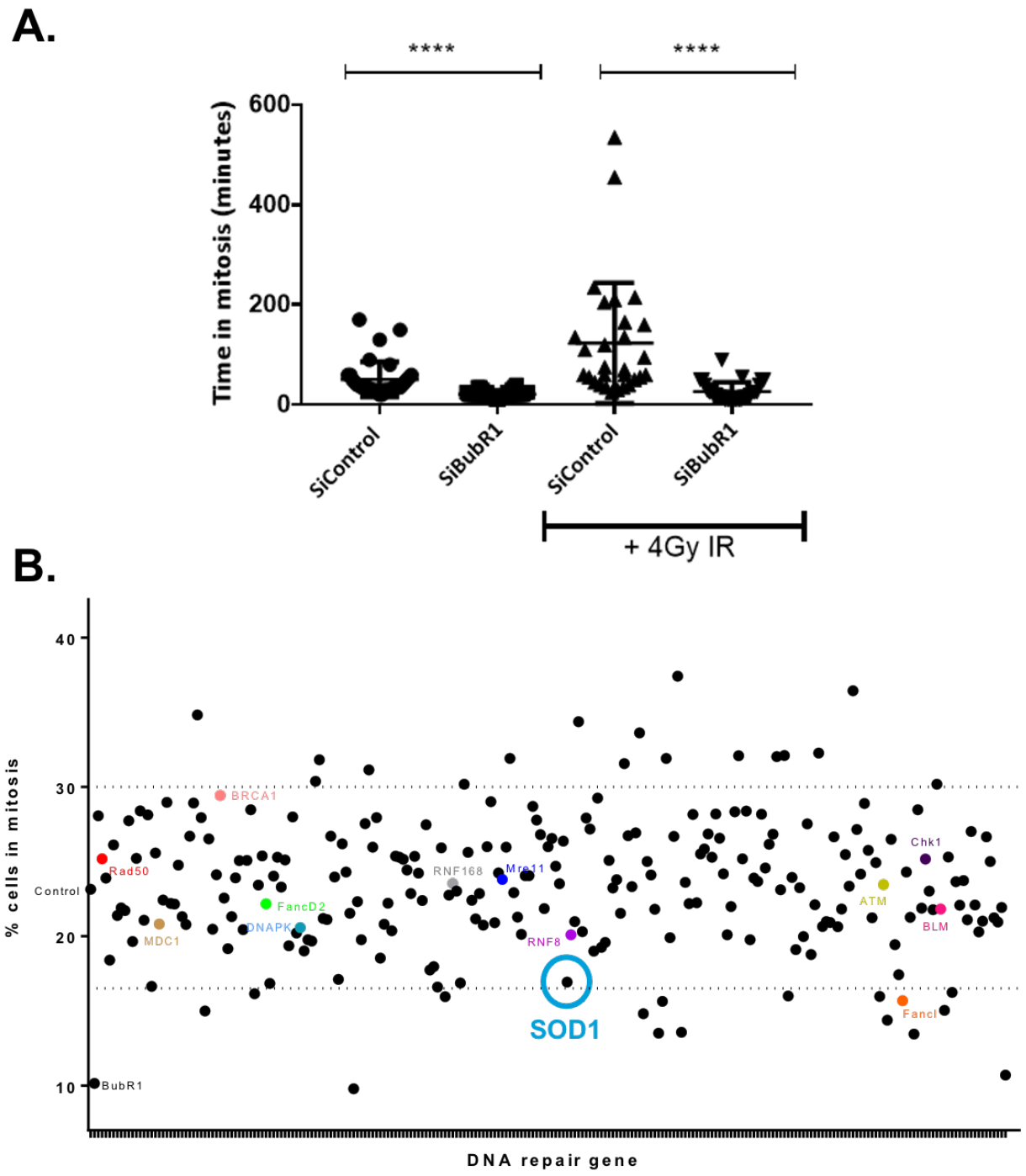

Figure 1.9: The preliminary findings in support of the existence of the MDDC and the identification of proteins involved in the checkpoint.

Legend on next page.

Figure 1.9: The preliminary findings in support of the existence of the MDDC and the identification of proteins involved in the checkpoint.

A. Mitotic transit was quantified over 24 hours via time-lapse microscopy, following the knockdown of BubR1 using siRNA and treatment of cells with IR (4 Gy). One-way ANOVA with Dunnett's correction test for multiple comparisons was performed to determine statistical significance (**** denotes $p \leq 0.0001$). **B.** High throughput fluorescent microscopy screen for mitotic population identified via pH3 staining (N= 5). Dharmacon siRNA DNA damage library was used, and cells were treated with IR (10 Gy and Chk1 inhibitor (Gö6976)). Each point represents a protein and known proteins involved in mitotic transit are labelled. The median Z score of +/- 1.5 is represented with the dotted lines and the error bars omitted for clarity.

1.6.2 Hypotheses and aims.

The first hypothesis of this thesis is that SOD1 has a novel role in the mitotic response to DNA damage.

The second hypothesis of this thesis is that the MDDC is also dependent on BubR1, and the identification and investigation into potential interacting proteins will reveal the role of BubR1 within the MDDC.

The aims of this thesis are:

1. Validate the involvement of SOD1 in the response to DNA damage during mitosis.
2. Determine how SOD1 is involved in the MDDC.
3. Identify the BubR1 DNA damage interactome.
4. Determine if the interactors of BubR1 are required for the MDDC.
5. Establish an initial pathway for the MDDC.

Chapter 2: Materials and Methods.

2.1 Materials.

2.1.1 Laboratory equipment.

Equipment	Supplier
7900 Real Time polymerase chain reaction (PCR) machine	Applied Biosciences
Aspirator	Integra Vascusafe
Autoclave	Scientific Laboratory Supplies
Balance	Thermo Fisher Scientific
Benchtop centrifuge	MSE
Class II A/B3 biological safety cabinet	Forma Scientific
CO_2 incubator	Thermo Fisher Scientific
DynaMag magnetised tube rack	Invitrogen
Electrophoresis tank	Apollo Instrumentation
FACSCalibur	BD Sciences
Film scanner	EPSON
Fluorescent Eclipse TE200 inverted microscope	Nikon
Fluorescent plate reader- SpectraMax M5e multi-mode microplate reader	Molecular devices
Gel doc XR imaging system	Bio-Rad
Haemocytometer	Neubauer
Heat/ magnetic stirrer	Stuart
Heating block DB-2A	Techne
High phase liquid chromatography (HPLC), Ultimate 3000	Thermo Fisher Scientific
Irradiator	CIS Bio International
Laboratory fume cupboard	Fumex Ltd
Leica LASAF-lite image microscope	Leica
Light microscope eclipse TS100	Nikon
LSM980 airyscan 2 confocal fluorescent Microscope	Zeiss
Microcentrifuge	Eppendorf
Mini-gyro rocker SSM3	Stuart
Mr. Frosty™ freezing container	Thermo Fisher Scientific
Multiscan™ FC microplate photometer	Thermo Fisher Scientific
Nanodrop ND-1000 UV-vis spectrophotometer	Thermo Fisher Scientific
pH 3510 meter	Jenway
Pipette boy	Drummond
Pipettes	Gibson
Power pack	Bio-Rad
Rocker	Stuart
Rotator SB3	Stuart

Equipment (continued)	Supplier
Shaker incubator	SciQuip
SRX 101A film processor	Konica
Thermocycler S1000	Bio-Rad
Ultrasonic bath	VWR
Vacuum centrifuge, concentrator plus	Eppendorf
Vortex-genie 2	Scientific Industries
Water bath	Gallenkamp
Western tanks	Bio-Rad

2.1.2 Reagents.

Reagent	Supplier
Acetic acid	Thermo Fisher Scientific
Acetonitrile (ACN) HPLC grade	Thermo Fisher Scientific
Agar	Melford
Agarose	Affymetrix
Ammonium bicarbonate (ABC)	Sigma-Aldrich
Ammonium persulfate (APS)	Sigma-Aldrich
Ampicillin	Thermo Fisher Scientific
Benzonase endonuclease	Merck
Blasticidin S Hydrochloride (HCL) powder	Melford
Bovine serum albumin (BSA)	Sigma-Aldrich
Bromophenol blue	Sigma-Aldrich
Calcium chloride ($CaCl_2$)	Thermo Fisher Scientific
Cell dissociation buffer	Gibco
CometAssay kit	R&D systems
Chloromethyl-2',7'-dichlorodihydrofluorescein diacetate (CM-H2DCFDA) general oxidative stress indicator kit	Invitrogen
DharmaFECT 1 transfection reagent	Horizon Dharmacon
Dharmafect duo	Horizon Dharmacon
4′,6-Diamidino-2-phenylindole dihydrochloride (DAPI)	Life technologies
Dimethyl sulfoxide (DMSO)	Thermo Fisher Scientific
Dimethylformamide (DMF) anhydrous	Sigma-Aldrich
Dithiothreitol (DTT)	Roche
Phenol red free DMEM	Gibco
DNA loading buffer blue (x5)	Bioline
Doxycycline Hyclate	Sigma-Aldrich
Dpn I restriction enzyme	Agilent Technologies
Dulbecco's Modified Eagle's Medium (DMEM)	Sigma-Aldrich
Dynabead protein G	Invitrogen
Enhanced chemiluminescence (ECL)	Thermo Fisher Scientific
Ethanol	Thermo Fisher Scientific
Ethidium bromide	Thermo Fisher Scientific

Reagent (continued)	Supplier
Ethylene glycol tetraacetic acid (EGTA)	Sigma-Aldrich
Ethylenediaminetetraacetic acid (EDTA)	Sigma-Aldrich
FITC annexin V apoptosis detection kit I	BD Biosciences
Foetal calf serum (FCS)	Life Science Productions
Formic acid	Thermo Fisher Scientific
Glycerol	Thermo Fisher Scientific
Glycylglycine	Alfa Aesar
Glycine	Thermo Fisher Scientific
High-Capacity RNA-to-cDNA reverse transcription kit	Applied Biosystems
HPLC grade water	Thermo Fisher Scientific
Hydrochloric acid (HCL)	Thermo Fisher Scientific
Hygromycin B	Roche
Hyperladder 1 kb	Bioline
Imidazole-HCL	Sigma-Aldrich
Epredia™ Immu-mount™	Thermo Fisher Scientific
Industrial methylated spirit (IMS)	Thermo Fisher Scientific
InstantBlue Protein Stain	Expedeon
Iodoacetamide	Sigma-Aldrich
Iodoacetamide (D4 isotope)	Cambridge isotope libraries
Isopropanol	Thermo Fisher Scientific
Kanamycin sulfate	Roche
KOD hot start DNA polymerase	Novagen
Lipofectamine 2000	Thermo Fisher Scientific
Luria broth base (LB) broth, Miller's modified	Merck
Magnesium chloride ($MgCl_2$)	Thermo Fisher Scientific
Magnesium Sulphate ($MgSO_4$)	Thermo Fisher Scientific
Methanol	Thermo Fisher Scientific
Methylene blue	Thermo Fisher Scientific
Dried skimmed milk powder	Marvel
Mix2Seq sequencing kit	Eurofins Genomics
MluI restriction enzyme	Promega
Monarch gel digest kit	New England Biolabs
Monarch PCR & DNA clean up kit	New England Biolabs
MOPS Run Buffer x20	Expedeon
NP-40 alternative	Merck
Nuclease-free water	Invitrogen
Paraformaldehyde (PFA) 4 %	Chem Cruz
PhosSTOP phosphatase inhibitor tablets	Roche
Polyethylene glycol (PEG)	Thermo Fisher Scientific
Potassium chloride (KCL)	Sigma-Aldrich
PP2A immunoprecipitation phosphatase assay kit	Merck
Precast gel	Expedeon
Precision plus molecular weight marker	Bio-Rad
Prolong Gold antifade reagent with DAPI	Life Technologies

Reagent (continued)	Supplier
Propidium iodide (PI)	Sigma-Aldrich
Protease cocktail inhibitor	Roche
Protein assay dye reagent	Bio-Rad
Protein tyrosine phosphatase activity assay kit	Abcam
ProtoGel 30 % Acrylamide mix	Geneflow
QuickChange II Site-Directed Mutagenesis Kit	Agilent Technologies
RNAse A	Sigma-Aldrich
RNaseZap	Sigma-Aldrich
RNeasy mini kit	Qiagen
SgfI restriction enzyme	Promega
siMAX universal buffer	Eurofins
siRNA universal buffer	Dharmacon
Sodium chloride (NaCl)	Thermo Fisher Scientific
Sodium deoxycholate	Sigma-Aldrich
Sodium dodecyl sulfate (SDS)	Sigma-Aldrich
Sodium hydroxide (NaOH)	Thermo Fisher Scientific
SuperSignal™ West Pico PLUS Chemiluminescent Substrate	Thermo Fisher Scientific
ß-Mercaptoethanol	Sigma-Aldrich
SYBR Gold	Thermo Fisher Scientific
T4 DNA ligase	New England Biolabs
TaqMan universal PCR master mix	Applied Biosystems
Tetramethylethylenediamine (TEMED)	Thermo Fisher Scientific
Threonine phosphopeptide (K-R-p-T-I-R-R)	Merck
Trifluoroacetic acid (TFA)	Thermo Fisher Scientific
Tris base	Sigma-Aldrich
Triton-X 100	Alfa Aesar
Trypan blue	Bio-Rad
Trypsin-EDTA	Sigma
Tween-20	Acros Organics
Trypsin protease, MS grade	ThermoFisher
Urea (Ultra-pure)	Kind gift from Dr Philip Jackson (University of Sheffield)
X-ray developer	Champion Photochemistry
X-ray fixer	Champion Photochemistry

2.1.3 Purified water.

A Triple Red nanopore water filter (Thermo Fisher Scientific) produced type 1 ultra-pure deionised water (ddH_2O).

2.1.4 Sterilisation.

Glassware and solutions were sterilised by autoclaving at 15 p.s.i and 120 °C for 15 minutes. Solutions that were not suitable for autoclaving were filter sterilised using a sterile syringe and a sterile 0.2 µM filter.

2.1.5 Mammalian cell lines.

Cell Line	Cell Type	Antibiotic Sensitivity	Supplier
HeLa	Cervical adenocarcinoma	-	ATCC
Hek293	Human embryonic kidney cells	-	ATCC
MCF7	Breast adenocarcinoma	-	ATCC
MRC5VA	Normal lung fibroblasts	-	ATCC
JSH601	HeLa Flp-In T-REx cell line	Hygromycin B and Blasticidin S Hydrochloride	A kind gift from Dr Don Cleveland (University of California San Diego)
UPF1-Flag HeLa	HeLa Flp-In T-REx cell line	Hygromycin B and Blasticidin S Hydrochloride	A kind gift from Professor Carl Smythe (University of Sheffield)

ATCC: American Type Culture Collection

2.1.6 Buffers and stock solutions.

Phosphate buffered saline (PBS)

Sterile 1x PBS was prepared by dissolving 1 PBS tablet (Oxoid) in ddH_2O (100 mL). The solution was made and autoclaved by departmental technical staff. PBS solution was stored at room temperature for tissue culture or at 4 ºC for laboratory work.

1 M Tris (pH 6.8, 7.5 and 8.0)

121.14 g tris base was dissolved in ddH_2O and pH 6.8, 7.5 or 8.0 was achieved through the addition of 10 M HCL. The final volume was made to 1 L with ddH_2O and stored at room temperature.

1.5 M Tris (pH 8.8)

181.71 g tris base was dissolved in ddH_2O and pH 8.8 was achieved through the addition of 10 M HCL. The final volume was made to 1 L with ddH_2O and stored at room temperature.

5 M NaCl

146.1 g NaCl was dissolved in 500 mL ddH_2O and stored at room temperature.

500 mM EDTA (pH 8.0)

186.1 g EDTA was dissolved in 1 L ddH2O after 5 M NaOH was added to achieve pH 8.0. 500 mM EDTA was stored at room temperature.

1 M EGTA (pH 8.0)

38 g EGTA was dissolved in 100 mL ddH2O after 5 M NaOH was added to achieve pH 8.0. 1 M EGTA was stored at room temperature.

10 % APS

1 g APS was dissolved in 10 mL ddH_2O and stored at 4 °C. 10 % APS was made fresh each month.

10 % SDS

100 g SDS was dissolved in 1 L ddH_2O and stored at room temperature.

5x Radioimmunoprecipitation assay (RIPA) lysis buffer

25 mL 1 M Tris pH 8.0 (250 mM), 15 mL 5 M NaCl (750 mM), 5 mL 10 % SDS (0.5 %), 5 mL NP-40 alternative (5 %) and 2.5 g sodium deoxycholate (2.5 %), made to 100 mL ddH_2O. 5x RIPA lysis buffer and stored at room temperature. This buffer was diluted to a 1x working solution in ddH_2O and stored at 4 ºC.

Immunoprecipitation (IP) wash buffer

20 µL Tween-20 (0.02 %) is added to 100 mL sterile PBS and stored at 4 °C.

5x Protein SDS-polyacrylamide gel electrophoresis (SDS-PAGE) loading dye

25 mL 1 M Tris pH 6.8 (250 mM), 50 mL glycerol (50 %), 5 mL ß-Mercaptoethanol (5 %), 20 mg bromophenol blue (0.02 %) and 10 g SDS (10 %), made to 100 mL with ddH_2O. 5x protein SDS-PAGE loading dye was stored at room temperature.

SDS-PAGE running buffer

The stock solution of 10x SDS-PAGE running buffer was prepared by dissolving 30.3 g tris base (250 mM) and 144 g glycine (1.9 M) in 900 mL ddH_2O, then 100 mL 10% SDS (1 %) was added for a final volume of 1 L. The working solution of 1x SDS-PAGE running buffer was prepared by diluting 100 mL 10x SDS running buffer with ddH_2O to a total volume of 1 L and stored at room temperature. Both buffers were stored at room temperature.

1x MOPS Run Blue running buffer

50 mL of 20x MOPS Run Blue running buffer for pre-cast gels was made to 1 L with ddH_2O and stored at room temperature.

Transfer buffer

The stock solution of 10x transfer buffer was prepared by dissolving 30.3 g tris base (250 mM) and 144 g glycine (1.9 M) in 1 L ddH_2O. 10x transfer buffer was stored at room temperature. The working solution of 1x transfer buffer was prepared by diluting 100 mL 10x transfer buffer with 200 mL methanol and made to 1 L with ddH_2O, with an additional 1 mL 10 % SDS (0.01 %) for larger proteins. 1x transfer buffer was made on the day of use.

10x Tris-buffered saline (TBS) (pH 7.6)

24.2 g tris base (200 mM) and 80 g NaCl (1.4 M) dissolved in ddH_2O and the pH altered with 10 M HCL to 7.6. Total volume was made to 1 L with ddH_2O and stored at room temperature.

1x TBS-Tween (TBS-T)

100 mL 10x TBS stock was diluted with 900 mL ddH_2O with the addition of 1 mL Tween-20 (0.1 %). 1x TBS-T was stored at room temperature.

5 % Milk

5 g milk powder was dissolved in 100 mL 1xTBS-T. 5 % Milk was stored at 4 °C.

Flow Buffer 1

2.5 g BSA (0.5 %) and 1.25 mL Triton-X 100 (0.25 %) were dissolved in 500 mL sterile PBS. Flow buffer 1 was stored at 4 °C.

Flow Buffer 2

1.25 mL Triton-X 100 (0.25 %) was dissolved in 500 mL sterile PBS. Flow buffer 2 was stored at 4 °C.

PBS-Triton-X (PBS-Tx)

0.75 g BSA (0.15 %) and 2.5 mL Triton-X 100 (0.5 %) was dissolved in 500 mL sterile PBS and stored at 4 °C.

BSA-Triton-X (BSA-Tx)

5 g BSA (5 %), 100 µL Triton-X 100 and 0.8 g NaCl (0.8 %) was dissolved in 100 mL sterile PBS and stored at 4 °C.

Tris-acetate-EDTA (TAE) buffer

The stock solution of 10x TAE buffer was prepared by dissolving 48.4 g tris base (400 mM), 20 mL 500 mM EDTA pH 8.0 (10 mM) and 11.42 mL acetic acid (1.1 %) in ddH_2O and the pH was altered with 10 M HCL to 7.6-7.8. Total volume was made to 1 L with ddH_2O. The working solution of 1x TAE buffer was prepared by diluting 100 mL 10x TAE stock with ddH_2O to a final volume of 1 L. Both buffers were stored at room temperature.

LB broth

10 g LB broth (2.5 %) dissolved in ddH_2O to a final volume of 400 mL. LB broth was autoclaved before use and stored at room temperature.

Agar

12 g agar (3 %) and 10 g LB broth (2.5 %) dissolved in ddH_2O to a final volume of 400 mL. Agar was autoclaved before use and stored at room temperature.

Kanamycin sulfate

500 mg kanamycin sulfate was dissolved in 10 mL ddH_2O to generate a stock solution of 50 mg/mL. The solution was filter sterilised before use and stored at -20 °C.

Ampicillin

1 g ampicillin was dissolved in 10 mL ddH_2O to generate a stock solution of 100 mg/mL. The solution was filter sterilised before use and stored at -20 °C.

5x KCM

25 mL 1 M potassium chloride (KCL) (500 mM), 7.5 mL 1 M $CaCl_2$ (150 mM), 12.5 mL 1 M $MgCl_2$ (250 mM) and ddH_2O (5 mL) to make a final volume of 50 mL. Filter sterilised and stored at room temperature.

Bacterial TBS

10 g polyethylene glycol (PEG) (10 %), 5 mL DMSO (5 %), 1 mL 1 M $MgCl_2$ (10 mM) and 1 mL 1 M $MgSO_4$ (10 mM) was added to 83 mL LB broth pH 6.1 to a final volume of 100 mL. This buffer was autoclaved and stored at 4 °C.

Phosphatase assay lysis buffer

418.16 mg imidazole-HCL (20 mM), 800 µL 500 mM EDTA pH 8.0 (2 mM), 400 µL 1 M EGTA pH 8.0 (2 mM) dissolved in ddH_2O and the pH altered with 10 M HCL to 7.0. Total volume was made to 200 mL with ddH_2O and stored at 4 °C.

Methylene blue staining solution

4 g methylene blue (0.4 %) dissolved in 700 mL methanol (70 %) and ddH_2O to a total volume of 1 L and stored at room temperature.

10x In vitro protein reaction buffer

0.132 g glycylglycine (100 mM) and 0.292 g NaCl (500 mM) was dissolved in 10 mL ddH_2O. The reaction buffer was filter sterilised before used and stored at room temperature.

1 M Dithiothreitol (DTT)

1.54 g DTT was dissolved in 10 mL ddH_2O and stored at -20 °C until freeze thawed once for use.

1 M Ammonium bicarbonate (ABC) solution

0.79 g ABC was dissolved in 10 mL HPLC grade ddH_2O and stored at room temperature. 1 M ABC was made fresh before use.

50 mM ABC solution

1 mL 1 M ABC solution was diluted in 19 mL HPLC grade ddH_2O. This was made fresh for each experiment.

25 mM ABC solution

500 µL 1 M ABC solution was diluted in 19.5 mL HPLC grade ddH_2O. This was made fresh for each experiment.

Reduction reagent

0.015 g DTT (10 mM) was dissolved in 10 mL 50 mM ABC solution. This was made fresh for each experiment and stored short-term at room temperature.

Alkylation reagent

0.102 g iodoacetamide (55 mM) was dissolved in 10 mL 50 mM ABC solution. This was made fresh for each experiment and stored short-term at room temperature protected from light.

Digestion buffer

37.5 µL 1 µg/µL trypsin protease, MS grade (12.5 ng/µL) was added to 15 µL 1 M $CaCl_2$ (5 mM) and made to a total volume of 3 mL in 50 mM ABC solution.

Mass spectrometry (MS) IP lysis buffer

500 µL 1 M Tris pH 8.0 (50 mM), 400 µL 5 M NaCl (200 mM), 100 µL Triton-X 100 (1 %), 10 µL 1 M DTT (1 mM), 20 µL 500 mM EDTA pH 8.0 (1 mM), 20 µL benzonase endonuclease (0.2 %), 1 phosSTOP inhibitor tablet (1x) and 1 complete EDTA protease cocktail inhibitor (1x) dissolved in sterile ddH_2O, to a final volume of 10 mL. This lysis buffer was made before use and stored on ice.

MS IP wash buffer

The MS IP wash buffer was prepared the same as the MS IP lysis buffer with the exception of the absence of benzonase endonuclease, which was replaced by 20 µL extra sterile ddH_2O for a final volume of 10 mL. This wash buffer was made before use and stored on ice.

On-bead wash buffer

10 µL 1 M Tris pH 7.5 (10 mM), 0.0088 g NaCl (150 mM), 1 mL 500 mM EDTA (500 mM) made to a total volume of 1 mL using HPLC grade ddH_2O. This buffer was prepared fresh and stored short-term on ice.

Elution buffer I

50 µL 1 M Tris pH 7.5 (50 mM), 0.12 g ultra-pure Urea (2 M), 10 µL 100 mM DTT (1 mM) and 5 µL 1 µg/µL trypsin protease, MS grade (5 µg/µL) made to a total volume of 1 mL using HPLC grade ddH_2O. This buffer was prepared fresh and stored short-term at room temperature.

Elution buffer II

50 µL 1 M Tris pH 7.5 (50 mM), 0.12 g ultra-pure Urea (2 M) and 50 µL 100 mM iodoacetamide (5 mM) made to a total volume of 1 mL using HPLC grade ddH_2O. This buffer was prepared fresh and short-term at room temperature protected from light.

OMIX C18 tip conditioning solution

For mass spectrometry sample clean up Bond Elut OMIX C18 tips (Aligent) were used and required certain buffers. 500 µL HPLC grade acetonitrile (ACN) (50 %) and 500 µL HPLC grade ddH_2O (50 %) was made for immediate use.

OMIX C18 tip wash solution

1 µL TFA (0.1 %) was added to 999 µL HPLC grade ddH_2O made for immediate use.

OMIX C18 tip elution solution

1 µL formic acid (0.1 %), 500 µL HPLC grade ACN (50 %) and 499 µL HPLC grade ddH_2O (49.9 %) made for immediate use.

Q-Extractive (QE) loading buffer

1 mL TFA (0.1 %) and 30 mL HPLC grade ACN (3 %) was added to HPLC grade ddH_2O to a final volume of 1 L. This buffer was stored at room temperature.

MS grade decontamination solution

500 µL acetic acid (0.1 %) and 50 mL isopropanol (10 %) was prepared in ddH_2O to a final volume of 500 mL. This buffer was stored at room temperature.

2.1.7 Treatment compounds.

Compound	Mechanism of action	Diluent	Supplier
Alisertib	Aurora A inhibitor	DMSO	Selleckchem
Carboplatin	Forms inter- and intra-DNA adducts	H_2O	Sigma-Aldrich
Hydrogen peroxide (H_2O_2)	Induces oxidative damage	H_2O	EMD Millipore Corp
Nocodazole	Inhibits microtubule polymerisation	DMSO	Sigma-Aldrich
Okadaic acid (OA)	PP1/PP2A inhibitor	DMSO	Sigma-Aldrich
Pyocyanin	Superoxide radical inducer	DMF	Sigma-Aldrich
Sodium selenite	Inorganic source of selenium, to enhance transcription and activity of antioxidant selenoenzymes	H_2O	Sigma-Aldrich
Temozolomide (TMZ)	Methylates DNA bases	DMSO	Sigma-Aldrich

2.1.8 Irradiation.

Cells were irradiated in a 3.8 L irradiation canister inserted into the CIB/IBL 437 CS-137 irradiator. Irradiation delivery was dependent on the experiment. Direct irradiation was performed with cells plated prior to treatment in 10 cm plastic culture plates or 6/24 well plates. Alternatively, cells plated post-treatment were administered with irradiation in 15 mL falcon tubes.

2.1.9 Short interfering ribonucleic acid (siRNA).

All siRNAs were made to a stock concentration of 20 μM with the manufacture recommended buffer and stored at -20 ºC. 1x siMAX universal buffer was generated by the dilution of 5x siMAX universal buffer (1 mL) in nuclease-free water (4 mL).

siRNA duplexes	Sequence (5'-3')	Resuspension buffer	Supplier (cat number)
siGENOME Non-targeting control pool 1	UAGCGACUAAACACAUCAA, UAAGGCUAUGAAGAGAUAC, AUGUAUUGGCCUGUAUUAG, AUGAACGUGAAUUGCUCAA	1x siRNA buffer	Horizon (D-001206-13)
Low GC content siControl	UAAUGUAUUGGAACGCAUA	1x siMAX universal buffer	Eurofins Genomics
siBubR1	CAGATTTAGCACATTTACTAT	Nuclease-free water	Qiagen (SI00060501 7)
siMDC1-1	AAUCCUGAGACCUCCUAAGG UUU	1x siMAX universal buffer	Eurofins Genomics
siMDC1-2	GUUGUAACUGAAAUCCAGC	1x siMAX universal buffer	Eurofins Genomics
siSOD1 smart pool	Made of the 4-individual siRNA (siSOD1-5-8)	1x siRNA buffer	Dharmacon (M-008364-01)
siSOD1-5	UCGUUUGGCUUGUGGUGUA	1x siRNA buffer	Dharmacon (D-008364-05)
siSOD1-6	ACAAAGAUGGUGUGGCCGA	1x siRNA buffer	Dharmacon (D-008364-06)
siSOD1-7	GUGCAGGGCAUCAUCAAUU	1x siRNA buffer	Dharmacon (D-008364-07)
siSOD1-8	UUAAUCCUCUAUCCAGAAA	1x siRNA buffer	Dharmacon (D-008364-08)
siSOD1-Q1	CACTTATTATGAGGCTATTAA	Nuclease-free water	Qiagen (SI00009947)

siRNA duplexes (continued)	Sequence (5'-3')	Resuspension buffer	Supplier (cat number)
siSOD1-Q2	AACCCTGTATGGCACTTATTA	Nuclease-free water	Qiagen (SI00009954)
siSOD1-Q3	CTGTAGTGAGAAACTGATTTA	Nuclease-free water	Qiagen (SI00009968)
siSOD1-Q4	CAGAATTTCTTTGTCATTCAA	Nuclease-free water	Qiagen (SI00009968)
siSOD1-Q5	ATGGCACTTATTATGAGGCTA	Nuclease-free water	Qiagen (SI02623474)
siSOD1-Q11	ATGGGTATTAAACTTGTCAGA	Nuclease-free water	Qiagen (SI04380222)
siUPF1 smart pool	Made of the 4-individual siRNA (siUPF1-1-4)	1x siRNA buffer	Dharmacon (M-011763-01)
siUPF1-1	GCUCCUACCUGGUGCAGUA	1x siRNA buffer	Dharmacon (D-011763-01)
siUPF1-2	UCAAGGUCCCUGAUAAUUA	1x siRNA buffer	Dharmacon (D-011763-02)
siUPF1-3	GGAAGUCGACCUCCUUUGA	1x siRNA buffer	Dharmacon (D-011763-03)
siUPF1-4	CAAGAUAACAUCACUGUCA	1x siRNA buffer	Dharmacon (D-011763-04)

siSOD1-Q refers to the Qiagen siRNAs which target the 3'untranslated region (UTR) of SOD1.

2.1.10 Antibodies.

2.1.10.1 Primary antibodies.

Primary Antibody	Host Animal	Application and Dilution	Supplier (cat number)
Bub3	Rabbit	WB (1:1000)	Cell Signalling (3049S)
Bub3 E-7	Mouse	WB (1:1000)	Santa Cruz (sc-376506)
BubR1	Mouse	WB (1:1000), IF (1:500), IP	Abcam (ab54894)
BubR1 (SBR1.1)	Sheep	IP	A gift from Professor Stephen Taylor (University of Manchester)
Cdc20	Rabbit	WB (1:1000)	Cell Signalling
Cdc20	Rabbit	WB (1:1000)	Abcam

Primary Antibody (continued)	Host Animal	Application and Dilution	Supplier (cat number)
CENPB	Rabbit	IF (1:500)	Santa Cruz
Flag	Mouse	IP	Sigma
Glutathione Peroxidase 1	Rabbit	WB (1:1000)	Novusbio (NBP1-33620)
Mad2	Rabbit	WB (1:2000)	Abcam (ab70385)
MDC1	Rabbit	WB (1:500), IP	Bethyl (A300-51A)
MDC1	Mouse	WB (1:1000)	Sigma (M2444)
Myc-Tag	Mouse	WB (1:1000), IP, IF (1:100)	Cell Signalling (2276S, 9B11)
Pericentrin	Rabbit	IF (1:1000)	Abcam (ab44448)
Phosphorylated H2AX (γH2AX) serine 139	Mouse	IF (1:100)	Santa Cruz (sc-517348)
Phosphorylated Histone 3 (pH3) serine 10	Rabbit	FACs (1:100)	EMD Millipore (3018868)
PP2A C subunit (clone 1D6)	Mouse	WB (1:1000), IP	Sigma-Aldrich (05-421)
RAD51	Rabbit	IF (1:100)	Abcam (ab63801)
Securin	Rabbit	WB (1:1000)	Abcam (ab79546)
β -Actin C-4	Mouse	WB (1:5000)	Santa Cruz (sc-47778)
β -Tubulin	Mouse	WB (1:5000), IF (1:100)	Sigma (T4026)
Superoxide dismutase 1	Rabbit	WB (1:1000), IF (1:100)	Abcam (ab13498)
Superoxide dismutase 1	Rabbit	WB (1:1000)	Cell Signalling (2770S)
UPF1	Rabbit	WB (1:500)	Proteintech (23379-1-AP)

Western blotting (WB), Immunofluorescence (IF), Immunoprecipitation (IP) and fluorescence-activated cell sorting (FACs).

2.1.10.2 Secondary antibodies.

Antibody	Host Animal	Application	Supplier (cat number)
Alexa Fluor™ 488 goat anti-mouse IgG	Goat	IF (1:200)	Invitrogen (A11017)
Alexa Fluor™ 594 goat anti-rabbit IgG	Goat	IF (1:200)	Invitrogen (A11012)
Goat Anti-Mouse horse radish peroxidase (HRP)	Goat	WB (1:5000)	Invitrogen (A16078)
Goat pAb anti-Rabbit IgG FITC	Goat	FACs (1:100)	Abcam (ab6717)
Polyclonal swine Anti-Rabbit Immunoglobulin HRP	Swine	WB (1:5000)	Dako (P0399)

2.1.11 RT-PCR probes.

All probes were labelled with a FAM dye.

Gene target	Supplier (cat number)
Bub3	Thermo Fisher Scientific (Hs00945687)
BubR1	Thermo Fisher Scientific (Hs01084828)
Cdc20	Thermo Fisher Scientific (Hs00426680)
Glyceraldehyde 3-phosphate dehydrogenase (GAPDH)	Thermo Fisher Scientific (Hs02786624)
Mad2	Thermo Fisher Scientific (Hs01554513)

2.1.12 Primers.

Name	Sequence (5'-3')	Melting Temperature (Tm °C)	Supplier
CMV forward	CGCAAATGGGCGGTAGGCGTG	65.7	Eurofins Genomics
SOD1 G85R mutant	Forward: GGGCGACCTGAGAAATGTGACCG Reverse: ACGTGCCGTTCCTCGTCC	74.5 68.8	Sigma-Aldrich
SOD1 G93A mutant	Forward: TGATAAGGACGCCGTCGCCGACG Reverse: GCGGTCACATTTCCCAGG	78.9 66.7	Sigma-Aldrich
SOD1 optimised	Forward: ATAGACTACAGCGATCGCCATGGCCACAAA Reverse: TATAAATCTAGACGCGTCTGGGCGATTCCA	77.6 75.0	Sigma-Aldrich
SOD1 S60A mutant	Forward: CGGATGTACCGCTGCCGGCCCCC Reverse: GCGGTGTTGTCGCCGAAC	83.5 70.4	Sigma-Aldrich
SOD1 S99A mutant	Forward: CGCCGACGTGGCTATCGAGGACA Reverse: ACGCCGTCCTTATCAGCG	77.6 66.3	Sigma-Aldrich

The SOD1 mutant primers are non-complementary and were designed using the NEBaseChanger for site-directed mutagenesis (SDM).

2.1.13 Plasmids.

Protein	Protein Tag	Plasmid	Antibiotic resistance	Supplier (cat number)
BubR1	Myc	pCDNA3	Ampicillin	A kind gift from Dr Samuel Sidi (Icahn School of Medicine at Mount Sinai)
CMV	Myc	pDEST	Ampicillin	A kind gift from Dr Spencer Collis (University of Sheffield)
OGG1	Myc	pCMV	Ampicillin	Addgene (18709) a gift from David Sidransky (Chatterjee *et al.*, 2006)
PP2A	Myc-DDK	pCMV6	Kanamycin	Origene (NM_002715, RC201334)
SOD1	Myc-DDK	pCMV6	Kanamycin	Origene (NM_000454, RC200725)
SOD1 optimised	-	pEX-A128	Ampicillin	Custom made by Eurofins

2.2 Methods.

2.2.1 Mammalian tissue culture.

2.2.1.1 Culture conditions and passaging.

Cell work was carried out in a sterile environment using a class II A/B3 biological safety cabinet. All cells lines were cultured in DMEM supplemented with 10 % FCS and incubated at 37 °C with 5 % CO_2. The Flp-In T-REx cell lines were grown within antibiotic selection with Hygromycin B (200 µg/µL) and Blasticidin S HCl (4 µg/µL) added to each flask. All cell lines were cultured in T75 flasks with 15 mL total media volume.

Passaging occurred once the cells had achieved 60-80 % confluency, which involved the removal of the media, duplicate washes in sterile PBS and the short incubation (5 minutes) with trypsin-EDTA (2 mL) at 37 °C for cell detachment. Pre-warmed media (8 mL) was then added to the detached cell solution which diluted the trypsin-EDTA, cells were then seeded into new flasks with fresh culture medium and selection reagents (if appropriate).

In preparation for plating, the diluted trypsin-EDTA cell solution was centrifuged at 1000 revolutions per minute (RPM) for 3 minutes in the benchtop centrifuge. The cell pellet

was resuspended in fresh media (10 mL) and cells were counted on a haemocytometer. The desired number of cells were taken to be plated for experimental purposes.

2.2.1.2 Cell freezing and thawing.

Similar to plating preparation, the diluted trypsin-EDTA cell solution was centrifuged at 1000 RPM for 3 minutes and the cell pellet was resuspended in fresh media (2 mL) with 10 % DMSO. The cell suspension was divided into each cryovial (1 mL) and stored in a Mr. Frosty^{TM} freezing container at -80 °C. For long term storage (> 1 year) cell stocks were transferred to liquid nitrogen.

Frozen cell stocks were defrosted at 37 °C in a water bath. The cell suspension was added to 9 mL fresh, pre-warmed culture medium and centrifuged at 1000 RPM for 3 minutes. The pellet was resuspended in media (10 mL) and transferred to a T25 culture flask. Cells were grown at 37 °C with 5 % CO_2 and passaged 3 times in T75 flasks before experimental work was performed.

2.2.1.3 Mycoplasma testing.

The Geneflow EZ PCR mycoplasma detection kit was used for mycoplasma contamination testing, which was routinely conducted in all cell lines by departmental technicians.

2.2.2 Bacterial culture and cloning.

2.2.2.1 Chemically competent bacteria stocks.

Two strains of chemically competent Escherichia coli (*E.coli*), DB3.1 (gifted from Dr Spencer Collis, Department of Oncology and Metabolism, University of Sheffield) and DH5α cells (Invitrogen) were grown to produce a large cell stock for cloning experiments, all conducted in the absence of antibiotic selection. A loop of the *E.coli* strain was grown overnight at 37 °C on an agar plate. Then a single colony was selected and mixed into a universal tube containing 5 mL LB broth, cells were grown overnight in a shaker incubator at 37 °C. 500 µL of the resulting culture was added to 400 mL LB broth in a conical flask, the culture was grown in a shaker incubator at 37 °C to promote exponential growth until the optical density (OD) reached 0.5-0.6 nm

measured at 595 nm wavelength using the Thermo Scientific MultiscanTM FC. The culture was pelleted and resuspended in 25 mL cold bacterial TBS, aliquoted and flash frozen. The cells were stored at -80 °C.

2.2.2.2 Transformation of plasmid DNA.

All mammalian expression vectors **(2.1.13)** were transformed into either strain of chemically competent *E.coli* cells. 5 µL plasmid DNA was added to 75 µL ddH_2O, 20 µL 5x KCM and 150 µL bacterial cells. This solution was mixed, incubated on ice for 20 minutes, followed by a 10-minute incubation at room temperature. Then 1 mL LB broth was added to the mixture and a further incubation at 37 °C for 1 hour in a shaker incubator. Bacterial cells were microcentrifuged at 4500 RPM for 5 minutes to generate a loose pellet, where the majority of the supernatant was discarded, and the pellet resuspended in the remaining solution. The bacterial cells were streaked onto agar plates with appropriate antibiotic selection (at the suppliers recommended concentration) and grown overnight at 37 °C. Multiple colonies were selected and grown in universal tubes containing 5 mL LB broth under antibiotic selection in a shaker incubator at 37 °C overnight. The plasmid DNA was extracted and purified using the Qiagen spin miniprep kit following the manufacturer instructions. The concentration of DNA (ng/µL) was quantified using the nanodrop spectrophotometer (ND-1000, Thermo Fisher) with the DNA-50 nucleic acid setting on the ND-1000 software.

2.2.2.3 Subcloning of optimised SOD1.

2.2.2.3.1 Optimised SOD1 sequence.

A codon optimised SOD1 wild-type sequence was generated using the GenSmart™ codon optimisation tool by GenScript. This manipulated the sequence complementary for the siRNA, resulting in a siRNA resistant SOD1 protein whilst ensuring function. Eurofins synthesised the optimised *SOD1* gene sequence, in addition to cloning sites and additional sequence, **(Figure 2.1)** and was inserted into a pEX-A128 vector **(2.1.13)**. The plasmid was resuspended in TE buffer to generate a 100 ng/µL stock concentration.

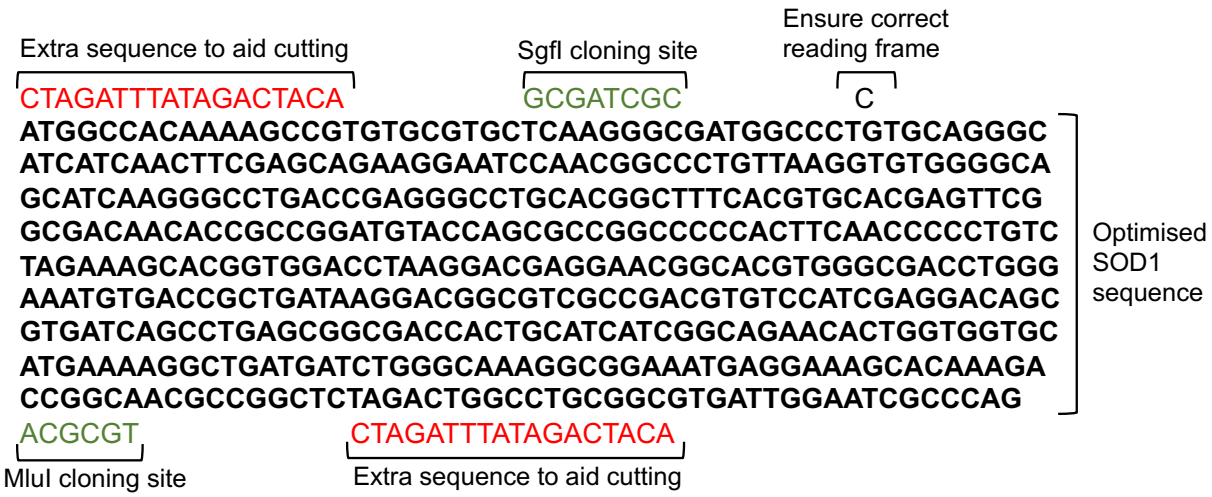

Figure 2.1: The annotated sequence of optimised SOD1.

The complete sequence was synthesised for the optimised SOD1 mammalian expression plasmid, featuring an additional sequence to aid in restriction site cutting, the desired restriction sites on either side of the SOD1 sequence.

2.2.2.3.2 Optimised SOD1 gene strand amplification.

The optimised *SOD1* gene was subcloned into the pCMV6-Myc-DDK tagged expression vector **(2.1.13)**, after extracting the original *SOD1* gene. This was conducted to insert the gene of interest into the desired vector and tag the gene with Myc, to distinguish it from endogenous SOD1 protein.

Optimised SOD1 was amplified in a KOD hot start polymerase reaction, according to manufacturer instructions (Novagen). The reaction set up involved; 5 µL 10x KOD reaction buffer (1x), 3 µL 25 mM $MgSO_4$ (1.5 mM), 5 µL 2mM each deoxyribonucleotides (dNTPs) mix (200 µM each), 1.5 µL 10 µM forward and reverse optimised SOD1 primers (0.3 µM) **(2.1.12)**, 50 ng DNA, 1 µL KOD polymerase (1 Unit (U)) and sterile H_2O to a total volume 50 µL. The reaction mixture was gently mixed via pipetting and microcentrifuged briefly. Cycling conditions were selected for genes 500-1000 bp (optimised SOD1 513 bp) and the lowest primer melting temperature (Tm °C) was used for the annealing temperature.

Step	Temperature and time (500-1000 bp)
1. Polymerase activation	95 °C for 2 minutes
2. Denature	95 °C for 20 seconds
3. Annealing	75 °C for 10 seconds
4. Extension	70 °C for 7.7 seconds (15 seconds/ Kbp)
25 cycles of steps 2-4	
5. Final extension	70 °C for 5 minutes
6. End	4 °C for forever

Table 2.1: SOD1 gene amplification cycling conditions.

2.2.2.3.3 PCR product clean up and visualisation.

The majority of PCR product was purified (2 µL PCR product kept for DNA gel) using the Monarch PCR & DNA clean up kit (New England Biolabs) following manufacturer instructions, and the concentration (ng/µL) of the resulting product was quantified using the nanodrop spectrophotometer. The amplification and purification of the optimised *SOD1* gene strand was visualised on an agarose gel following the PCR reaction. A 1 % agarose gel was prepared by dissolving 2 g agarose gel in 200 mL 1x TAE buffer with heat and allowed to cool sufficiently before the addition of 4 µL 10 mg/mL ethidium bromide (200 µg/mL). The gel solution was mixed and allowed to set in the gel insert apparatus with the comb inserted. Once set, the gel apparatus was placed in the electrophoresis tank, immersed in 1x TAE buffer and the comb removed. 2 µL of PCR product (pre-clean up and post-clean up) were mixed with 0.5 µL 5x DNA loading buffer (1x) each and the total volumes were loaded into the gel for comparison, in addition to 5 µL Hyperladder 1 Kbp. A current of 100 V was used for 15-30 minutes and the DNA bands were visualised on the gel doc XR imaging system using ultraviolet (UV).

2.2.2.3.4 Restriction digest.

To insert the optimised *SOD1* gene into the desired pCMV6-Myc-DDK expression vector, both required restriction digestion to generate complementary ligation sites. The restriction enzymes (SgfI and MluI) used different buffers (C and D respectively), but MluI was 50-75 % reactive in buffer C, so this was selected for the reaction. A 5-fold excess of the restriction enzymes to DNA concentration was added to the reaction

following manufacturer instructions (Promega). The restriction digest reaction mixture was composed of; 2 µL 10x reaction buffer C (1x), 0.2 µL 10 µg/µL acetylated BSA (0.1 µg/µL), 500 ng DNA (plasmid or optimised SOD1), 0.25 µL of 10 U/µL restriction enzyme (2.5 U) and sterile H_2O to a total volume 20 µL. The reaction mixture was mixed gently and incubated at 37 °C for 4 hours, followed by enzyme inactivation at 65 °C for 20 minutes in the S1000 thermocycler. 2 µL plasmid restriction digest (approximately 50 ng) and the equivalent plasmid DNA concentration the undigested plasmid (50 ng) was visualised on a 1 % agarose gel as previously described **2.2.2.3.3**, to ensure the plasmid was successfully digested. The concentration (ng/µL) of both digestion products were quantified using the nanodrop spectrophotometer.

2.2.2.3.5 Ligation reaction.

The vector: insert ratio was amended from the manufacturer's instructions (New England Biolabs) as the digested plasmid product was not purified by gel extraction (insufficient yield), so the desired insert (digested optimised SOD1) needed to outcompete the previous insert (SOD1) for the digested pCMV6 Myc-DDK tagged vector during the ligation reaction. The ligation reaction mixture contained; 2 µL 10x ligase reaction buffer (1x), 50 ng vector, 10 ng insert, 1 µL T4 DNA ligase and sterile H_2O to a total volume of 20 µL. The reaction mixture was mixed gently, microcentrifuged briefly and incubated at room temperature for 10 minutes. The enzyme was inactivated at 65 °C for 10 minutes and chilled on ice before transformation. The ligation product was transformed into DH5α chemically competent *E.coli* cells, grown under kanamycin selection (50 µg/µL) as described in section **2.2.2.2**.

2.2.2.3.6 Sequencing.

The extracted plasmid DNA from the bacterial culture using the Qiagen spin miniprep kit following the manufacturer's instructions and the concentration (ng/µL) quantified using the nanodrop spectrophotometer. Sequencing of samples were conducted by Eurofins genomics using the Mix2Seq kit, which required 1.5 µg DNA in sterile H_2O to a total volume of 15 µL. Then 1 µL of a suitable primer (10 µM) was added to each sample, in the case of all sequencing conducted in this thesis the CMV forward primer was used.

2.2.2.4 Glycerol bacterial stocks.

Before DNA extraction, 500 µL bacterial culture containing the plasmids used in this thesis **(2.1.13)** were mixed with 500 µL 50 % sterile glycerol and stored at – 80 °C. To utilise this stock, a small amount of the frozen bacterial glycerol solution was collected using a loop and streaked on an agar plate containing the appropriate antibiotic. Colonies were selected, grown in LB broth containing antibiotic selection and the DNA extracted using Qiagen spin miniprep kit following the manufacturer's instructions and the concentration (ng/µL) quantified using the nanodrop spectrophotometer.

2.2.3 Gene manipulation and expression assays.

2.2.3.1 Site-directed mutagenesis.

The pCMV6 Myc-DDK tagged optimised SOD1 plasmid (wildtype (WT)) was used to create a range of siRNA resistant SOD1 mutants (G93A, G85R, S99A and S60,99A). This was conducted using both the QuickChange II site-directed mutagenesis (SDM) kit and the KOD hot start DNA polymerase kit.

The SDM reaction mixture was adapted from the KOD hot start DNA polymerase protocol and was composed of; 5 µL 10x KOD reaction buffer (1x), 5 µL 25 mM $MgSO_4$ (2.5 mM), 2 µL 2mM each dNTPs mix (80 µM each), 2 µL 2.5 µM forward and reverse mutant SOD1 primers (0.1 µM) **(2.1.12)**, 100 ng DNA, 0.5 µL KOD polymerase (1 Unit (U)) and sterile H_2O to a total volume 50 µL. The reaction mixture was gently mixed via pipetting and microcentrifuged briefly. The cycling conditions were as instructed in the QuickChange II SDM kit and configured for the SOD1 size (462 bp).

Step	Temperature and time
1. Polymerase activation	95 °C for 1 minute
2. Denature	95 °C for 50 seconds
3. Annealing	60 °C for 50 seconds
4. Extension	68 °C for 8 minutes (1 minute/ Kbp)
18 cycles of steps 2-4	
5. Final extension	68 °C for 7 minutes
6. End	3 °C for forever

Table 2.2: SDM cycling conditions.

3 µL SDM products were visualised on a 1 % agarose gel (as described in **2.2.2.3.3**) to ensure amplification. Then 1 µL 10 U/µL Dpn I restriction enzyme (0.21 U) was added to the remaining SDM product to digest the parental supercoiled dsDNA (non-mutated). The solution was mixed gently and microcentrifuged for 1 minute and incubated at 37 °C for 1 hour in the thermocycler. 5 µL of each mutant sample was transformed into DH5α chemically competent *E.coli* cells, grown under kanamycin selection (50 µg/µL), as described in section **2.2.2.2**. Colonies were selected and cultured, then plasmid DNA was extracted using the Qiagen spin miniprep kit following the manufacturer's instructions and the concentration (ng/µL) quantified using the nanodrop spectrophotometer. 1.5 µg of each sample was sequenced by Eurofins genomics with the Mix2Seq kit (as described in **2.2.2.3.6**).

For the S60,99A double mutant, the S99A was generated first and the process repeated with the S60A primers on the S99A plasmid, rather than the WT plasmid.

2.2.3.2 Plasmid DNA transfection.

$1x10^5$ cells were seeded into a 6 well plate and left to adhere overnight. 1 µg plasmid DNA was diluted in 200 µL warm serum-free DMEM media (SFM) per well. In a separate tube, 5 µL lipofectamine 2000 (Invitrogen) was diluted in 200 µL SFM per well. These mixtures were incubated for 5 minutes, then mixed in equal volumes and incubated for a further 20 minutes. 400 µL were added to each well dropwise. Transfected cells were incubated for 24-72 hours before harvesting.

2.2.3.3 siRNA transfection.

siRNA (reverse) transfection was performed at the same time as plating the cells. For each transfection reaction 5 µL siRNA (20 µM stock) was added to 245 µL SFM and 3 µL DharmaFECT 1 transfection reagent was added to 247 µL SFM. These solutions were incubated for 5 minutes. After incubation, these solutions were mixed in equal volumes and incubated for a further 20 minutes. 500 µL of the final transfection solution was added to the well. $1.5x10^5$ cells were plated per well in a 6-well plate with a total volume of 2 mL (50 nM total siRNA concentration). siGENOME non-targeting control pool (Dharmacon) or low GC content siControl (Eurofins) siRNAs were used in parallel

as a negative control. These plates were typically treated 48 hours post-transfection and harvested after 72 hours or shortly before at treatment termination.

Forward transfection involved cells plated before transfection. $1.5x10^5$ cells were plated per well in a 6-well plate and left to adhere overnight. The siRNA was prepared the same as reverse transfection, added dropwise to the cells to a final well volume of 2 mL. The same negative controls were used as reverse transfection. These plates were treated at 48 hours and harvested after 72 hours post-transfection.

2.2.3.4 Double transfection of siRNA and DNA with Dharmafect duo.

$1x10^5$ cells were seeded into a 6 well plate and left to adhere overnight. DNA concentration was dependent on the plasmid, for Myc-SOD1 WT, Myc-SOD1 mutants and the CMV-Myc (empty vector control) 150 ng were used and for Myc-PP2A and Myc-OGG1 1 µg were used. To the DNA, 5 µL siRNA (20 µM stock) was added and 200 µL SFM (calculation for an individual well). In a separate tube, 5 µL Dharmafect duo transfection reagent was added to 200 µL SFM (calculation for an individual well). Each reaction tube was incubated for 5 minutes, then mixed in equal volumes and incubated for a further 20 minutes at room temperature. 400 µL of the DNA-siRNA-Dharmafect duo solution was added to each well. Cells were incubated for 48-72 hours post-transfection depending on experimental design.

2.2.3.5 Double transfection of 3' UTR siRNA and plasmid DNA.

$1\text{-}2x10^5$ cells were plated per well in a 6-well plate and incubated overnight. Forward transfection using a 3' UTR siRNA for SOD1 was conducted as described **2.2.3.3**. A coding region SOD1 siRNA was also included as a positive control for SOD1 knockdown. 48 hours post-transfection 250 ng unmodified Myc-SOD1 expression vector (Origene) was transfected into the cells with lipofectamine 2000 or 250 ng CMV-Myc empty vector as a negative control **(2.2.3.2)**. 24 hours post-DNA transfection and 72 hours post-siRNA transfection the cells were harvested.

2.2.4 Protein assays.

2.2.4.1 Cell harvesting for SDS-PAGE.

$1.5x10^5$ cells were plated in 6 well plates and harvesting times were dependant on the treatments administered and experimental type. All siRNA transfection experiments were harvested after 72 hours post-transfection or shortly before with the termination of treatment. Other assays involved cells to be left to adhere overnight and then treated for the allotted time before harvesting.

The media for each sample was collected into a 15 mL falcon tube on ice. Wells were washed in duplicate with cold PBS (1 mL), the wash was collected into the corresponding tubes. 1 mL trypsin-EDTA was added to the wells and incubated for 5 minutes at 37 °C for cell detachment. Using the media-PBS solution already collected cells were washed down the wells and collected into the corresponding tubes. The cell solution was centrifuged at 1000 RPM for 3 minutes, pellets were resuspended in 1 mL PBS and transferred to 2 mL Eppendorf tubes. Samples were then centrifuged in a microcentrifuge at 13,000 RPM (supplied by Eppendorf) for 3 minutes and washed in PBS a further time. Pellets were placed on ice for lysis.

2.2.4.2 Cell harvesting for immunoprecipitation (IP).

$2.5x10^5$-$1x10^6$ cells were seeded into multiple 10 cm culture dishes per condition, quantity and cell number were dependant on treatment times and cell line. All plates were allowed to adhere overnight before treatment administration. All experiments included bead-only or FLAG antibody negative control conditions which were untreated.

Before harvesting, the plates were chilled at 4 °C for 15 minutes. The media was collected into corresponding 50 mL falcon tubes (on ice), then the cells were removed from the plates via a cell scraper and pipetted into the correct tubes. The cell solutions were centrifuged at 1000 RPM for 3 minutes, pellets resuspended in cold PBS (1 mL) and transferred to a 2 mL Eppendorf tube. The samples were then microcentrifuged at 13,000 RPM for 3 minutes and washed again in PBS. Pellets were placed on ice for lysis.

2.2.4.3 Lysate preparation.

Lysis buffer was generated through the addition of phosSTOP inhibitor tablet and protease inhibitor cocktail tablet to 1x RIPA lysis buffer. For the SDS-PAGE samples from 6 well plates, 1 of each tablet was dissolved individually in 1 mL ddH_2O (10x stock solution) and 100 µL of each were added to 1 mL 1x RIPA buffer on ice (1x working solution). The remaining tablet solution was stored at -20 °C for future use. Pellets were lysed in 100 µL lysis buffer for 20 minutes on ice.

The resultant pellets for IP were resuspended in 1 mL cold lysis buffer, produced from 10 mL 1x RIPA lysis buffer containing 1 whole tablet of the protease inhibitor cocktail and phosSTOP inhibitor (1x working solutions). The samples were incubated on ice for 30 minutes.

After the incubation samples were then microcentrifuged at 4 °C for 15 minutes at 13,000 RPM. The supernatants composed of soluble protein were then transferred into a new Eppendorf tube for quantification.

2.2.4.4 Protein quantification.

The Bradford Assay was conducted to determine the concentration of the protein in each sample. A protein standard curve was produced from a 1 mg/mL BSA stock solution at a range of known concentrations (0-0.1 mg/mL). 40 µL of each standard was added in triplicate to a 96 well plate.

Concentration (mg/mL)	1 mg/mL BSA (mL)	ddH_2O (mL)	Protein assay dye reagent (mL)
0	0	1	0.2
0.02	1 mL of 0.1 concentration	4	0.2
0.03	1 mL of 0.1 concentration	2.33	0.2
0.04	0.5	12	0.2
0.05	0.5	9.5	0.2
0.06	0.5	7.83	0.2
0.08	0.5	5.75	0.2
0.1	0.5	4.5	0.2

Table 2.3: Volumes for a BSA standard curve of known protein concentrations.

The protein samples were diluted 1:100 (samples from 6 well plates) or 1:400 (samples for IP) and 40 µL was added in triplicate into a 96 well plate. 200 µL of protein assay dye reagent (Bio-Rad) was also added to each well. The OD for all samples and standards were measured at 595 nm wavelength using the Multiscan^{TM} FC microplate photometer.

The BSA known protein concentrations were plotted against the average OD of each standard, to generate the standard curve where $y = mx+c$ **(Figure 2.2)**. The average OD of each sample was inserted into the equation and the dilution factor was accounted for, resulting in the protein concentration of each sample.

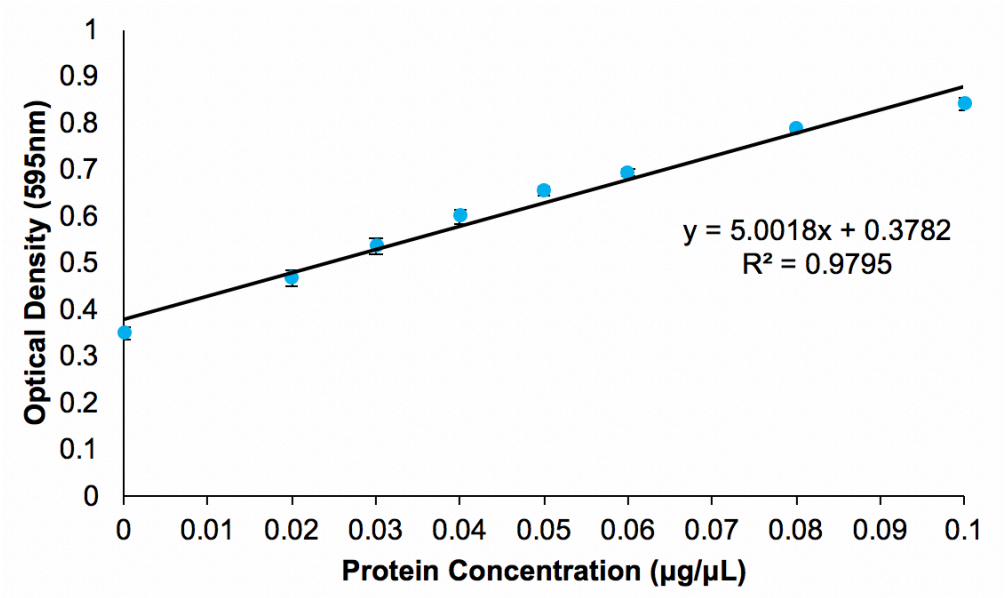

Figure 2.2: Protein Standard Curve.

One example of the standard curve generated using the BSA standards, to determine the protein concentration in the samples.

For SDS-PAGE samples, the maximum amount of protein for the total lysis volume was calculated for the sample with the lowest protein concentration. All other samples were made to this concentration and to an equal volume with excess 1x RIPA lysis buffer. 5x protein SDS-PAGE loading dye was diluted 1:4 in the final protein sample, then samples were heated at 70 °C for 10 minutes. All samples were used immediately or stored at -20 °C until use.

For IP 200 µg of the whole cell lysate of each sample was calculated to produce an input sample. All inputs were made to an equal volume with 1x RIPA lysis buffer, 5x protein SDS-PAGE loading dye (1:4 dilution) was added and heated at 70 °C for 10 minutes and stored at -20 °C until use. The remaining lysate was used for the IP, like SDS-PAGE samples, the maximum amount of protein was calculated for the sample with the lowest protein concentration, using the remaining volume of the whole cell lysate. This protein concentration was made uniform across all samples.

2.2.4.5 Immunoprecipitation.

20 µL Dynabead protein G (Invitrogen) were added to an Eppendorf tube for each sample. The preservative residue was removed using the DynaMag magnetised tube rack (Invitrogen) and the beads were washed twice with IP wash buffer (200 µL). The beads were incubated on a rotator (Stuart) with the antibody for the protein of interest at 5 µg/mL in 100 µL of wash buffer for 10 minutes at room temperature. A FLAG antibody or no antibody for bead-only conditions were included as negative controls. The lysates calculated for the samples during protein quantification were then added to the beads achieving a final volume of 1 mL with 1x RIPA lysis buffer. The beads were incubated with the whole cell lysates for 1 hour at 4 °C on a rotator. The lysates were then discarded, and excess or non-specific proteins were washed multiple times from the beads with wash buffer (200 µL). The buffer was removed, and the beads were resuspended in 44 µL 1x protein SDS-PAGE loading dye (5x protein SDS-PAGE loading dye diluted 1:4 with lysis buffer). The samples were heated at 90 °C for 10 minutes with mixing at 2-minute intervals. The dye-eluted protein solution was separated from the beads and transferred into a new Eppendorf tube. Samples were used immediately or stored at -20 °C until use.

2.2.4.6 SDS-PAGE and western blotting.

Polyacrylamide gels were prepared at differing percentages for the resolving gel with a 5 % stacking gel **(Table 2.4)**. The percentage was dependant on the desired proteins molecular weight. Alternatively, the 4-12 % precast gels (Expedeon) were for IP samples.

Reagents	Resolving gel (20 mL)		Stacking gel (10 mL)
	6 %	15 %	5 %
	Volume (mL)		Volume (mL)
ddH$_2$O	10.6	4.6	6.8
ProtoGel	4.0	10.0	1.7
Tris	5.0 (1.5 M, pH 8.8)	5.0 (1.5 M, pH 8.8)	1.25 (1 M, pH 6.8)
10 % SDS	0.2	0.2	0.1
10 % APS	0.2	0.2	0.1
TEMED	0.016	0.008	0.01

Table 2.4: The SDS-PAGE gel recipes.

For all gels, 6 µL of the Bio-Rad precision plus molecular weight marker ranging 10-250 kDa was loaded parallel to samples. For SDS-PAGE and IP input samples 10-30 µg protein were loaded into each lane. Whereas 20 µL of IP samples were loaded into the gels.

The 1x SDS running buffer was prepared for all hand cast gels and a 1x MOPS Run Blue running buffer (Expedeon) for the precast gels. With the appropriate running buffer and equipment, the proteins were separated at 120-180 V until the loading front completely descended through the gel. The protein was transferred onto a nitrocellulose membrane (GE Healthcare) between Whatmann paper with 1x transfer buffer at 4 °C for 2-3 hours at 100 V. The membrane was blocked in 5 % milk for 1 hour on a gyrorocker (Stuart), then incubated with the primary antibody in 5 % milk at 4 °C overnight with gentle rocking. After this incubation, the membrane was washed in 1x TSB-T five times for 5 minutes on the gyrorocker. The corresponding HRP-labelled secondary antibody was diluted 1:5000 in 5 % milk and incubated on the membrane for 1 hour at room temperature whilst gently rocked. After this incubation the membrane was washed five times for 5 minutes in 1x TSB-T on the gyrorocker. To activate the HRP reaction and visualise the protein, enhanced chemiluminescence (ECL) (Thermo Fisher Scientific) reagent was prepared in equal measures and dispersed evenly onto

the membrane for 1 minute. The Kuji medical X-ray film (Fujifilm) was exposed to the membrane in the darkroom. The signal was developed and fixed using the RG universal X-ray developer and RG universal X-ray fixer in the SRX 101A film processor (Konica).

2.2.4.6.1 Western blot quantification.

Where appropriate films with reasonable exposures were scanned and opened in FIJI Image J software to calculate band densitometry. The band density of a protein of interest was normalised against the band density of the control protein β-Tubulin or β-actin of the same sample. The relative intensity of the protein of interest was then compared between samples.

2.2.5 Phosphatase activity assays.

2.2.5.1 Protein tyrosine phosphatase activity assay.

2.2.5.1.1 Sample preparation and assay.

$1.5x10^5$ HeLa cells per well in a 6 well plate were reverse transfected with siControl and siSOD1-5 as described in methods section **2.2.3.2**. 72 hours post-transfection the desired treatment was administered.

The protein tyrosine phosphatase (PTP) activity assay (Abcam) was conducted according to the manufacturer instructions. Prior to sample harvesting, a sufficient amount of PTP assay buffer for each reaction was aliquoted, then DTT (100 mM stock) was diluted 1:50 in the buffer and stored on ice. Then samples were harvested via the removal of the media, the addition of 500 µL PTP-DTT assay buffer to each well, cells were removed using a cell scraper and collected in 2 mL Eppendorf tubes on ice. The cell solution was then sonicated (Vibra Cell, Sonics) on ice for 10 seconds at 70 % amplitude, incubated on ice for 5 minutes and centrifuged at 13,000 RPM for 15 minutes. The supernatant was collected and incubated on ice.

Each reaction (samples, background, negative (suramin) and positive control) was prepared as a master mix and 80 µL was added to each well in duplicate **(Table 2.5)**. Suramin required reconstitution with 110 µL ddH_2O to generate a 10 mM stock, this

was diluted to 2 mM in ddH_2O for the reaction and stored at -20 °C. The PTP positive control was also reconstituted with 110 µL ddH_2O and stored at -80 °C.

Component	Samples (µL)	Background (µL)	Negative control (µL)	Positive control (µL)
Sample	20	-	20 of control sample only	-
PTP positive control	-	-	-	10
Suramin (2 mM)	-	-	10	-
PTP-DTT assay buffer	60	80	50	70

Table 2.5: The composition of each reaction.

The plate was incubated in the dark for 10 minutes at room temperature. Then 500x PTP substrate stock solution was reconstituted in 44 µL ddH_2O and stored at -20 °C. A 5x PTP substrate solution was prepared from a 1:100 dilution of 500x PTP substrate stock solution in PTP-DTT assay buffer. 20 µL of the 5x PTP substrate solution was added to each well. The fluorescence was measured after 5 minutes at 360 nm using the Fluorescent SpectraMax M5e multi-mode microplate reader (Molecular Devices).

2.2.5.1.2 Analysis.

The average PTP activity was calculated from the duplicate wells and the percentage difference was calculated relative to the siControl untreated condition (100% activity). Analysis was conducted using Microsoft Excel software.

2.2.5.2 PP2A IP activity assay.

2.2.5.2.1 Sample preparation and IP.

$1.5x10^5$ HeLa cells per well in a 6 well plate were reverse transfected with siControl and siSOD1-5 as described in methods section **2.2.3.2**. 48 hours post-transfection each siRNA condition was replated at 50,000 cells per well in a 6 well plate per treatment condition. Cells were incubated overnight to adhere to the plates and then the desired treatment was administered.

The PP2A IP activity assay was conducted using the PP2A immunoprecipitation phosphatase assay kit (Merck) and the manufacturer's protocol was optimised. 10% w/v protease inhibitor cocktail was added to phosphatase assay lysis buffer to generate the working solution of phosphatase assay lysis buffer, which was made fresh for each assay. The media was discarded, and cells were removed from the plates using 100 µL of the lysis buffer and a cell scraper, then the solution was collected in 2 mL Eppendorf tubes on ice. The cell-lysis solution was then sonicated (Vibra Cell, Sonics) on ice for 10 seconds at 70 % amplitude and centrifuged at 13,000 RPM for 5 minutes. The supernatant composed of the soluble protein fraction was collected and incubated on ice.

The Dynabeads protein G were diluted in a 2:1 ratio with phosphatase buffer (from the kit). 10 µL of the bead mix was aliquoted into individual tubes for each sample and a blank (assay control sample). The beads were washed in 1x TBS using the DynaMag magnetised tube rack (Invitrogen). The PP2A subunit C antibody (Sigma-Aldrich) was diluted in a 1:50 ratio with phosphatase buffer. 34 µL of the antibody mixture was used to resuspend each tube of IP beads, then 100 µL of the cell lysate of each sample was added to the corresponding tubes. For the blank sample, the IP beads were resuspended in the antibody mixture and 100 µL phosphatase buffer. The beads were incubated with the cell lysates for 2 hours at 4 °C on a rotator. The supernatant was removed, and IP beads were washed in 100 µL 1x TBS three times. The beads for all samples were then resuspended in 100 µL phosphatase buffer, transferred into 1.5 mL Eppendorf tubes and the wash was removed. 10 µL threonine phosphopeptide (Merck) from a 1 mM stock and 3.3 µL phosphatase buffer were added to the beads and incubated at 30 °C for 10 minutes with mixing every minute. 6 µL eluted PP2A protein solution was transferred to a 96 well microtiter plate (½ volume flat bottom plate supplied in kit) in duplicate wells for each sample. Malachite green phosphate detection solution was composed of Malachite green additive diluted 1:100 in Malachite green solution A and 24 µL of the detection solution was added to each well (both supplied in kit). The absorbance was measured at 620 nm using the Fluorescent SpectraMax M5e multi-mode microplate reader (Molecular Devices).

2.2.5.2.2 Analysis.

The average PP2A activity was calculated from the duplicate wells and the percentage difference was calculated, relative to the siControl untreated condition (100% activity). Analysis was conducted using Microsoft Excel software.

2.2.6 Cell cycle analysis.

2.2.6.1 Sample harvesting.

Cells were seeded at $1x10^6$ cells in 10 cm culture dishes or $1.5x10^5$ cells per well of a 6 well plate and treated as specified. The media from each plate was collected into corresponding 15 mL falcon tubes (on ice). Each plate was washed with cold PBS and added to the media. 1 mL trypsin-EDTA was added to each plate and incubated for 5 minutes at 37 °C, detached cells were then washed down the plate and added into the corresponding tubes. The samples were centrifuged at 1000 RPM for 3 minutes, the resulting pellets were resuspended in cold PBS and centrifuged again with the same conditions. The PBS wash was discarded, and the pellets fixed via the addition of cold 70 % ethanol dropwise, whilst samples were vortexed (Scientific Industries). Samples were then stored at -20 °C for at least 24 hours before staining.

2.2.6.2 Phosphorylated serine 10 Histone 3 and PI co-staining technique.

The ethanol was removed via centrifugation at 1000 RPM for 3 minutes and each sample pellet was resuspended in cold PBS. The samples were centrifuged again to remove the PBS wash and cells were permeabilised on ice for 15 minutes in flow buffer 1 (500 µL). Flow buffer 1 was removed by centrifugation and the cell pellets were incubated with 100 µL phosphorylated Histone 3 (pH3) antibody (EMD Millipore) diluted 1:100 in flow buffer 1 for 1 hour and 30 minutes at room temperature. Flow buffer 2 (500 µL) was added to the samples and centrifuged at 1000 RPM for 3 minutes. The pellets were then resuspended in 100 µL goat pAb anti-rabbit IgG FITC secondary antibody, diluted 1:100 in flow buffer 1 and incubated for 30 minutes at room temperature in the dark. The samples were then washed in duplicate with 500 µL PBS. The cell pellets were resuspended in 5 µL RNAse A (2 mg/mL stock) and 400 µL PI (10 µg/µL stock solution in PBS) and incubated for at least 30 minutes at 4 °C protected from the dark. Samples were processed on the FACSCalibur (BD Sciences), to collect 10,000 events for each sample using the Cell Quest Pro software. PI only, no primary

antibody and no secondary antibody controls were included in each experiment to determine any non-specific staining.

2.2.6.3 Analysis.

Data were analysed using FlowJo software version 10. The FL3 (PI)-Area (FL3-A) was plotted against FL3 (PI)-Width (FL3-W) allowing for the isolation of the single cell population for analysis **(Figure 2.3A)**. This gated region was applied to the whole sample set. Each cell cycle phase was then determined either through plotting FL3 (PI)-Height (FL3-H) histogram **(Figure 2.3B)**, which provided the number of events for each phase or through plotting FL1-H (pH3 (ser 10) staining) against FL3-H **(Figure 2.3C)** which distinguished between G2 and mitotic cell populations. On either plot, the population of cells in G1 were represented as an increase in signal intensity at ~200 FL3-H with two copies of the chromosomes (2N or diploid cells) and the G2/Mitotic (M) proportion of cells were represented as an increase in signal intensity at ~400 FL3-H with four copies of the chromosomes (4N or tetraploid cells). The sub G1 proportion of cells were identified to the left of G1, S phase was defined as the signal between G1 and G2 and the polyploid (> 4N) cells were identified to the right of G2. The FL1-H plot separated the G2 and M populations via pH3 (ser 10) staining, as the mitotic cells were positive for the stain and were identified on the plot as a distinct signal ≥ 0.5 logs greater than the G2 population. The percentage of cells in each cell cycle phase were compared between samples, with a main focus on the mitotic cell population. The percentages of each cell population for each condition were recalculated to equal 100% in Microsoft Excel software. Then the overall average for all repeats were calculated.

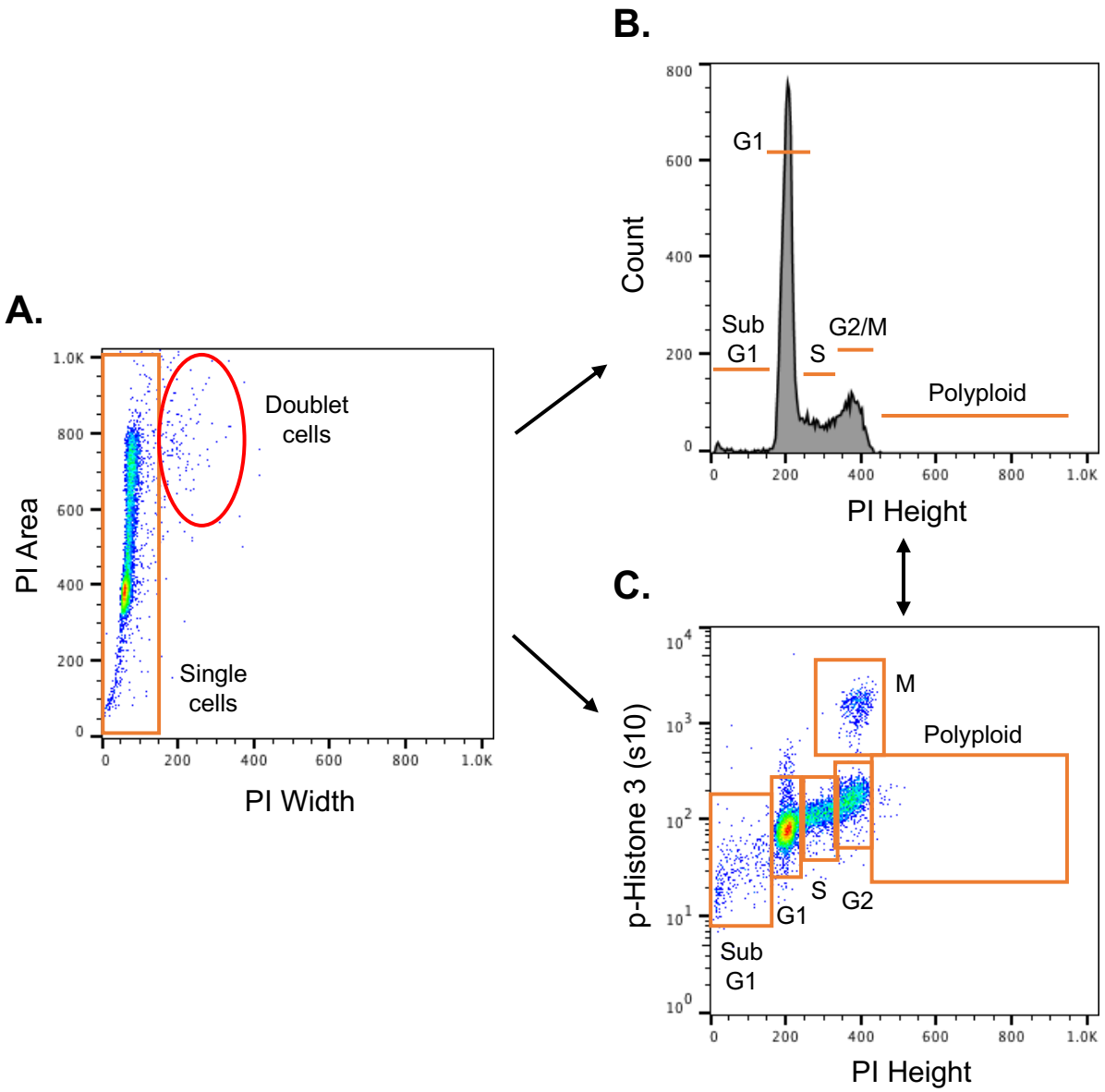

Figure 2.3: Cell cycle analysis method using FlowJo software.

A. The single cell population was selected using the gate shown in orange, excluding the doublet cells (indicated with the red circle). This gate is applied to the whole sample set. **B.** The FL3 (PI)-Height (H) histogram where each cell cycle phase; sub G1, G1, S, G2/mitosis (M) and polyploid can be identified and quantified. **C.** The FL1-H p-Histone 3 against FL3-H plot represents p-Histone 3 positivity of the cell population. Each cell population can be quantified, as well as the distinction between the G2 and M populations.

2.2.7 Immunofluorescence assays.

2.2.7.1 JSH601 exogenous BubR1 phenotype.

2.2.7.1.1 Staining method.

JSH601 cells were seeded at $2x10^5$ in a 6-well plate onto 70 % ethanol sterilised 22 mm x 22 mm microscope glass coverslips and the overexpression of the Myc and green fluorescent protein (GFP) tagged BubR1 protein (MycGFP-BubR1) was induced with 1 µg/mL doxycycline (stock 10 mg/mL) for 24 hours. Then cells were treated with nocodazole (200 ng/mL) for 4 hours before harvesting. After nocodazole treatment, the media was removed, slides were washed multiple times with cold PBS (500 µL) and fixed with 4 % paraformaldehyde (PFA) for 20 minutes at 4 °C. The coverslips were washed gently in PBS (500 µL) and stored in PBS (2 mL) at 4 °C until staining.

The cells were permeabilised with 0.5 % v/v Triton-X 100-PBS for 5 minutes at room temperature and washed twice gently in PBS (500 µL). The coverslips were blocked in 3 % w/v BSA-PBS (2 mL) for 30 minutes at room temperature. After the incubation, coverslips were gently washed in 0.2 % v/v Triton-X 100-PBS three times for 5 minutes. Anti-BubR1 (Abcam) or anti-Myc-tag (Cell Signalling) were co-stained with anti-CENPB (Santa Cruz), all primary antibodies were diluted 1:500 in 1 % w/v BSA-PBS, 1 mL was added to each coverslip and incubated overnight at 4 °C. After the incubation the coverslips were gently washed again in 0.2 % v/v Triton-X 100-PBS multiple times. Anti-mouse Alexa 488 and Anti-rabbit Alexa 594 secondary antibodies were diluted 1:200 in 3 % w/v BSA-PBS, coverslips were inverted onto 150 µL of the secondary antibody solution on a 6 well plate lid and incubated in a humidified chamber for 1 hour in the dark. Then coverslips were transferred back into the 6 well plates and washed gently twice with 0.2 % v/v Triton-X 100-PBS and washed once in cold PBS for 5 minutes per wash. Coverslips were inverted and mounted to microscope slides using the Prolong Gold antifade mountant with 4′,6-Diamidino-2-phenylindole Dihydrochloride (DAPI) (Life Technologies). Slides were set in the dark and stored long term at 4 °C.

2.2.7.1.2 Analysis.

Images of mitotic cells were taken on the 60x/1.4 oil immersion objective lens on the Eclipse TE200 inverted fluorescent microscope (Nikon) using Velocity software (Perkin

Elmer). Images were processed using FIJI Image J software. The association of the CENPB and BubR1 or Myc-Tagged proteins provided insight into the actions of exogenous MycGFP-BubR1 overexpressed in the JSH601 cell line.

2.2.7.2 SOD1 cellular localisation.

2.2.7.2.1 Staining method.

This experiment was conducted by Priya Lata. $1.5x10^5$ HeLa cells were plated per well in a 6 well plate onto 70 % ethanol sterile glass microscope coverslips. 24 hours post-plating IR treatment was administered at 5 Gy and incubated for 0.5, 1, 2, 4, 8 and 16 hours. Also including an untreated control condition. All cells were then fixed by transferring the coverslips directly into a 6 well plate containing 2 mL 4% PFA for 20 minutes at 4 °C. Fixed coverslips were washed twice in cold PBS and stored in 2 mL PBS at 4 °C until staining.

The cells were permeabilised with 0.1 % v/v Triton-X 100-PBS for 5 minutes at room temperature and washed twice gently in PBS (500 µL). The coverslips were blocked in cold 1 % w/v BSA-PBS (2 mL) for 30 minutes at room temperature. After the incubation, coverslips were gently washed in 0.1 % v/v Triton-X 100-PBS three times for 5 minutes. Anti-β-tubulin (Sigma-Aldrich) and anti-SOD1 (Abcam) primary antibodies were diluted 1:100 in 1 % w/v BSA-PBS, coverslips were inverted onto 150 µL of the antibody solution on a 6 well plate lid. The coverslips were incubated in a humified chamber for 1 hour at 37 °C. After the incubation the coverslips were transferred to the well plate and gently washed again in 0.1 % v/v Triton-X 100-PBS three times. Anti-mouse Alexa 488 and anti-rabbit Alexa 594 secondary antibodies were diluted 1:200 and 1 mg/mL DAPI was diluted 1:1000 in 1 % w/v BSA-PBS, coverslips were inverted onto 150 µL of the staining solution on a 6 well plate lid and incubated in a humidified chamber for 30 minutes in the dark. Then coverslips were transferred back into the 6 well plates and washed gently twice with 0.1 % v/v Triton-X 100-PBS, then washed once in cold PBS with 1 µg/mL DAPI (1 mg/mL stock) and again in PBS alone (all 5 minutes per wash). Coverslips were inverted and mounted to microscope slides using the Immu-mount™ (Thermo Fisher Scientific). Slides were set in the dark and stored long term at 4 °C. A secondary antibody alone control slide was also prepared, to assess the non-specific staining of the secondary antibodies.

2.2.7.2.2 Analysis.

Images of 100 cells per repeat were taken on the 60x/1.4 oil immersion objective lens on the Eclipse TE200 inverted fluorescent microscope (Nikon) using Velocity software (Perkin Elmer). The nuclear intensity of SOD1 was determined by measuring the integrated density of the SOD1 staining using a threshold image of the corresponding DAPI image in FIJI Image J software.

2.2.7.3 Abnormal mitotic phenotype assessment.

2.2.7.3.1 Staining method.

$1.5x10^5$ HeLa cells per well were plated in a 6 well plate onto sterile glass microscope coverslips and reverse transfected with siControl, and siSOD1-5 as described in methods section **2.2.3.2**. One coverslip was plated for a secondary antibody alone staining control. 48 hours post-transfection, IR treatment was administered at 5 Gy and incubated for 16 hours, with each knockdown including an untreated condition. Cells were then fixed by transferring coverslips directly into a 6 well plate containing 2 mL 4% PFA for 20 minutes at 4 °C. Fixed coverslips were washed twice in cold PBS and stored in 2 mL PBS at 4 °C until staining.

The staining protocol was the same as the SOD1 cellular localisation assay (methods section **2.2.7.2.1**), with the exception that only β-tubulin was stained for and anti-mouse Alexa 488 secondary antibody was only required.

2.2.7.3.2 Analysis.

Images of 100 cells per repeat were taken on the 60x/1.4 oil immersion objective lens on the Eclipse TE200 fluorescent microscope (Nikon) using NIS Elements software (Nikon). Images were processed using FIJI Image J software. Cells were characterised using typical abnormal mitotic phenotypes such as micronuclei or multi-micronuclei, DNA/anaphase bridges and multinucleate, in addition to normal/ undamaged cells. Micronucleated cells were defined as cells containing the presence of one or more (multi-Micronucleated) small nuclei containing DNA fragments separate from the nucleus within one cell. DNA/anaphase bridges were defined as a cell with a DNA tether between two nuclei or between the sister chromatids in anaphase. Multinucleated was defined as a cell with > 1 nuclei or fused nuclei. Finally, cells that

featured two or more of these different characteristics were termed multiple phenotypes.

2.2.7.4 Centrosome assessment.

2.2.7.4.1 Staining method.

HeLa cells were plated, transfected, treated and harvested as in the abnormal mitotic phenotypes assay (methods section **2.2.7.3.1**). The staining protocol was the same as the SOD1 cellular localisation assay (methods section **2.2.7.2.1**), with the exception that β-tubulin was co-stained with Pericentrin (Abcam) at 1:1000.

2.2.7.4.2 Analysis.

Images of 50 mitotic cells per repeat were taken on the 60x/1.4 oil immersion objective lens on the Eclipse TE200 fluorescent microscope (Nikon) using NIS Elements software (Nikon). Images were processed using FIJI Image J software. Pericentrin fragmentation was defined as the identification of multiple smaller or elongated pericentrin staining compared to 1 complete pericentrin protein focus. Centrosome amplification was defined as > 2 distinct centrosomes within one cell.

2.2.7.5 DNA damage time course.

2.2.7.5.1 Staining method.

HeLa cells were plated, transfected and treated as in the abnormal mitotic phenotypes assay (methods section **2.2.7.3.1**), but samples were harvested at 0, 0.5, 1, 2, 4, 8, 16 and 24 hours post-IR (5 Gy), plus untreated control samples. The staining protocol was the same as the SOD1 cellular localisation assay (methods section **2.2.7.2.1**), with the exception that only anti-γH2AX (Santa Cruz) primary antibody was stained for at 1:100, which only required the anti-mouse Alexa 488 secondary antibody.

2.2.7.5.2 Analysis.

Images 100 cells per repeat were taken on the 60x/1.4 oil immersion objective lens on the Eclipse TE200 fluorescent microscope (Nikon) using NIS Elements software (Nikon). For each time point and siRNA condition, the number of nuclear γH2AX foci were counted per nucleus in each image using the foci counter macro in the FIJI Image J software.

2.2.7.6 SAC protein co-localisation assessment.

2.2.7.6.1 Staining method.

HeLa cells were plated, transfected, treated and harvested as in the abnormal mitotic phenotypes assay (methods section **2.2.7.3.1**). The staining protocol was the same as the SOD1 cellular localisation assay (methods section **2.2.7.2.1**), with the exception that anti-BubR1 (Abcam) diluted 1:500 was co-stained with anti-CENPB (Santa Cruz) at 1:500.

2.2.7.6.2 Analysis.

Z stacks images of 5 metaphase or anaphase cells were taken on the 63x/1.4 oil immersion objective lens using the Zeiss LSM980 confocal fluorescent microscope and Zen Blue software (version 3.1). FIJI Image J software was used to process the images.

2.2.7.7 DNA repair assessment.

2.2.7.7.1 Staining method.

HeLa cells were plated, transfected and treated as in the abnormal mitotic phenotypes assay (methods section **2.2.7.3.1**), but samples were harvested at 4 hours post-IR (5 Gy), plus untreated control samples. Cells were then fixed by transferring coverslips directly into a 6 well plate containing 2 mL 4% PFA for 20 minutes at 4 °C. Fixed coverslips were washed twice in cold PBS and stored in 2 mL PBS at 4 °C until staining.

The cells were permeabilised with 0.5 % v/v Triton-X 100-PBS for 5 minutes at room temperature and washed gently in cold PBS-Tx (1 mL) for 15 minutes four times. Anti-RAD51 (Abcam) primary antibody diluted 1:100 in BSA-Tx and co-stained with γH2AX (Santa-Cruz) diluted 1:100. Coverslips were inverted onto 150 µL of the antibody solution on a 6 well plate lid. The coverslips were incubated in a humified chamber overnight at 4 °C. After the incubation, the coverslips were transferred to the well plate and gently washed again in PBS-Tx for 15 minutes four times. Anti-mouse Alexa 488 secondary antibody was diluted 1:200 and anti-rabbit Alexa 594 secondary antibody diluted 1:500 in 5 % w/v BSA. Coverslips were inverted onto 150 µL of the staining solution on a 6 well plate lid and incubated in a humidified chamber for 1 hour in the dark. Then coverslips were transferred back into the 6 well plates and washed gently

twice with PBS-Tx for 15 minutes, then washed once in cold PBS with 1 µg/mL DAPI (1 mg/mL stock) for 5 minutes and then washed a further two times with PBS-Tx for 15 minutes. Coverslips were inverted and mounted to microscope slides using the Immu-mount™ (Thermo Fisher Scientific). Slides were set in the dark and stored long term at 4 °C.

2.2.7.7.2 Analysis.

Images 100 cells per repeat were taken on the 60x/1.4 oil immersion objective lens on the Eclipse TE200 fluorescent microscope (Nikon) using NIS Elements software (Nikon). Cells with ≥ 5 RAD51 foci were considered positive and the average of positive cells were calculated across all conditions and repeats.

2.2.8 Live cell microscopy.

2.2.8.1 Cell plating and treatment.

Reverse transfection of cells were conducted on a smaller experimental scale. 1 µL of each siRNA (20 µM stock) was diluted in 50 µL warm SFM per well, in a separate tube 0.6 µL DharmaFECT transfection reagent was diluted in 50 µL SFM per well and each solution incubated for 5 minutes at room temperature. An equal volume of the DharmaFECT solution was mixed into each siRNA solution and incubated a further 20 minutes. 100 µL of the siRNA-DharmaFECT mixture was added to each well of a 24 well plate, $1x10^4$ cells were plated in each well and cultured at 37 °C and 5 % CO_2. 48 hours post-transfection wells were treated with the appropriate treatments either 4 hours or immediately before imaging commenced.

For some conditions such as IR or rescue experiments, $1.5x10^5$ cells were plated in a 6-well plate with the desired transfection (if required). Cells were harvested and re-plated into the 24 well plate on the day of imaging, the media of these conditions were removed and washed once in PBS. Cells were dislodged from the wells with 1 mL trypsin-EDTA for 5 minutes at 37 °C, then diluted in media and collected in 15 mL falcon tubes. Pellets were obtained through centrifugation at 1000 RPM for 3 minutes and the pellets were resuspended in 1 mL media. Cells were counted and $4x10^4$ cells were diluted in 2 mL per condition. IR (if applicable) was administered whilst cells were in solution. 1 mL of the cell solution was re-plated to the live cell 24 well plate, and cells

were left to adhere for 4 hours before imaging commenced. Other treatments were administered immediately before imaging commenced (if required).

2.2.8.2 Imaging.

The cells were imaged on the Leica AF6000 time-lapse microscope overnight (approximately 16-19 hours) with conditions maintained at 37 °C and 5 % CO_2. Cells were visualised using phase contrast and a 20x phase contrast objective. 6-10 images were captured at different positions/well every 5 minutes using the LAX software.

2.2.8.3 Analysis.

FIJI Image J software was used to generate a time-lapse video of each position imaged. The time required for mitotic transit was measured using the image number for 50 cells per condition per repeat. Cells were scored from mitotic initiation, defined as when the cell underwent nuclear envelope breakdown to completed cytokinesis **(Figure 2.4)**. Cell fate was also quantified, such as cell death in mitosis or death after cell division, aberrant mitosis, which included cells which divided into > 2 daughter cells, and mitotic slippage, which was defined as the cell failing to divide and returning to interphase.

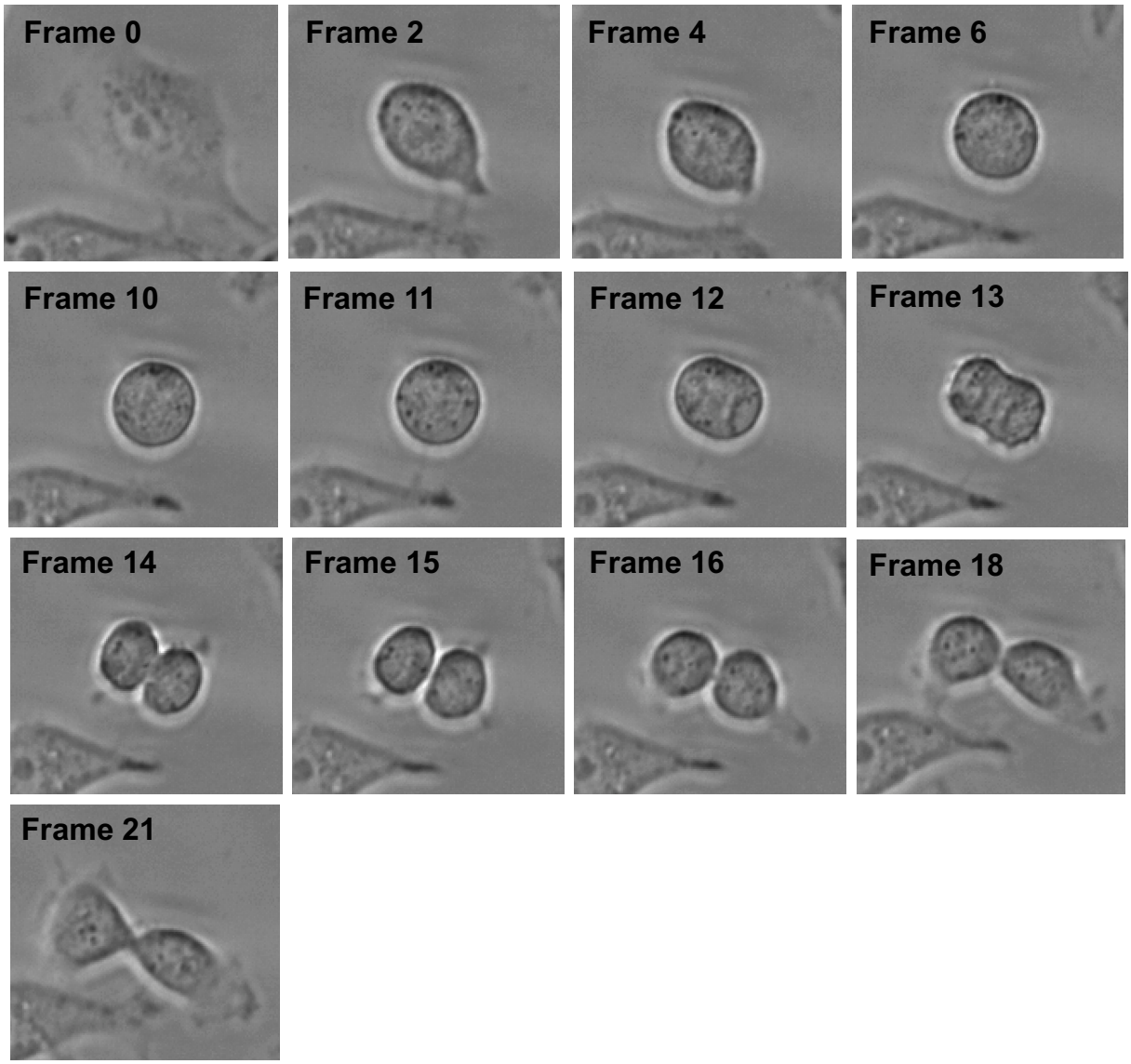

Figure 2.4: Representative images of a HeLa cell undergoing mitosis.

In Frame 0 the cell is in interphase and enters mitosis in Frame 6 when the nuclear envelope breaks down and the cell rounds up from the plate. At Frames 12 and 13, the chromatids can be seen transitioning to opposing cellular poles during anaphase. Cytokinesis is initiated in Frame 14 and mitosis is completed in Frame 16. Therefore, mitosis was completed in 10 frames (6-16) or 50 minutes.

2.2.9 Cell survival assays.

2.2.9.1 Trypan blue assay.

HeLa cells were seeded at $1x10^6$ cells in 10 cm culture dishes per condition. Cells were incubated overnight for cell adhesion. Cells were treated with 10 Gy IR and incubated for 16 hours. An untreated condition was also included as a control. All conditions were

harvested via the collection of media into a falcon tube, washed with PBS and cells were detached through incubation with trypsin-EDTA (2 mL) for 5 minutes at 37 °C. The detached cell solution was added to the collected media and centrifuged at 3000 RPM for 3 minutes. The cell pellet was resuspended in 1 mL media and 10 µL of cells were mixed in an equal ratio with trypan blue solution (10 µL). 10 µL of the cell-trypan blue solution was counted using a haemocytometer. Cells that absorbed the trypan blue solution were considered unviable. Three independent measurements were taken from each sample per experimental repeat. The overall average percentage of viable cells was calculated.

2.2.9.2 Annexin V and PI apoptosis detection assay.

2.2.9.2.1 Cell plating and staining.

HeLa cells were seeded at $1x10^6$ cells in 10 cm culture dishes per condition in 6 mL media and left to adhere overnight before the administration of treatments. Cells were treated with 10 Gy IR and 6 µL 1 mM camptothecin (1 µM; Sigma-Aldrich) as a positive control. In addition to treated samples, a stained, unstained, PI only and annexin V only untreated control conditions were included in the sample set. All conditions were harvested prior to the 16 hours post-IR time point, which allowed for cell preparation and staining to process the live cells at the desired 16 hour time point.

The BD Biosciences FITC annexin V apoptosis detection kit I was used to manufacturer's instructions for cell harvesting and staining. The media was collected into 15 mL falcon tubes for each condition on ice, washed gently in cold PBS (wash was collected) and cells were detached after incubation with trypsin-EDTA (2 mL) for 5 minutes at 37 °C. The cells were added to the corresponding media solution on ice and centrifuged at 3000 RPM for 3 minutes. The pellets were resuspended in 1 mL PBS and transferred to a 2 mL Eppendorf tube. Cells were washed a further time in PBS through microcentrifugation at 13,000 RPM. The 10x annexin V binding buffer was diluted 1:10 to a 1x annexin V binding buffer working solution. The pellets were resuspended in 100 µL 1x annexin V binding buffer, then 5 µL of both annexin V and PI solutions were added to the cells and gently vortexed. The cells were incubated for 15 minutes at room temperature in the dark and 400 µL of 1x annexin V binding buffer

was added to each sample. All samples were processed on the FACSCalibur (BD Sciences) and 10,000 events per sample were collected.

2.2.9.2.2 Analysis.

Data were analysed using FlowJo software version 10 **(Figure 2.5)**. The side scatter was plotted against forward scatter to gate the cell population of interest. The gate was applied to the whole sample set. The FL3-H (PI) was plotted against FL1-H (annexin V) to determine the fate of the cells within the population following the various treatments. The distinct signal intensities produced from the staining process corresponded to different cell fates and were gated, in turn generating a percentage population. Annexin V^-/PI^- was defined as live cells, Annexin V^+/PI^- was defined early apoptotic, Annexin V^+/PI^+ as apoptotic and Annexin V^-/PI^+ as late apoptotic or necrotic. When necessary a compensation matrix was applied to FL1-H, to better distinguish between the different fate populations.

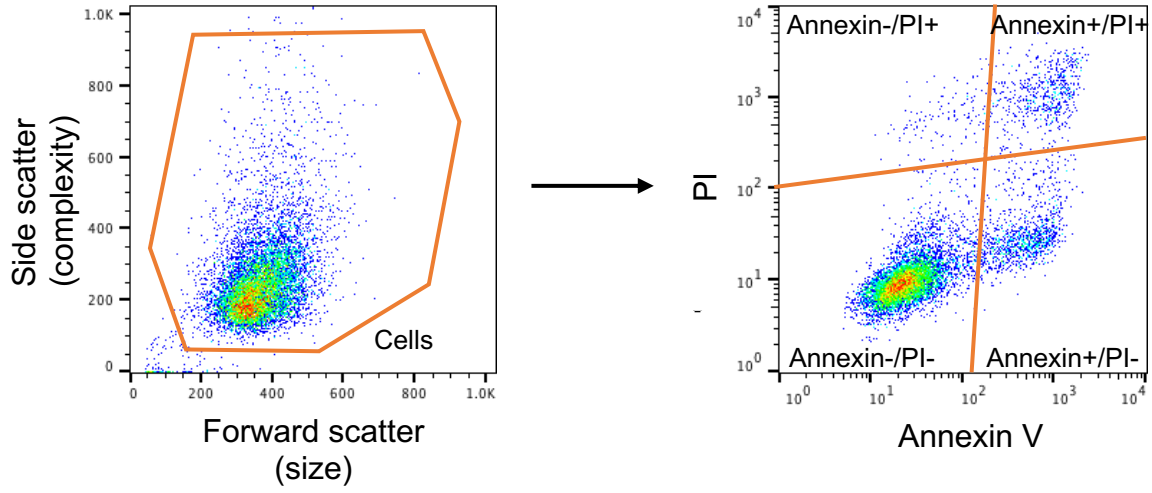

Figure 2.5: Annexin V and PI apoptosis analysis method in FlowJo software.
The cell population of interest was selected using the gate shown in orange (left plot), excluding cellular debris. This gate was applied to the whole sample set. The FL3-H (PI) against FL1-H (Annexin V) plot shows the distinct signal intensities for each combination of stains, indicating the fate of the cells within the population.

2.2.9.3 Clonogenic survival assay.

2.2.9.3.1 Cell plating and staining.

$1.5x10^5$ HeLa cells were plated per well in a 6 well plate and reverse transfected with siControl and siSOD1-5, as described in methods section **2.2.3.2**. 48 hours post-transfection each condition was counted and replated in 6 well plates at 200 and 1000 cells per well in triplicate for untreated and low treatment doses or 500 and 2000 cells per well in triplicate for higher treatment doses. The cells were incubated overnight to adhere to the plates and then treated with varying doses of IR (0.5, 1, 3, 5 Gy). Cells were then incubated for 10 days post-treatment for sufficient colony formation.

The media was removed from the wells and methylene blue staining solution was added to stain the colonies. Plates were incubated for 30 minutes at room temperature and then the staining solution was washed from the plates using alternate washes of cold and hot water. Plates were dried at room temperature.

2.2.9.3.2 Analysis.

The number of colonies were counted for each condition and triplicate cell number per repeat. A colony was defined as ≥ 50 cells per cluster. In this thesis, the lower number of cells plated for each condition was selected for analysis. The average number of cells per condition were calculated using Microsoft Excel software. The plating efficiency for the untreated condition was then calculated as depicted below:

$$Plating\ efficiency\ = \frac{Number\ of\ colonies\ counted}{Number\ of\ cells\ plated}$$

The plating efficiency of the untreated was used to then calculate the survival fraction of all conditions. The survival fraction was calculated as depicted below:

$$Survival\ Fraction = \frac{Number\ of\ colonies}{(Number\ of\ cells\ plated \times\ plating\ efficiency)}$$

The IR dose response data was plotted with the linear quadratic model of cell death in GraphPad Prism (version 8) software.

2.2.10 ROS quantification assay.

2.2.10.1 Cell plating and treatment.

HeLa cells were reverse transfected (methods section **2.2.3.2**), and 48 hours post-transfection cells were replated into a 96 well plate at $1x10^4$ cells/well in 100 µL phenol red free DMEM media. For each condition cells were plated in triplicate, including the control wells; blank (media and probe), unstained media (media without probe) and unstained cells (cells without probe). Cells were incubated overnight to adhere.

2.2.10.2 Staining.

ROS were detected using the chloromethyl-2',7'-dichlorodihydrofluorescein diacetate (CM-H2DCFDA) general oxidative stress indicator kit (Invitrogen). The CM-H2DCFDA probe was reconstituted in DMSO (865.36 µL) to generate a 100 µM stock solution, which was prepared fresh for each assay. Then the probe was diluted to 10 µM working solution in warm PBS. Phenol red free DMEM was removed from the wells and 100 µL of the diluted probe was added to each well, excluding certain control wells where the media was replaced. Cells were incubated in the probe at 37 °C and 5 % CO_2 for 1 hour in the dark. The probe was then removed, and fresh media was added to the wells. Various chemotherapeutics, ROS inducers and IR treatment was administered to cells and incubated for the allotted time. The fluorescence was measured at 495/ 527 nm bottom read on the Fluorescent SpectraMax M5e multi-mode microplate reader (Molecular Devices).

2.2.10.3 Analysis.

The average fluorescent ROS intensity was calculated from the triplicate wells and normalised against the average of the blank control condition. Analysis was conducted using Microsoft Excel software.

2.2.11 DNA damage comet assay.

2.2.11.1 Sample preparation and staining.

HeLa cells were reverse transfected in a 6 well plate with siControl, and siSOD1-5 as described in methods section **2.2.3.2**. 72 hours post-transfection cell were treated with 5 Gy IR or 50 µM H_2O_2 for 4 hours, plus an untreated control for each siRNA.

The media was discarded, and cells were transferred to 2mL Eppendorf tubes with PBS and a cell scraper. Cells were resuspended in PBS (1 mL) and counted. 100,000 cells per condition were isolated for the experiment. Alkaline comet assay protocol was performed as instructed in the CometAssay kit (Trevigen).

2.2.11.2 Analysis.

Images of the cells per repeat were taken on the 10x/0.25 objective lens on the Eclipse TE200 fluorescent microscope (Nikon) using NIS Elements software (Nikon). The FITC channel was used to visualise the cells. Images were converted to the BNP file format to process using the CometScore software. The average percentage of DNA in Tail were calculated for 50 cells per condition and the overall mean was determined across the experimental repeats.

2.2.12 Reverse transcription-quantitative polymerase chain reaction.

Reverse transcription-quantitative polymerase chain reaction (RT-qPCR) quantifies the mRNA expression level of a gene of interest relative to a control (housekeeping) gene.

2.2.12.1 RNA extraction.

HeLa cells were reverse transfected as described in methods section **2.2.3.2** and treated with IR (5 Gy) 48 hours post-transfection and incubated a further 16 hours. Untreated conditions were also included. After treatment incubation, the media was removed from the cells and RNA extraction was performed using the manufacturer's protocol and reagents from the RNeasy mini kit (Qiagen).

The concentration (ng/µL) of the eluted RNA was quantified using the Nanodrop spectrophotometer (ND-1000) using the RNA-40 nucleic acid setting. RNA quality was also determined using the A_{260}/A_{280} ratio, where RNA purity was considered acceptable with a ratio of 1.8-2.0.

2.2.12.2 Reverse transcription.

The RNA extracted underwent reverse transcription using the high-capacity RNA to cDNA kit (Applied Biosystems). For each RNA sample, 10 µL 20x Enzyme mix, 2 µg RNA made to a maximum total volume of 8 µL with nuclease-free water and 2 µL RT

enzyme were added to a 0.2 mL PCR tube. The PCR solution was then gently mixed and centrifuged briefly in a benchtop centrifuge. The RT-PCR reaction was incubated in the PCR machine at 37 °C for 1 hour, followed by 95 °C for 5 minutes and 4 °C until incubation was terminated.

2.2.12.3 Messenger RNA (mRNA) relative expression via TaqMan assay.

A TaqMan solution was prepared for each gene of interest and the housekeeping gene *GAPDH*, for each sample in triplicate and the marginal error accounted for. The solution was comprised of 18.56 µL 2x TaqMan universal mastermix (Applied Biosystems), 1.86 µL probe for the gene of interest (listed in materials section **2.1.11**) and 9.28 µL nuclease-free water and scaled to accommodate the total number of samples. For each gene, 9 µL of the corresponding TaqMan solution was added to a 384 well plate. Then 1 µL of the cDNA samples from the RT-PCR reaction was added to the wells in triplicate for each probe. The well plate was then sealed and briefly centrifuged.

2.2.12.4 Analysis.

The TaqMan well plate was processed on the 7900 RT-PCR machine using the SDS 2.4 software. The reporter was set to FAM which corresponded to probe dye and the cycles were maintained at 45-50 depending on the amount of RNA processed in the RT-PCR reaction. The data was exported to Microsoft Excel and the relative fold change expression was calculated. This involved determining an average Ct value of the triplicate wells, then the delta (Δ) Ct values were calculated as depicted below:

$$\Delta\text{Ct} = \text{average Ct value of gene of interest} - \text{average Ct value of housekeeping gene}$$

Then the fold change of the experimental conditions in relation to the control condition was calculated as depicted below:

$$\text{Fold change expression} = \frac{\Delta\text{Ct of sample of interest}}{\Delta\text{Ct of control sample}}$$

2.2.13 Mapping of PP2A cysteine oxidation.

2.2.13.1 Sample preparation and reaction.

The cysteine oxidation of PP2A alpha GST (N-term) recombinant protein (Novus Biologicals, cat number H00005515-P01) was analysed following reactions with either a SOD1 (Cu-Zn) recombinant protein (Novus Biologicals, cat number NBP2-34942) or H_2O_2. 28.58 µL PP2A protein (2 µg) was mixed with either 1 µL SOD1 (1 µg) or 2.8 µL H_2O_2 (50 µM), in addition to 2.8 µL 10x in vitro reaction buffer (1x) and made to a total volume of 34 µL with PBS in Lobind Eppendorf tubes. PP2A protein with the reaction buffer and PBS was conducted as the control. The reactions were incubated at 37 °C for 10 minutes and the reactions were inactivated by storing at -20 °C until further processing.

2.2.13.2 Reduced cysteine residue labelling and MS.

The labelling and MS analysis were conducted by Dr Caroline Evans from the Dickman group (Department of Chemical and Biological Engineering, University of Sheffield). Isotopically labelled iodoacetamide (D4) was added to the samples containing the SOD1 and H_2O_2, to label reduced cysteine residues. Whereas unlabelled iodoacetamide was used to label PP2A alone control sample. All samples were then prepared for input into the Ultimate 3000 high performance liquid chromatography (HLPC) system coupled to Q-Extractive HF (QE) Orbitrap mass spectrometer.

2.2.13.3 Analysis.

All data were input into Mascot software, in consideration of the appropriate modifications. A list of peptides identified was generated for the PP2A in each reaction, indicating any modifications. Carbamidomethyl (modification of cysteine residues by iodoacetamide) was of interest, which indicated the reduced cysteines following the reaction.

2.2.14 Mass Spectrometry Screen.

2.2.14.1 Cell plating and treatment.

The Flp-In T-REx cell line JSH601 were plated $2.5x10^5$ in twenty 10 cm plates per condition. Cells were allowed to adhere for 6 hours before the MycGFP-BubR1 overexpression was induced with doxycycline (1 µg/mL) for 48 hours. The other

condition involved no induction of the MycGFP-BubR1 protein to provide a negative control. Then both conditions were treated with IR (5 Gy) for a further 16 hours before harvesting.

2.2.14.2 GFP-Trap immunoprecipitation.

Plates were incubated at 4 °C for 10 minutes before the termination of treatment. Then the media was collected into 50 mL falcons on ice per condition, cells were removed from the plates using cell scrapers (Thermo Fisher Scientific). Cells were pelleted via centrifugation at 13,000 RPM and 4 °C, then resuspended in PBS (5 mL) and transferred into 15 mL falcon tubes per condition. Cells were washed again with PBS, then resuspended in 4 mL MS IP lysis buffer and incubated on ice for 30 minutes with occasional mixing. The soluble protein was separated through centrifugation at 13,000 RPM and at 4 °C, then transferred into a new cold 15 mL falcon. The protein was quantified as in methods section **2.2.4.4**. At this point, the soluble protein could be split for dual MS digestion techniques (on-bead and in-gel).

For in-gel digestion GFP-Trap magnetic agarose beads (ChromoTek) were precleared from preservative solution and washed in the cold MS IP wash buffer twice using the DynaMag magnetised tube rack (Invitrogen). Alternatively, for on-bead digestion, the same process was conducted but the MS IP wash buffer did not contain Triton-X 100 and DTT. The maximum amount of protein was added to the beads in 15 mL tubes and mixed on a rotator for 3 hours at 4 °C. 200 µg was taken for input samples too and made like SDS-PAGE samples (methods section **2.2.4.4**). The remaining protein was discarded, and the beads were washed three times in the appropriate MS IP wash buffer. For in-gel digestion, the IP beads were then transferred to a 1.5 mL Eppendorf tube with wash buffer (1 mL) and resuspended in 55 µL 1x Protein SDS-PAGE loading dye (diluted 1:4 in wash buffer). The beads were heated for 15 minutes at 90 °C with mixing at 5-minute intervals. The protein-dye solution was transferred into new tubes and the beads discarded. The IP samples were stored at -20 °C. Alternatively, for on-bead digestion, the IP beads were stored at -20 °C after washing.

2.2.14.3 SDS-PAGE and protein staining.

A 4-12 % precast tris-glycine gel (Expedeon) was prepared with the 1x MOPS Run Blue running buffer. All of the in-gel digestion IP samples were double loaded (25 µL loaded and ran to the bottom of the well and then 25 µL added into the same well again) into each lane along with a Bio-Rad precision plus molecular weight marker (6 µL). The proteins were separated at 120-180 V until the loading front completely descended through the gel.

The gel was immersed completely in InstantBlue Protein Stain (Expedeon) and incubated for 15 minutes at room temperature with gentle rocking. Once protein bands were visible, the lanes were excised with sterile scalpels and stored in nuclease-free water at 4 °C.

2.2.14.4 Gel de-staining and In-gel digestion.

The gels were transported to the Department of Chemical and Biological Engineering (University of Sheffield) for MS preparation and analysis. Each gel lane was excised into 1 mm bands with scalpels sterilised with decontamination solution, bands were then cut into smaller pieces and each band was placed into separate 1.5 mL sterile Lobind Eppendorf tubes (Thermo Fisher Scientific). Gel bands were de-stained through the incubation with 30 % IMS (200 µL) for 20 minutes at 65 °C. This was repeated 3 times until the gel was clear for the digestion protocol.

The digestion protocol was initiated with the gel bands incubated in 50 mM ABC solution (100 µL) for 5 minutes at room temperature. The ABC solution was removed, and gel bands were dehydrated through the incubation in 100 µL LC grade acetonitrile (ACN) for 10 minutes at room temperature, with vortexing at different intervals. The 50 mM ABC and ACN incubations were repeated once more, so the gel pieces appeared white at the end of these incubations. The proteins were reduced through the incubation with the reduction reagent (50 µL) at 56 °C for 30 minutes. After this incubation, the samples were briefly centrifuged to collect the condensation and the remaining reduction reagent was discarded. Gel pieces were then incubated in ACN (50 µL) for 10 minutes with occasional vortexing, resulting in dehydrated gel bands (appeared white). Alkylation of the proteins was then performed through the addition

of 50 µL alkylation reagent, which was incubated for 20 minutes at room temperature in the dark. The alkylation reagent was discarded, and the rehydrated gel bands were incubated in 50 mM ABC solution (100 µL) for 10 minutes at RT. Excess reagents were removed from the gel pieces through incubation with ACN (100 µL) for 10 minutes at room temperature and the resulting solution was discarded. The 50 mM ABC and ACN incubations were repeated once more, and the solvents were discarded from the dehydrated white gel bands. The bands were dried in a vacuum centrifuge (Concentrator plus, Eppendorf) set to V-AL for 10 minutes at a time until gel pieces appeared granular. The tubes were transferred to ice and protein was digested in digestion buffer (20 µL). After 20 minutes, more digestion buffer was added to cover the gel pieces and incubated for a further 25 minutes. Excess digestion buffer was removed and 1 M $CaCl_2$ diluted 1:200 (5 mM) in 50 mM ABC was added to cover the gel pieces (65 µL) and incubated at 37 °C overnight. After the incubation the peptides had diffused from the gel into the buffer, the condensation was collected through brief centrifugation and the extracts were transferred into a new 1.5 mL Lobind tube, labelled for each gel segment and placed on ice. 25 mM ABC solution (15 µL) was added to the gel pieces and incubated at room temperature for 10 minutes with interval vortexing. The resulting solution was added into the corresponding tubes on ice. The gel pieces were then dehydrated through incubation with 100 µL ACN for 15 minutes at 37 °C, with vortexing every 5 minutes. The condensation was collected through brief centrifugation and the solution was added into the corresponding extract tubes. 150 µL 5 % v/v formic acid (400 µL formic acid diluted in 7.6 mL HPLC grade water) was added to the gel pieces for 15 minutes at RT, with vortexing after 10 minutes. The samples were briefly centrifuged, and the formic acid solution was transferred into the corresponding tubes containing the pooled extracts. ACN (100 µL) was added to the gel pieces for 15 minutes at 37 °C, with vortexing every 5 minutes. The samples were briefly centrifuged and the ACN solution was transferred to the pooled extracts. The extracts were then placed into the vacuum centrifuge until dry and stored at -20 °C.

2.2.14.5 On-bead digestion.

For on-bead digestion, the protocol performed was adapted from ChromoTek instructions. The frozen IP samples **(2.2.14.2)** were resuspended and washed twice times in 500 µL cold on-bead wash buffer using the DynaMag magnetised tube rack

(Invitrogen). Then the IP samples were resuspended in 25 µL elution buffer I and incubated at 37 °C for 30 minutes with mixing every 5 minutes. The resulting supernatant was composed of the protein digest and transferred into a Lobind Eppendorf tube for each sample. The IP beads were resuspended twice in 50 µL elution buffer II and the supernatant was added to the corresponding digest solution for each sample. The samples were then incubated at 37 °C in the dark overnight and the digestion reaction was stopped with the addition of 1 µL TFA. The samples were then placed into the vacuum centrifuge until dry and stored at -20 °C.

2.2.14.6 Bond Elut OMIX C18 tip clean up.

The peptides were de-salted before MS analysis with Bond Elut OMIX C18 tips (10 µL) (Aligent). First, the in-gel samples were resuspended and merged into six fractions using 20 µL Q-Extractive (QE) loading buffer, where the on-bead samples were resuspended in 20 µL QE loading buffer. All samples were then cleaned following the manufacturer instructions. The tip was primed through aspiration with OMIX C18 conditioning solution (10 µL) twice, then equilibrated through aspiration twice with OMIX C18 wash solution (10 µL). Then the sample was aspirated (10 µL) into and dispended from the tip ten times to allow optimum peptide binding to the hydrophobic monolithic silica surface within the tip. The tip was cleaned with OMIX C18 wash solution four times and peptides were eluted from the tip with OMIX C18 elution solution (10 µL) twice into a new Lobind Eppendorf tube. The resulting peptides were vacuum dried and stored at -20 °C prior to MS analysis.

2.2.14.7 HPLC-MS/MS.

Each sample was resuspended in 5 µL QE loading buffer, sonicated for 5 minutes at 37 °C in an ultrasonic bath (VWR) and the condensation was collected through centrifugation at 13,000 RPM for 2 minutes. 3 µL was transferred to a micro-vial with a snap ring cap (VWR). Samples were input into the Ultimate 3000 HLPC system (Thermo Fisher Scientific) with a C18 column. Peptides were eluted onto an Easy-spray PepMap C18 column with a flow rate gradient (300 nL/minute). The HPLC was coupled to QE HF Orbitrap and data acquisition was performed with a positive ion mode full scan (375 to 1500m/z) with an MS1 resolution of 120 000, Automatic Gain Control (AGC) target of $1x10^6$ and a maximum fill time of 60 ms. Then MS2 resolution

of 30 000 with AGC target of $1x10^5$, a maximum fill time of 60 ms and an isolation window of 2 m/z. The total run time was 55 minutes per sample.

2.2.14.8 Analysis.

The raw data collected from the MS screen was analysed in Max Quant software. The settings used were trypsin/P digestion, with up to 2 missed cleavages, the fixed modification was Carbamidomethyl, variable modifications were oxidation and acetylation (Protein N-term), Label-free Quantification was performed with the minimum neighbour of 3 and an average number of neighbours of 6. Peptide tolerance was set at 4.5 ppm and minimum peptide length of 7 amino acids, maximum peptide mass of 4600Da, protein FDR was set at 0.01. The identifier was set to Uniprot with the human genome FASTA file (11107229296-1).

The protein list was exported to Microsoft Excel software. Firstly, both proteins lists were ordered through unique peptides and those ≥ 2 were taken forward for analysis. Both proteins lists were then ordered by IBAQ intensity and unidentified or Uniprot identified contaminants (keratin) were removed. Then using the BioGrid database, the known interactors of BubR1 with evidence of ≥ 2 studies, were highlighted in both conditions. This was supported using the STRING database, which also identifies the known interactors of the protein of interest using the literature. It was key to identify the known interactors first to ensure confidence within the screen.

A study by Trinkle-Mulcahy (2008) analysed the non-specific interactors of the GFP tag and several bead matrixes (bead proteomes), including agarose, sepharose and magnetic (Trinkle-Mulcahy *et al.*, 2008). This paper was used to identify and eliminate the majority of contaminants from the screen lists. Trinkle-Mulcahy (2008) Figure 2C (a list of frequently detected GFP interacting proteins), Table I/II (sepharose bead proteomes) and supplementary Table 1 (comparison of Dynabeads and sepharose bead non-specific interactors) were compared to both protein lists and contaminants were removed (Trinkle-Mulcahy *et al.*, 2008).

Once the majority of contaminants were removed, the -Dox list was compared to the +Dox list. The iBAQ intensity of each protein was compared between the conditions,

those with greater intensity in the -Dox were considered non-specific and discarded and those with greater intensity in the +Dox were considered a potential interactor. The proteins in both lists but the greater intensity in +Dox were not discarded as these may be genuine BubR1 interactors but have an affinity for or are involved with other proteins with an affinity for the beads. This step of analysis provided a preliminary list of potential interactors.

The next step of analysis used the CRAPome database, which features numerous lists of MS experiments categorised by experimental details. The preliminary list of interactors was assessed in the CRAPome database and the proteins that were identified in 50 % or greater experiments were considered contaminants. Additionally, the proteins which were identified in 30-50 % of all MS experiments in the database were analysed further, through experimental details. If these proteins were identified in 50 % or greater of experiments that used magnetic agarose beads, these were also removed from the list.

An on-bead digestion optimisation experiment was conducted with the negative control sample (-Dox) and the proteins identified (non-specific) with a unique peptides number of ≥ 2 were eliminated from the potential interactors list from the in-gel digest. Finally, a 0.1 % false discovery rate of the iBAQ intensity of BubR1 (top hit) was applied to the potential interactors list, to produce the final list of 175 interacting proteins of BubR1.

2.2.15 Statistical analysis.

GraphPad Prism (version 8) software was used to perform statistical data analysis. Single data points from each experiment were represented through means +/- standard deviation (SD). Whereas multiple data points from each condition from each independent experiment, were expressed as a mean of means were represented as +/- standard error of the mean (SEM). SD and SEM represented parametric data. For non-parametric data, the median was plotted.

For parametric data, statistical significance was determined between means via unpaired T-test or between multiple means by One-way ANOVA with Dunnett correction test for multiple comparisons. For non-parametric data, statistical

significance was determined between means via Mann-Whitney or between multiple means by Kruskal-Wallis test with Dunn's multiple comparisons. A p value ≤ 0.05 was regarded significant (* p ≤ 0.05, ** p ≤ 0.01, *** p ≤ 0.001, **** p ≤ 0.0001 and ns p = non-significant).

Chapter 3: SOD1 regulates mitotic progression following DNA damage.

3.1 Introduction, aims and hypothesis.

The Thompson laboratory deduced that cells traverse through mitosis slower post-irradiation (IR), indicating the existence of a mitotic DNA damage checkpoint (MDDC), as previously stated in section **1.6.1**. Preliminary data also found that this arrest was dependent on BubR1. Furthermore, a high throughput fluorescence microscopy siRNA screen was conducted by the Thompson laboratory **(Figure 1.9),** to identify other proteins involved in the MDDC. Following further refinement of the initial screen via a secondary screen, the final protein list was generated and superoxide dismutase 1 (SOD1) was selected for investigation in this chapter.

SOD1 is an abundant antioxidant enzyme involved in the dismutation of superoxide ($O_2^{\bullet-}$) radicals into hydrogen peroxide (H_2O_2) (Wang *et al.*, 2018), which is then further detoxified downstream. The imbalance of redox homeostasis (reactive oxygen species (ROS) production and clearance) causes oxidative stress, which can in turn damage DNA (Pizzino *et al.*, 2017). ROS such as H_2O_2 has been implicated in the regulation of numerous signalling pathways via non-damaging reversible oxidative modifications, indicating a vital redox role in canonical cellular pathways (Zhang *et al.*, 2016). Then in addition to SOD1's enzymatic role in the regulation of redox homeostasis, SOD1 has also been implicated in H_2O_2 mediated gene expression of redox and DNA damage related proteins (Tsang *et al.*, 2014; X. Li, Qiu, *et al.*, 2019), in which SOD1 was activated by DNA damage response (DDR) proteins ATM and Chk2 (Tsang *et al.*, 2014; Bordoni *et al.*, 2019). SOD1 is widely known to be mutated in amyotrophic lateral sclerosis (ALS), which results in protein dysregulation and insoluble aggregation of SOD1 in neuronal cells, ultimately leading to oxidative damage and neurotoxicity (Pansarasa *et al.*, 2018). Finally, to my knowledge, a role for SOD1 in mitosis has not been previously established. Taken together, I deemed SOD1 to be an interesting and promising target to examine in the context of mitotic DNA damage.

In this chapter, a thorough investigation was conducted to determine the role of SOD1 in the MDDC. The siRNA screen was validated to confirm SOD1's involvement in the checkpoint. Then as SOD1 is associated with both the oxidative stress and DNA damage responses, these were analysed further to determine which or how both interplay in the MDDC. Furthermore, SOD1's specific mechanism of action in the MDDC was explored, to aid in the clarification of the pathway responsible for the checkpoint.

The hypothesis of this chapter is:

SOD1 has a novel role in the response to DNA damage during mitosis, revealing the mechanism of the MDDC.

The aims of this chapter are:

1. To confirm SOD1 is involved in the response to DNA damage during mitosis.
2. To investigate SOD1's involvement in mitosis and the MDDC.

The objectives of this chapter are:

1. To validate the involvement of SOD1 in the MDDC via mitotic cell population, mitotic progression and complementation assays.
2. To determine how ROS affects SOD1's role in the MDDC.
3. To determine the effect of SOD1 on the DDR and DNA repair pathways.
4. To investigate the mechanism in which SOD1 functions within the MDDC.
5. To determine if the enzymatic or transcription factor capability of SOD1 is responsible for the phenotype observed via SOD1 functional mutants.

3.2 Results.

3.2.1 Assays to determine the MDDC.

To determine and validate proteins that have a role in the MDDC, it was important to establish assays that were capable of observing the checkpoint. An IR dose response was conducted to demonstrate the MDDC via mitotic cell population and mitotic progression assays.

Firstly, the mean cell cycle distribution and the mean mitotic population was determined through pHistone 3 (pH3) (serine 10) staining in combination with propidium iodide (PI) **(Figure 3.1A-C)**. Both IR doses analysed, 5 and 10 Gy significantly increased the mitotic population of HeLa cells after 16 hours compared to the untreated condition ($p = 0.0003$ and $p < 0.0001$ respectively), in a dose dependent manner. The same trend was observed when the mitotic progression following each IR dose was examined. Again, each dose of IR significantly increased the mean time for the completion of mitosis, compared to the untreated condition (5 Gy $p = 0.0037$ and 10 Gy $p < 0.0001$) **(Figure 3.1D)**.

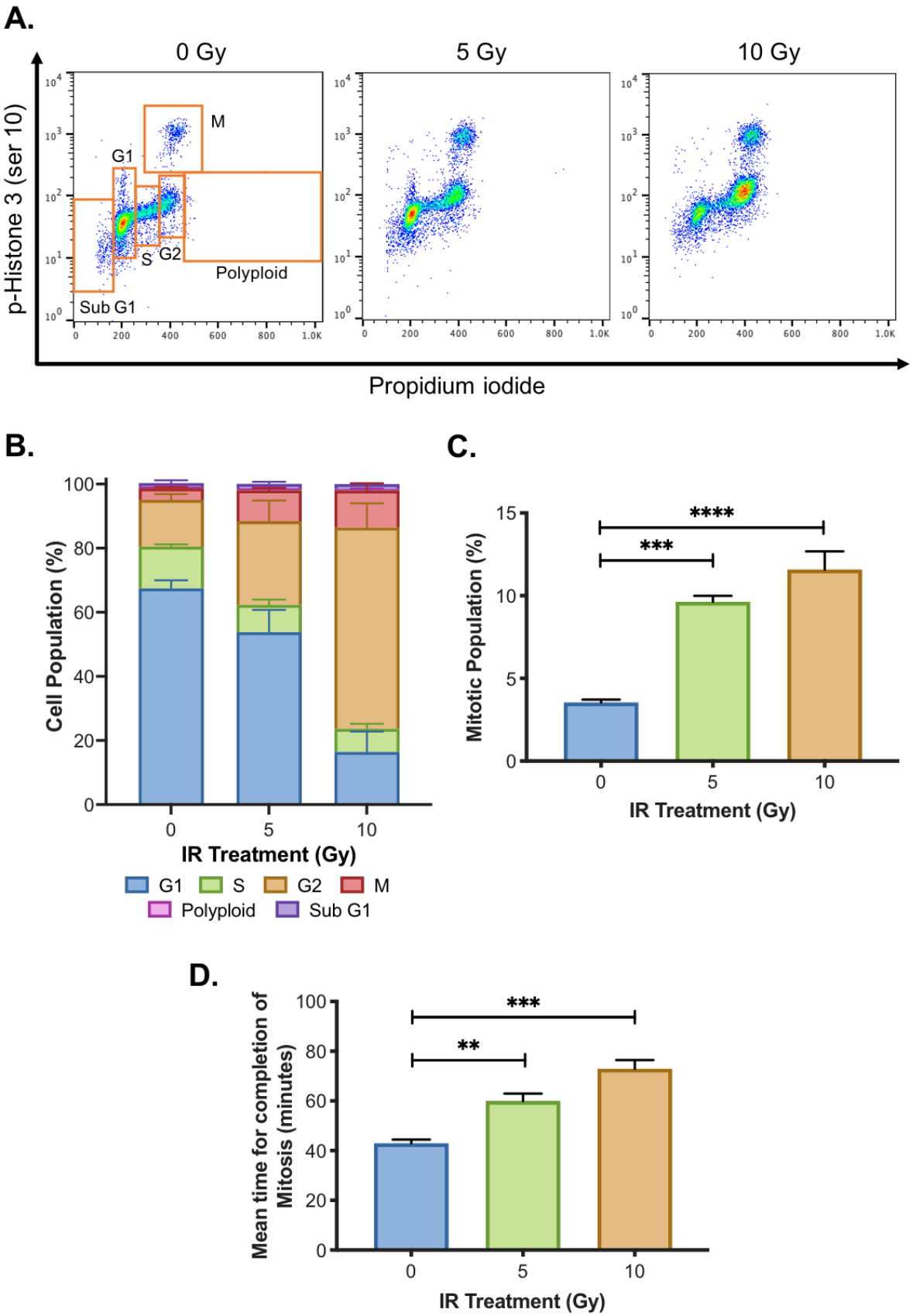

Figure 3.1: The analysis of the MDDC after IR treatment using the mitotic cell population and mitotic progression assays.

Legend on next page.

Figure 3.1: The analysis of the MDDC after IR treatment using the mitotic cell population and mitotic progression assays.

A. Representative HeLa FACs plots for FL1-H p-Histone 3 against FL3-H propidium iodide (PI) staining 16 hours post-IR treatment (0, 5 and 10 Gy). Gating examples are presented in orange on the untreated plot, where a minimum of 10,000 single cells was analysed and p-Histone 3 positivity quantified. **B.** Mean cell cycle phase distribution following 16 hours post-5 or 10 Gy IR treatment +/- SEM (N= 4). **C.** Mean mitotic cell population following each IR dose represented on a different scale for clarity +/- SEM (N= 4). One-way ANOVA with Dunnett's correction test for multiple comparisons was performed to determine statistical significance (*** denotes $p \leq 0.001$ and **** $p \leq 0.0001$). **D.** Time-lapse live cell microscopy analysis of the mean time taken to complete mitosis after each IR treatment. A maximum of 50 cells per condition were counted and the data represents the overall mean of each independent experiments +/- SEM (N= 4). One-way ANOVA with Dunnett's correction test for multiple comparisons was performed to determine statistical significance (** denotes $p \leq 0.01$ and *** $p \leq 0.001$).

These assays demonstrate the MDDC in an asynchronous cell population, uninfluenced by anti-mitotic agents such as nocodazole, which is common in other studies in this area (Smits *et al.*, 2000; Nitta *et al.*, 2004). This more natural approach supports the existence of the MDDC, which may provide a mechanism of tumour cell evasion to current anti-cancer therapeutics. Throughout this thesis, the MDDC is represented and assessed using mitotic cell population and mitotic progression assays, to identify proteins involved in the checkpoint.

3.2.2 SOD1 is required for the MDDC.

3.2.2.1 The validation of the role of SOD1 in the MDDC.

SOD1 was initially identified as a potential protein involved in the mitotic response to DNA damage via the siRNA DNA damage screen conducted in the Thompson laboratory **(Figure 1.9)**. It was also deduced from the literature that SOD1 is a promising hit to investigate further and to my knowledge has not previously been identified to have a role in mitosis or mitotic DNA damage. To confirm if SOD1 has a role in the MDDC, the assays discussed in section **3.2.1** were performed to analyse the MDDC following SOD1 knockdown.

Firstly, the siRNA knockdown of SOD1 was optimised through western blot analysis. The efficiency of the knockdown was determined for the smart pool and the four deconvoluted siRNAs for SOD1. It was concluded that siSOD1-5 and siSOD1-7 were consistently most effective at reducing SOD1 protein levels **(Figure 3.2A)**.

Then the mean cell cycle distribution analysis through pH3 and PI co-staining was conducted using all siRNAs, to assess the effect of SOD1 depletion on the cell cycle and the mitotic population in the absence and presence of IR (16 hours post-10 Gy IR) **(Figure 3.2B-C)**. There was no significant effect of SOD1 knockdown on the mitotic cell population in the untreated conditions. As expected, there was a significant enrichment in the mitotic population following IR treatment compared to untreated cells ($p < 0.0001$) in the siControl condition **(Figure 3.2C)**. Following the induction of DNA damage all SOD1 siRNA's but siSOD1-8, significantly reduced the mitotic cell population compared to the treated siControl condition ($p < 0.0001$ for each siRNA). The degree to which siSOD1-5, siSOD1-7 and siSOD1-8 affected the mitotic population following DNA damage, corresponds to the efficiency of the knockdown observed via western blot analysis. For future experiments, siSOD1-5 and siSOD1-7 were used.

Finally, mitotic progression following SOD1 knockdown in untreated and irradiated cells (5 Gy) was quantified via time-lapse microscopy **(Figure 3.2D-G)**. In support of the cell cycle analysis **(Figure 3.2B-C)**, in untreated HeLa cells, there was no effect of SOD1 depletion on the time required for the completion of mitosis, compared to the siControl condition **(Figure 3.2D)**. However, upon the induction of DNA damage via IR treatment, conditions depleted of SOD1 (siSOD1-5 and siSOD1-7) shown a significantly reduced mitotic transit time compared to the treated siControl in cancerous HeLa (both $p < 0.0001$) **(Figure 3.2E)** and MCF7 cells (both $p< 0.0001$) **(Figure 3.2F)**. A similar response was observed in the non-cancerous cell line MRC5VA, yet only siSOD1-5 significantly reduced the mitotic transit time compared to the siControl condition ($p= 0.0054$) **(Figure 3.2G)**. Furthermore, it is of interest that the depletion of SOD1 following DNA damage significantly reduced the mitotic transit time compared to the untreated SOD1 knockdown conditions in HeLa cells (siSOD1-5 untreated vs siSOD1-5 irradiated $p = 0.033$ and siSOD1-7 untreated vs siSOD1-7 irradiated $p = 0.0477$) **(Figure 3.2D-E)**. Then siBubR1 was included in each live cell microscopy

experiment as the positive control, which as expected, significantly reduced the mitotic completion time in the untreated and irradiated HeLa cells compared to the siControl ($p = 0.0004$ and $p < 0.0001$ respectively) and in MCF7 ($p < 0.0001$) and MRC5VA cells ($p < 0.0001$).

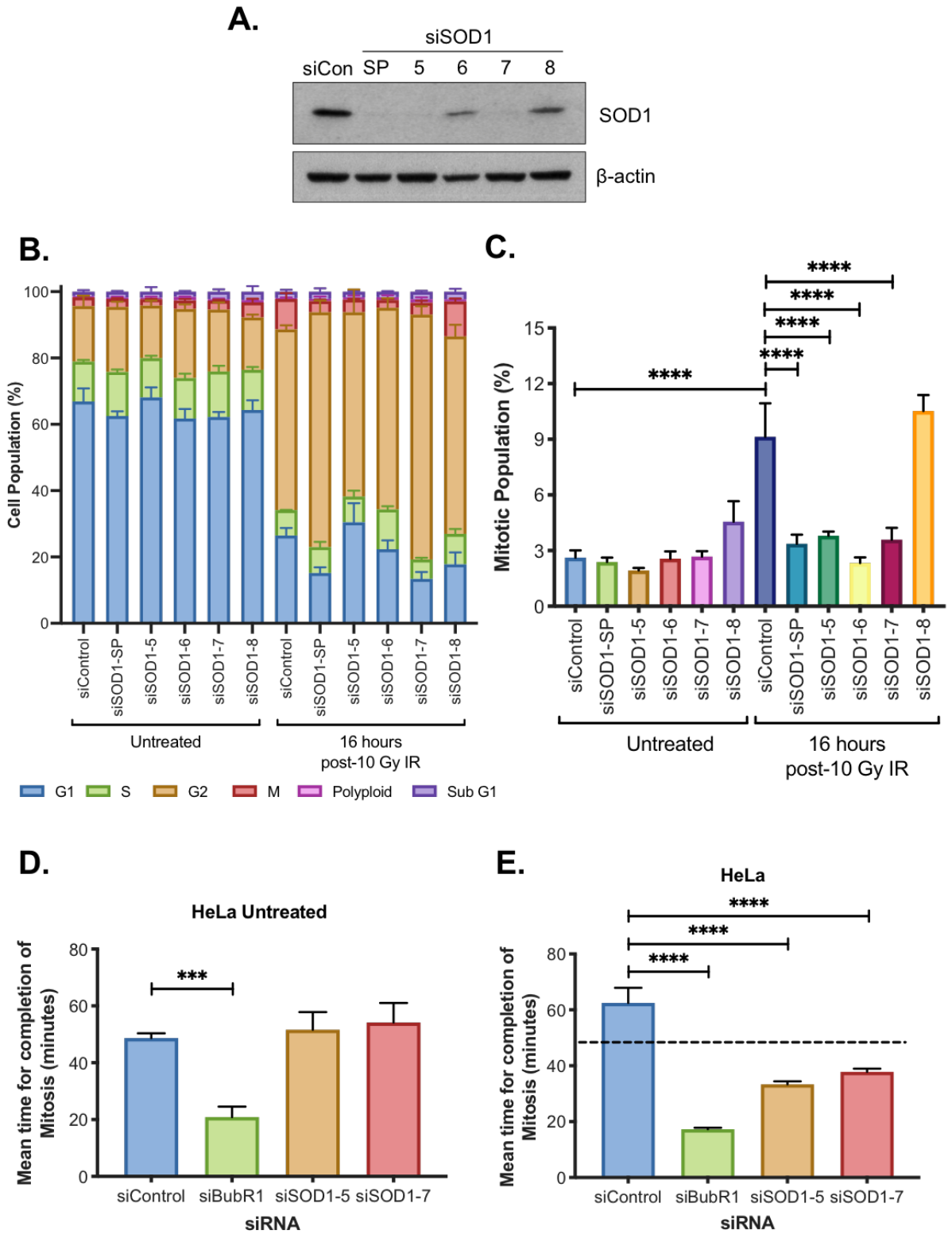

Figure 3.2: The optimisation of SOD1 knockdown and the analysis of the MDDC in the absence of SOD1 following DNA damage.

Legend on next page.

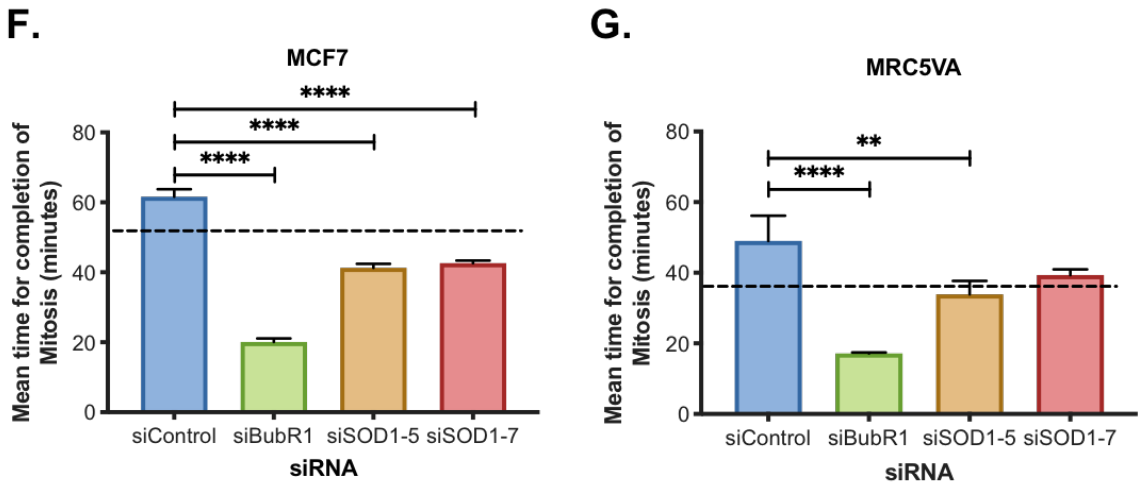

Figure 3.2: The optimisation of SOD1 knockdown and the analysis of the MDDC in the absence of SOD1 following DNA damage.

A. A representative western blot showing the levels of SOD1 and β-actin after transfection with each siRNA (siControl and siSOD1 smart pool (SP) and individual SOD1 siRNA's 5-8) (N= 3). **B.** Mean cell cycle phase distribution following SOD1 depletion with a control siRNA, in untreated cells or 16 hours post-10 Gy IR treatment +/- SEM (N= 3). **C.** Mean mitotic cell population following transfection with each siRNA and 16 hours post-10 Gy IR treatment represented on a different scale for clarity +/- SEM (N= 3). One-way ANOVA with Dunnett's correction test for multiple comparisons was performed to determine statistical significance (**** denotes $p \leq 0.0001$). **D.** Time-lapse live cell microscopy analysis of the mean time taken to complete mitosis after BubR1 (positive control) or SOD1 knockdown (siSOD1-5 and -7) in untreated HeLa cells. A maximum of 50 cells for each siRNA was counted and the data represents the overall mean of each independent experiments +/- SEM (N= 3). One-way ANOVA with Dunnett's correction test for multiple comparisons was performed to determine statistical significance (*** denotes $p \leq 0.001$). **E.** as in **D.** with the exception of HeLa cells were treated with 5 Gy IR (+/- SEM, N= 3). One-way ANOVA with Dunnett's correction test for multiple comparisons was performed to determine statistical significance (**** denotes $p \leq 0.0001$). **F.** as in **E.** with the exception of MCF7 cells were treated with 5 Gy IR (+/- SEM, N= 3). One-way ANOVA with Dunnett's correction test for multiple comparisons was performed to determine statistical significance (**** denotes $p \leq 0.0001$). **G.** as in **E.** with the exception of MRC5VA cells were treated with 5 Gy IR (+/- SEM, N= 3). One-way ANOVA with Dunnett's correction test for multiple comparisons was performed to determine statistical significance (** denotes $p \leq 0.01$ and **** $p \leq 0.0001$). The dotted lines indicate the untreated transit time of the corresponding cell line, **E.** HeLa; 48 minutes, **F.** MCF7; 53 minutes and **G.** MRC5VA; 36 minutes.

Therefore, SOD1 was required for the prolonged mitotic transit observed following DNA damage induced by IR treatment, validating an involvement in the MDDC.

3.2.2.2 SOD1 is involved in the DNA damage response in mitosis following treatment with DDR and oxidative stress inducing agents.

Next, alternative DNA damage inducing chemotherapeutics agents were examined, such as the alkylating reagents, carboplatin and temozolomide (TMZ). Carboplatin is a derivative of cisplatin and binds to DNA to form inter- and intra-DNA adducts which cause DSBs (Galluzzi *et al.*, 2014). TMZ forms various methylation lesions on the DNA bases, which can result in SSBs and DSBs (Erasimus *et al.*, 2016). Both chemotherapeutic agents would first determine if other DNA damage inducing treatments activate the MDDC and also reveal if the response to these agents is SOD1 dependent.

Time-lapse live cell microscopy was conducted to determine the effect of carboplatin and TMZ on the mitotic progression in the presence and absence of SOD1. Both the treatment with carboplatin and TMZ significantly increased the mitotic transit time compared to the untreated siControl condition ($p = 0.0022$ and $p = 0.0004$ respectively) **(Figure 3.3)**. Furthermore, upon the knockdown of SOD1, there was a significant reduction in the time taken to complete mitosis after both carboplatin and TMZ treatment compared to the treated siControl condition (both $p < 0.0001$) **(Figure 3.3)**. The DNA damage inducing agents produced a similar response observed following IR treatment (siControl untreated vs siControl irradiated $p = 0.0015$ and siControl irradiated vs siSOD1 irradiated $p < 0.0001$), which was included to provide a direct comparison **(Figure 3.3)**.

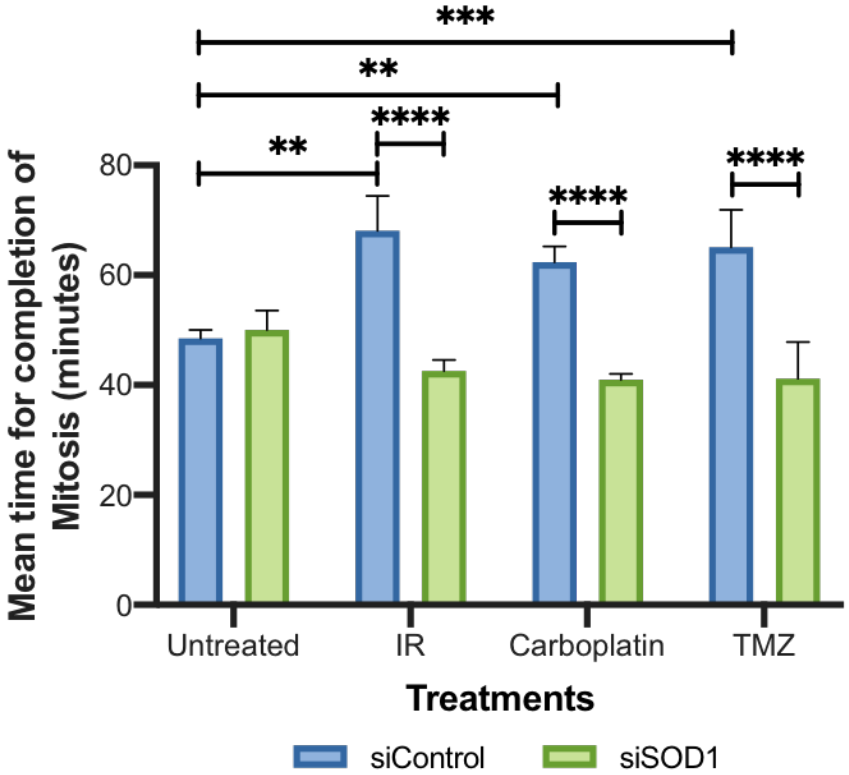

Figure 3.3: The analysis of chemotherapeutics on the MDDC in the absence of SOD1. Time-lapse live cell microscopy analysis of the mean time taken to complete mitosis following SOD1 knockdown (siSOD1-5) in HeLa cells treated with IR (5 Gy), carboplatin (1 μM) and TMZ (1 μM) approximately 2-4 hours prior to the initiation of the experiment. A maximum of 50 cells for each condition was counted and the data represents the overall mean of each independent experiments +/- SEM (N= 3). One-way ANOVA with Dunnett's correction test for multiple comparisons was performed to determine statistical significance (** denotes $p \leq 0.01$, *** $p \leq 0.001$ and **** $p \leq 0.0001$).

In summary, both chemotherapeutic agents activated the MDDC in a SOD1 dependent manner.

Then as the primary function of SOD1 is as an antioxidant enzyme, it was of interest to determine if oxidative stress inducing agents had any effect on the MDDC and if SOD1 was required for any cell cycle arrest observed. The oxidative stress inducing agents H_2O_2 and pyocyanin were administered to cells to test this. Pyocyanin is an agent produced by *P. aeruginosa* and is a known $O_2^{\bullet-}$ and H_2O_2 radical producer, most likely due to damage to the mitochondria and reduction of H_2O_2 detoxifying enzyme,

catalase expression (O'Malley *et al.*, 2003). Therefore, this agent would activate SOD1 antioxidant activity. Whereas H_2O_2 is a cellularly stable and a common type of ROS, which is known to be involved in many cellular processes and signalling pathways (Harris and Denicola, 2020). Furthermore, this is the product of the dismutase reaction of $O_2^{\bullet-}$ by SOD1. These oxidative stress inducing agents were tested in the presence and absence of SOD1 and the effects on mitotic progression were assessed via time-lapse live cell microscopy **(Figure 3.4)**.

Pyocyanin increased the mitotic transit time in the siControl condition **(Figure 3.4A)**. Then in the absence of SOD1, there was a reduction in the mean mitotic completion time after pyocyanin treatment compared to the siControl treated condition. Despite this effect being deemed non-significant, the trend observed was similar to treatment with DDR inducing agents. For H_2O_2, different doses (0-500 μM) were administered to HeLa cells and the effect on mitosis was assessed **(Figure 3.4B)**. Most doses (50, 100 and 500 μM) in the siControl condition, exhibited a significant increase in mean mitotic transit time compared to the untreated siControl condition (siControl untreated vs siControl 50 μM; $p = 0.0216$, siControl untreated vs siControl 100 μM; $p = 0.0244$ and siControl untreated vs siControl 500 μM; $p = 0.002$). However, the same trend was observed after 25 and 200 μM H_2O_2 treatment. All H_2O_2 doses increased the mitotic transit time to similar levels. Furthermore, in the absence of SOD1 there was a reduction in mean mitosis completion time in the majority of H_2O_2 doses administered compared to the corresponding siControl treated condition, with exception of 500 μM treatment potentially due to an increase in toxicity. However, this effect was only significant following 50 μM ($p < 0.0022$) H_2O_2, which was used for future experimentation.

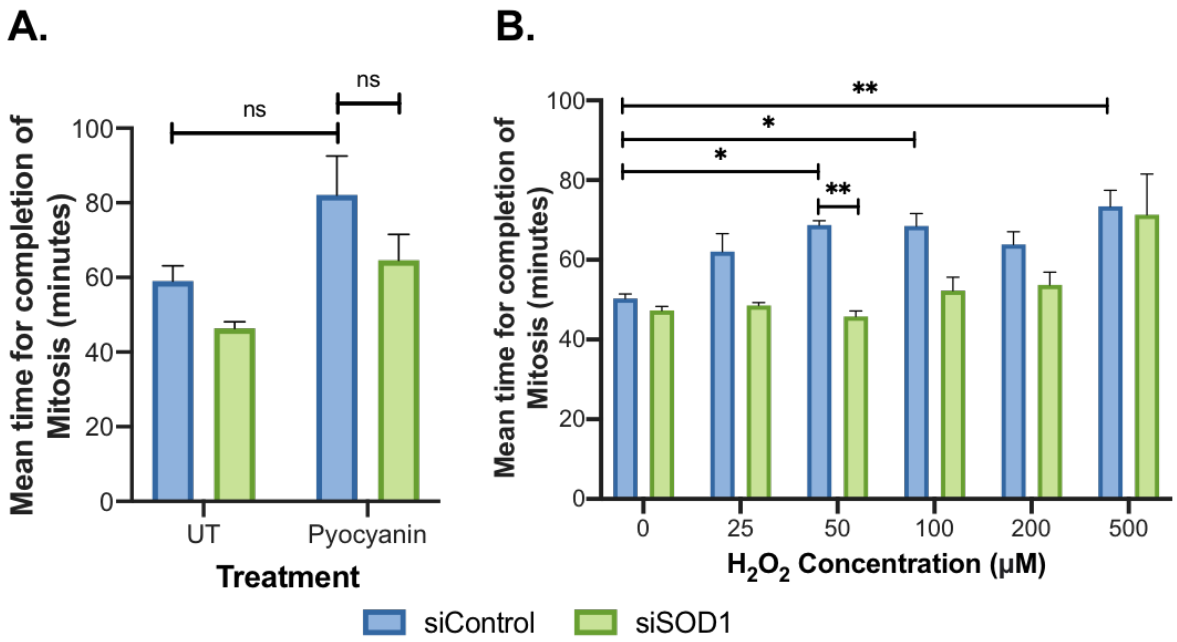

Figure 3.4: The analysis of ROS inducing agents in the absence of SOD1 on the MDDC. **A.** Time-lapse live cell microscopy analysis of the mean time taken to complete mitosis following SOD1 knockdown (siSOD1-5) in HeLa cells treated with pyocyanin (50 μM) 2 hours prior to the initiation of the experiment. A maximum of 50 cells for each condition was counted and the data represents the overall mean of each independent experiment +/- SEM (N= 3). One-way ANOVA with Dunnett's correction test for multiple comparisons was performed to determine statistical significance (ns denotes p = non-significant). **B.** as in **A.** with the exception HeLa cells treated with 0-500 μM H_2O_2 2 hours prior to the initiation of the experiment (+/- SEM N= 4). One-way ANOVA with Dunnett's correction test for multiple comparisons was performed to determine statistical significance (* denotes $p \leq 0.05$ and ** $p \leq 0.01$).

Therefore, oxidative stress inducing agents activated the MDDC in a SOD1-dependent manner, similarly to DNA damage inducing agents.

Next, the effect of H_2O_2 (50 μM) and IR (5 Gy) treatments on mitotic progression following SOD1 knockdown was analysed further. The cell cycle phase and cellular fate were represented for each cell assessed throughout the imaging period **(Figure 3.5)**. The delay in mitotic transit was observed throughout the imaging period (over 16 hours) after each treatment in the siControl condition. In SOD1 knockdown cells following treatment with H_2O_2 and IR, the reduction in mitotic transit time was clearly visible and also occurred throughout the entire experiment. Furthermore, this alternate

data analysis allowed the cellular fate of each condition to be visualised. The majority of cells were viable and proceeded into interphase after mitosis. Few cells died in mitosis or died after division and these fates did not correspond to a particular condition.

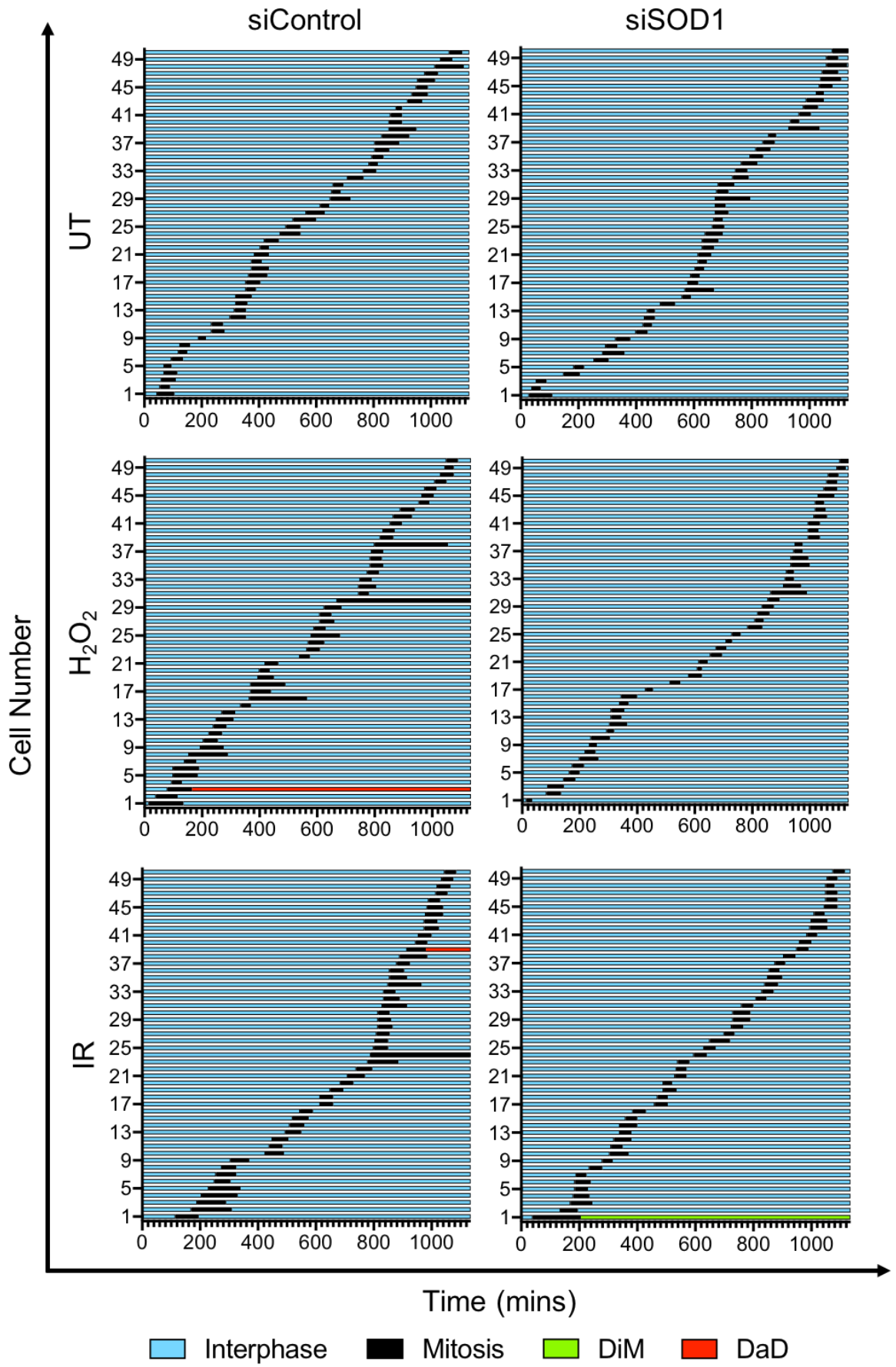

Figure 3.5: The analysis of mitotic progression and cell fate of each cell.

Legend on next page.

Figure 3.5: The analysis of mitotic progression and cell fate of each cell.
Re-analysis of previous time-lapse live cell microscopy data representing when mitosis occurred and the resulting cellular fate following SOD1 knockdown (siSOD1-5) in HeLa cells treated with H_2O_2 (50 μM) and IR (5 Gy). A maximum of 50 cells for each condition was counted and the initiation and completion of mitosis were presented in time order for one experimental repeat (N=1). The time the cell was in mitosis is represented in black and the interphase is shown in blue. Alternative cellular fates including dead in mitosis (DiM) is shown in green and dead after division (DaD) in red.

The delay in mitosis was observed following H_2O_2 and IR treatment of interphase cells. This suggests that these damaged cells are evading the interphase DDR checkpoints and relying upon the MDDC. As the majority of cells continue to cycle into interphase following mitosis, this indicates that the cells may experience a degree of repair in mitosis.

3.2.2.3 The effect of SOD1 knockdown on the MDDC can be rescued with the addition of an exogenous SOD1 protein.

In order to confirm the role of SOD1 in mitotic progression following DNA damage and ROS inducing treatments, a complementation experiment using an exogenous form of SOD1 was optimised. Typically, an siRNA for the 3' untranslated non-coding region (UTR) of the gene of interest is used to deplete the cells of the endogenous protein and instead an exogenous protein, via a gene expression vector that does not feature a 3'UTR is expressed within the cell. This will rescue the phenotype and mimic the desired control condition, providing evidence in support of the protein of interest specifically causing the effect being assessed. Six 3'UTR siRNAs for SOD1 (Qiagen) were thoroughly examined to knockdown endogenous SOD1 (Appendix **Figure 7.1**). Despite this, none of the siRNAs tested produced a consistent or efficient knockdown of SOD1 and there were no alternative commercially available 3'UTR siRNAs for SOD1 to examine. Therefore, it was concluded that the siSOD1-5 siRNA would be used for the rescue experiment. However, this targets the coding region of the gene and would affect the endogenous and exogenous forms of SOD1.

To overcome this, a codon optimised SOD1 sequence was generated using the GenSmart™ Codon optimisation tool by GenScript. This also manipulated the sequence complementary for siSOD1-5, resulting in a siRNA resistant SOD1 protein whilst ensuring SOD1 function. Eurofins synthesised the optimised *SOD1* gene and insert it into a pEX-A128 vector. In preparation for the rescue using the 3'UTR siRNA, a Myc-SOD1 expression vector in a pCMV6 plasmid was purchased from Origene. As this exogenous protein would be targeted by siSOD1-5, the optimised SOD1 was subcloned into the pCMV6 plasmid featuring a Myc-Tag to allow differentiation of endogenous and exogenous forms of SOD1. This wildtype (WT) exogenous form of SOD1 was then termed Myc-SOD1^{WT}. Optimisation of the rescue experiment using siSOD1-5 and Myc-SOD1^{WT} was conducted to obtain efficient knockdown and overexpression of the variations of the SOD1 proteins (Appendix **Figure 7.2**).

Firstly, to ensure that the simultaneous knockdown of SOD1 and expression of Myc-SOD1^{WT} was effective, the protein levels were examined through western blot analysis. It was deduced that the appropriate knockdown and overexpression for each condition was consistently achieved **(Figure 3.6A)**. SOD1 complementation experiments were conducted for mitotic progression assays following treatment with both IR (5 Gy) **(Figure 3.6B)** and H_2O_2 (50 μM) **(Figure 3.6C)**. An empty Myc-Tagged expression vector was used as a control vector. Overall, the same results were obtained following both treatments. As expected, there was a significant increase in mitotic transit time after IR and H_2O_2 treatment in the siControl conditions in the absence and presence of both the control vector and Myc-SOD1^{WT}, compared to the untreated siControl conditions (all $p < 0.0001$). Moreover, as previously observed there was a significant reduction in mitotic transit time in the absence of SOD1 following IR and H_2O_2 treatments compared to the corresponding siControl treated conditions (both $p < 0.0001$) and in the same conditions with the addition of the control vector (both $p < 0.0001$). Then the complementation with Myc-SOD1^{WT} following SOD1 knockdown and each treatment significantly increased the mean mitotic transit time, compared to the corresponding siControl untreated conditions (both $p < 0.0001$) and similarly to the other treated siControl conditions.

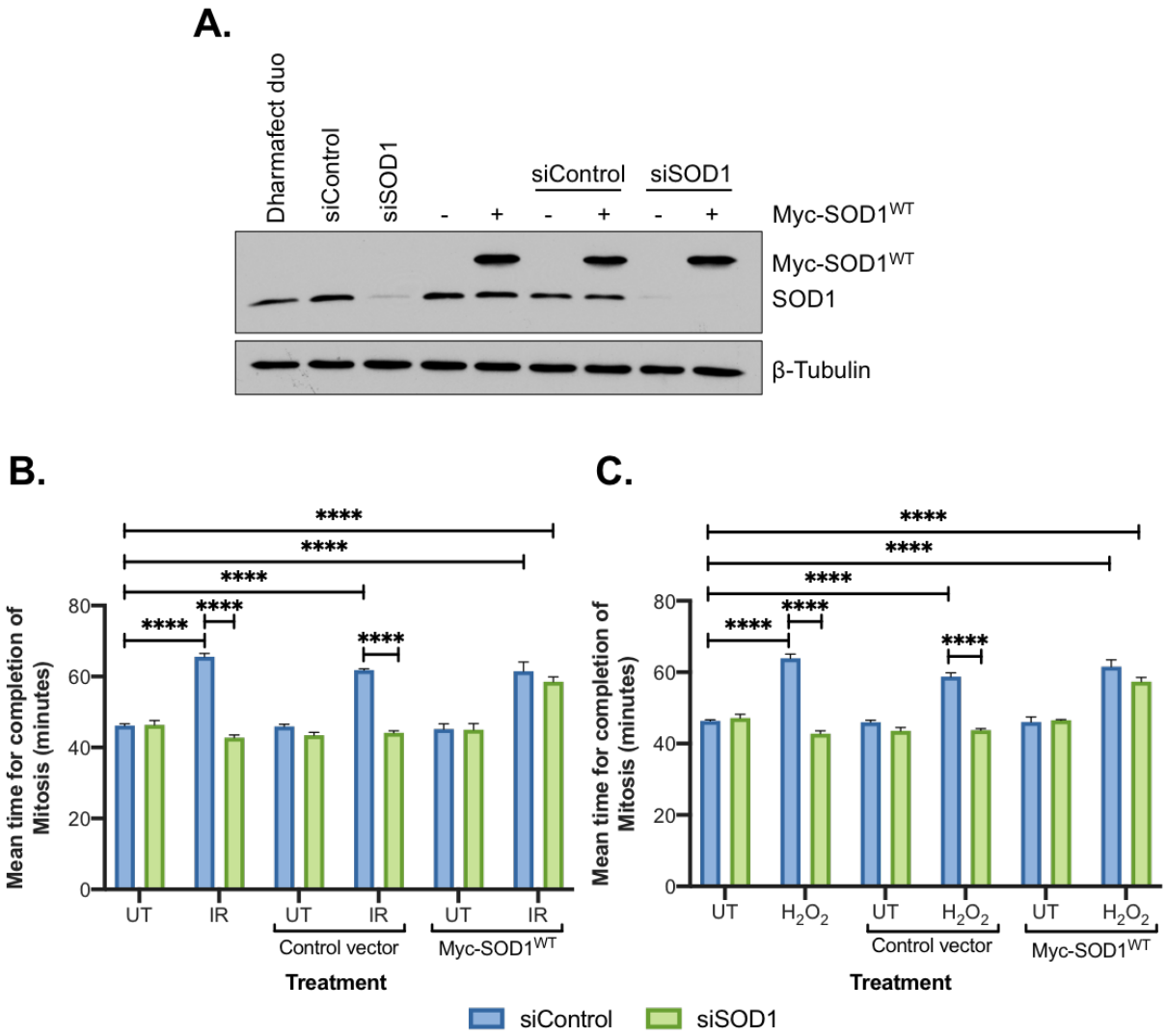

Figure 3.6: The complementation of SOD1 restored the mitotic arrest observed after IR and H_2O_2 treatment.

A. Representative western blot showing the knockdown and overexpression of SOD1 using siSOD1-5 and Myc-SOD1^{WT} (N= 2). Extracts were probed for SOD1, Myc-Tag to represent Myc-SOD1^{WT} and β-Tubulin. **B.** Time-lapse live cell microscopy analysis of the mean time taken to complete mitosis following SOD1 knockdown (siSOD1-5) and complementation with 250 ng Myc-SOD1^{WT} in HeLa cells treated with IR (5 Gy). A maximum of 50 cells for each condition was counted and the data represents the overall mean of each independent experiment +/- SEM (N= 3). One-way ANOVA with Dunnett's correction test for multiple comparisons was performed to determine statistical significance (**** denotes $p \leq 0.0001$). **C.** as in **B.** with the exception of HeLa cells treated with 50 μM H_2O_2 2 hours prior to the initiation of the experiment +/- SEM (N= 3). One-way ANOVA with Dunnett's correction test for multiple comparisons was performed to determine statistical significance (**** denotes $p \leq 0.0001$).

Overall, it can be concluded that SOD1 is required for the prolonged mitotic transit observed following DNA damage, hence involved in the MDDC.

3.2.3 ROS levels do not impact the MDDC.

3.2.3.1 ROS levels were investigated after treatment with DNA damage and oxidative stress inducing agents.

It was demonstrated that both DNA damaging agents and oxidative stress inducers activated the MDDC in a SOD1 dependent manner. This highlights the involvement of the DDR and oxidative stress pathways in mitosis, potentially via the induction of oxidative DNA damage. To determine if the SOD1-dependent mitotic arrest was due to oxidative damage, the ROS levels were quantified after each treatment and it was investigated how the depletion of SOD1 impacted these levels.

A fluorescence chloromethyl-2',7'-dichlorodihydrofluorescein diacetate (CM-H2DCFDA) probe (Invitrogen) was used to detect general ROS levels. This probe was effective at determining the ROS levels after differing doses of H_2O_2 (0-500 μM). The fluorescent ROS intensity increased to different degrees after 50-500 μM H_2O_2 **(Figure 3.7A)**. However, only the higher H_2O_2 doses (200 μM and 500 μM) tested, significantly increased the ROS levels in siControl conditions ($p = 0.0417$ and $p < 0.0001$ respectively). The ROS levels were reduced in the absence of SOD1 compared to comparative siControl conditions of each H_2O_2 dose, but not to a significant degree.

Furthermore, the ROS intensity following IR treatment (5 and 10 Gy) slightly increased in siControl conditions **(Figure 3.7B)**. Whereas carboplatin and TMZ did not affect ROS intensity. Then the absence of SOD1 appeared to reduce the level of ROS caused by treatment with TMZ and both IR doses, compared to the siControl corresponding conditions. Overall, the levels of ROS exhibited from DNA damaging agents was much lower than the levels produced by H_2O_2.

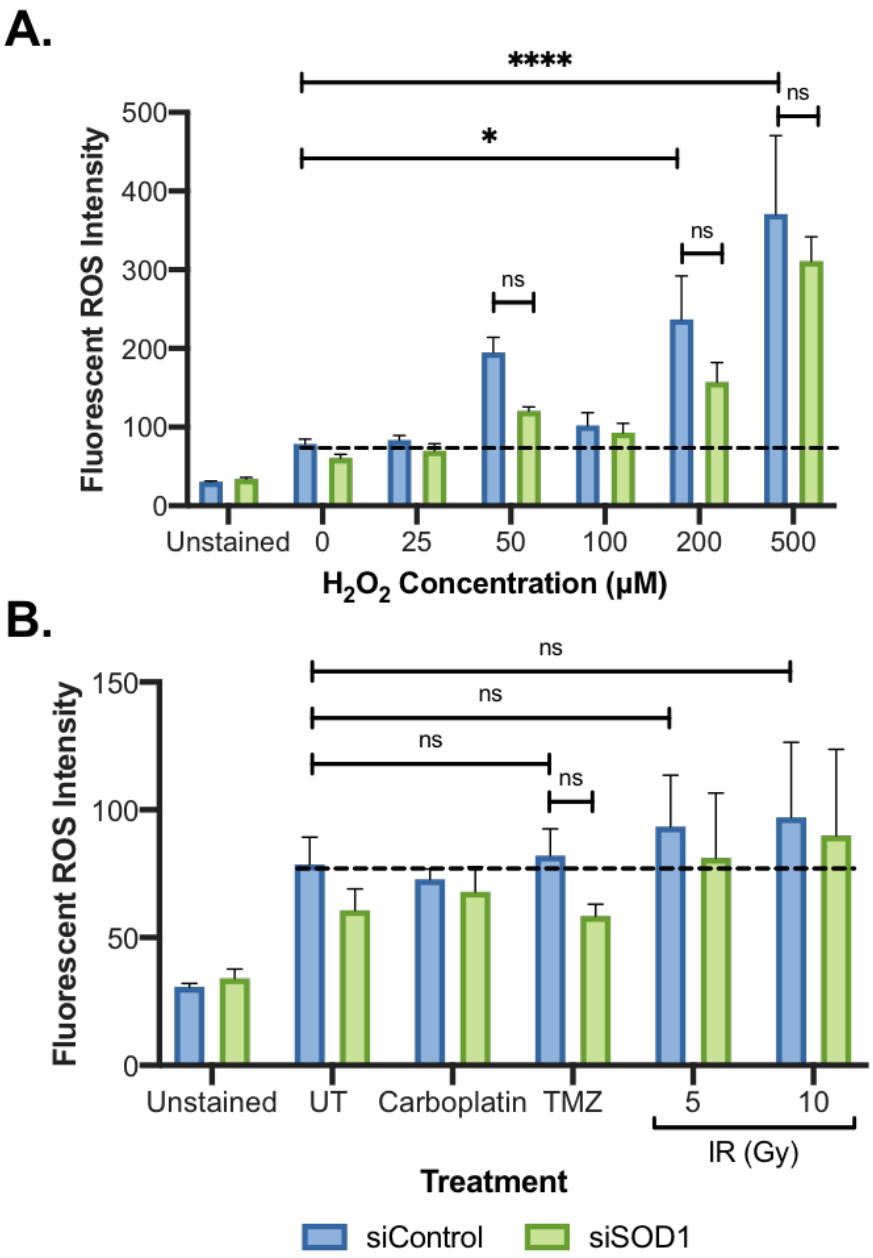

Figure 3.7: The analysis of ROS levels after treatment with H_2O_2, IR, carboplatin and TMZ.

A. HeLa cells fluorescent ROS intensity was analysed after treatment with H_2O_2 (0-500 μM) for 1 hour and in the presence of siSOD1-5. The dotted line represents the ROS levels in the untreated control for comparison. Each condition was measured in triplicate, averaged and normalised against the unstained control for each independent repeat +/- SEM (N= 3), courtesy of Priya Lata. One-way ANOVA with Dunnett's correction test for multiple comparisons was performed to determine statistical significance (* denotes $p \leq 0.05$ and **** $p \leq 0.0001$). **B.** as in **A.** with the exception of HeLa cells treated with Carboplatin (1 μM), TMZ (1 μM) and IR (5 and 10 Gy) for 1 hour prior to the reading the fluorescent intensity +/- SEM (N= 3). One-way ANOVA with Dunnett's correction test for multiple comparisons was performed to determine statistical significance (ns denotes p = non-significant).

As expected, there was an increase in ROS levels following H_2O_2 treatment. However, the chemotherapeutics assessed, TMZ and carboplatin are not well recognised to produce ROS, which was exemplified in these findings. The absence of SOD1 reduced ROS levels, predominantly following H_2O_2 treatment. Furthermore, a more SOD1 specific ROS probe was used to analyse these treatments further, which measured $O_2^{\bullet-}$ radicals (ENZO). However, there was no consistent increase in $O_2^{\bullet-}$ levels following any treatment, but a unified increase was observed following SOD1 knockdown (data not shown). Overall, these findings suggest that the SOD1-dependent activation of the MDDC was not due to a redox imbalance.

3.2.3.2 Selenium rescued the mitotic transit time following treatment with DNA damage and oxidative stress inducing agents.

To further analyse the effect of ROS levels on mitotic progression following the various treatments used in this research, it was proposed that an investigation into the effect of the reduction of the intracellular ROS concentration was performed and the effect on mitotic transit examined. First, supplementation with the commonly used antioxidant N-Acetyl-L-cysteine (NAC) was assessed in this research. NAC is a precursor of the non-enzyme antioxidant glutathione, so increases H_2O_2 detoxification through the increase of glutathione synthesis and the enhancement of antioxidant glutathione peroxidase (GPx) enzymes activity (Lauterburg, Corcoran and Mitchell, 1983). However, in this thesis, the NAC was deemed unsuitable to test mitotic progression as it produced inconsistent data (data not shown), potentially due to the toxicity induced following the variety of doses examined (0.01-10 mM) and in the literature NAC has been demonstrated to arrest cells in G1 (Liu, Wikonkal and Brash, 1999; Kim *et al.*, 2001).

Alternatively, supplementation of cells with selenium was utilised as the mechanism to reduce the intracellular ROS concentration. Selenium is important in the detoxification of H_2O_2, as it is a key component of the GPx enzyme family. The element resides in the enzyme active site with cysteine, to form a selenocysteine active site (Rotruck *et al.*, 1973). Selenium reacts with H_2O_2 undergoing oxidation and this is ultimately recovered via reduction to its active state through reactions with the co-factor glutathione (Bhowmick and Mugesh, 2015). Enrichment of the intracellular

concentration of selenium is known to positively impact the transcription and activity of the GPx enzymes, specifically GPx1 (Jerome-Morais *et al.*, 2013). Therefore, the level of H_2O_2 clearance will be enhanced, reducing intracellular ROS levels.

Firstly, the most effective selenium concentration was determined via the administration of a series of selenium concentrations (0-200 nM) to HeLa cells for 72 hours and GPx1 protein levels were analysed **(Figure 3.8)**. It was deduced that all selenium doses enhanced GPx1 expression, but 50 nM of selenium was most efficient and was used for future experimentation. GPx1 protein levels reduced slightly following the higher doses of 100 and 200 nM of selenium.

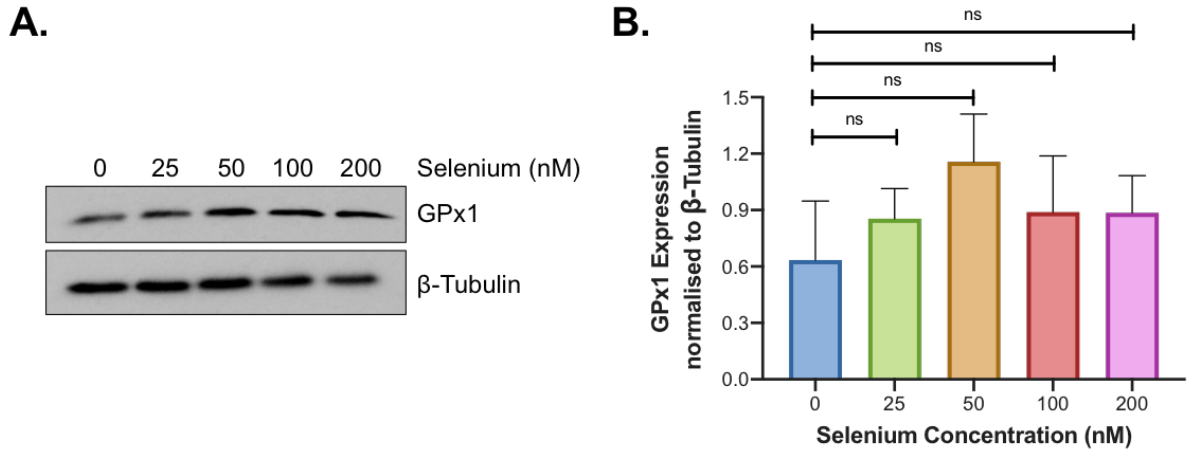

Figure 3.8: The optimal doses of selenium to enhance GPx1 expression.

A. A representative western blot of whole cell extracts of HeLa cells cultured in the presence of selenium (0-200 nM) for 72 hours (N= 3). Extracts were probed with GPx1 and β-Tubulin (control) antibodies. **B.** The relative expression of GPx1 compared to β-Tubulin expression was calculated from western blot images via measuring the band densitometries in FIJI. Each condition for three independent repeats was measured to give the overall expression of GPx1 +/- SD. Significance was determined using a One-way ANOVA with Dunnett's multiple comparisons (ns denotes p = non-significant).

Next, the effect of selenium (50 nM) on mitotic progression was analysed with H_2O_2 (50 μM), IR (5 Gy), TMZ (1 μM) and carboplatin (1 μM) treatments, in the presence and absence of SOD1. This would determine the impact of the reduction of intracellular ROS on mitotic transit and test if SOD1 was required for any effect observed. Additionally, the fluorescent ROS intensity was measured to complement the mitotic

progression assays. This would reveal the levels of ROS after each treatment and how the ROS concentration was impacted by both selenium and SOD1.

As expected, the treatment of siControl cells with H_2O_2 **(Figure 3.9A)**, IR **(Figure 3.9C)**, carboplatin **(Figure 3.9E)** and TMZ **(Figure 3.9G)** significantly increased the mean mitotic transit time compared to siControl untreated HeLa cells (all $p < 0.0001$). As well as the absence of SOD1 causing a significant reduction in mitotic duration after each treatment compared to the corresponding siControl treated conditions (all $p < 0.0001$). Overall, selenium alone did not affect mitotic duration in either the presence or absence of SOD1 in untreated cells. However, the selenium supplementation significantly reduced the mean mitotic transit time to similar to untreated cells, in combination with all treatments analysed in the siControl conditions, compared to the corresponding treated siControl conditions alone (all $p < 0.0001$). Finally, selenium in combination with each treatment had no additional effect in the absence of SOD1.

The ROS intensity was significantly increased following H_2O_2 treatment, despite the SOD1 status of the cells and selenium supplementation (siControl untreated vs siControl H_2O_2; $p < 0.0001$, siControl untreated vs siSOD1 H_2O_2; $p < 0.0001$, siControl untreated vs siControl combination; $p = 0.0003$ and siControl untreated vs siSOD1 combination; $p = 0.0002$) **(Figure 3.9B)**. Selenium appeared to slightly reduce ROS levels between the siControl H_2O_2 treatment alone and combination conditions **(Figure 3.9B)**. Whereas the absence of SOD1 did not affect the average ROS intensity in the presence of H_2O_2 or the combined treatment **(Figure 3.9B)**. Then all conditions treated with IR slightly increased the average ROS concentration **(Figure 3.9D)**. However, there was no effect of selenium supplementation on ROS levels after IR in siControl conditions. The absence of SOD1 indicated a slight reduction in ROS levels compared to the siControl after IR, yet selenium did not affect this **(Figure 3.9D)**. Carboplatin alone and in combination with SOD1 knockdown and/or selenium did not affect the average ROS intensity **(Figure 3.9F)**. Whereas the average ROS intensity appeared to slightly decrease following all TMZ treated conditions regardless of SOD1 status and/or selenium **(Figure 3.9H)**.

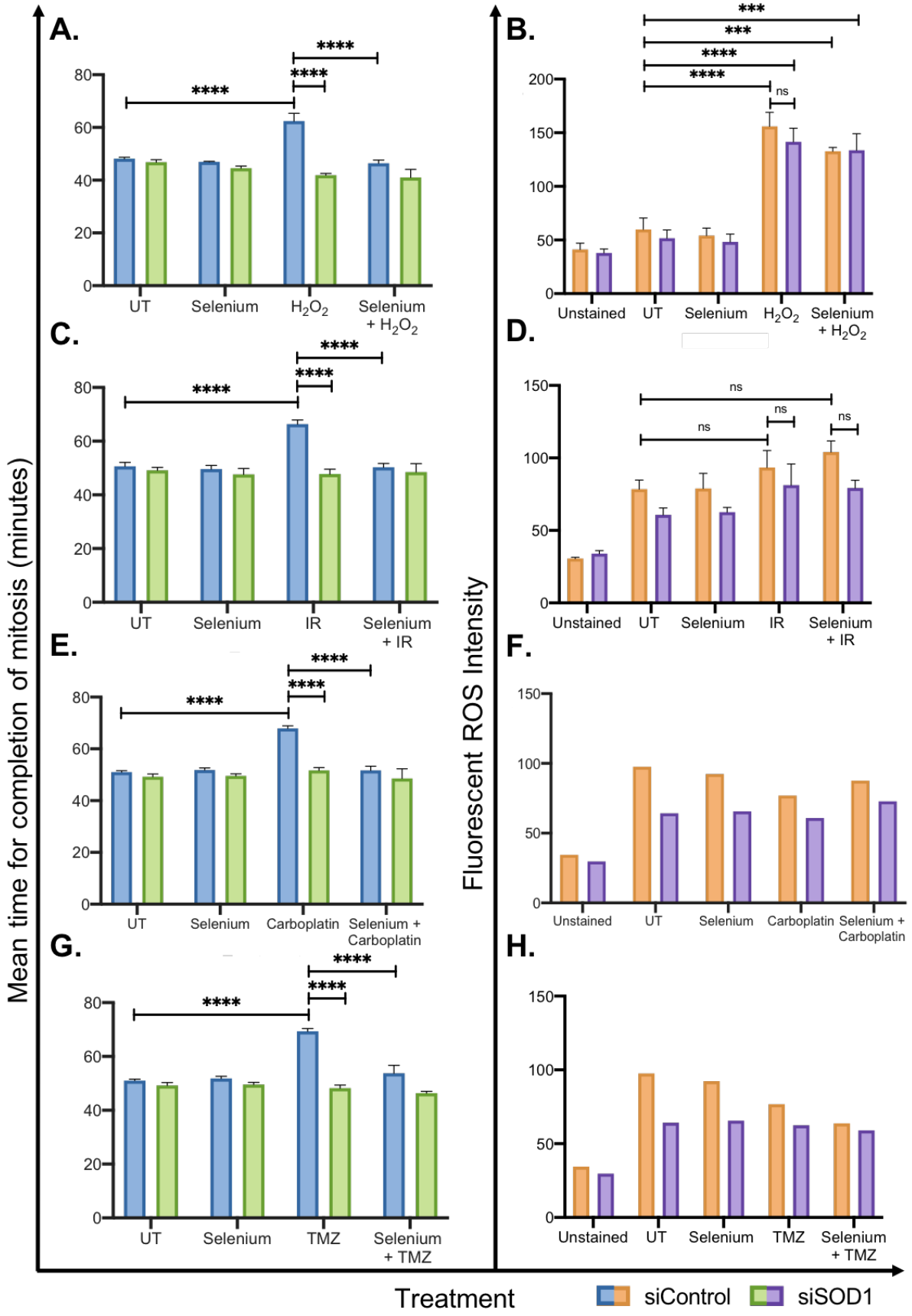

Figure 3.9: The effect of selenium supplementation on mitotic progression and intracellular ROS levels after varying treatments.

Legend on next page.

Figure 3.9: The effect of selenium supplementation on mitotic progression and intracellular ROS levels after varying treatments.

Time-lapse live cell microscopy analysis of the mean time taken to complete mitosis following SOD1 knockdown (siSOD1-5) in HeLa cells treated with **A.** 50 μM H_2O_2, **C.** 5 Gy IR, **E.** 1 μM carboplatin and **G.** 1 μM TMZ approximately 2-4 hours prior to the initiation of the experiment. A maximum of 50 cells for each condition was counted and the data represents the overall mean of each independent experiments +/- SEM (N= 3). One-way ANOVA with Dunnett's correction test for multiple comparisons was performed to determine statistical significance (**** denotes $p \leq 0.0001$). **B.** HeLa cells fluorescent ROS intensity was analysed after treatment with 50 μM H_2O_2 and **D.** 5 Gy IR for 1 hour and in the presence of siSOD1-5. Each condition was measured in triplicate, averaged and normalised against the unstained control for each independent repeat +/- SEM (N= 3) courtesy of Priya Lata. One-way ANOVA with Dunnett's correction test for multiple comparisons was performed to determine statistical significance (*** denotes $p \leq 0.001$, **** $p \leq 0.0001$ and ns p = non-significant). **F. and H.** as in **B.** with the exception of HeLa cells treated with carboplatin (1 μM) and TMZ (1 μM) respectively for 1 hour prior to the reading the fluorescent intensity (N= 1).

Overall, this data suggests that the addition of selenium rescued the mitotic arrest in the presence of all the agents tested. However, this effect is unlikely to be due to the reduction of intracellular ROS, as selenium had little effect on ROS levels in combination with the MDDC activating agents. Whereas in the absence of SOD1, selenium did not affect mitotic transit or ROS concentration. Overall, these findings support that the SOD1-dependent activation of the MDDC was not due to a redox imbalance.

3.2.4 SOD1 regulates DNA damage and repair.

This research has confirmed a role of SOD1 in the MDDC activated by DNA damage and oxidative stress inducing agents. After the examination into the oxidative stress axis, it was found that the DNA damaging agents did not induce substantial ROS levels yet were capable of inducing the SOD1-dependent mitotic arrest, and ROS levels were not reduced following selenium supplementation despite its ability to rescue the mitotic arrest. Overall, these findings suggest the SOD1-dependent activation of the MDDC was due to DNA damage rather than a redox imbalance, as all agents analysed are

known to induce DNA damage. Therefore, the DNA damage axis was addressed and an investigation into the impact of SOD1 on the DDR was performed.

3.2.4.1 SOD1 levels increase in the nucleus following DNA damage.

Recently numerous papers have observed in yeast, Human FT169 A-T fibroblasts (Tsang *et al.*, 2014), HeLa (X. Li, Qiu, *et al.*, 2019) and neuroblastoma cells (Bordoni *et al.*, 2019), that SOD1 re-localised to the nucleus after treatment with ROS inducing agents, such as H_2O_2. This phenomenon was suggested to be mediated by ATM and its downstream signalling proteins (Tsang *et al.*, 2014; Bordoni *et al.*, 2019). In the context of this research, the enrichment of SOD1 to the nucleus following H_2O_2 treatment, may provide evidence of SOD1 recruitment to the DNA and support its involvement in the response to DNA damage. Firstly, it was replicated and confirmed by Priya Lata that following the administration of H_2O_2, SOD1 protein levels were enhanced in the nucleus in HeLa cells (data not shown).

To test this further, SOD1 nuclear concentration was analysed by immunocytochemistry at various time intervals over 16 hours following IR (5 Gy) treatment **(Figure 3.10)**. Representative images from a selected range of time points are shown in **Figure 3.10A**. The nuclear-integrated density of SOD1 was measured and the entire data set from the three biological repeats (N= 300) was plotted **(Figure 3.10B)**. It was determined that 0.5-16 hours after IR treatment that the levels of nuclear SOD1 significantly increased compared to the untreated cells (0.5, 1, 4, 8 and 16 hours post-IR vs untreated; $p < 0.0001$ and 2 hours post-IR vs untreated; $p = 0.0001$). Furthermore, the overall mean of each experimental repeat was analysed, and no significant difference was determined, yet the same trend was observed **(Figure 3.10C)**. The level of SOD1 in the nucleus appears to fluctuate over the time period analysed and only begins to return to untreated nuclear SOD1 density after 16 hours post-IR treatment.

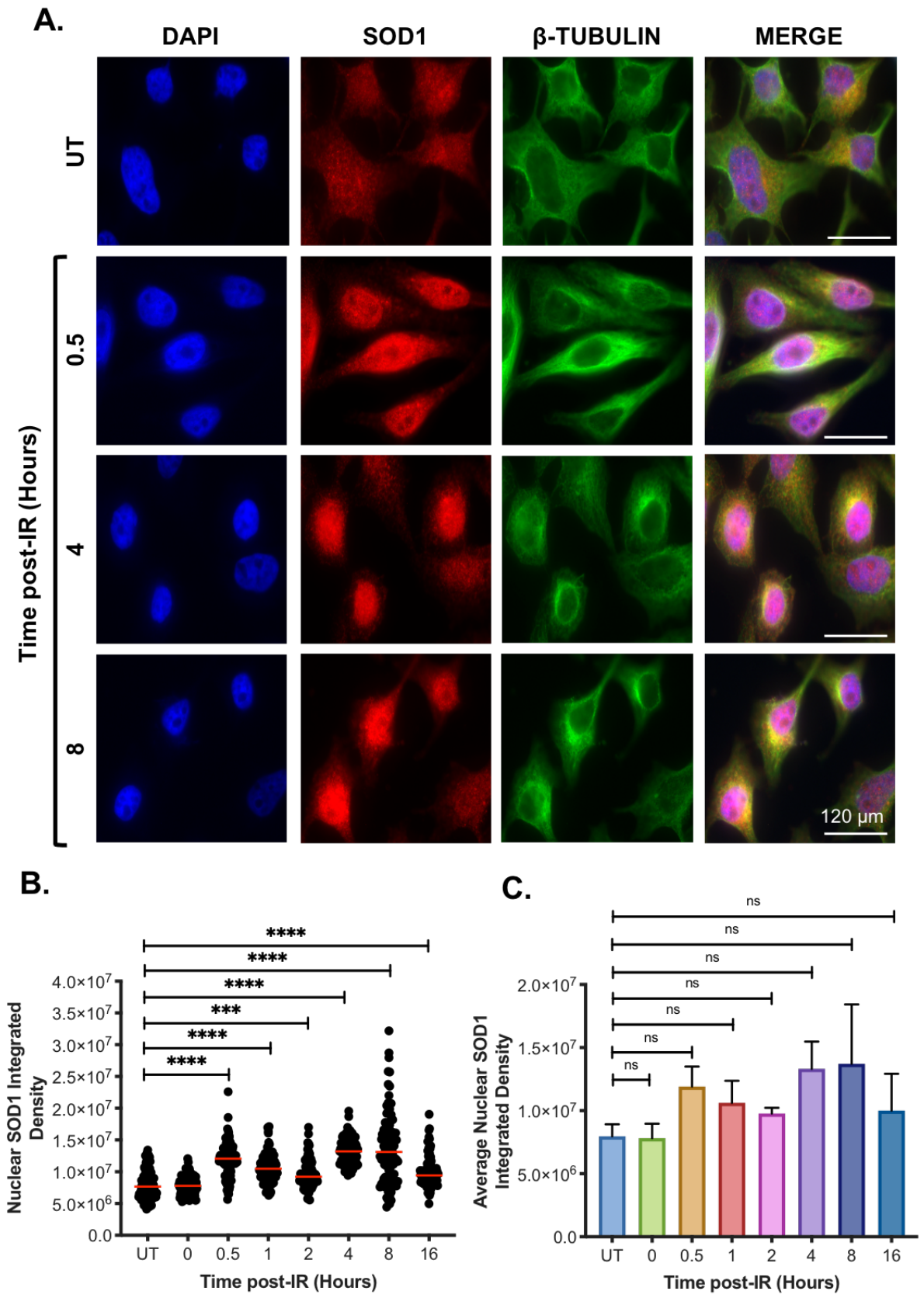

Figure 3.10: The analysis of SOD1 cellular location after IR treatment.

Legend on next page.

Figure 3.10: The analysis of SOD1 cellular location after IR treatment.

A. HeLa cells were treated with 5 Gy IR and fixed at a variety of time points (0, 0.5, 1, 2, 4, 8 and 16 hours) post-treatment over 16 hours. Cells were stained using immunofluorescence for SOD1 and β-Tubulin. Images were taken on a Nikon TE200 inverted fluorescent microscope at a 60X magnification, courtesy of Priya Lata. A panel of representative images illustrating the cellular location of SOD1 in a selection of time points was analysed. **B.** The nuclear SOD1 intensity (integrated density) was measured in FIJI for 100 cells per condition for three independent repeats. The pooled data from all repeats is represented as black dots and the median highlighted in red. Kruskal-Wallis test was performed to determine statistical significance (*** denotes $p \leq 0.001$ and **** $p \leq 0.0001$). **C.** The overall mean nuclear SOD1 intensity of each independent experiments +/- SEM. One-way ANOVA with Dunnett's correction test for multiple comparisons was performed to determine statistical significance (ns denotes p = non-significant).

Overall, SOD1 is enhanced in the nucleus following induction of H_2O_2 and IR treatment, suggesting that SOD1 responds to DNA damage.

3.2.4.2 DNA damage levels increase in the absence of SOD1.

Next, it was assessed how and if the amount of DNA damage experienced was influenced by SOD1 following both IR and H_2O_2 treatments. HeLa cells were treated with 5 Gy IR and 50 μM H_2O_2 for 4 hours in the presence and absence of SOD1. Then the number of DNA breaks was quantified via the alkaline comet assay **(Figure 3.11)**. In the siControl conditions, a significant increase in DNA damage was observed in IR and H_2O_2 treated cells compared to the untreated condition ($p = 0.0007$ and $p = 0.0076$ respectively) **(Figure 3.11B)**. Furthermore, following H_2O_2 treatment there was a significant increase in DNA damage experienced in SOD1 knockdown cells compared to the siControl ($p = 0.0045$). The same trend was observed after IR treatment but to a lesser effect.

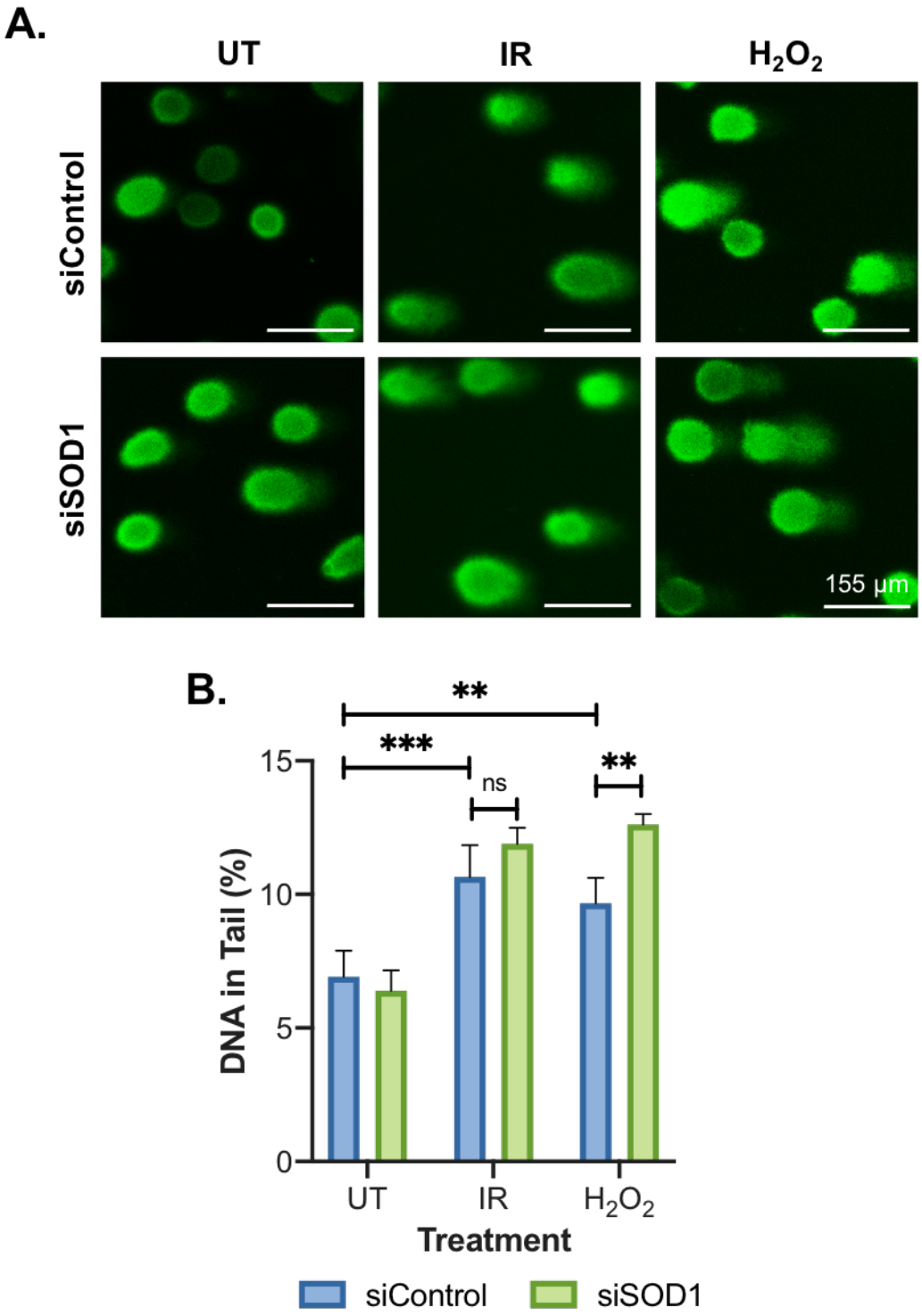

Figure 3.11: The effect of SOD1 on the amount of DNA damage experienced after IR and H_2O_2 treatment.

Legend on next page.

Figure 3.11: The effect of SOD1 on the amount of DNA damage experienced after IR and H_2O_2 treatment.

A. HeLa cells were transfected with siControl or siSOD1-5 and treated with 5 Gy IR or 50 μM H_2O_2 for 4 hours prior to harvesting. An alkaline comet assay was performed, and images were taken on a Nikon TE200 inverted fluorescent microscope at a 10X magnification. Representative images illustrating the amount of DNA damage in the form of a distinct nucleus featuring tails composed of diffused DNA fragments for each condition analysed. **B.** The percentage of DNA in the tail was measured for 50 cells for each condition using Comet software, where the data represents the overall mean of each independent experiment +/- SEM (N= 3). One-way ANOVA with Dunnett's correction test for multiple comparisons was performed to determine statistical significance (** denotes $p \leq 0.01$, *** $p \leq 0.001$ and ns p = non-significant).

These findings confirm that MDDC activating agents, H_2O_2 and IR induce DNA damage and support the role of SOD1 in the protection against DNA damage. Therefore, the SOD1-dependent MDDC may be activated by DNA damage.

Next, the DDR initiation and recovery was specifically analysed using the DNA damage biomarker γH2AX (Rogakou *et al.*, 1998). This upstream DDR protein which when activated by ATM and ATR (phosphorylation at serine (S) 139) accumulates at the DNA break site forming foci and then recruits other downstream DDR and repair proteins (Rogakou *et al.*, 1999; Jackson and Bartek, 2009). γH2AX foci indicate an active DDR, which will dissipate when the DNA damage is resolved. The number of foci per HeLa cell nucleus was quantified at various time intervals over 24 hours following IR (5 Gy) treatment **(Figure 3.12)**. Representative images from selected time points are shown in **Figure 3.12A**. The number of γH2AX foci was counted for each condition and the entire data set from the three biological repeats (N= 300) was plotted **(Figure 3.12B)**. Over the 24 hours, siControl cells were experienced a significant increase in DNA damage from 0-16 hours post-IR (0, 0.5, 1, 2, 4, 8 and 16 hours post-IR vs untreated; $p < 0.0001$). 16 hours post-IR observed a reduction in γH2AX foci indicating repair and returning to normal levels 24 hours post-treatment. However, cells in the absence of SOD1 exhibited significantly more damage compared to the corresponding siControl treated conditions (0, 0.5, 2, 4, 8 and 16 post-IR siSOD1 vs siControl; $p < 0.0001$, $p = 0.001$, $p = 0.0002$, $p = 0.0168$, $p = 0.0007$ and $p < 0.0001$

respectively). The overall mean of each experimental repeat was analysed, and the same trend was observed with significant statistical differences **(Figure 3.12C)**.

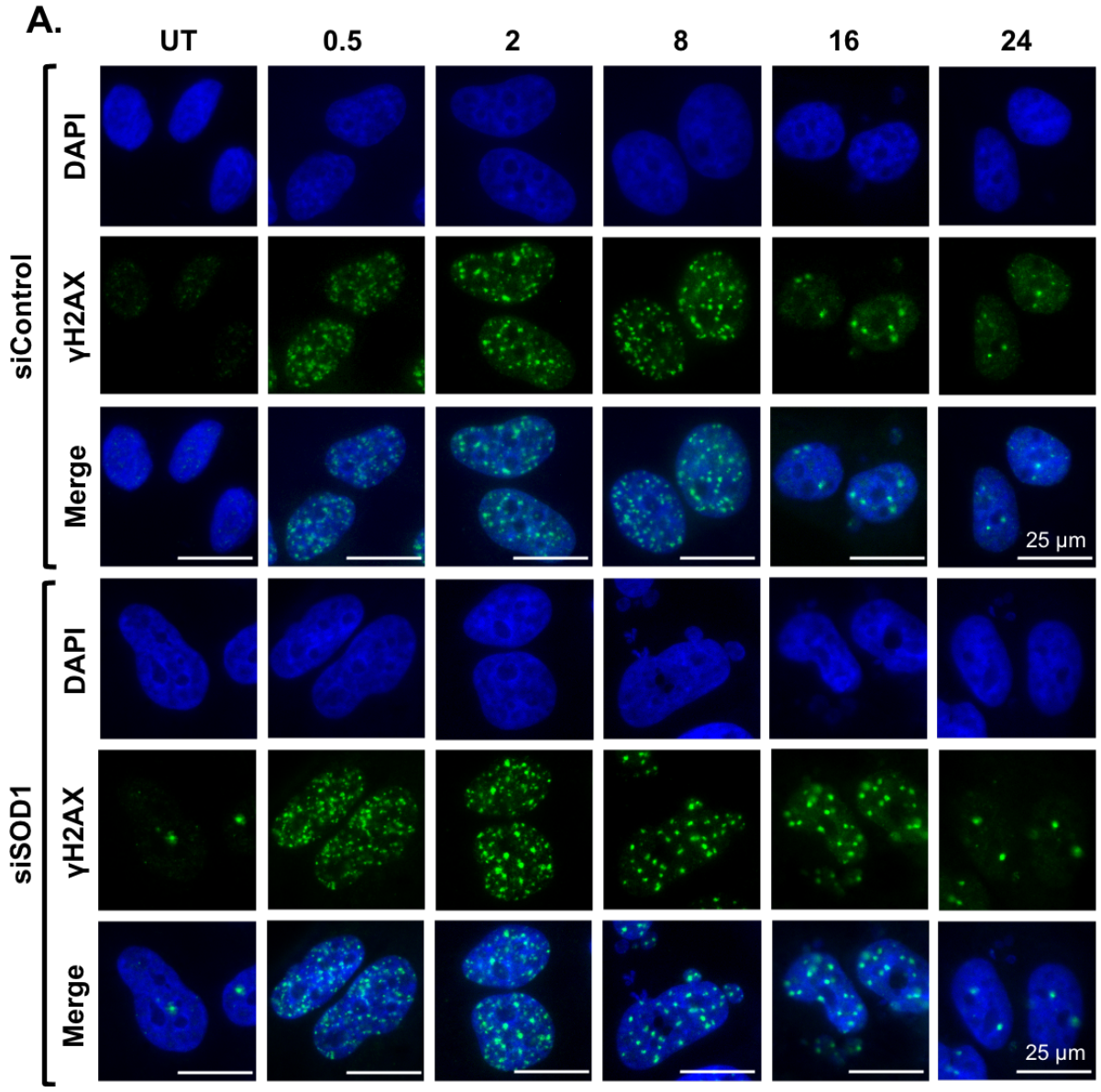

Figure 3.12: The effect of SOD1 on the duration of DNA damage.

Legend on next page.

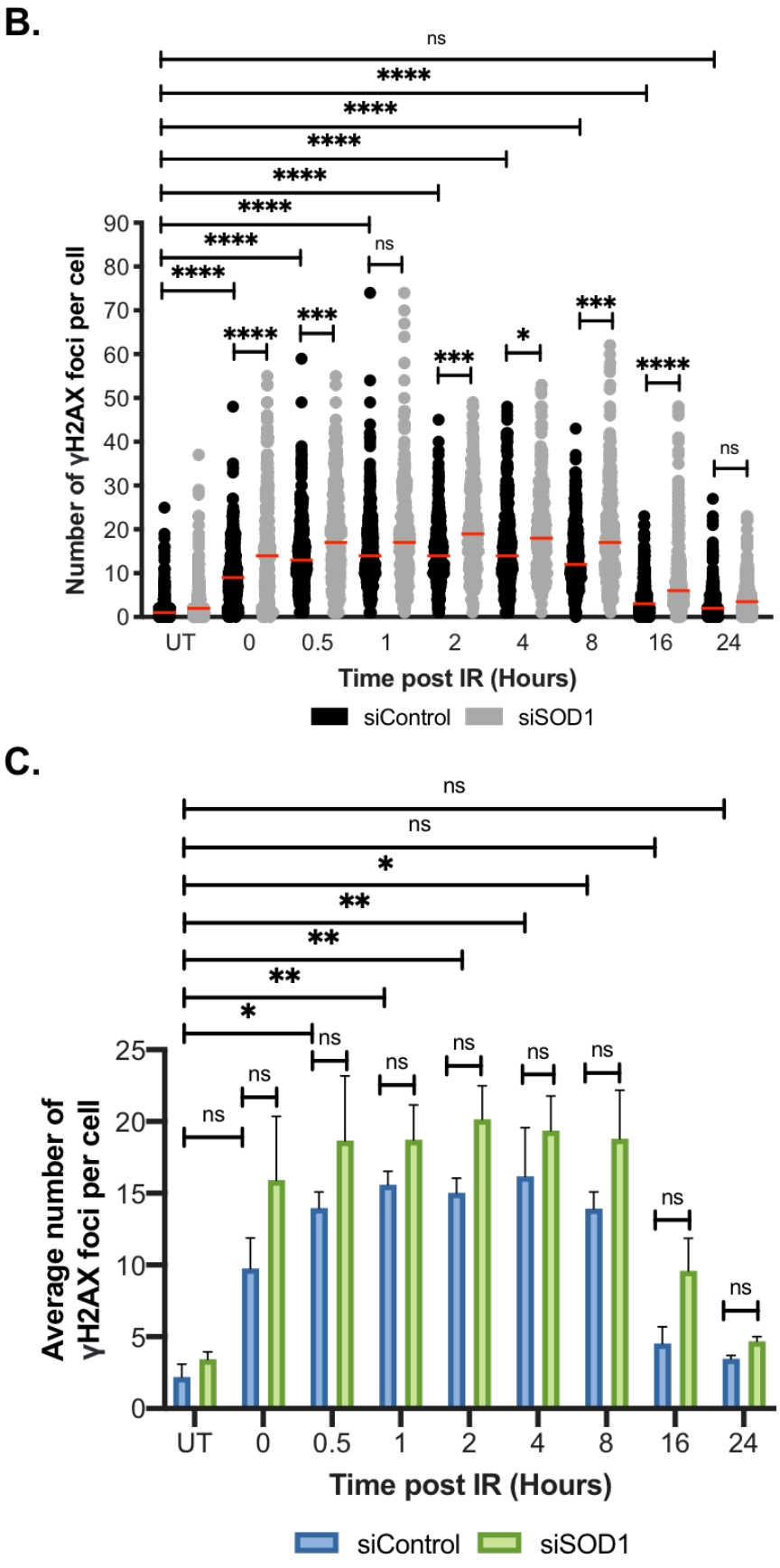

Figure 3.12: The effect of SOD1 on the duration of DNA damage.

Legend on next page.

Figure 3.12: The effect of SOD1 on the duration of DNA damage.
A. After knockdown of SOD1 using siSOD1-5, HeLa cells were treated with 5 Gy IR and fixed at a variety of time points post-treatment over 24 hours. Cells were stained using immunofluorescence for γH2AX. Images were taken on a Nikon TE200 inverted fluorescent microscope at a 60X magnification. A panel of representative images illustrating DNA damage in a range of time points was assessed. **B.** The number of γH2AX foci was quantified with the particle counter in FIJI for 100 cells per condition for three independent repeats. The pooled data from all repeats are represented as black dots (siControl) and grey dots (siSOD1-5) and the median highlighted in red. Kruskal-Wallis test was performed to determine statistical significance (* denotes $p \leq 0.05$, *** denotes $p \leq 0.001$, **** $p \leq 0.0001$ and ns p = non-significant). **C.** The average number of γH2AX foci for each independent experiment +/- SEM (N= 3). One-way ANOVA with Dunnett's correction test for multiple comparisons was performed to determine statistical significance (* denotes $p \leq 0.05$, ** $p \leq 0.01$ and ns p = non-significant).

In summary, in the absence of SOD1, the level of DNA damage was enhanced and the DDR prolonged. This indicates that SOD1 may act within the DDR to stimulate repair to protect the cells against damage.

3.2.4.3 SOD1 regulates DNA damage repair.

In the absence of SOD1, there is an enhanced amount of DNA damage and an extended recovery period, suggesting a role of SOD1 in the DDR. The increased levels of damage observed may require more time to be repaired or SOD1 may influence the DNA repair mechanisms. To investigate if SOD1 affects DNA damage repair, the localisation of the homologous recombination (HR) repair pathway protein, RAD51 was utilised as a biomarker for repair functionality. HR responds to DSBs which are primarily generated after IR (Vignard, Mirey and Salles, 2013). The number of RAD51 positive HeLa cells were quantified 4 hours post-IR in siControl and siSOD1 conditions **(Figure 3.13)**. Additionally, γH2AX was co-stained to monitor DNA damage in comparison to repair mechanisms. Representative images are shown in **Figure 3.13A**. As expected, the HR repair pathway was significantly activated following IR treatment compared to the untreated condition in siControl cells ($p < 0.0001$) **(Figure 3.13B)**. However, in the absence of SOD1 in IR treated cells, whilst there were elevated damage levels seen by the enhanced numbers of γH2AX foci **(Figure 3.13C)**, there

was a significant reduction in RAD51 foci compared to the siControl treated condition ($p = 0.0029$) **(Figure 3.13B)**.

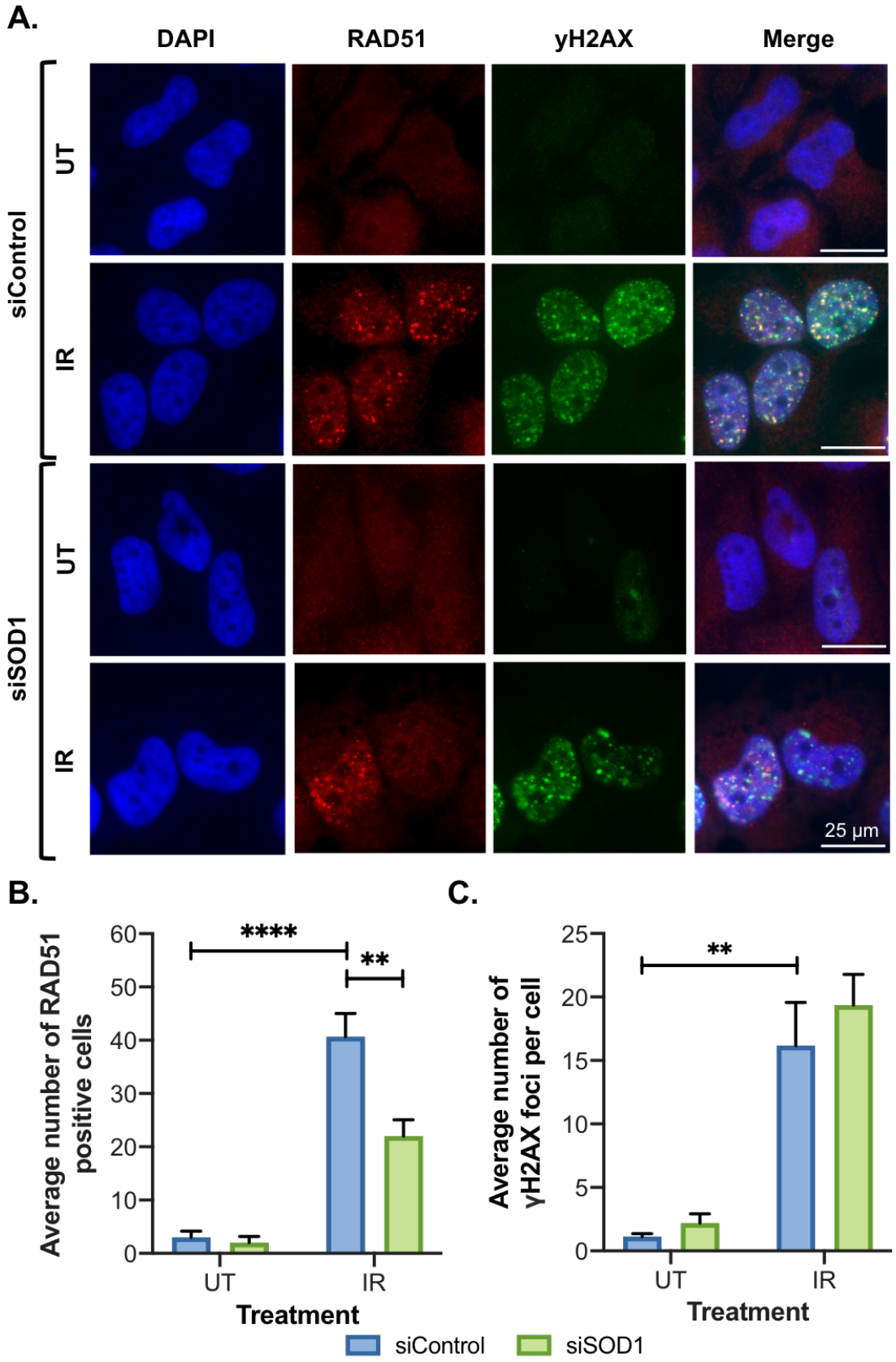

Figure 3.13: The effect of SOD1 on DNA damage repair.

Legend on next page.

Figure 3.13: The effect of SOD1 on DNA damage repair.

A. HeLa cells depleted of SOD1 using siSOD1-5 were treated with 5 Gy IR and harvested after 4 hours. Cells were stained using immunofluorescence for RAD51 and γH2AX. Images were taken on a Nikon TE200 inverted fluorescent microscope at a 60X magnification. A panel of representative images illustrating the DNA damage and repair was assessed. **B.** The number of nuclei positive for RAD51 foci was quantified for 100 cells per condition for three independent repeats +/- SEM. Cells were considered positive if the nucleus contained ≥ 5 distinct RAD51 foci. One-way ANOVA with Dunnett's correction test for multiple comparisons was performed to determine statistical significance (** denotes $p \leq 0.01$ and **** $p \leq 0.0001$).

These findings support the involvement of SOD1 in the DDR and indicate the increased and prolonged levels of DNA damage observed in the absence of SOD1 was due to the lack of sufficient DNA repair via the mediation of RAD51 activity.

3.2.4.4 The influence of SOD1 on cellular sensitivity to IR.

Overall, it can be concluded that SOD1 is involved in regulating the DDR and in the absence of SOD1, irradiated cells experience enhanced levels of DNA damage and a reduction in repair. These findings may suggest that that in the absence of SOD1, there will be an increase in cellular death via sensitivity to DNA damage. The potential of SOD1 to sensitise cells to a range of IR treatments (0-5 Gy) was examined following SOD1 knockdown. However, it was deduced that the absence of SOD1 did not sensitise cells to any dose of IR treatment administered, compared to the siControl condition **(Figure 3.14)**.

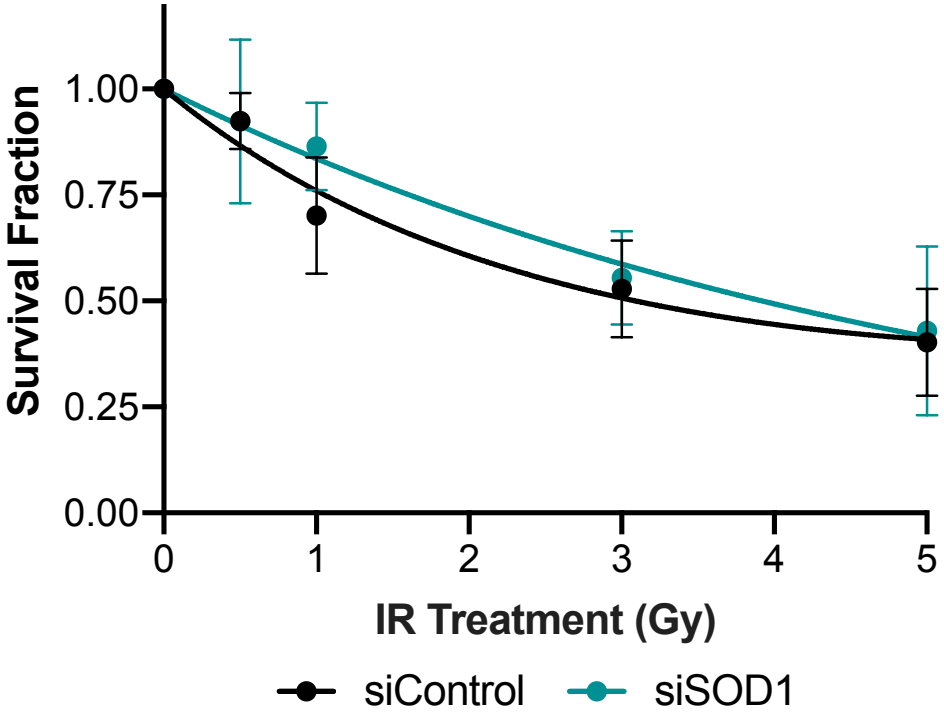

Figure 3.14: The effect of SOD1 on cell survival after treatment with IR.
Clonogenic survival assay was conducted with HeLa cells were treated with 0-5 Gy IR in the presence and absence of SOD1 knockdown (siSOD1-5). 10 days post-treatment colonies with at least 50 cells were counted in triplicate per experimental repeat +/- SEM (N= 3). Students unpaired T-test was performed to determine the statistical significance of SOD1 knockdown at each IR dose administered.

In summary, SOD1 knockdown did not sensitise cells to IR treatment, indicating SOD1 does not impact the DDR-mediated cell fate, potentially due to a more predominant alternative survival pathway. In support of this, I found the DDR was prolonged in the absence of SOD1 and repair was not completely diminished, suggesting the absence of SOD1 would not induce large scale cell death.

3.2.5 The examination of the mechanism of SOD1 in mitotic DNA damage.

The role of SOD1 has now been investigated via both oxidative stress and DNA damage pathways, to support SOD1's involvement in the mitotic DNA damage response. Despite informative findings throughout this chapter, no clear mechanism of how SOD1 regulates the MDDC has yet been determined and further exploration was required. Various aspects surrounding the MDDC and SOD1 were considered,

including the assessment of mitotic structural integrity, involvement of the spindle assembly checkpoint (SAC), the requirement of oxidative DNA damage repair pathway, the assessment of specific SOD1 functional capabilities and the influence of oxidative agents and SOD1 on mitotic regulators.

3.2.5.1 The role of SOD1 on the occurrence of physical and structural abnormalities in mitosis following DNA damage.

3.2.5.1.1 The assessment of SOD1 on abnormal mitotic cell division following DNA damage.

It is known that the DSB lesions generated by IR treatment, typically causes aberrations in mitotic cell division, deriving a variety of observable nuclear defects, which can indicate IR sensitivity leading to cell death due to genomic instability (Cohen-Jonathan, Bernhard and McKenna, 1999). The abnormal nuclear phenotypes include micronucleated or multi-micronucleated cells; the microencapsulation of fragmented chromosomes generating one or more small nuclei caused by chromatid segregation errors (Cohen-Jonathan, Bernhard and McKenna, 1999), DNA bridges; a cell with a DNA tether between two nuclei or between the sister chromatids in anaphase (anaphase bridge) usually caused by dicentric chromosomes (Acilan, Potter and Saunders, 2007; Ganem and Pellman, 2012), and finally, multinucleated cells; which is defined as the presence of more than one nucleus within a single cell or a cell containing a fused nucleus. Cells that featured two or more of these different characteristics were termed multiple phenotypes. Overall, it is conceivable that such physical abnormalities may delay mitotic transit, so the effect of SOD1 on the occurrence of mitotic defects was assessed.

To quantify the effect of SOD1 on the occurrence of aberrant mitotic phenotypes, cells were characterised by the presence of defective phenotypes in the absence of SOD1 and the presence of DNA damage (IR). HeLa cells were treated with 5 Gy IR and harvested 16 hours post-treatment in the presence or absence of SOD1 **(Figure 3.15)**. Representative images for each condition and treatment are shown in **Figure 3.15A**. The number of cells featuring one or more micronuclei significantly increased after IR treatment (siControl and siSOD1), compared to the siControl untreated condition **(Figure 3.15B-C)**. Furthermore, between the IR treated conditions, the number of

multi-micronucleated cells and cells with multiple phenotypes were significantly increased in the absence of SOD1 **(Figure 3.15B-C)**. Multinucleated cells were observed, but usually in the presence of another phenotype. Whereas the presence of DNA bridges was not significantly enhanced in any condition. Overall, it was deduced that in the absence of SOD1 there was a significant increase in all mitotic defects observed compared to the control and in presence of DNA damage ($p < 0.0001$) **(Figure 3.15D)**. Representative images to specifically illustrate each mitotic defective phenotype are shown in **Figure 3.15E**.

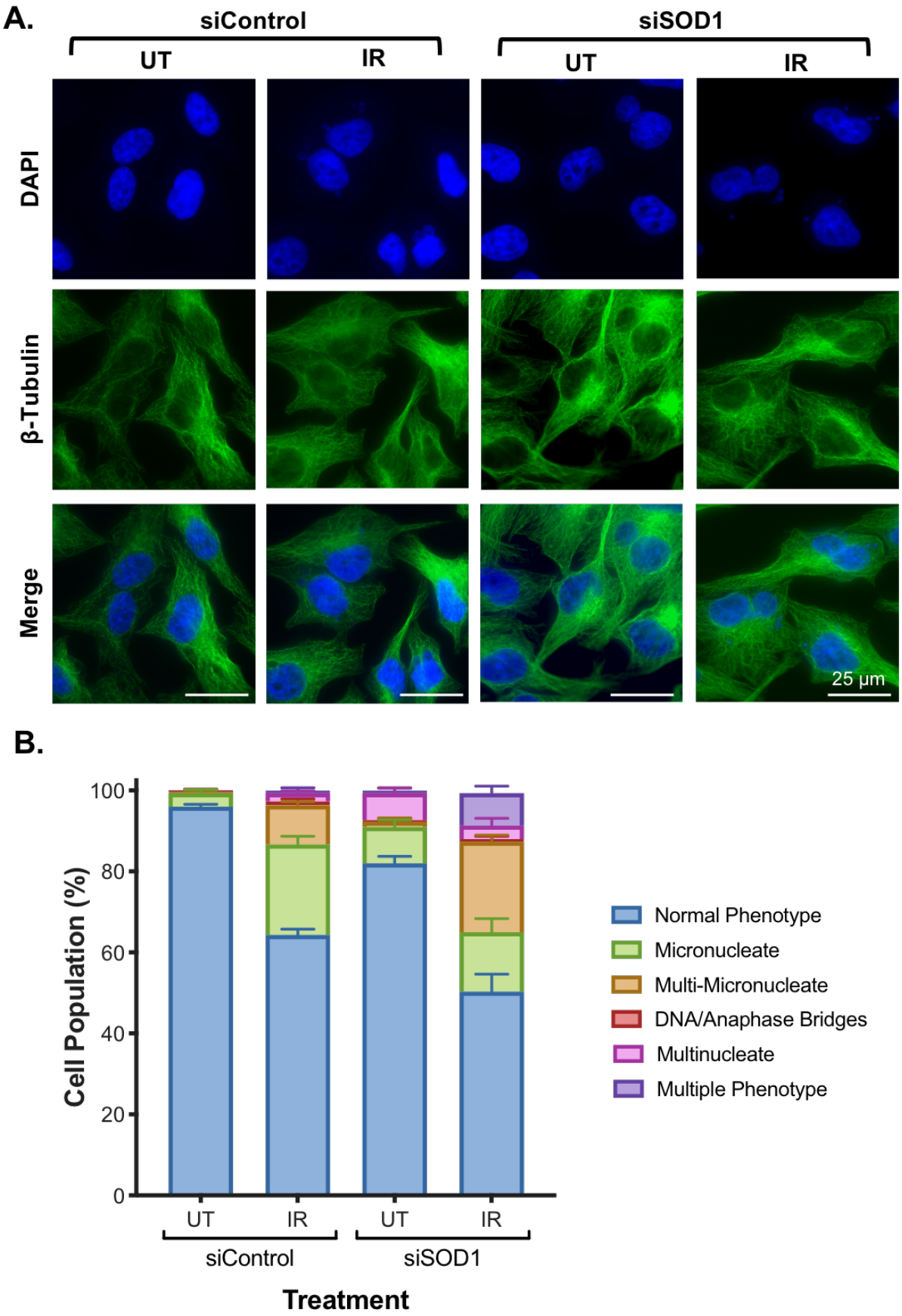

Figure 3.15: The effect of SOD1 on the occurrence of abnormal mitotic phenotypes.

Legend on next page.

C.

	Normal					DNA/Anaphase bridges			
	siControl UT	siControl IR	siSOD1 UT	siSOD1 IR		siControl UT	siControl IR	siSOD1 UT	siSOD1 IR
siControl UT		<0.0001	<0.0001	<0.0001	siControl UT		>0.9999	>0.9999	>0.9999
siControl IR				<0.0001	siControl IR				>0.9999
	Micronucleate					**Multinucleate**			
	siControl UT	siControl IR	siSOD1 UT	siSOD1 IR		siControl UT	siControl IR	siSOD1 UT	siSOD1 IR
siControl UT		<0.0001	0.2637	0.0001	siControl UT		>0.9999	0.0862	0.9685
siControl IR				0.0238	siControl IR				>0.9999
	Micro-Micronucleate					**Multiple Phenotypes**			
	siControl UT	siControl IR	siSOD1 UT	siSOD1 IR		siControl UT	siControl IR	siSOD1 UT	siSOD1 IR
siControl UT		0.0022	>0.9999	<0.0001	siControl UT		>0.9999	>0.9999	0.0151
siControl IR				<0.0001	siControl IR				0.0371

D.

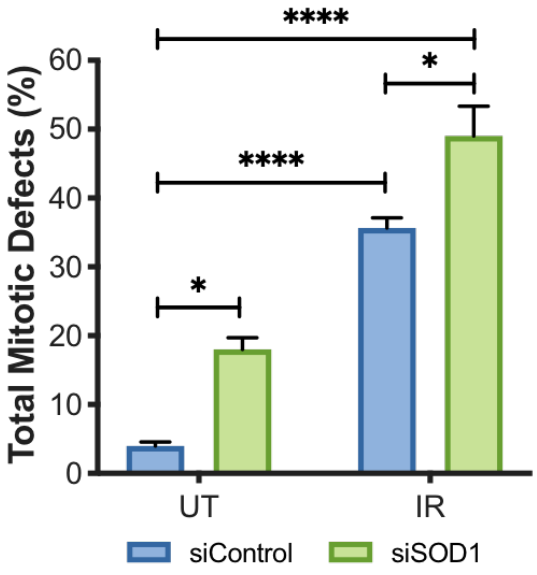

Figure 3.15: The effect of SOD1 on the occurrence of abnormal mitotic phenotypes. Legend on next page.

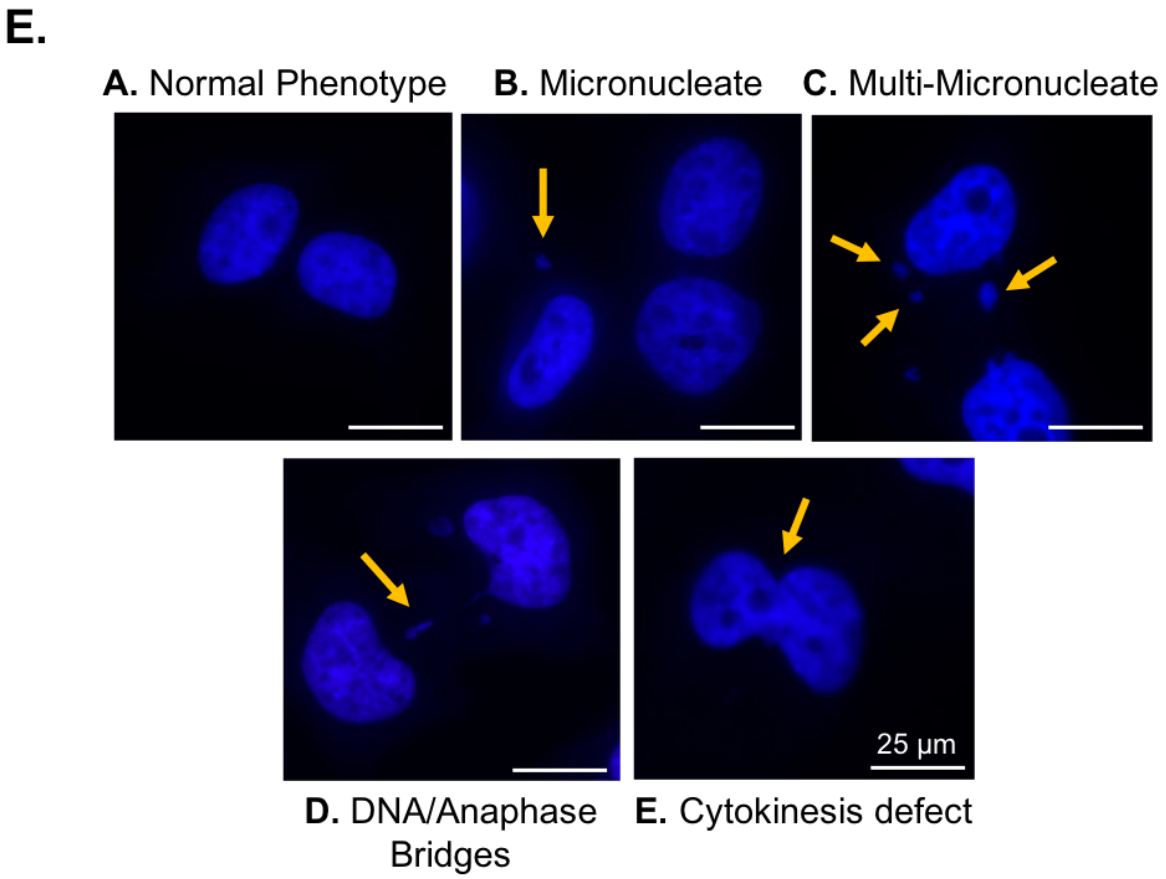

Figure 3.15: The effect of SOD1 on the occurrence of abnormal mitotic phenotypes.
A. HeLa cells depleted of SOD1 using siSOD1-5 were treated with 5 Gy IR and harvested 16 hours post-treatment. Cells were stained using immunofluorescence with standard nuclear marker DAPI and β-Tubulin. A panel of representative images from the images taken on a Nikon TE200 inverted fluorescent microscope at a 60X magnification. **B.** Cells exhibiting one or more mitotic defects were quantified for 100 cells per condition for three independent repeats (+/- SEM). **C.** Table of p-values from One-way ANOVA with Dunnett's correction test for multiple comparisons with significance highlighted in yellow. **D.** The total percentage of cells exhibiting mitotic defects, the individual phenotype data was collated for all conditions and repeats analysed. One-way ANOVA with Dunnett's correction test for multiple comparisons was performed to determine statistical significance (* denotes $p \leq 0.05$ and **** $p \leq 0.0001$). **E.** Representative images illustrating each of the mitotic defective phenotypes assessed. The yellow arrow highlights the defining characteristic of the defect.

As expected, the number of mitotic defects increased following IR treatment and further increased in the absence of SOD1. This suggests that the delay in mitotic transit was not due to these physical mitotic defects and that SOD1 did not induce arrest via this

mechanism, as a reduction in mitotic defects in the absence of SOD1 would be expected. However, these findings indicate that SOD1 possess a role in DNA protection in mitosis.

3.2.5.1.2 SOD1 did not affect centrosomal integrity.

Considering there was an increase in errors in mitotic cell division observed following SOD1 knockdown in the presence of DNA damage, mitotic spindle organisation and segregation functionality was examined, specifically through centrosomal analysis. The characteristics examined were centrosomal over-amplification (greater than two centrioles) and centrosomal fragmentation.

To elucidate if the increase in abnormal mitotic phenotypes observed in the absence of SOD1 is due to the ability of SOD1 to regulate centrosomal integrity, the centrosomal component pericentrin was assessed via immunocytochemistry. HeLa cells were treated with IR and the centrosomal integrity was measured in the presence and absence of SOD1 **(Figure 3.16)**. A significant enhancement in centrosomal fragmentation was observed in IR treated siControl cells compared to the untreated condition ($p = 0.0336$). However, there was a slight increase in centrosomal fragmentation following SOD1 knockdown in both untreated and irradiated cells, compared to the siControl untreated condition, but the differences were not deemed statistically significant **(Figure 3.16A)**. Finally, no substantial differences in centrosomal amplification were observed following SOD1 knockdown and/or irradiation treatment, compared to the untreated control condition. Representative images of the characteristics quantified are shown in **Figure 3.16B**.

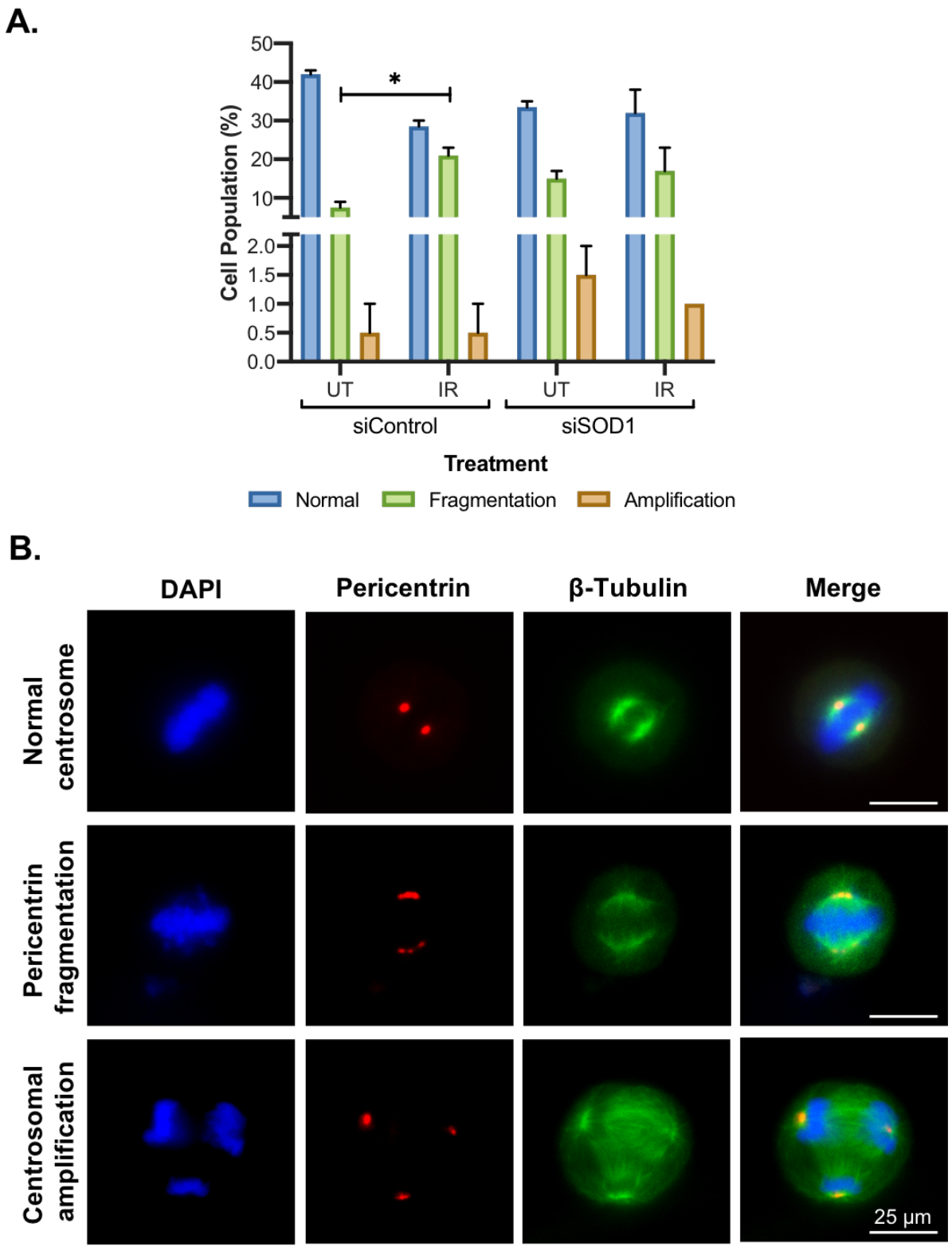

Figure 3.16: The effect of SOD1 on centrosomal integrity.

Legend on next page.

Figure 3.16: The effect of SOD1 on centrosomal integrity.

A. HeLa cells depleted of SOD1 using siSOD1-5 were treated with 5 Gy IR and harvested 16 hours post-treatment. Cells were stained using immunofluorescence with pericentrin and β-Tubulin. The images were taken on a Nikon TE200 inverted fluorescent microscope at a 60X magnification. 50 cells per condition were quantified by centrosomal characteristics for each independent repeat +/- SEM (N= 2). Statistical significance was determined by One-way ANOVA with Dunnett's correction test for multiple comparisons (* denotes $p \leq 0.05$). **B.** A panel of representative images to illustrate each characterised assessed.

SOD1 had no effect on centrosomal integrity, which indicates the enhanced number of mitotic defects following the SOD1 knockdown and DNA damage was not caused by impairment of the centrosome. Overall, it can be deduced that the IR-mediated prolonged mitotic transit was not due to an enrichment of structural and mechanical defects via abnormal mitotic phenotypes or centrosomal dysfunction. Finally, SOD1 was not involved in causing these defects.

3.2.5.2 SOD1's mechanism of action does not act through the spindle assembly checkpoint.

The vital regulatory mitotic checkpoint, the SAC ensures proper microtubule attachment to the chromosomes in metaphase for the cell cycle continuation and successful cell division. The SAC functionality is dependent on the mitotic checkpoint complex (MCC), composed of BubR1, Bub3, Mad2 and Cdc20 (Musacchio and Salmon, 2007). Many papers describe a SAC-mediated mitotic arrest in response to DNA damage (Mikhailov, Cole and Rieder, 2002; Nitta *et al.*, 2004; Kim and Burke, 2008). Furthermore, preliminary data conducted in the Thompson laboratory determined BubR1 may be key in the MDDC **(Figure 1.9)**. In consideration of this, it was proposed that the SAC was examined in the presence and absence of SOD1 and DNA damage, to identify if SOD1 activates the SAC to induce mitotic arrest following DNA damage.

Firstly, the overall protein levels of each MCC protein (BubR1, Bub3, Mad2 and Cdc20) and metaphase-anaphase transition protein securin were analysed via western blot. HeLa cells were transfected with two individual SOD1 siRNAs (siSOD1-5 and siSOD1-

7), treated with 5 Gy IR and harvested 16 hours post-treatment. Overall, there was no effect of IR alone and/or SOD1 knockdown on the levels of any of the mitotic proteins assessed **(Figure 3.17A)**.

Next, the MCC proteins were assessed at the transcriptional level via reverse transcription-quantitative polymerase chain reaction (RT-qPCR). Samples were treated similarly to those for the western blot analysis, with the exception upon harvesting as total cellular RNA was extracted. SOD1 protein levels were examined to confirm the knockdown of SOD1 and was conducted in parallel to each gene expression test **(Figure 3.17B)**. In support of the protein level data **(Figure 3.17A)**, as a collective, there was no significant difference in the MCC gene levels following SOD1 knockdown in the absence and presence of DNA damage **(Figure 3.17C)**. Although siSOD1-7 appeared to enhance gene expression levels of the MCC proteins particularly after IR treatment, which was only significant for Mad2 ($p = 0.0061$). As this was not observed at the protein level and was not reciprocated with siSOD1-5, it renders the effects to be due to potential off-target effects of the siRNA.

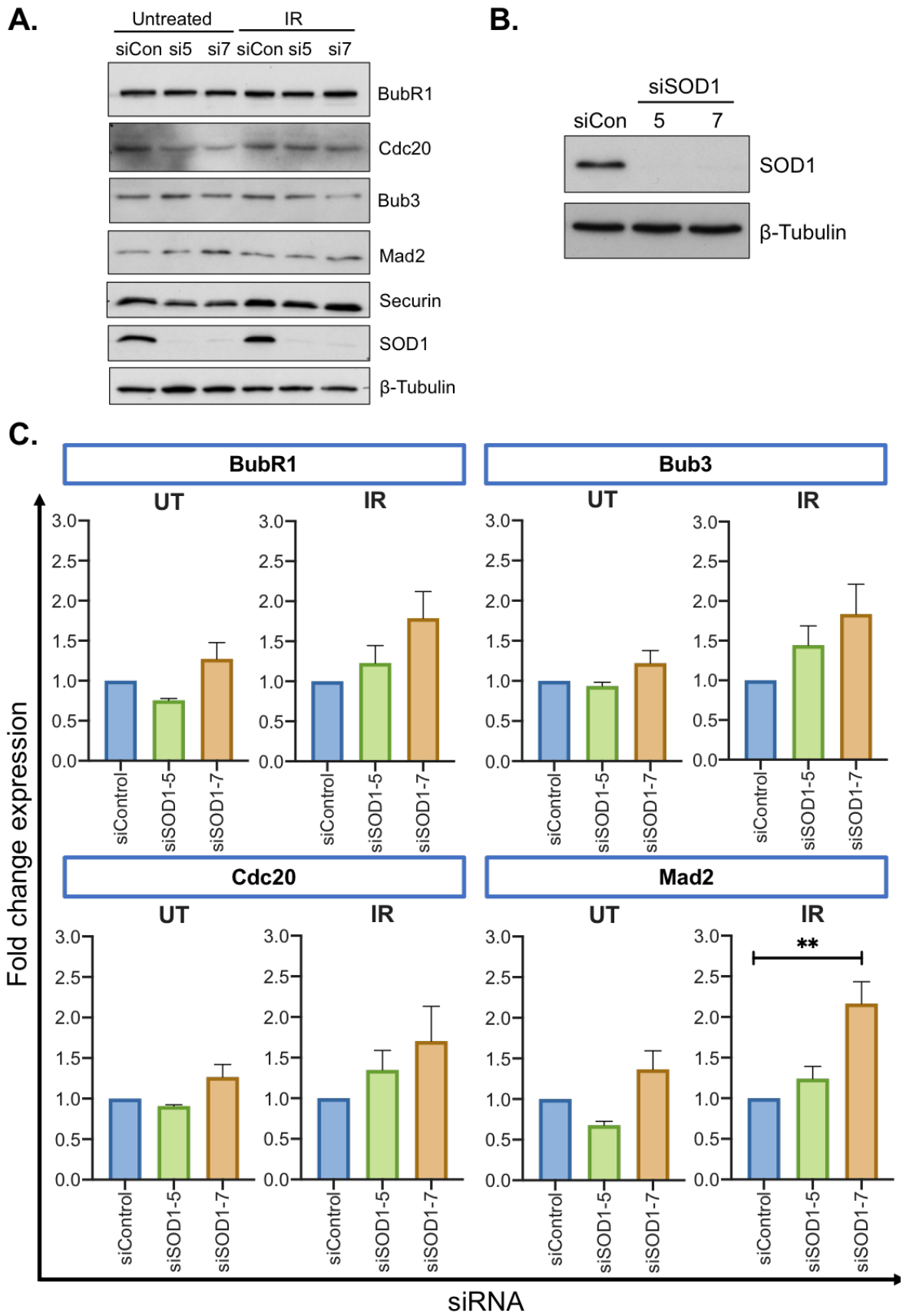

Figure 3.17: The analysis of the MCC functionality after SOD1 knockdown and DNA damage.

Legend on next page.

SAC functionality was also specifically assessed through the treatment of cells with the anti-mitotic agent; nocodazole. Nocodazole inhibits microtubule polymerisation through binding to β-tubulin (a main component of microtubules) (Hoebeke, Van Nijen and De Brabander, 1976), preventing further elongation (Vasquez *et al.*, 1997). The consequences of this agent on mitosis involve the disruption of microtubule attachment to the kinetochores, causing unsatisfactory SAC conditions and metaphase arrest. If SOD1 regulates the SAC it would be expected that in the absence of SOD1, the response to nocodazole treatment would be disrupted. HeLa cells were transfected with siSOD1-5 and siBubR1 as a positive control, then treated with 200 ng/mL nocodazole prior to the initiation of time-lapse microscopy. Mitotic cell fate throughout the experiment was assessed, including mitotic arrest, death, slippage and division. Mitotic slippage is defined as the cell exiting mitosis after failing to divide and returning to interphase. It was deduced that SOD1 had no effect on SAC functionality following nocodazole treatment, as the majority of cells experienced a sustained mitotic arrest or died in mitosis, similarly to the control cells **(Figure 3.17D)**. This further suggests that SOD1 does not act through the SAC, as it would be expected that cells respond similarly to BubR1 knockdown, which resulted in the significant increase in mitotic slippage due to SAC inactivity, compared to control cells ($p < 0.0001$).

Finally, an initial assessment of the MCC proteins recruitment to the kinetochore-centromeric regions during mitosis was conducted. HeLa cells were transfected with siSOD1-5 and treated with 5 Gy IR, cells were harvested 16 hours post-treatment. Immunofluorescent analysis of BubR1 co-stained with centromeric protein, CENPB was performed and metaphase cells were visualised. It was anticipated that BubR1 would not localise (degree may vary) at the kinetochore-centromeric region (CENPB) if SOD1 was required for SAC functionality after DNA damage for the MDDC. However, it was found that IR and SOD1 knockdown alone or in combination did not affect BubR1 localisation to the kinetochores **(Figure 3.17E)**. To mention, mitotic abnormalities were observed following both IR treatments.

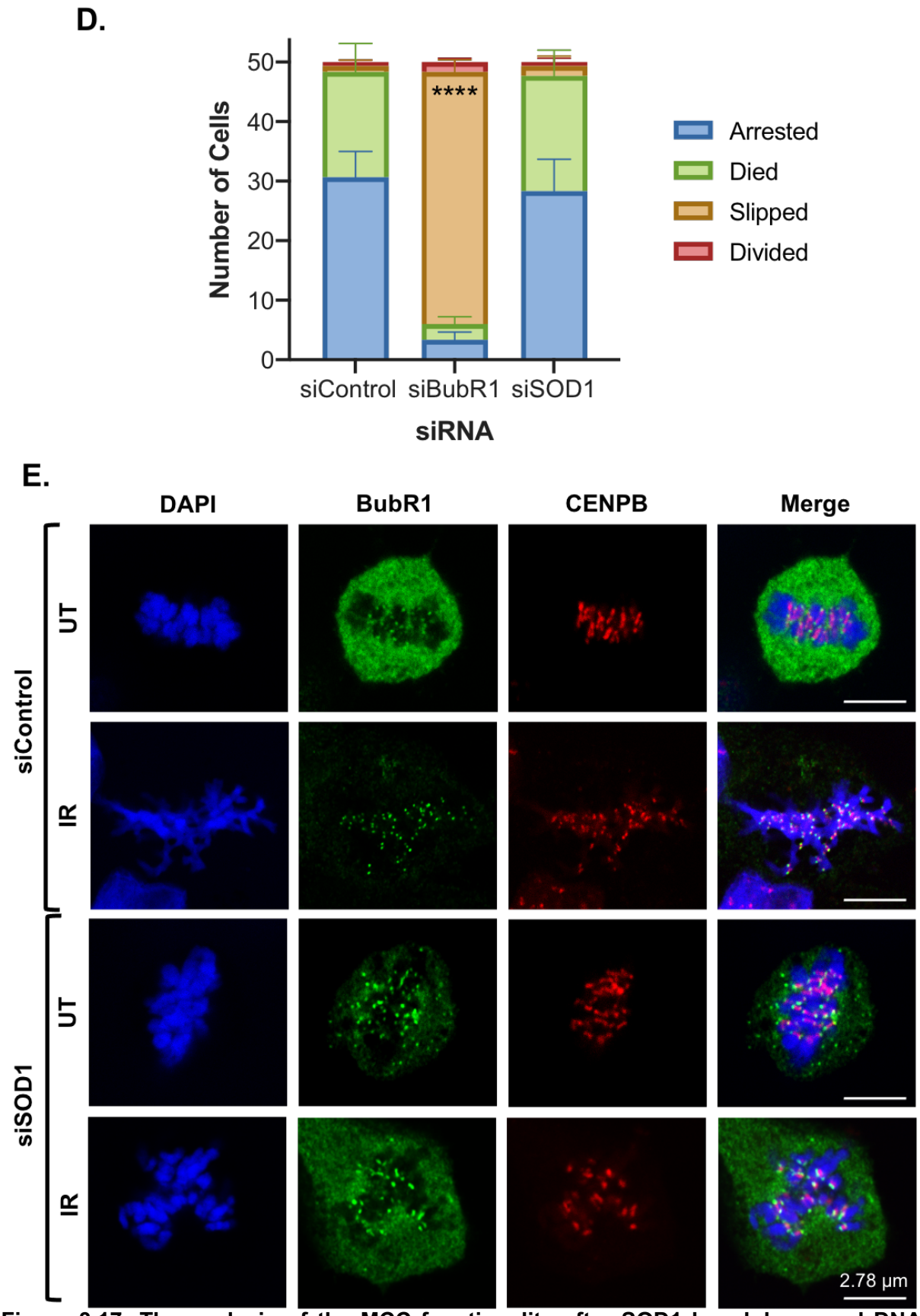

Figure 3.17: The analysis of the MCC functionality after SOD1 knockdown and DNA damage.

Legend on next page.

Figure 3.17: The analysis of the MCC functionality after SOD1 knockdown and DNA damage.

A. Representative western blot showing the levels of mitotic SAC proteins after the knockdown of SOD1 using siSOD1-5 and siSOD1-7 in HeLa cells, which were harvested 16 hours post-treatment with IR (5 Gy) treatment (N≥ 2). Extracts were probed for BubR1, Cdc20, Bub3, Mad2, Securin, SOD1 and β-Tubulin. **B.** Representative western blot showing the knockdown of SOD1 using siSOD1-5 and siSOD1-7 in HeLa cells (N= 3). These samples were conducted in parallel to **C.** Extracts were probed for SOD1 and β-Tubulin. **C.** MCC proteins; BubR1, Bub3, Cdc20 and Mad2 gene expression was quantified relative to *GAPDH* via RT-qPCR in HeLa cells transfected with siSOD1-5 and harvested 16 hours post-IR (5 Gy). The fold change of the delta CT values for all conditions were plotted and the data represents the overall mean of each independent experiments +/- SEM (N= 3). One-way ANOVA with Dunnett's correction test for multiple comparisons was performed to determine statistical significance (** denotes $p \leq 0.01$). **D.** Time-lapse live cell microscopy analysis of mitotic cell fate following BubR1 and SOD1 knockdown (siSOD1-5) in HeLa cells treated with nocodazole (200 ng/mL). A maximum of 50 cells for each condition was counted and the data represents the overall mean of each independent experiments +/- SEM (N= 3). One-way ANOVA with Dunnett's correction test for multiple comparisons was performed to determine statistical significance (**** denotes $p \leq 0.0001$). **E.** HeLa cells depleted of SOD1 using siSOD1-5, treated with 5 Gy IR and harvested 16 hours post-treatment, were stained using immunofluorescence with BubR1 and CENPB. The images were taken on a Zeiss LSM980 confocal fluorescent microscope at a 63X magnification. 5 metaphase-anaphase cells per condition were assessed for one independent repeat.

Overall, the loss of SOD1 does not affect SAC functionality, hence the SOD1-dependent mitotic delay observed was likely not due to SAC-mediated mitotic arrest.

3.2.5.3 Overexpression of 8-oxoguanine glycosylase does not rescue the SOD1-dependent mitotic arrest following DNA damage.

It is known that oxidative stress damages DNA and the cell possesses a protective repair pathway to overcome this damage. The resulting lesion is commonly the formation of 8-oxo-7,8-dihydro-2′-deoxyguanosine (8-oxodG) adducts via the reaction of ROS with guanine bases, which are classed as biomarkers of oxidative damage (Kasai, 1997). Base excision repair (BER) is performed to remove and repair the

lesions, which is initiated by 8-oxoguanine glycosylase (OGG1) (Lu, Nash and Verdine, 1997). I hypothesised that the DNA damage-induced mitotic cell cycle arrest regulated by the antioxidant enzyme, SOD1, may act through the BER pathway, providing a potential mechanism for the mitotic arrest.

To test this theory, an exogenous OGG1 protein featuring a Myc-Tag (Myc-OGG1) was transfected into HeLa cells in the presence and absence of SOD1 (siSOD1-5) and the mitotic transit time assessed upon activation of MDDC with 50 μM H_2O_2 treatment **(Figure 18A)**. The treatment of siControl cells with H_2O_2 in the presence of Myc-OGG1, induced mitotic arrest compared to the transfected untreated cells ($p < 0.0001$). Then the mitotic transit time was significantly reduced after SOD1 knockdown, H_2O_2 treatment and Myc-OGG1 overexpression compared to the parallel siControl condition ($p < 0.0001$). This effect was the same as the Myc-OGG1 negative control conditions (siControl or siSOD1 cells untreated or treated). Excess cells obtained when replating the time-lapse microscopy experiment were utilised as western blot samples to ensure overexpression of Myc-OGG1 and knockdown of SOD1 was achieved **(Figure 18B)**.

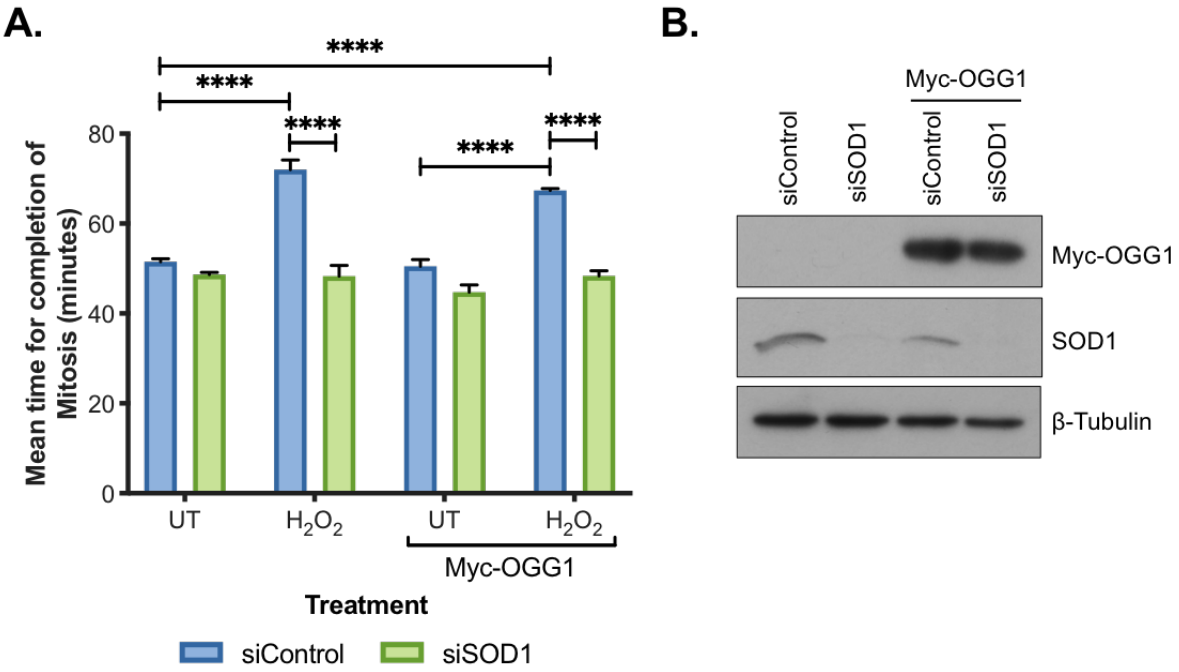

Figure 3.18: The analysis of OGG1 overexpression on mitotic transit time in the presence and absence of SOD1.

Legend on next page.

Figure 3.18: The analysis of OGG1 overexpression on mitotic transit time in the presence and absence of SOD1.

A. Time-lapse live cell microscopy analysis of the mean time taken to complete mitosis following SOD1 knockdown (siSOD1-5) and overexpression of Myc-OGG1 (1 µg) in HeLa cells treated with H_2O_2 (50 µM) 2 hours prior to the initiation of the experiment. A maximum of 50 cells for each condition was counted and the data represents the overall mean of each independent experiment +/- SEM (N= 3). One-way ANOVA with Dunnett's correction test for multiple comparisons was performed to determine statistical significance (**** denotes $p \leq 0.0001$). **B.** Representative western blot showing the knockdown of SOD1 and overexpression of Myc-OGG1 (N= 3). Extracts were collected following replating each mitotic progression assay and probed for SOD1, Myc-Tag to represent Myc-OGG1 and β-Tubulin.

Overall, SOD1 did not act through OGG1 to induce mitotic arrest, indicating that the MDDC probably does not require or specifically activate the BER pathway.

3.2.5.4 SOD1 enzymatic activity is required for the DNA damage induced mitotic arrest.

SOD1 is a well-characterised and well-researched antioxidant enzyme. Recently, evidence has emerged in support of a novel role of SOD1 in gene expression mediated by H_2O_2 (Tsang *et al.*, 2014; Bordoni *et al.*, 2019; X. Li, Qiu, *et al.*, 2019). SOD1 was first identified to act as a nuclear transcription factor in yeast, independent of its dismutase function (Tsang *et al.*, 2014). This study found that H_2O_2 stimulated Dun1 (a Chk2 related protein) activation of SOD1 via phosphorylation at S60 and S99, leading to SOD1 localisation to the nucleus (Tsang *et al.*, 2014). Dun1 is a downstream effector of Mec1, the yeast homolog of ATM, providing a potential link to the DNA damage response. Tsang *et al*. (2014) also conducted a microarray to determine the genes dependent on SOD1, which were those involved in protective mechanisms against ROS, maintenance of redox homeostasis, ROS-induced DNA replication stress and the DNA damage response. This study was later supported by similar findings by Bordoni *et al.* (2019) in neuroblastoma cells and by Li *et al.* (2019) in HeLa cells (Bordoni *et al.*, 2019; X. Li, Qiu, *et al.*, 2019). This promising novel function of SOD1 may reveal the mechanism in which SOD1 induces mitotic cell cycle arrest following DNA damage.

To determine if SOD1's enzymatic or transcription factor activity is responsible for the DNA damage induced mitotic arrest, various functional SOD1 mutants were generated via site-directed mutagenesis using the Myc-SOD1^{WT} expression vector. The functional mutants include glycine to alanine mutation at position 93 (G93A), glycine to arginine mutation at position 85 (G85R), serine to alanine mutation at position 99 (S99A) and positions 60 and 99 (S60,99A). G93A and G85R are common pathogenic SOD1 variants, typically associated with ALS. The G93A mutation is located within a vital structural component of SOD1 and is often referred to as a WT-like mutation, as SOD1 enzymatic activity is sustained (Hayward *et al.*, 2002; Boyd *et al.*, 2020). Whereas G85R causes complete enzymatic inactivity through the disruption of zinc-binding motifs at the active site (Hayward *et al.*, 2002). To disable transcription factor activity S99A and S60,99A mutants were generated. Tsang *et al.* (2014) reported a reduction in SOD1 nuclear localisation with an S99A mutation alone compared to total abolition with the double variant (Tsang *et al.*, 2014). The single variant for transcription factor activity will support any effect observed with the double mutant.

The effect of these four SOD1 functional mutants were assessed via the mitotic progression assay, to determine which was required for the SOD1-dependent mitotic delay. Similar to the WT alone complementation experiment (section **3.2.2.3**), HeLa cells were transfected with siSOD1-5 and the WT, G93A, G85R, S99A and S60,99A expression vectors **(Figure 3.19)**. An empty Myc-Tagged expression vector was also implemented into the experiment as a control vector. Mitotic arrest was stimulated with H_2O_2 (50 μM) treatment. In addition to the control vector, G85R, S99A and S60,99A significantly reduced mitotic transit time in H_2O_2 treated siSOD1 cells compared to siControl treated conditions ($p < 0.0001$, $p < 0.0001$, $p = 0.03$ and $p = 0.0468$ respectively) **(Figure 3.19A).** The G85R mutation was most prominent and similar to the control vector. Excess cells from each condition that were not used for the microscopy were utilised for western blot analysis for each repeat to ensure the correct overexpression and knockdown was achieved **(Figure 3.19B)**. It is of note that the G85R mutant was observed to have abnormal electrophoretic mobility, as the protein bands were lower than the other mutants. This phenomenon has also been reported in the literature (Hayward *et al.*, 2002) and was proposed to be due to this mutants metal deficiency, leading to an enhanced overall negative charge through the loss of

metal ions or a conformational change which increased SDS binding during sample preparation.

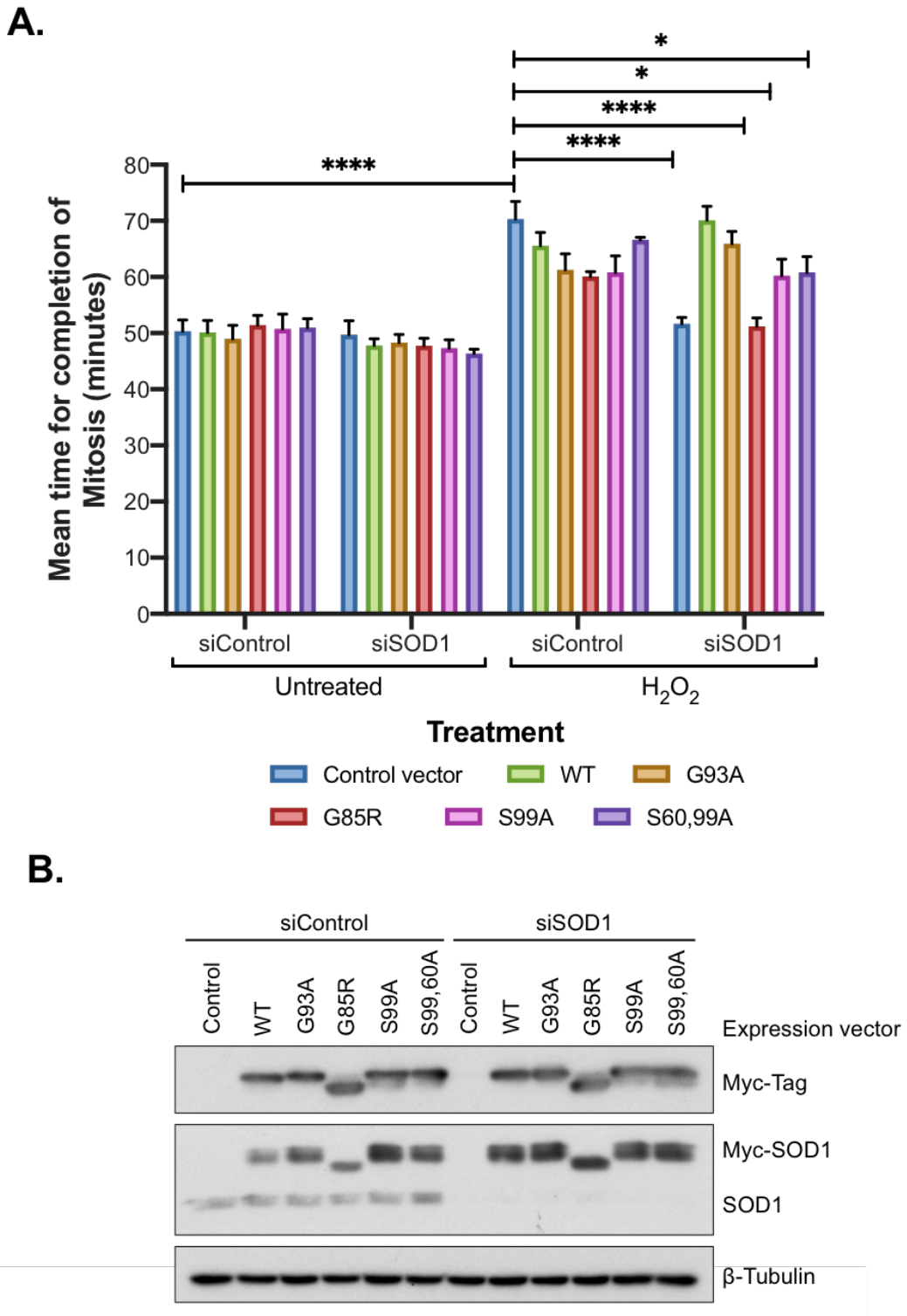

Figure 3.19: The assessment of SOD1 functional mutants on mitotic arrest induced by H_2O_2.

Legend on next page.

Figure 3.19: The assessment of SOD1 functional mutants on mitotic arrest induced by H_2O_2.

A. Time-lapse live cell microscopy analysis of the mean time taken to complete mitosis following SOD1 knockdown (siSOD1-5) and complementation with 250 ng Myc-SOD1 expression vectors; WT, G93A, G85R, S99A and S60,99A in HeLa cells treated with H_2O_2 (50 μM) 2 hours prior to the initiation of the experiment. A maximum of 50 cells for each condition was counted and the data represents the overall mean of each independent experiments +/- SEM (N= 3). One-way ANOVA with Dunnett's correction test for multiple comparisons was performed to determine statistical significance (* denotes $p \leq 0.05$ and **** $p \leq 0.0001$). **B.** Representative western blot showing the knockdown of SOD1 and overexpression of the various Myc-SOD1 expression vectors (N= 3). Extracts were collected following replating of each mitotic progression assay and probed for SOD1, Myc-Tag to represent each Myc-SOD1 vector and β-Tubulin.

To summarise, this data suggests that the mitotic arrest observed is dependent on SOD1's enzymatic activity. However, as the S99A and S60,99A mutants also had an effect on mitotic arrest, this implies SOD1 nuclear localisation may have a supporting role in the MDDC.

3.2.5.5 SOD1-dependent mitotic arrest acts synergistically with Aurora A inhibition.

In mitosis, Aurora A is involved in numerous events such as the promotion of mitotic entry by CDK1/cyclin B (Hirota *et al.*, 2003) and Plk1 (Macůrek *et al.*, 2008) activation, centrosome maturation (Hirota *et al.*, 2003), chromosome alignment during metaphase (Marumoto *et al.*, 2003), kinetochore-microtubule attachment (Ma *et al.*, 2011) and cytokinesis for mitotic exit (Marumoto *et al.*, 2003). Aurora A kinase activity has also been found to be regulated by redox through a series of oxidative modifications (Lim *et al.*, 2020), which results in inactivation by hyperphosphorylation (Wang *et al.*, 2017). The inhibition of Aurora A by oxidative stress disrupted spindle assembly inducing mitotic arrest (Wang *et al.*, 2017). Therefore, Aurora A may provide a mechanism for the SOD1-dependent mitotic arrest upon DNA damage.

To test this, alisertib, an inhibitor of Aurora A was administered to the cell in the presence and absence of SOD1, to determine the effect on the MDDC activated by

H_2O_2 treatment **(Figure 3.20)**. Alisertib significantly increased the mitotic transit time in siControl conditions, alone or in combination with H_2O_2 compared to the untreated condition (both $p < 0.0001$). Then a significant reduction in mitotic transit was observed following SOD1 knockdown and alisertib treatment alone and in combination with H_2O_2, compared to the corresponding siControl conditions ($p = 0.011$ and $p < 0.0001$ respectively), similar to the H_2O_2 alone ($p = 0.0004$). However, there was a lesser effect observed in the alisertib treatment alone. Furthermore, the combination treatment in siControl cells significantly increased the mitotic transit time compared to H_2O_2 alone ($p = 0.0027$).

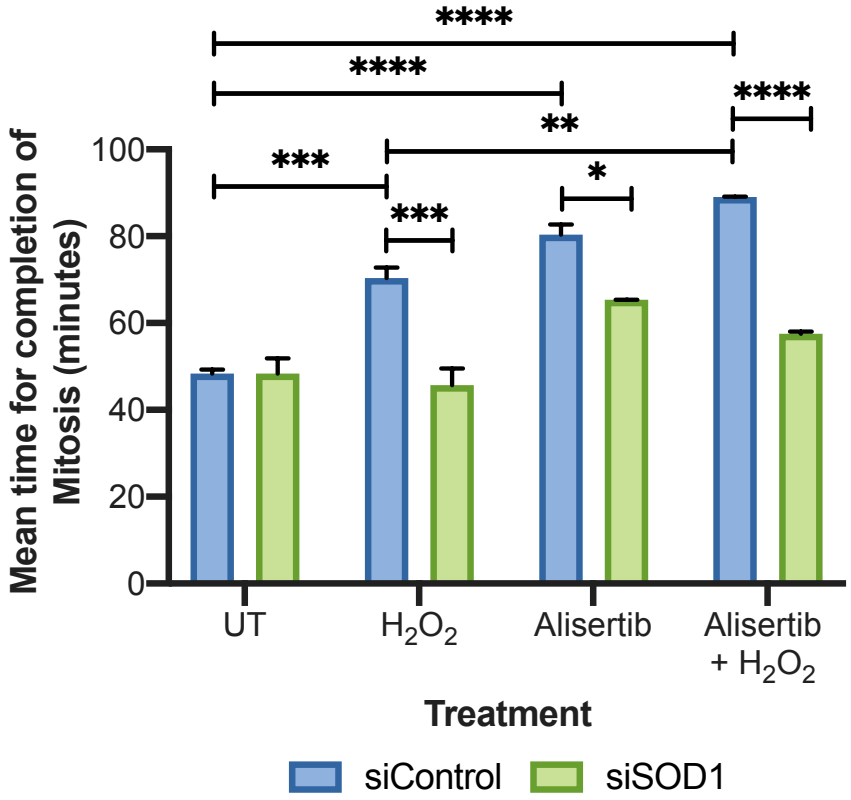

Figure 3.20: The effect of alisertib on mitotic progression.

Time-lapse live cell microscopy analysis of the mean time taken to complete mitosis following SOD1 knockdown (siSOD1-5) in HeLa cells treated with 25 nM alisertib approximately 2 hours prior to the initiation of the experiment. A maximum of 50 cells for each condition was counted and the data represents the overall mean of each independent experiments +/- SEM (N= 2). One-way ANOVA with Dunnett's correction test for multiple comparisons was performed to determine statistical significance (* denotes $p \leq 0.05$, ** $p \leq 0.01$, *** $p \leq 0.001$ and **** $p \leq 0.0001$).

The inhibition of Aurora A demonstrated an additive effect with H_2O_2 treatment, whereas the loss of mitotic arrest following SOD1 knockdown was less prominently observed with alisertib alone. From these findings, it was deduced that SOD1 probably did not act through Aurora A to induce the prolonged mitotic transit activated by H_2O_2 treatment.

3.2.5.6 SOD1 regulates PP2A activity following DNA damage to induce mitotic arrest.

It is known that ROS is involved in the regulation of various signalling pathways, through reversible modifications to proteins. This includes the oxidation of cysteine and methionine residues changing the protein structure, which in turn affects activity, function and interactions (Reichmann, Voth and Jakob, 2018). It has been observed that phosphorylation events are enriched after treatment with H_2O_2, suggesting that this oxidative stress inducer targets regulatory phosphatases for inhibition (Rao and Clayton, 2002). There are different types of phosphatases that target specific phosphorylation sites on various proteins, such as protein tyrosine phosphatases (PTPs) and protein serine-threonine phosphatases (PSPs). Both types of phosphatases are negatively regulated by H_2O_2 oxidation, most likely targeting cysteine residues within the enzymes active sites (Sullivan *et al.*, 1994; Raman and Pervaiz, 2019). Hence providing the mechanism in which oxidative stress regulates signalling pathways. Furthermore, SOD1 has also been implicated in phosphatase regulation via H_2O_2 generation (Juarez *et al.*, 2008) or may act through direct cysteine oxidation (Winterbourn, Peskin and Parsons-Mair, 2002; Bakavayev *et al.*, 2019). Therefore, the effect of SOD1 on phosphatase activity was investigated.

Firstly, the effect of SOD1 and H_2O_2 on total PTPs activity was measured, via a fluorescent assay **(Figure 3.21A)**. It was expected that activity would be reduced following the administration of H_2O_2 to HeLa cells due to phosphatase inhibition, and activity would increase following SOD1 knockdown if SOD1 was involved in the inhibition. It was observed that SOD1 knockdown generated an increase in general phosphatase activity in both untreated and H_2O_2 treated conditions, yet the increase in activity was not as profound in H_2O_2 treated cells. However, there was a similar increased activity level following H_2O_2 treatment between the siControl and siSOD1

conditions. Overall, the differences obtained were not significant. Therefore, I decided to focus on a single phosphatase.

More specifically, the serine-threonine phosphatase PP2A dephosphorylates various kinases throughout mitosis promoting mitotic entry, progression and exit (Raman and Pervaiz, 2019). H_2O_2 is known to inactivate PP2A activity (Rao and Clayton, 2002; Ahn *et al.*, 2019), which has specifically impacted mitosis (Ahn *et al.*, 2019). The inactivation is suggested to occur via oxidation of cysteine residues in the catalytic domain (Foley *et al.*, 2007). Hence, highlighting PP2A to be a potential target in the SOD1-dependent MDDC. PP2A activity levels were exclusively measured via a colourimetric assay involving immunoprecipitation of the PP2A catalytic (PP2A-C) domain **(Figure 3.21B)**. A slight reduction of PP2A activity was measured after H_2O_2 treatment of siControl cells compared to the untreated siControl condition. However, following SOD1 knockdown in both untreated and H_2O_2 treated conditions, the activity of PP2A was greatly enhanced compared to the untreated siControl cells.

SOD1's influence on PP2A activity was investigated further via mitotic progression assays. Firstly, the PP2A inhibitor okadaic acid (OA) was administered to HeLa cells in the presence and absence of SOD1 and H_2O_2 treatment, and the effect on mitotic progression was measured. The treatment with OA caused a significantly prolonged mitotic transit time, despite H_2O_2 treatment or SOD1 knockdown compared to siControl untreated cells (all $p < 0.0001$ except siControl untreated vs siSOD1 + OA; $p = 0.0019$) **(Figure 3.21C)**. Furthermore, complementation of HeLa cells with an exogenous PP2A-C domain expression vector (Myc-PP2A) was used to determine if an excess of PP2A could overcome the mitotic arrest observed following H_2O_2 treatment, to indicate if PP2A inhibition might be responsible for the SOD1-dependent mitotic arrest **(Figure 3.21D)**. It was deduced that the increase of PP2A expression significantly reduced the mitotic transit time after H_2O_2 treatment in the siControl condition, compared to the corresponding control treated condition ($p < 0.0001$). Whereas there was no effect of PP2A overexpression following SOD1 knockdown and/or H_2O_2 treatment. To ensure the overexpression was successful, the excess cells were utilised for western blot analysis. It was confirmed for each independent mitotic progression assay that Myc-PP2A was expressed and SOD1 was knocked down **(Figure 3.21E)**.

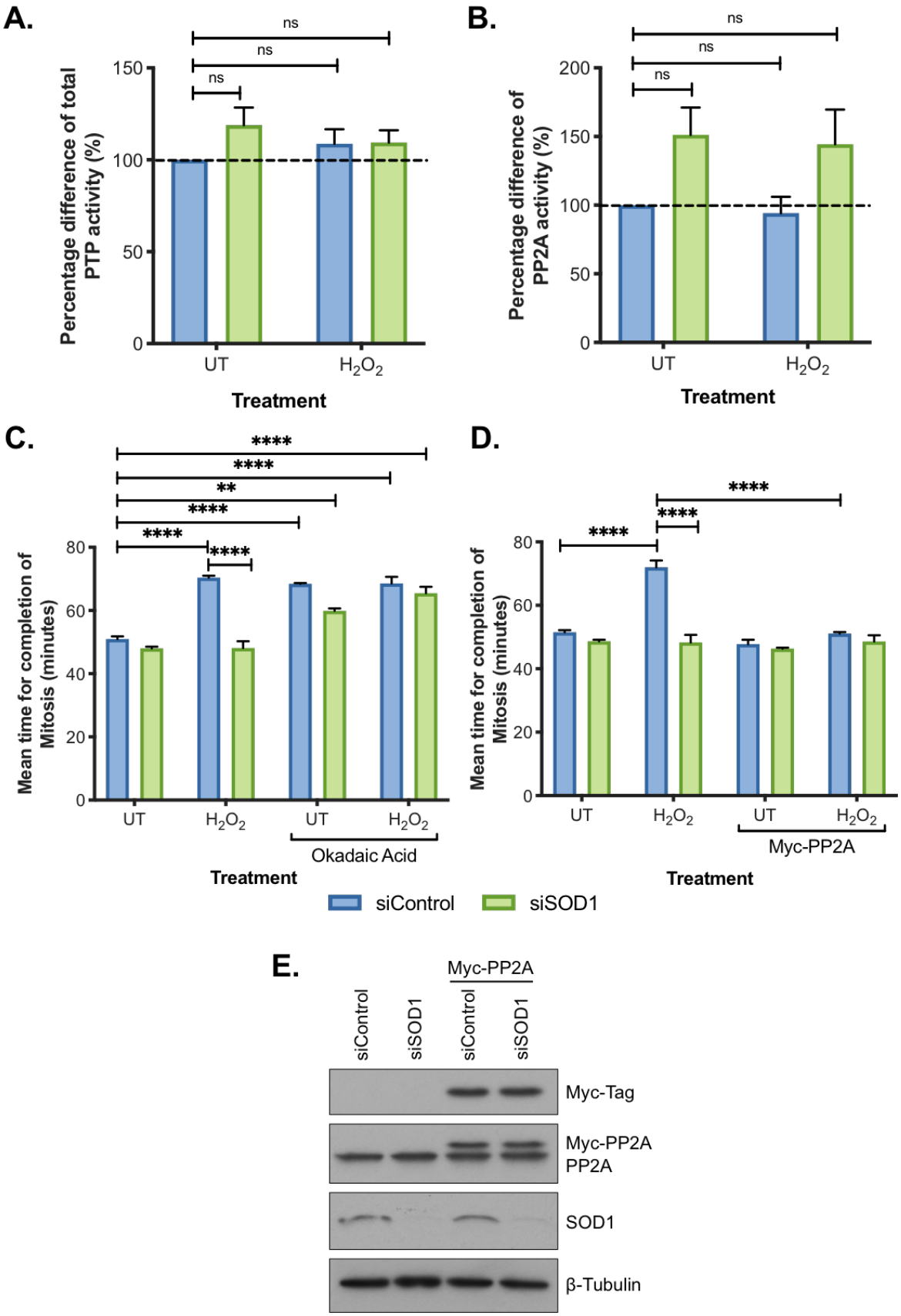

Figure 3.21: The investigation into the potential role of PP2A on mitotic arrest induced by H_2O_2.

Legend on next page.

Figure 3.21: The investigation into the potential role of PP2A on mitotic arrest induced by H_2O_2. A. The protein tyrosine phosphatase activity was measured in cells treated with H_2O_2 (50 μM) for 1 hour, in the presence and absence of SOD1 (siSOD1-5). Each condition was measured in duplicate and averaged for each independent repeat +/- SEM (N= 4). The dotted line represents the baseline phosphatase activity in the untreated control for comparison. One-way ANOVA with Dunnett's correction test for multiple comparisons was performed to determine statistical significance (ns denotes p = non-significant). **B.** as in **A.** with the exception PP2A activity was specifically measured +/- SEM (N= 3). The dotted line represents the baseline PP2A activity in the untreated control for comparison. One-way ANOVA with Dunnett's correction test for multiple comparisons was performed to determine statistical significance (ns denotes p = non-significant). **C.** Time-lapse live cell microscopy analysis of the mean time taken to complete mitosis following SOD1 knockdown (siSOD1-5) in HeLa cells treated with 20 nM okadaic acid and/or H_2O_2 (50 μM) 2 hours prior to the initiation of the experiment. A maximum of 50 cells for each condition was counted and the data represents the overall mean of each independent experiments +/- SEM (N= 3). One-way ANOVA with Dunnett's correction test for multiple comparisons was performed to determine statistical significance (** denotes $p \leq 0.01$ and **** $p \leq 0.0001$). **D.** as in **C.** with the exception that cells were transfected with 1 μg Myc-PP2A expression vector and treated with H_2O_2 (50 μM) 2 hours prior to the initiation of the experiment +/- SEM (N= 3). One-way ANOVA with Dunnett's correction test for multiple comparisons was performed to determine statistical significance (**** denotes $p \leq 0.0001$). **E.** Representative western blot showing the knockdown of SOD1 and overexpression of Myc-PP2A (N= 3). Extracts were collected following replating of each mitotic progression assay and probed for SOD1, Myc-Tag to represent Myc-PP2A, PP2A and β-Tubulin.

To summarise, SOD1 appeared to regulate PP2A activity levels and PP2A inhibition and overexpression influenced mitotic progression, indicating that PP2A may be involved in the SOD1-dependent MDDC. SOD1 has been described to exhibit pro-oxidant activity and I theorise SOD1 regulates phosphatase activity through cysteine oxidation, via the direct reaction of SOD1 with cysteine residues (Winterbourn, Peskin and Parsons-Mair, 2002; Bakavayev *et al.*, 2019) or indirectly via H_2O_2 generation (Juarez *et al.*, 2008). To elucidate the mechanism behind PP2A regulation by SOD1, I first aimed to identify the specific cysteine (C) residues that undergo oxidation in the presence of SOD1 via a mass spectrometry (MS) screen. The specific residues are

currently unknown, yet it is theorised in the literature that the vicinal C266 and C269 residues proximal to the PP2A-C domain's active site may be of significance (Foley *et al.*, 2007). These residues may form a disulphide bridge following oxidation, leading to PP2A inactivity.

Prior to the MS analysis, the PP2A-C domain was visualised using PyMOL Molecular Graphics System software, to identify cysteine residues of particular interest **(Figure 3.22A)**. The assessment of the 3D phosphatase structure deduced that there were three cysteine residues proximal to the active site (His-118), C196, C266 and C269. These would be of particular interest for the MS oxidation screen. Next, a theoretical digest was performed on the PP2A-C domain using the PeptideMass software by Expasy, to determine if the peptides would be detected and where the residues of interest would reside **(Figure 3.22B)**. Each of the three residues of interest were featured on individual peptides, which will aid in the detection of any modifications.

The MS mapping of PP2A cysteine oxidation involved the reaction of exogenous recombinant proteins for PP2A-C domain and SOD1 in vitro. PP2A was analysed alone and in the presence of SOD1. Reduced cysteine residues were labelled with iodoacetamide in the PP2A alone control sample and isotopically labelled iodoacetamide D4 in the PP2A samples containing SOD1. Iodoacetamide reacts with reduced cysteines to produce a detectible Carbamidomethyl modification, whereas oxidised cysteine residues would not exhibit this modification. The preliminary data collected for the mapping of PP2A cysteine oxidation in the presence of SOD1 demonstrated that the residues of interest were not detected, with exception of C269 which was reduced **(Figure 3.22C)**. All residues of interest were reduced in the PP2A alone control sample. Further details are featured in Appendix **Table 7.1**.

A.

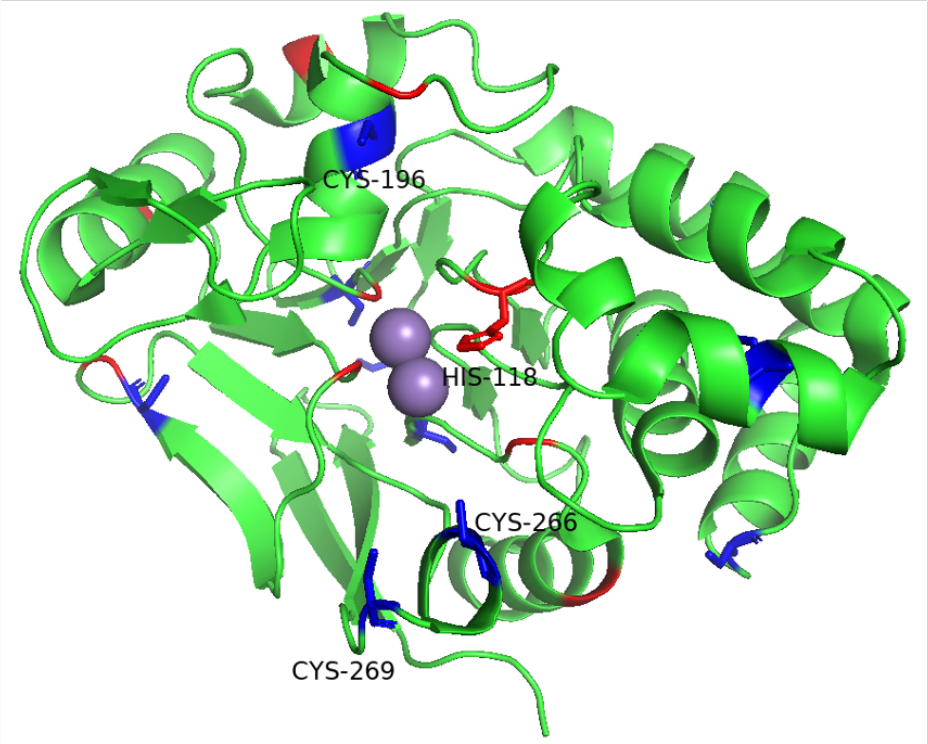

B.

Sequence coverage: 92.6 %

	mass	position	#MC	modifications	peptide sequence
	4166.0942	145-181	0		YFTDLFDYLPLTALVDGQIF CLHGGLSPSIDTLDHIR
	2655.2797	215-239	0		GAGYTFGQDISETFNHANGL TLVSR
C196	2452.0907	186-206	0		LQEVPHEGPMCDLLWSDPDD R
	2403.1042	50-70	0		CPVTVCGDVHGQFHDLMELF R
	1858.8112	240-254	0		AHQLVMEGYNWCHDR
	1792.7846	75-89	0		SPDTNYLFMGDYVDR
	1734.8156	122-135	0		QITQVYGFYDECLR
	1655.9254	90-104	0		GYYSVETVTLLVALK
	1647.7683	9-21	0		ELDQWIEQLNECK
C266	1646.7995	255-268	0		NVVTIFSAPNYCYR
C269	1621.7560	269-283	0		CGNQAAIMELDDTLK
	1340.6633	284-294	0		YSFLQFDPAPR
	960.4745	42-49	0		ESNVQEVR
	951.4683	137-144	0		YGNANVWK
	918.4891	22-29	0		QLSESQVK
	829.4315	207-214	0		GGWGISPR
	795.4107	296-302	0		GEPHVTR
	755.3610	304-309	0	METH: 309 769.3767 PHOS: 307 835.3273	TPDYFL
	699.3169	116-121	0		GNHESR
	615.4188	111-115	0		ITILR
	603.3712	37-41	0		EILTK
	579.2807	30-34	0		SLCEK
	522.2228	1-4	0		MDEK

Figure 3.22: Preliminary data for the mapping of PP2A oxidation in the presence of SOD1.

Legend on next page.

C.

PP2A Residue	Modification	
	PP2A	PP2A + SOD1
C196	Reduced	Not detected
C266	Reduced	Not detected
C269	Reduced	Reduced

Figure 3.22: Preliminary data for the mapping of PP2A oxidation in the presence of SOD1.

A. A 3D model of the catalytic C subunit of PP2A generated by PyMOL Molecular Graphics System, indicating the cysteine residues proximal to the active site (HIS-118). Courtesy of Patricia Belver. **B.** The data from the theoretical digest of the PP2A-C subunit using trypsin was performed using PeptideMass software. The residues of interest are highlighted. **C.** Preliminary data for the mapping of PP2A cysteine residues, indicating if the residues of interest were modified in the error tolerance search.

Overall, the preliminary data confirms the identification of reduced cysteine residues. Yet as the PP2A residues of interest were mainly undetected following the reaction with SOD1, further work is required to elucidate the effect of SOD1 on PP2A.

3.3 Discussion.

In this chapter, the novel role of SOD1 in the MDDC was successfully confirmed and explored, revealing a potential mechanism of action, which involves the regulation of PP2A activity, to facilitate the response to mitotic DNA damage. Furthermore, a role of SOD1 in DNA damage repair was also identified.

3.3.1 SOD1 is required for the mitotic DNA damage checkpoint.

SOD1 was confirmed to be involved in the MDDC via numerous methods including, mitotic population **(Figure 3.2)**, mitotic progression **(Figures 3.2, 3.3 and 3.4)** and

complementation assays **(Figure 3.6)**. The prolonged mitotic transit/activation of the MDDC was observed in response to DNA damage inducers (IR, carboplatin and TMZ) and oxidative stress inducers (pyocyanin and H_2O_2), in a SOD1-dependent manner. The IR-induced arrest was conducted in cancer (HeLa and MCF7) and non-cancer (MRC5VA) cell lines **(Figure 3.2)**. Interestingly, in MRC5VA cells the DNA damage-induced mitotic delay was not consistently observed, bringing down the mean and generating a larger error bar compared to the cancer cell lines. The loss of mitotic delay following SOD1 knockdown was also less prominent, compared to the cancer cell lines. I hypothesise that the non-cancerous cell line possesses functional and robust interphase DDR checkpoints, compared to the cancerous cell lines. MRC5VA cells were expected to utilise the interphase checkpoints to repair the majority of damage induced and fewer cells with excess or unrepaired DNA damage progressed into mitosis, activating the MDDC.

Furthermore, in the literature, IR (Strasser-Wozak *et al.*, 1998), carboplatin (Wang *et al.*, 2010), TMZ (Hirose, Berger and Pieper, 2001) and H_2O_2 (Li *et al.*, 2009) have been found to cause G_2/M cell cycle arrest. The specific mitotic cell population was not assessed in these studies, yet an enrichment in mitotic cells may have contributed to the enhanced G_2/M peak observed. More specifically, in a recent publication, H_2O_2 has been shown to induce a SAC-independent mitotic arrest in budding yeast (Atalay *et al.*, 2017). Whilst this study is simplistic in content, with the little data presented and in a little-known journal, I believe the conclusions drawn are reliable and supports the findings in this thesis.

3.3.2 Intracellular ROS levels did not influence MDDC.

The MDDC was found to be associated with oxidative stress pathways, as the checkpoint was activated by oxidative stress inducers and is dependent on the antioxidant, SOD1. Therefore, it was important to assess if the arrest observed was in response to an enrichment of ROS levels. A fluorescent CM-H2DCFDA probe to detect general ROS levels was used in this chapter, yet the mechanism of the probe activation was primarily in response to the detection of H_2O_2 levels (BioTek, 2021). Therefore, it was expected that the levels of ROS detected would increase in an H_2O_2 dose dependent manner **(Figure 3.7A)**. Whilst this was the general effect observed, a

consistent dose response was not achieved due to 25 and 100 μM H_2O_2 doses unexpectedly demonstrating the little effect on ROS levels. Furthermore, there were only small and non-significant increases in the ROS concentration detected after IR (5 and 10 Gy) treatment **(Figure 3.7B)**. It is known and has been demonstrated (Lee *et al.*, 2012; Sun *et al.*, 2020), that IR greatly enhances intracellular ROS levels. A comparison of the methodology used in this research and the Lee *et al.* (2012) and Sun *et al.* (2020) studies revealed numerous similarities, including IR dose (5 and 10 Gy, 5 Gy and 8 Gy respectively), IR treatment times (1 hour, 30 minutes and 2 hours respectively), probe concentration (10 μM) and the probe incubation time in this research and the Sun *et al.* (2020) study was both 1 hour. The main difference was that the probe was incubated with the cells prior to treatment in this research, compared to post-treatment in both the studies. This factor was considered during the assay optimisation conducted for this research, but no difference was obtained when comparing when probe incubation occurred, so the manufacturer's instructions were followed in which probe incubation was conducted before treatment. To summarise, a major fault in the methodology could not be determined to explain the low levels of ROS observed following IR treatment.

Then my data demonstrated carboplatin and TMZ treatment did not affect intracellular ROS levels **(Figure 3.7B)**. However, as these chemotherapeutics are not widely recognised to induce ROS this was to be expected. In the literature, TMZ treatment has been found to induce superoxide ($O_2^{\bullet-}$) radicals 30 minutes post-treatment, potentially due to damage to the mitochondria (Svilar *et al.*, 2012). Therefore, the CM-H2DCFDA probe would be inadequate to detect the specific type of ROS induced by TMZ treatment, yet this was still not observed using the superoxide probe 20 minutes post-TMZ treatment (data not shown). Then there is little information on carboplatin inducing ROS in the literature, one paper demonstrates an increase in H_2O_2 (using the CM-H2DCFDA probe) following a 24-hour treatment (He *et al.*, 2018), but this could be accounted for by an increase in cellular damage following the extended treatment period. Throughout these experiments, there was a consistent observable decrease in the levels of ROS following SOD1 knockdown. This was determined to be due to the reduction of H_2O_2 produced by SOD1 antioxidant inactivity, yet the levels of $O_2^{\bullet-}$ radicals would increase, as observed by the superoxide probe (data not shown).

To further investigate the potential involvement of oxidative stress in instigating mitotic arrest, I set out to reduce ROS levels via selenium supplementation, following treatment with the various agents (IR, TMZ, carboplatin and H_2O_2) analysed **(Figure 3.9)**. Selenium is an important active site component of the antioxidant glutathione peroxidase (GPx) enzyme family. The enrichment of the intracellular concentration of selenium aids in the detoxification of H_2O_2 by positively impacting the transcription and activity of the GPx enzymes, specifically GPx1 (Jerome-Morais *et al.*, 2013). It was deduced that selenium supplementation significantly reduced the mitotic transit time induced by DNA damage and oxidative stress inducing agents in siControl cells. However, this effect observed was not deduced to be due to the reduction of ROS levels, as again it was found that all treatments did not substantially or consistently induce high levels of ROS, and surprisingly selenium did not reduce ROS levels adequately or at all. The dose of selenium (50 nM) used in this research was shown to be sufficient to increase GPx1 levels, hence should reduce intracellular ROS. This is supported in the literature as 30 nM of selenium was adequate to increase GPx1 activity levels in the colon cancer cell line; HCT116 (Jerome-Morais *et al.*, 2013) and leukaemia cell line; HL-60 (Speier, Baker and Newburger, 1985), as well as enhance the GPx1 protein levels (Jerome-Morais *et al.*, 2013) and sufficiently reduce the H_2O_2 concentration (Speier, Baker and Newburger, 1985). Therefore, this indicates that the mitotic arrest and effect observed by selenium was not dependent on the levels of ROS. The mechanism of selenium in the reduction of mitotic duration is proposed in section **3.3.6**.

In the literature, levels of ROS have been demonstrated to increase in mitosis which is further enhanced during mitotic arrest and results in increased protein oxidation, suggesting ROS levels may act as a signal during mitosis (Patterson *et al.*, 2019). Despite the strong association of the MDDC with the oxidative stress pathway, the findings of this thesis indicate the checkpoint is independent of oxidative stress, as the DNA damaging agents did not induce substantial ROS levels yet were also capable of inducing the SOD1-dependent mitotic arrest, and ROS levels were not reduced following selenium supplementation, despite its ability to rescue the mitotic arrest. Overall, this indicates the SOD1-dependent activation of the MDDC is not due to redox impairment. Furthermore, the induction of oxidative stress by H_2O_2 has been found to impair Aurora A activity via hyperphosphorylation, which disrupted spindle assembly

inducing mitotic arrest, similar to the use of a small molecule inhibitor (MK-5108) (Wang *et al.*, 2017). Therefore, it was hypothesised that SOD1 may act through Aurora A to induce the mitotic arrest observed. However, the additive effect obtained following alisertib (Aurora A inhibitor) and H_2O_2 treatment in the siControl conditions **(Figure 3.20)**, suggests that the prolonged mitotic duration induced by each treatment individually are independent of each other. Then the effect of alisertib treatment in the absence of SOD1 increased mitotic transit similar to H_2O_2 treatment in the control condition and exhibited less of a reduction in mitotic transit time, compared to SOD1 knockdown and H_2O_2 treatment alone or in combination with alisertib. Therefore, these findings indicate the SOD1-dependent mitotic arrest does not act through Aurora A inactivation. Further supporting the activation of the MDDC is independent of redox impairment.

Finally, the involvement of BER, the repair mechanism which responds to oxidative DNA damage lesions, was also analysed to determine if the SOD1-dependent MDDC utilised this pathway to induce mitotic arrest **(Figure 3.18)**. A key upstream BER enzyme, OGG1 was overexpressed using a Myc-OGG1 expression vector with H_2O_2 treatment, but this demonstrated the same effect as the untransfected conditions. Then the complementation with Myc-OGG1 had no effect in either SOD1 knockdown conditions, regardless of treatment. Overall, this indicates that SOD1 did not activate BER for the MDDC, again indicating the MDDC is independent of oxidative stress. Interestingly another BER enzyme, Human MutT Homolog 1 (MTH1) was recently identified to be involved in mitotic progression through the maintenance of microtubule polymerisation and the inhibition of this enzyme caused mitotic cell cycle arrest and enrichment in oxidative DNA damage lesions (Gad *et al.*, 2019). The MTH1 association with mitotic arrest may be of interest in future work.

3.3.3 The enzymatic function of SOD1 is responsible for mitotic arrest.

Functional SOD1 mutants were generated to help determine how this enzyme mediates mitotic arrest. It was deduced that the enzymatically inactive G85R SOD1 mutant in the absence of WT SOD1, failed to rescue the mitotic arrest following H_2O_2 treatment, obtaining similar mitotic transit times to the untreated control condition **(Figure 3.19)**. Here, I have identified that SOD1 requires its enzymatic active site to

stimulate mitotic arrest following DNA damage. To link this with my findings that SOD1 inactivates PP2A phosphatase to induce mitotic arrest, a study by Juarez *et al.* (2008) found that SOD1 regulated phosphatase activity during other cellular pathways, via the production of H_2O_2. However, an overall increase in H_2O_2 production following DNA damage has not been consistently observed in this thesis. Rather, I hypothesise a localised production of H_2O_2 by DNA damage activated SOD1, which will negatively impact phosphatase activity (specifically PP2A) causing mitotic arrest. Interestingly, another pro-oxidant role of SOD1 has been found, where SOD1 was capable of catalysing thiol oxidation, with specificity for cysteine residues which can render proteins inactive, implying SOD1 can directly mediate protein activity independent of dismutase activity (Winterbourn, Peskin and Parsons-Mair, 2002; Bakavayev *et al.*, 2019). Therefore, I also hypothesise that SOD1 could directly regulate the activity of PP2A in response to DNA damage, to activate and regulate the MDDC.

Furthermore, the S99A and S60,99A mutants did not completely rescue the mitotic transit time after H_2O_2 treatment in the absence of WT SOD1 **(Figure 3.19)**. It was reported by Tsang *et al.* (2014) that SOD1 activation at S60 and S99 was dependent on oxidative stress (Tsang *et al.*, 2014; Bordoni *et al.*, 2019). As I found that these mutants did not have a profound effect on mitotic transit and the effect observed was to a lesser degree than the G85R mutant, this supports my deduction that oxidative stress is not the activating influence of the SOD1-dependent MDDC. Then the phosphorylation of S60 was determined to be vital for effective SOD1 nuclear localisation and was enhanced by S99 phosphorylation (Tsang *et al.*, 2014). As both S99A and S60,99A mutants produced the same effect on mitotic transit, it can be deduced that the effect observed was dependent on the integrity of the S99 phosphorylation site, which is most likely independent of SOD1 localisation in the nucleus. In support of this, Bordoni *et al.* (2019) deduced the phosphorylation of S60 and S99 were found in the nucleus and cytoplasm respectively, during an MS screen of SOD1 phosphorylation events (Bordoni *et al.*, 2019). Furthermore, the G93A SOD1 mutant has been reported to be restricted in the cytoplasm, potentially via protein misfolding (J. Li *et al.*, 2019), yet this mutant did not affect mitotic transit in this thesis. Taken together, it can be concluded that the effect of the S99 phosphorylation site is independent of nuclear localisation, indicating a potential secondary supportive function of SOD1 within mitotic arrest. Interestingly, two MS screens investigating the

phospho-proteome of the cell cycle, have identified the SOD1 S101 phosphorylation site, which corresponded to S99 in the amino acid sequence (Dephoure *et al.*, 2008; Olsen *et al.*, 2010). Both screens did not find SOD1 phosphorylation to be significantly changed within the context of the research interest of 'normal' cell cycle phosphorylation events. However, the study by Olsen *et al.* (2010) did hypothesise that the mitotic kinase polo-like kinase 1 (Plk1) may target the S99 phosphorylation motif of SOD1 (Olsen *et al.*, 2010). Overall, the S99 phosphorylation site requires further investigation within the MDDC.

3.3.4 SOD1 is involved in the DNA damage response and repair.

As the MDDC activation was concluded to be independent of redox impairment, and it is known that each treatment used to activate this SOD1-dependent checkpoint (IR, carboplatin, TMZ and H_2O_2) inflict DNA damage, the DNA damage axis was examined. Firstly, IR can cause damage directly and indirectly (radiolysis of water to produce hydroxyl ($^{\bullet}OH$) radicals) leading to DNA base damage, SSBs and the most toxic DSBs (Jackson and Bartek, 2009; Schipler and Iliakis, 2013). Similarly, H_2O_2 causes DNA damage via the production of $^{\bullet}OH$ radicals by the Fenton reaction, which also leads to DNA base damage, SSBs and eventual DSBs (Schipler and Iliakis, 2013). Then the DNA platinum adducts generated by carboplatin treatment results in DSBs (Galluzzi *et al.*, 2014). Finally, TMZ induces methylation of DNA bases, causing damage and removal via BER or mismatch repair (MMR), failure to do this results in SSBs and eventual DSBs (Jackson and Bartek, 2009; Erasimus *et al.*, 2016). (Eventual DSBs refers to unrepaired SSBs or SSBs generated during BER or MMR, that then forms DSBs through damage site proximity or following DNA replication (Schipler and Iliakis, 2013; Erasimus *et al.*, 2016).)

It was determined that in response to DNA damage there was a significant enrichment of SOD1 in the nucleus 0.5-16 hours post-IR treatment **(Figure 3.10)**. This indicates SOD1 may localise in the nucleus to participate within the DDR. Similarly, the Thompson laboratory and other groups in the literature have observed the same phenomenon following H_2O_2 treatment 15 minutes-4 hours post-treatment (Tsang *et al.*, 2014; Bordoni *et al.*, 2019; X. Li, Qiu, *et al.*, 2019). Furthermore, phosphorylation of SOD1 at S60 and S99 was found to enable SOD1 localisation to the nucleus, which

was regulated by DDR proteins, Chk2 via ATM (Tsang *et al.*, 2014; Bordoni *et al.*, 2019). Yet Tsang *et al.* (2014) and Li *et al.* (2019) determined this occurred to enable SOD1 stimulation of gene expression. However, it is feasible to assume the ATM-Chk2 activation of SOD1 occurs following DNA damage. Overall, I propose that DNA damage stimulates the enrichment of nuclear SOD1.

DNA damage levels were assessed via alkaline comet assays **(Figure 3.11)** and immunofluorescent analysis of γH2AX foci **(Figure 3.12)**. The data from both assays demonstrate the enhanced level of DNA damage upon SOD1 knockdown. Similar findings have been observed in ALS models with mutant SOD1 (G93A) exhibiting higher DNA damage than WT SOD1 (Sau *et al.*, 2007). Taken together, my data suggest that either SOD1 is involved in the regulation of the DDR or the loss of SOD1 leads to more DNA damage through enrichment of toxic ROS radicals. A study by Inoue *et al.* (2010) supports that the increase in $O_2^{\bullet-}$ radicals upon SOD1 depletion, negatively impacted genome stability. However, this study has shown the enrichment of $O_2^{\bullet-}$ radicals occurs 108-120 hours post-SOD1 depletion, which then initiated the damage (Inoue *et al.*, 2010). In my research, the effects observed on DNA damage were demonstrated at 72 hours post-knockdown, which then debates if the effects observed are due to oxidative stress. Furthermore, if the increase in damage was due to oxidative stress rather than reduced repair, an increase in DNA damage in the untreated cells would also be expected, as there would be more $O_2^{\bullet-}$ radicals to generate damage in this condition too. However, this was not observed, hence SOD1 is more likely to be involved in the DDR and indicates the SOD1-dependent activation of the MDDC is due to DNA damage.

As the level of DNA damage was enhanced and prolonged in the absence of SOD1, and I have concluded this is unlikely to be due to an increase in ROS, the cells ability to repair the damage was also assessed. DNA repair capacity was measured via RAD51 foci formation following IR treatment **(Figure 3.13)**. As expected, RAD51 foci formation was significantly enhanced after IR treatment in the control condition, but interestingly, irradiated SOD1 knockdown cells exhibited a significant reduction in RAD51 foci. This supports the presence of more damage in the absence of SOD1, as the ability to repair the lesions by HR is impaired. Recently a decrease in RAD51 and DNA ligase 4 was observed in SOD1 knockout mice (Nguyen-Powanda and Robaire,

2021), indicating that as well as HR, nonhomologous end-joining (NHEJ) may also be regulated by SOD1. Another recent study by Godinez *et al.* (2020) shown that HR and NHEJ repair pathways are activated upon DNA damage encountered in mitosis (Godinez *et al.*, 2020). This also strengthens the association of SOD1 with DNA repair following mitotic DNA damage. Furthermore, in yeast cells, the knockout of SOD1 was demonstrated to cause a defective Mec1 (ATM/ATR) mediated repair pathway (Carter *et al.*, 2005). The ATM/ATR pathway has been shown to mediate the recruitment and activation of RAD51 via phosphorylation (Sørensen *et al.*, 2005; Flott *et al.*, 2011; Weinberg, 2014), which is vital for its DNA binding capability and functional ATPase activity (Flott *et al.*, 2011). In this chapter SOD1 was associated with phosphatase regulation (section **3.3.6**), hence it is theorised that the reduction in RAD51 accumulation at the DNA lesions may be due to enhanced phosphatase activity in the absence of SOD1, impairing this vital phosphorylation event of RAD51. The association of SOD1 and the ATM pathway is frequently reported, plus the activation of HR repair is downstream of ATM. I theorise the existence of a positive feedback loop between ATM and SOD1, as the ATM DDR pathway potentially activates nuclear SOD1 in response to DNA damage and in turn, SOD1 appears to regulate the ATM-mediated HR repair pathway. Overall, these findings support a role of SOD1 in the response to DNA damage, specifically in DNA repair.

Currently, within cancer therapeutics, DNA damage proteins are targeted in combination with standard radiotherapy and chemotherapy (ClinicalTrials.gov, 2016, 2021a, 2021b; Lee *et al.*, 2018). This disables the DDR enhancing cellular sensitivity to the DNA damage inducing agents. As I have determined SOD1 to be involved in effective DNA repair, this highlights SOD1 as a potential anti-cancer target. Hence the impact of SOD1 knockdown on cell survival in combination with IR treatment was measured. However, SOD1 knockdown did not sensitise cells to any dose of IR treatment (0-5 Gy) administered **(Figure 3.14)**. This was unexpected as it has been consistently concluded within the literature that the reduction of SOD1 activity by depletion (siRNA and shRNA) and inhibition (ATN-224, LD100 and LCS-1), reduced cell viability via apoptosis in a variety of cancer cell lines and patient tumour samples (Somwar *et al.*, 2011; Glasauer *et al.*, 2014; X. Li, Chen, *et al.*, 2019; Liu *et al.*, 2020). The effects observed were even reversed via SOD1 overexpression via expression vectors (Somwar *et al.*, 2011) or the SOD1 mimetic MnTBAP (Glasauer *et al.*, 2014).

But these studies do not investigate the potential sensitisation of cells to current anti-cancer therapies upon SOD1 inhibition or knockdown. Furthermore, it has been determined that the SOD1 inhibitor imposed a greater anti-proliferative effect compared to the use of siRNA, due to only a partial reduction in SOD1 (Juarez *et al.*, 2008). It may be beneficial to measure SOD1 activity levels following siRNA treatment to quantify the effectiveness of knockdown in this research.

There are numerous mechanisms described to explain how SOD1 influences cancer cell proliferation, such as the increase in H_2O_2 intracellular levels which encourage proliferative pathways (X. Li, Chen, *et al.*, 2019), enhancing lipid metabolism (Li *et al.*, 2018), and via the increase of SOD1 in fibroblasts within the tumour microenvironment (Li *et al.*, 2020). The vast differences in these mechanisms may highlight a more complex role of SOD1 within the cell, which when inhibited impacts many pathways contributing to cell death. Alternatively, this demonstrates that the role of SOD1 in tumorigenesis is unknown and requires further work involving the consolidation of the current mechanisms described within the literature before SOD1 can be considered an anti-cancer target. Furthermore, I determined SOD1 contributes to the DNA repair, but SOD1 knockdown does not completely diminish the cells ability to overcome damage leading to large scale cell death, unlike with key DDR proteins such as ATM. Therefore, the lack of sensitisation of cells in the absence of SOD1 to IR treatment found in this thesis, indicates that there might be an alternative more predominant pathway which ensures cell survival. Overall, further work is required before SOD1 can be exploited in cancer treatment.

3.3.5 SOD1 regulates the MDDC independent of the SAC.

Furthermore, the SOD1-mediated mitotic delay was also independent of the SAC, as there was no effect of SOD1 on MCC protein and mRNA levels, SAC functionality and BubR1 recruitment to the kinetochore-centromeric region in the absence or presence of DNA damage **(Figure 3.17)**. In contrast, within the literature, many studies support the existence of a mitotic response to DNA damage, which causes a SAC-mediated mitotic arrest (Mikhailov, Cole and Rieder, 2002; Nitta *et al.*, 2004; Kim and Burke, 2008). In yeast, it was proposed the arrest was due to ATM and ATR activation of the SAC, independent of spindle attachment (Kim and Burke, 2008), but these findings did

not translate to human cells as the arrest was determined to be due to kinetochore defects caused by the damage affecting spindle attachment, independent of ATM (Mikhailov, Cole and Rieder, 2002). The Thompson laboratory has also demonstrated that the following DNA damage (IR treatment), there was an increase in the number of damaged centromeres, however, this was unaffected by SOD1 knockdown (data not shown). Again, indicating that the SOD1-dependent mitotic arrest does not act through the SAC. Furthermore, the study by Mikhailov *et al*. (2002) synchronised cells with nocodazole treatment, which activated the SAC leading to metaphase arrest, then proceeded to induce DNA damage. Therefore, it is feasible to assume the effects observed in Mikhailov's study were influenced by the use of the anti-mitotic agent. Whereas the analysis conducted in this thesis has demonstrated the DNA damage induced mitotic arrest in a more natural setting, plus SOD1 had no effect following nocodazole treatment on SAC-mediated arrest. Overall, my data suggests the SOD1-mediated mitotic arrest acts independently of the SAC. Furthermore, a post-SAC, pre-anaphase arrest has been described following DNA damage, due to securin phosphorylation by Chk1 which prevents its degradation by APC/C (Wang *et al.*, 2001). In summary, it is important to determine the specific phase of mitosis in which the SOD1-dependent activation of the MDDC occurs, to further elucidate the mechanism.

3.3.6 PP2A activity regulates SOD1-dependent mitotic arrest after DNA damage.

Initially, the total level of PTP activity was measured following SOD1 knockdown and H_2O_2 treatment, it seemed that SOD1 knockdown appeared to increase PTP activity in all conditions **(Figure 3.21A)**. Unexpectedly a similar effect was obtained in H_2O_2 treated siControl cells. Overall, the impact on total PTP activity was not substantial enough to suggest that this is the specific mechanism involved in the MDDC. This may be explained by PTP re-activation at the 1-hour time point assessed, as observed in the study by Sullivan *et al.* (1994). However, it is expected that the inhibition would occur over the 16-18 hours period mitotic arrest was measured during mitotic progression assays. Furthermore, the kit manufacturer's notes highlighted that PSPs may contribute to the substrate metabolism measured, indicating the effects observed may be non-specific to PTPs (Abcam, 2021). Taken together, I decided to focus on the single phosphatase PP2A, as it is a key mitotic phosphatase and has been found to

be regulated by H_2O_2. Similarly, SOD1 knockdown in both untreated and H_2O_2 treated conditions elevated PP2A activity levels approximately 1.44-1.51 fold, compared to the control untreated condition **(Figure 3.21B)**. Then a reduction in PP2A activity was indicated in H_2O_2 treated control cells. The increase in PP2A activity following SOD1 knockdown was more profound, compared to the slight influence observed on PTP activity, suggesting SOD1 mediates PP2A activity. In support of this, it was shown that PP2A gene expression was upregulated following both SOD1 inhibition and knockdown (X. Li, Chen, *et al.*, 2019).

Again the previously published inhibitory effect of H_2O_2 on PP2A activity (Rao and Clayton, 2002; Ahn *et al.*, 2019) was not obtained, despite the similar experimental parameters to the literature used in this thesis (H_2O_2 concentration and treatment time). However, one main difference is Ahn *et al.* (2019) isolated the mitotic cells for the activity assay. Therefore, the assay may not have been sensitive enough to detect the changes in PP2A activity by H_2O_2 in the asynchronous cell population used in this thesis. Alternatively, the data obtained may also be due to PP2A reactivation at the time point assessed. However, the specificity of H_2O_2 has been reported, as it has been determined that only PTPs are affected by H_2O_2 and not PSPs (Denu and Tanner, 1998). Furthermore, in regards to PSPs, it has been observed that only PP2A was inactivated and PP1 and PP2C were unaffected (Rao and Clayton, 2002). Despite, the previously published inhibitory effect of H_2O_2 not being consistently observed with either phosphatase assay, these findings highlight a role of SOD1 in PP2A regulation. Overall, I hypothesise SOD1 exhibits pro-oxidant activity to regulate phosphatases, specifically PP2A. This could occur via SOD1 binding to and directly oxidising cysteine residues leading to phosphatase inactivity, or SOD1 oxidising PP2A via the localised production of H_2O_2. These mechanisms would also allow SOD1 to maintain the cysteine oxidation state of PP2A over long time periods. In support of this theory, it is known that the level of cysteine oxidation in mitosis is enhanced and is further enhanced during mitotic arrest (Patterson *et al.*, 2019). The mechanism of how SOD1 mediates PP2A activity and the specific PP2A cysteine residues affected will be revealed in further oxidation mapping MS experiments.

The impact of SOD1 on PP2A activity was investigated further via mitotic progression assays using PP2A inhibitor, OA **(Figure 3.21C)** and a PP2A expression vector (Myc-

PP2A) **(Figure 3.21D)**. Firstly, the inhibition of PP2A via OA treatment significantly induced mitotic cell arrest in all conditions, regardless of H_2O_2 treatment or SOD1 knockdown status. The treatment with OA was also similar to the effect of H_2O_2 treatment alone and did not exhibit an additive affect like alisertib treatment **(Figure 3.20)** in the combination condition. These findings indicate the involvement of PP2A in mitotic transit, as the inhibition of PP2A with OA produced similar effects to H_2O_2 and reinstated the mitotic delay in the absence of SOD1. Furthermore, OA was reported to induce mitotic arrest via prolonged metaphase, independent of the SAC (Vandre and Wills, 1992). In support of these findings, the overexpression of Myc-PP2A was shown to significantly reduce and rescue the mitotic arrest induced by H_2O_2 treatment, similar to the untreated cells in the siControl conditions. This supports that PP2A is inactivated to induce the mitotic arrest, as the enrichment of active PP2A overcomes the arrest and reinstates 'normal' mitotic transit. The overexpression of PP2A had no effect in SOD1 knockdown conditions, as SOD1 would not inactivate PP2A and the arrest would not be induced. In summary, these findings support my hypothesis that SOD1 inactivates PP2A in response to DNA damage, leading to mitotic arrest during the MDDC.

Furthermore, other findings obtained within this chapter also provide support to the involvement of PP2A in the SOD1-dependent MDDC. Similarly, to the reducing effects observed on mitotic transit time upon PP2A overexpression in the treated control condition, selenium supplementation also significantly produced the same effect **(Figure 3.9)**. In addition to the enhancement of GPx1 activity, selenium supplementation has also been found to increase γ-glutamylcysteine synthetase and glutathione reductase activity, which act within glutathione biosynthesis and recovery of oxidised glutathione (GSSG) to reduced glutathione (GSH) respectively (Chung and Maines, 1981). Glutathione metabolism has also been implicated in PP2A regulation, as it was found that GSH reduced oxidised PP2A, thus reactivating the phosphatase's activity (Rao and Clayton, 2002). Alternatively, selenium has been identified to potently stimulate PP2A activity directly (Corcoran *et al.*, 2010). Therefore, the rescue of the mitotic arrest observed by selenium supplementation may be explained through the ability of selenium to stimulate PP2A activity, leading to mitotic progression. This hypothesis is further supported by the fact that selenium did not affect SOD1 knockdown cells (similar to PP2A overexpression), as in this situation PP2A would not

be inactivated. Overall, this finding further supports the theory that SOD1 inactivation of PP2A is responsible for the DNA damage induced MDDC.

Then it is well documented that PP2A is involved in the regulation of the DDR and repair pathways following DSBs. However, the SOD1 inactivation of PP2A does not explain the role of SOD1 in DNA damage and repair. In the literature, it was deduced that upon the depletion of PP2A, there was an enrichment of γH2AX foci and reduction of RAD51 foci formation at DNA lesions following IR treatment. This was determined to be due to PP2A regulation of ATM activity (Kalev *et al.*, 2012) and PP2A dephosphorylation of γH2AX for its removal from DNA lesions (Li *et al.*, 2015). These findings contradict the similar observations following SOD1 knockdown shown in this thesis **(Figure 3.12 and 3.13)** and as PP2A was shown to be enhanced in SOD1 attenuated cells, it is unexpected that the depletion of SOD1 and PP2A would produce the same effect on the DDR pathway. This may be explained by the longevity of PP2A knockdown treatment would dysregulate the majority of PP2A mediated signalling pathways leading to defectivity, compared to the transient inactivation by SOD1 reversible oxidation. Or this indicates that the role of SOD1 in the DDR is independent of PP2A and may be due to the targeting of another phosphatase. In summary, it is theorised that SOD1 targets a range of phosphatases and possibly even kinases, to regulate several cellular pathways.

3.3.7 Future work and limitations.

The mitotic phase in which the SOD1-dependent DNA damage mitotic arrest occurs is currently unknown. To determine this, it is proposed that fluorescently tagged histone H2B HeLa cells are utilised to replicate previously conducted mitotic progression assays, such as IR and H_2O_2 treatments with SOD1 knockdown. This will allow for better characterisation and comprehension of the MDDC for future experimentation.

It is also important to determine which proteins are responsible for the pro-oxidant activation of SOD1. ATM and Chk2 have previously been identified to activate SOD1 for nuclear localisation (Tsang *et al.*, 2014; Bordoni *et al.*, 2019), which I hypothesise to occur following DNA damage for SOD1's role in DNA repair. However, the

knockdown of ATM and Chk2 did not influence the mitotic population in the siRNA DNA damage screen conducted by the Thompson laboratory. Therefore, it is unlikely that either ATM or Chk2 activate SOD1 in response to mitotic DNA damage, rather other kinases are involved. The mutation of SOD1 at the S99 phosphorylation site (S99A) was found to influence mitotic progression following DNA damage, and has been hypothesised to be a target of the mitotic kinase, Plk1 (Olsen *et al.*, 2010). The activators of SOD1 for DNA repair and the MDDC could be determined via co-immunoprecipitation (co-IP) of SOD1 under the stimulatory conditions and probe for the hypothesised activators, or the SOD1 interactome could be identified via MS analysis. Overall, this will aid in the establishment of the roles of SOD1 in DNA repair and the MDDC.

To determine how SOD1 reduced RAD51 loading, upstream HR factors of RAD51 such as RPA, should also be analysed, as well as the level of phosphorylation of RAD51 at the vital sites for functionality, S192 (Flott *et al.*, 2011) and Threonine (T) 309 (Sørensen *et al.*, 2005), in the absence of SOD1. In addition to HR repair, NHEJ has also been identified as a repair mechanism in mitosis (Godinez *et al.*, 2020) and may be influenced by SOD1 (Nguyen-Powanda and Robaire, 2021). Therefore, the recruitment of NHEJ factors such as DNA ligase 4 (studied by Nguyen-Powanda and Robaire *et al.* (2021)), should be analysed in the absence of SOD1. Then the analysis of both repair mechanisms should be further analysed following the expression of the SOD1 functional mutants, to confirm the same pro-oxidant effect of SOD1 also regulates DNA repair. Finally, DNA repair during the MDDC should be analysed using a similar method to Godinez *et al.* (2020), which involved the DNA incorporation of 5'Ethynyl-2'-deoxyuridine (EdU; a thymidine analogue) to indicate if repair was occurring and the analysis of HR and NHEJ factors in mitotic cells. Overall, this will investigate the role of SOD1 in DNA repair and link this to the MDDC.

The specific mechanism by which PP2A inhibition causes the DNA damage-induced mitotic arrest requires investigation, to confirm the involvement of PP2A in the MDDC and contribute to the establishment of the MDDC pathway. However, there is a level of complexity regarding this, as PP2A is involved in numerous cellular pathways, including multiple aspects of mitosis, making it extremely difficult to specifically determine how mitotic arrest occurs. The determination of where DNA damage-

induced mitotic arrest occurs within mitosis will help to identify specific targets of PP2A in which to investigate.

Furthermore, PP2A cysteine oxidation by SOD1 requires further work to determine if the hypothesis is true. In future analysis, a different method adapted from the study by Prescher *et al.* (2021) will be used, which will indicate cysteine oxidation compared to the current method, which only indicates reduction. This will involve the incubation of the proteins post-reaction in unlabelled iodoacetamide to react with reduced cysteine residues, then the proteins will be separated via SDS-PAGE and undergo in-gel digestion, in which oxidised cysteines will be reduced and reacted with the labelled iodoacetamide D4 before MS analysis (Prescher *et al.*, 2021). Therefore, the D4 label will identify the oxidation sites of PP2A following the reaction with SOD1. In addition to this, a more generalised method to indicate the levels of cysteine oxidation should be conducted to determine the significance of this during the MDDC and the effect of SOD1 via knockdown. This can be achieved via the irreversible reaction of dimedone with oxidised cysteine residues, which can be identified using a specific antibody, along with pH3 for FACs analysis (as described in (Patterson *et al.*, 2019)).

As SOD1 has been implicated in the regulation of PP2A for the MDDC, it is hypothesised that SOD1 likely regulates other phosphatases too. This is supported in this chapter as determined within the literature the role of SOD1 in DNA repair is not likely to be due to PP2A regulation. Again, it will be difficult to determine which phosphatases and what the effect specifically is, due to the complexity of these proteins, as each phosphatase is involved in a plethora of pathways and possess numerous targets. Overall, SOD1 may function as a master regulator of phosphorylation events through phosphatase regulation in numerous cellular pathways.

3.4 Summary.

This chapter successfully identified the involvement of SOD1 in the MDDC in response to DNA damage anti-cancer therapeutics and oxidative stress inducing agents. It was concluded that the MDDC was activated upon DNA damage and not via redox

impairment. Then the SOD1 mechanism of action to activate the MDDC was concluded to be due to the regulation of PP2A phosphatase. The current hypothesis is that SOD1 possesses pro-oxidant activity, which involves the reversible inactivation of PP2A by cysteine oxidation, to induce the mitotic arrest during the MDDC. This role of SOD1 is independent of its antioxidant activity. Furthermore, a role of SOD1 within DNA damage repair was identified, which is likely to be due to the regulation of another phosphatase. Therefore, SOD1 has potentially been identified as a master regulator of cellular phosphorylation events, which requires further analysis within the MDDC and other cellular pathways such as the DDR. Overall, I have provided the initial exploration into the role of SOD1 in the MDDC.

Chapter 4: The mass spectrometry screen of the BubR1 interactome during the MDDC.

4.1 Introduction, aims and hypothesis.

This thesis has demonstrated that following the induction of DNA damage, cells exhibit slower mitotic transit, which was determined to be dependent on the antioxidant enzyme, superoxide dismutase 1 (SOD1) **(Chapter 3)**. DNA damage induced mitotic arrest has been described within the literature, but the arrest is typically proposed to be due to the spindle assembly checkpoint (SAC) (Mikhailov, Cole and Rieder, 2002; Nitta *et al.*, 2004; Kim and Burke, 2008). The SAC is a vital regulatory mitotic checkpoint, which regulates metaphase-anaphase transition by ensuring the correct attachment of the microtubules to the chromosomes (Farr and Cohen-Fix, 1999). This is regulated by a protein complex termed the mitotic checkpoint complex (MCC), composed of BubR1, Bub3, Mad2 and Cdc20, which arrest the cells in metaphase until the attachment process is completed (described in detail in section **1.2.2**) (Musacchio and Salmon, 2007). It is currently recognised that upon DNA damage, kinetochore attachment is disrupted leading to SAC-mediated mitotic arrest (Mikhailov, Cole and Rieder, 2002). However, I have found the SOD1-dependent mitotic DNA damage checkpoint (MDDC) does not act through the SAC to induce the mitotic arrest. However, it is conceivable that the mitotic SAC proteins possess additional roles independent of the SAC, to contribute to mitotic arrest in the MDDC. This is supported in the literature, as numerous studies have demonstrated crosstalk between the DNA damage response (DDR) and SAC proteins (discussed in section **1.3**).

Many studies have identified BubR1 as a prominent and multi-functional factor for the mitotic response to DNA damage (as described in section **1.3.2.6)**. BubR1 has been found to be hyperphosphorylated (Choi and Lee, 2008) and accumulate at the kinetochores following damage, contributing to a SAC-mediated mitotic arrest (Nitta *et al.*, 2004; Royou, Macias and Sullivan, 2005; Choi and Lee, 2008). Then BubR1 has

also been demonstrated to crosstalk with DDR proteins, including Chk1 in undamaged (Zachos *et al.*, 2007) and damaged (Royou, Macias and Sullivan, 2005) conditions, interact with ATM following IR treatment (Komura *et al.*, 2021) and also associate with PARP1 at the kinetochore in response to damage (Fang *et al.*, 2006). Furthermore, the deficiency of BubR1 is known to abrogate mitotic arrest in the presence of DNA damage (Nitta *et al.*, 2004; Fang *et al.*, 2006), supporting the vital role BubR1 possesses in the DDR pathway in mitosis. An alternative function of BubR1 has also been described in *Drosophila*, as along with the mitotic kinases, Plk1 and Aurora B, BubR1 was found to accumulate at DNA double strand breaks (DSBs) and form a tether structure between the break ends, facilitating chromatid segregation and protection against chromosome instability. It was also proposed that BubR1 enrichment at the damage site may facilitate DNA repair. (Royou *et al.*, 2010). To summarise, it can be deduced that BubR1 may act as a vital upstream DDR sensory and signalling protein in mitosis. Preliminary data from the Thompson laboratory **(Figure 1.9A)** has also identified BubR1 to be key in the MDDC. Then the current findings in this thesis have demonstrated that SOD1 regulates a BubR1 interactor, protein phosphatase 2A (PP2A) following DNA damage during the MDDC. Therefore, I decided to screen the BubR1 interactome, to identify the role of BubR1 and other members influencing the MDDC, in particular proteins known to be involved in DNA damage recognition and repair.

Proteomic screening experiments typically involve the mass spectrometry (MS) analysis of affinity purification (AP) or co-immunoprecipitation (co-IP) samples, which are composed of the protein of interest and its binding partners. AP-MS/MS has become a widely recognised proteomic technique, which produces large scale information into protein-protein interactions in numerous biological systems. The data obtained has enabled the identification of protein functions, the existence of protein complexes and the establishment of protein networks, as well as characterising proteins during disease development. (Morris *et al.*, 2014). AP-MS/MS experiments have contributed important information into mitosis, such as the formation of the MCC (Overlack *et al.*, 2015). Therefore, in this chapter, a screen was conducted to determine the interactome of BubR1 following DNA damage, via AP-High Performance Liquid Chromatography (HPLC)-MS/MS, which aimed to unveil the additional proteins involved in the MDDC and aid in the clarification of the pathway responsible for the

checkpoint. Optimisation of the various stages of the screen was conducted and the resulting interactors were validated. To my knowledge, this is the first screen of BubR1 interactors in the presence of DNA damage.

The hypothesis of this chapter is:

The MDDC is dependent on BubR1, a co-IP of BubR1 during an activated checkpoint will determine the interactome of BubR1 and may help in identifying proteins involved in the MDDC.

The aims of this chapter are:

1. To conduct an MS screen of BubR1 interactors.
2. To confirm screen hits.
3. To investigate interactors involvement in mitosis and the MDDC.

The objectives of this chapter are:

1. To optimise the sample preparation for the screen.
2. To determine the interactome of BubR1 during the MDDC.
3. To validate a novel interactor of BubR1 via co-IP.
4. To determine if the interactor is required for the MDDC via mitotic cell population and mitotic progression assays.

4.2 Results.

4.2.1 The optimisation of the MS screen workflow.

4.2.1.1 Examining co-IP technique for the MCC.

For the initial determination and to provide further optimisation for an appropriate co-IP technique, it was important to first prove that the established and common interactors of BubR1, the MCC proteins (Cdc20, Bub3 and Mad2) could be obtained using an IP. HeLa cells were treated with nocodazole to induce mitotic arrest and prolonged SAC activation thus enhancing the MCC formation. All members of the MCC were successfully identified and the interactions were amplified following nocodazole treatment indicating that the parameters of this co-IP were suitable **(Figure 4.1A)**.

Furthermore, the strength of the MCC interaction was tested through the alteration of the sodium chloride (NaCl) concentration of the lysis buffer. An enrichment of salt to the lysis buffer will increase the ionic strength of the solution, affecting the structure and interactions of the proteins (Arakawa and Timasheff, 1991). Increasing the salt concentration also reduces protein solubility due to the salt's effect on protein hydration, eventually resulting in protein aggregation and precipitation (Salting Out). This is commonly used as a method of protein purification and crystallisation. (Voet and Voet, 2011). The NaCl concentration of the standard lysis buffer for this research was 150 mM and was increased exponentially to 300 and 600 mM to determine the strength of the MCC protein complex **(Figure 4.1B)**. The MCC features strong interactions, as there is only a noticeable reduction in the complex association following 600 mM NaCl (4 times greater than the standard lysis buffer salt concentration). Furthermore, NaCl is considered a poor salting-out agent (Mcpherson, 2001; Dumetz *et al.*, 2007) and has been demonstrated to have little effect on protein interactions (Dumetz *et al.*, 2007), which is also exemplified here. This indicates the lysis buffer is appropriate to effectively obtain BubR1 interactors.

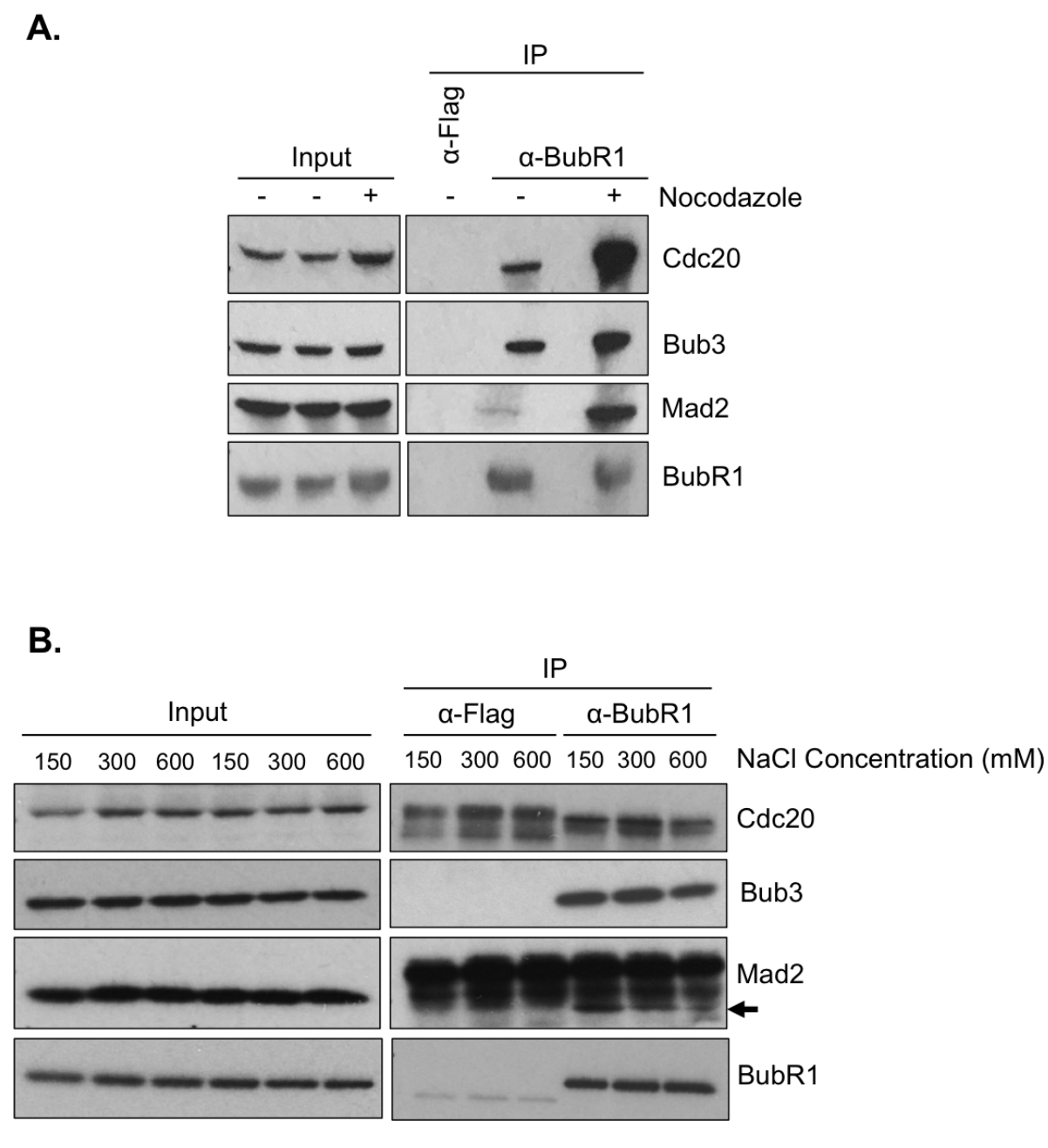

Figure 4.1: The co-IP results for the MCC.

A. Western blot showing the levels of the MCC proteins bound to BubR1 in HeLa cells treated with nocodazole (200 ng/mL) and harvested 4 hours post-treatment along with untreated cells for co-IP with antibodies against Flag (negative control) or BubR1 (N= 1). Immunoprecipitates were probed for BubR1, Cdc20, Mad2 and Bub3. **B.** Western blot showing the levels of the MCC proteins bound to BubR1 in HeLa cells lysed in RIPA buffer with varying concentrations of NaCl (150-600 mM) for co-IP with antibodies against Flag or BubR1 (N= 1). Immunoprecipitates were probed for BubR1, Cdc20, Mad2 and Bub3.

Overall, the MCC proteins were successfully obtained via a BubR1 co-IP. Therefore, the experimental parameters of the IP were sufficient, including the salt concentration of the current lysis buffer, which may support other weaker interactors of BubR1 in the MS screen. The next stage of optimisation involved the scaling of the experiment to be able to visualise the protein bands within an SDS-PAGE gel via incubation with InstantBlue Protein Stain (Expedeon). This would indicate the success of the co-IP through the visualisation of potential interactors and provide a sample clean up step prior to MS analysis. However, I found that BubR1 proteins levels from the IP were insufficient to continue the screen (data not shown). To overcome this, an exogenous BubR1 protein was examined to enhance protein levels for the screen.

4.2.1.2 Optimisation of the exogenous BubR1 expression.

The JSH601 cell line is derived from HeLa cells, gifted by Dr Don Cleveland (University of California San Diego). This cell line was generated using the Invitrogen Flp-In™ T-Rex™ system (Invitrogen, 2018) and features a doxycycline-inducible expression of a Myc and green fluorescent protein (GFP) tagged BubR1 protein (MycGFP-BubR1). The JSH601 cells were ideal for the MS screen, as the overexpression of an exogenous form of BubR1 would enhance BubR1 obtainment and the number of interactors identified during co-IP.

To enrich the number and frequency of interactors with BubR1 in the JSH601 cells for the MS screen, the expression levels of MycGFP-BubR1 were analysed over time (24-72 hours). This would clarify how effective the doxycycline-induced expression was over 72 hours and reveal the optimum time for treatment and harvesting of the cells for the MS screen. It was observed that after 48 hours of doxycycline-induced expression, the levels of MycGFP-BubR1 were sufficiently elevated, compared to 24 hours **(Figure 4.2)**. This enrichment began to decline at 72 hours. Therefore, JSH601 cells were supplemented with doxycycline 48 hours before treatment and experimental use.

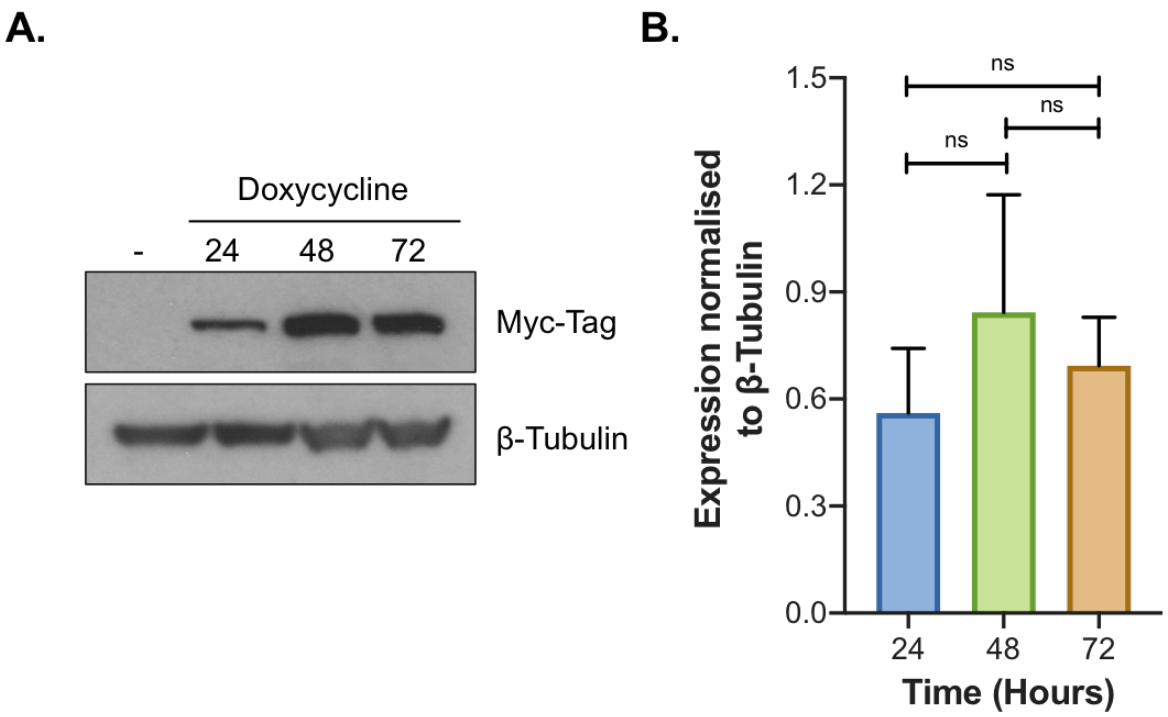

Figure 4.2: The optimal induction time of MycGFP-BubR1 expression.

A. A representative western blot of whole cell extracts of JSH601 cells cultured in the presence of doxycycline (1 µg/mL) for 24, 48 and 72 hours (N= 3). The absence of doxycycline was used as a negative control. Extracts were probed with Myc-Tag to represent MycGFP-BubR1 and β-Tubulin (control) antibodies. **B.** The relative expression of Myc-Tag compared to β-Tubulin expression was calculated from western blot images via measuring the band densitometries in FIJI. Each time point for each of the three independent repeats was measured to give the overall expression of MycGFP-BubR1. Significance was determined using a One-way ANOVA with Dunnett's multiple comparisons (ns denotes p = non-significant).

Next, it was determined that the exogenous form of BubR1 functioned as the endogenous. This was analysed through immunofluorescent staining of both forms of BubR1 in the JSH601 cell line alongside the constitutive centromeric protein B (CENPB). It was anticipated that both forms of BubR1 would co-localise with CENPB at the kinetochore-centromeric region during mitosis. It was clear to see that the expression of exogenous BubR1 was specific to the nucleus and only in the presence of doxycycline, as expected **(Figure 4.3B)**. Furthermore, initial analysis has shown that like endogenous BubR1 **(Figure 4.3A)**, the exogenous form appeared to localise at the centromere during mitosis **(Figure 4.3B)**.

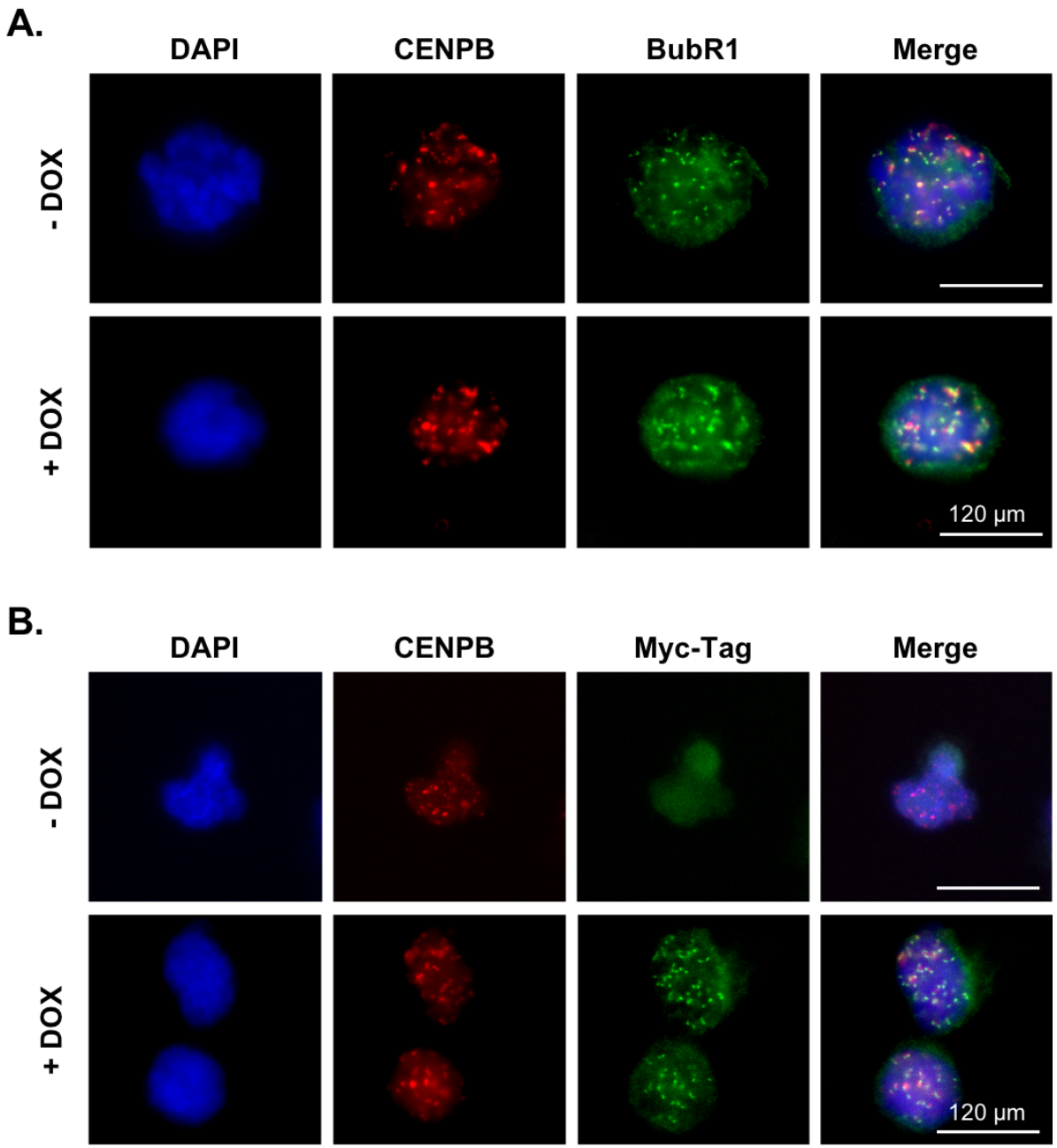

Figure 4.3: The Immunofluorescent analysis of the JSH601 cells.

A. In JSH601 cells, exogenous BubR1 (MycGFP-BubR1) expression was induced through treatment with doxycycline (DOX) (1 µg/mL) for 48 hours and the mitotic cell population was enriched through nocodazole (200 ng/mL) treatment for 4 hours. Cells were stained using immunofluorescence for CENPB and BubR1. Images of mitotic cells were taken on a Nikon TE200 inverted fluorescent microscope at a 60X magnification. Representative images illustrating the relationship between endogenous BubR1 with CENPB in mitotic JSH601 cells (N= 1). **B.** as in **A.** with the exception exogenous BubR1 was stained using Myc-Tag antibody (N= 1).

It was determined that both endogenous and exogenous BubR1 proteins exhibited identical functions regarding the localisation at the kinetochore-centromere region. The exogenous BubR1 protein will be used and further optimisation using this cell line was conducted for the MS screen.

4.2.1.3 The optimisation of GFP-Trap beads for co-IP.

The standard IP beads used throughout this research are the Invitrogen magnetic Dynabeads protein G, which require a short incubation with an antibody. However, this adds a further element of contamination in the form of heavy and light antibody chains within the bound protein fraction (can be seen in the Mad2 blot in **Figure 4.1B**). To overcome this the ChromoTek GFP-Trap beads were examined. These beads feature a GFP-binding domain (an anti-GFP nanobody), eliminating the need for antibodies **(Figure 4.4A)**. As the doxycycline-inducible form of BubR1 expressed in the JSH601 cells is GFP tagged, this is a viable option.

The initial assessment of the GFP-Trap beads involved co-IP for the MCC with the JSH601 cells using the same co-IP method used previously in **Figure 4.1A**. This would determine if the GFP-Trap beads were compatible with the current co-IP method. It was determined that the GFP-Trap beads were successful in obtaining large levels of the exogenous BubR1 and the majority of MCC proteins **(Figure 4.4B)**. However, the enhanced interaction of the MCC proteins following nocodazole treatment was not observed like previously. In attempts to repeat this data, it was difficult to obtain all or even any MCC proteins (data not shown). Overall, it was deduced that further optimisation of the co-IP methodology was required to complement these beads.

The next stage of optimisation involved the buffers, as the composition of lysis and IP wash buffers can affect the protein-protein interactions. The current RIPA lysis and IP wash buffers were compared to the MS IP lysis buffer used by the Collis laboratory (Department of Oncology and Metabolism, University of Sheffield). Then the Collis group used the same buffer (minus the benzonase) as wash buffer, which unlike the current IP wash buffer contained phosphatase and proteinase inhibitors, aiding in the protection the protein interactome on the bead throughout the whole co-IP process. It was demonstrated that all MCC proteins were obtained in MS IP buffer samples

compared to RIPA samples **(Figure 4.4C)**. There was also a noticeable difference in the level of exogenous BubR1 in the IP samples between the buffers too **(Figure 4.4C)**.

A.

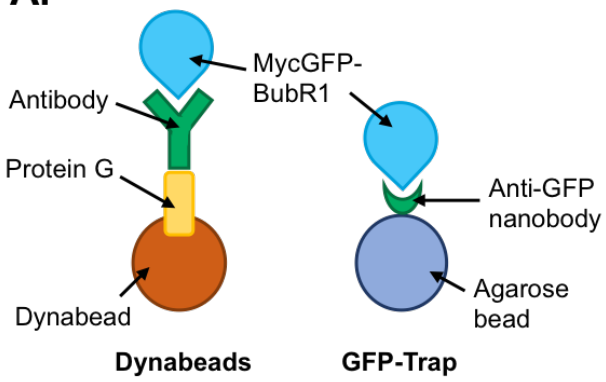

Feature	Dynabead™	GFP-Trap
Manufacturer	Invitrogen	ChromoTek
Bead matrix	Dynabead	Agarose
Separation feature	Magnetic	Magnetic
Ligand type	Protein G	GFP nanobody
Antibody required?	Yes	No

B.

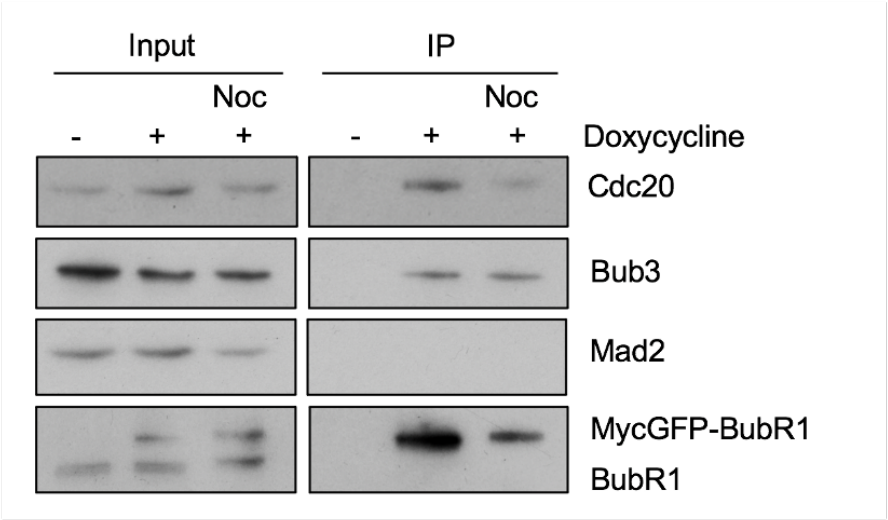

C.

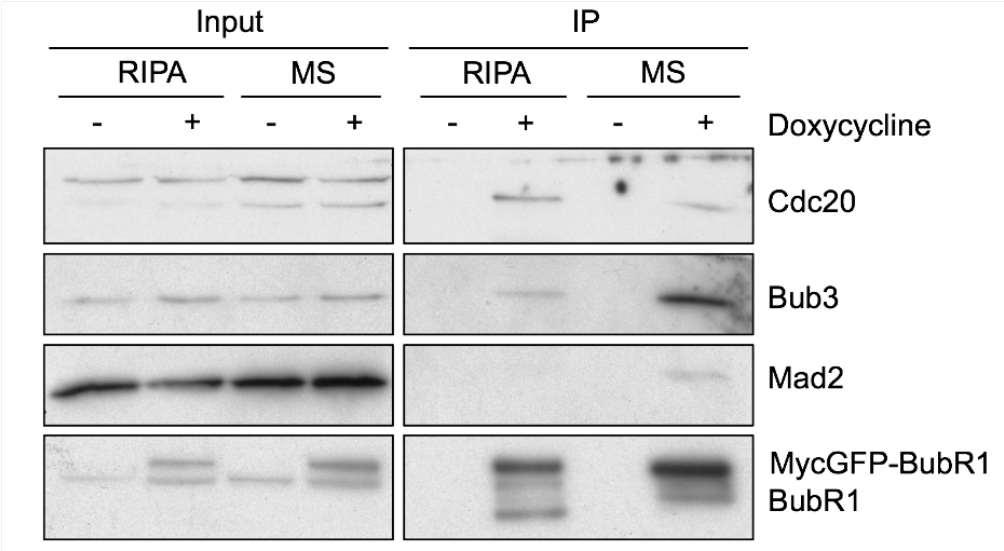

Figure 4.4: The optimisation of the GFP-Trap beads.

Legend on next page.

Figure 4.4: The optimisation of the GFP-Trap beads.

A. A comparison between the Invitrogen Dynabead™ and the ChromoTek GFP-Trap immunoprecipitation beads illustrated with a systematic diagram and table. **B.** Western blot showing the levels of the MCC proteins bound to MycGFP-BubR1 in JSH601 cells treated with nocodazole (200 ng/mL) and harvested 4 hours post-treatment along with untreated cells for co-IP with the GFP-Trap beads (N= 1). The absence of doxycycline was included as a negative control. Immunoprecipitates were probed for BubR1, Cdc20, Mad2 and Bub3. **C.** Western blot showing the levels of the MCC proteins bound to MycGFP-BubR1 in JSH601 cells following lysis in RIPA or MS lysis buffer prior to co-IP with GFP-Trap beads (N= 1). The absence of doxycycline was included as a negative control. Immunoprecipitates were probed for BubR1, Cdc20, Mad2 and Bub3.

Overall, the MS IP buffers were more compatible with the beads and the exogenous BubR1, compared to the RIPA buffer. The main difference between these lysis buffers is the type of detergent used. The MS IP lysis buffer contains the non-denaturing detergent; Triton-X 100, which allowed for the preservation of protein-protein interactions and structures. Whereas the RIPA buffer contains SDS, which is known to completely disrupt protein-protein interactions, leading to the denaturation of proteins which was undesirable for this experiment (ThermoFisher, 2021). Furthermore, the MS IP buffer composition was almost identical to the ChromoTek recommended IP lysis and wash buffer for the GFP-Trap beads (ChromoTek, 2020). In summary, the MS IP buffers were used for the MS screen.

4.2.1.4 Scaling up the co-IP.

Having optimised the co-IP methodology, the next experimental phase involved the scaling up of the co-IP for the visualisation of the protein bands within the SDS-PAGE gel via incubation with InstantBlue Protein Stain (Expedeon). It was important to increase the scale of the co-IP to enhance the sample size of interactors for the MS analysis. It was also beneficial to be able to see the bands within the IP samples, as this would indicate the quantity and intensity of the interactors of the protein of interest, confirming that the co-IP was successful and allow for continuation to sample preparation for MS analysis.

The standard bead amount of 20 µL (used throughout the previous optimisation) was increased initially to 50 µL. The capture of MycGFP-BubR1 was very efficient with this bead concentration, as definitive bands can be seen in SDS-PAGE gel **(Figure 4.5A)**. However, no interactors could be visualised, causing low confidence in the co-IP. The co-IP was scaled up further to 150 µL of beads, which was effective at obtaining high levels of MycGFP-BubR1 and numerous potential interacting partners **(Figure 4.5B)**.

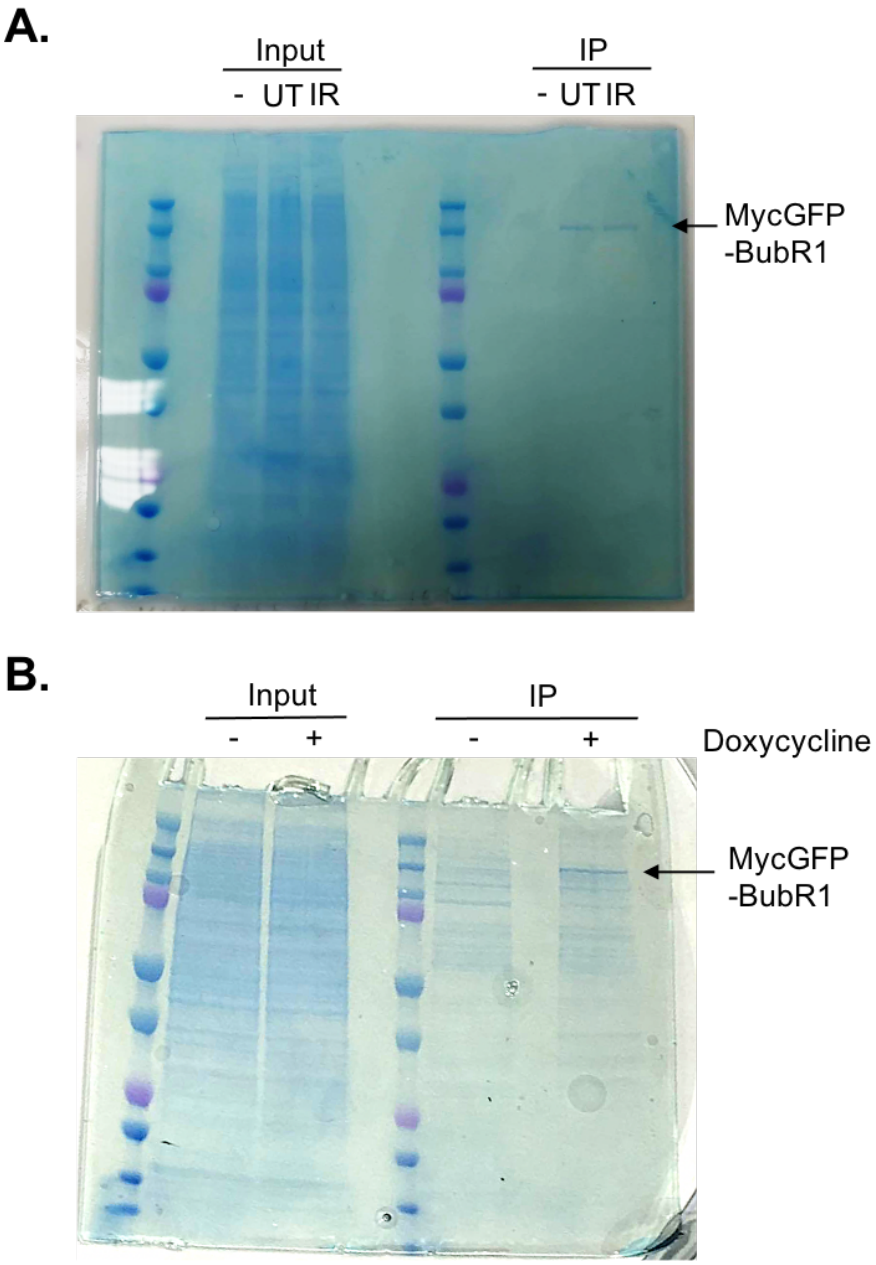

Figure 4.5: InstantBlue Protein stained SDS-PAGE gels representing the scaling up of IP experiments in preparation of MS.

Legend on next page.

Figure 4.5: InstantBlue Protein stained SDS-PAGE gels representing the scaling up of IP experiments in preparation of MS.

A. The SDS-PAGE-stained gel illustrating the co-IP (50 µL GFP-Trap beads) of untreated (UT), irradiated (IR) and doxycycline negative (-) samples (N= 1). The arrow indicates the MycGFP-BubR1 band. **B.** The SDS-PAGE-stained gel demonstrating bands for the co-IP (150 µL GFP-Trap beads) of samples in the absence (-) or presence (+) of doxycycline (N= 1). The arrow shows the MycGFP-BubR1 band and the other bands represent the potential interacting proteins.

Overall, the optimisation of the co-IP method was suitable, and the scale of the experiment was optimum to proceed to the configuration of the samples for MS.

4.2.1.5 Differing bead elution and digestion techniques.

To enhance the confidence in the proteomic analysis of this screen, it was proposed that prior to the elution of the proteins from the beads, the bead volume was split, and half the sample would be eluted for in-gel digestion and the other half would undergo on-bead digestion. On-bead and in-gel digestion methods are popular techniques of MS sample preparation with differing benefits. In-gel digestion involves SDS-PAGE, which acts as a clean-up step for the samples from detergents used in the co-IP buffers. Whereas on-bead digestion preserves the integrity of the interactome and is an overall faster method with fewer steps reducing chances of contamination. The use of both these methods would provide two independent analyses of the same screen samples, providing comparative lists and ensuring confidence in the interactors found, due to the differences in bead elution and protein digestion methods. It would be expected that the proteins found in both analyses would be true interactors. The proteins not found in both would indicate that these are more likely to be non-specific interactors maintained during sample preparation. Optimisation of the on-bead digestion was performed on an untreated control sample in the absence of doxycycline and a list of non-specific interactors was generated (Appendix **Table 7.2**). However, upon the on-bead digestion of the screen samples, no proteins were obtained (data not shown). Hence, the screen data was attained from the in-gel digestion method only **(Figure 4.6 steps 3 and 4)**. Yet the on-bead non-specific list contributed to data analysis.

4.2.1.6 Implementation of sample de-salting.

A de-salting step was required before input into the MS **(Figure 4.6 step 5)**. The end-stage of the in-gel digestion involved vacuum drying the samples, but a salt precipitate contaminant was present. Salt within the sample would reduce the sensitivity of electrospray ionisation (ESI) (Wang and Cole, 1994), which is used to generate ions during the input into the MS. During ESI salt adducts can form on protein ions affecting the charged state of the protein and broadening the spectral peaks affecting protein identification (Cassou and Williams, 2014). Therefore, the Aligent Bond Elut OMIX C18 tips were used to remove contaminants for MS. These tips feature a resin that binds the peptides, allowing for sample clean up and then elution of purer samples for MS.

4.2.1.7 The MS screen workflow.

As a result of the various and thorough optimisation of the techniques involved in the MS screen sample preparation, a final workflow was determined **(Figure 4.6)**.

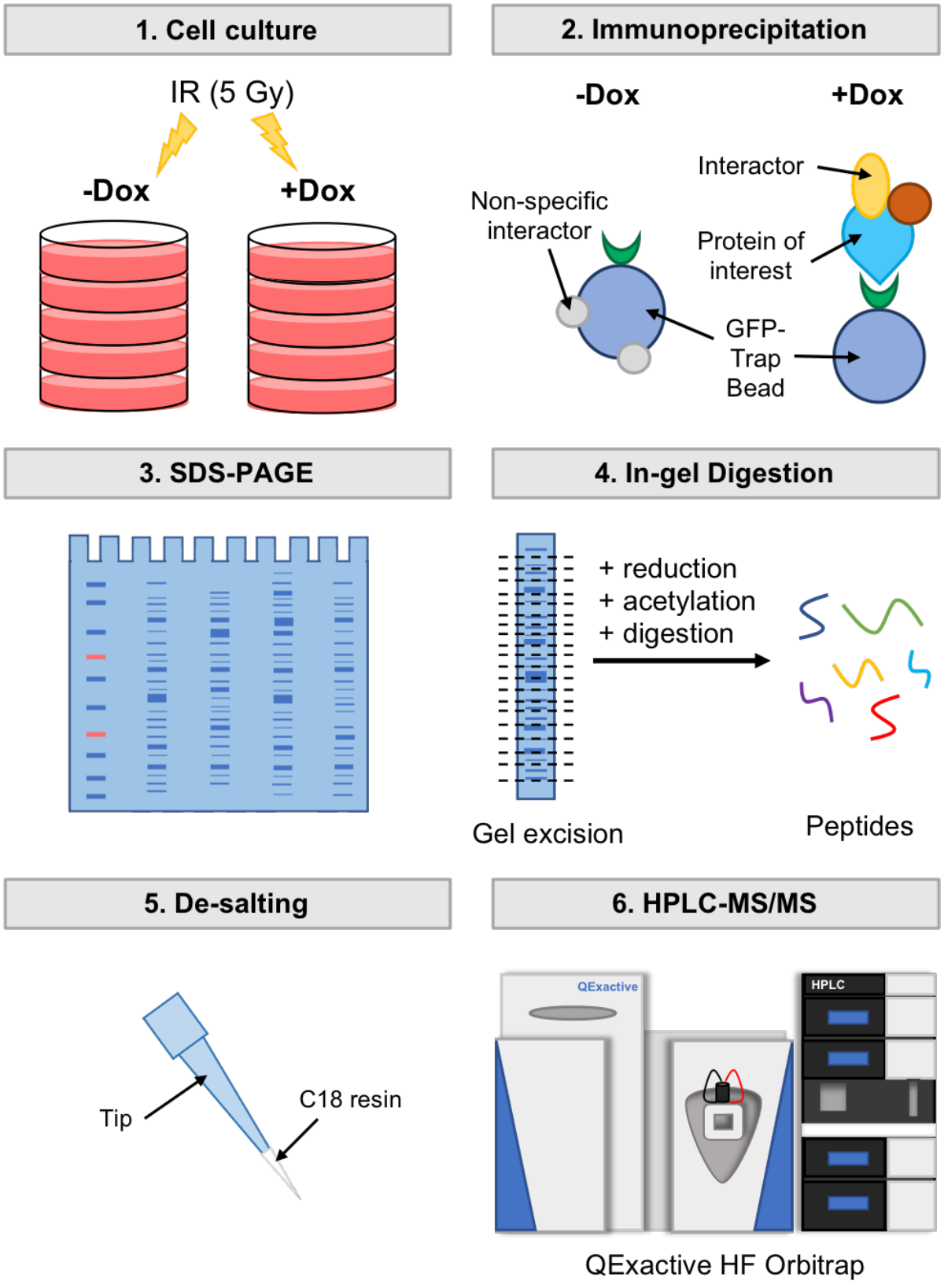

Figure 4.6: A schematic explanation of the workflow of the MS screen.

Legend on next page.

Figure 4.6: A schematic explanation of the workflow of the MS screen.
JSH601 cells were treated with doxycycline (+Dox) (1 µg/mL) for 48 hours, all conditions were then irradiated (5 Gy) for 16 hours. The absence of doxycycline was used as the negative control (-Dox) **(1)**. The co-IP was performed using the ChromoTek GFP-Trap beads (150 µL) with the MS buffers **(2)**. Immunoprecipitates were separated on an SDS-PAGE gel, proteins were then stained **(3)**, and gel bands excised before undergoing in-gel digestion (reduction, acetylation and tryptic digestion) producing peptides **(4)**. Samples were de-salted using the C18 tips **(5)**, prior to fractionation on the HPLC and analysis on the QExactive HF Orbitrap **(6)**.

4.2.2 The analysis of the MS screen of the BubR1 interactome during the MDDC.

The raw data collected from the MS screen was analysed in Max Quant software, which matched the sequences to proteins via the human FASTA software. The screen featured two samples, doxycycline negative (-Dox) and positive (+Dox), and through Max Quant analysis 953 and 845 proteins were initially identified for each sample respectively **(Figure 4.7A)**. The absence of doxycycline is the negative control and was used to identify non-specific interactors in the +Dox condition. It was expected that there would be fewer proteins in this condition than in +Dox. However, before the comparison between samples, a thorough analysis of both lists of proteins was performed to eliminate contaminants and frequently occurring proteins in affinity purification MS experiments. Contaminants were removed using several methods (described in methods section **2.2.14.8**) including **(Figure 4.7A)**, Uniprot identified contaminants (keratin) and the use of the CRAPome database, which features numerous protein lists from MS experiments categorised by experimental details, allowing the removal of proteins which occurred in the majority of similar MS experiments. Then proteins found in the on-bead digestion optimisation experiment (non-specific interactors list) (Appendix **Table 7.2**) were also removed, and finally, the removal of contaminants identified by the study by Trinkle-Mulcahy (2008), which analysed the non-specific interactors of the GFP tag and several bead matrixes (bead proteomes), including agarose, sepharose and magnetic beads (Trinkle-Mulcahy *et al.*, 2008).

Next, the comparison of the -Dox list with the +Dox list was conducted using the iBAQ intensity of each protein (the overall peptide intensity divided by the number of peptides found for the particular protein) **(Figure 4.7A)**. Proteins with greater intensity in the -Dox were considered non-specific and discarded and those with greater intensity in the +Dox were considered a potential interactor. The proteins found in both lists but with greater intensity in +Dox were not discarded, as these may be genuine BubR1 interactors but have an affinity for the beads. This step of analysis provided a preliminary list of potential interactors. Then using the BioGrid and STRING proteomic databases, the known interactors of BubR1 were highlighted **(Figure 4.7A and 4.7B)**. Finally, following the comparison between the samples, the addition of a false discovery rate of 0.1 % of the iBAQ intensity of BubR1 was applied to generate the final list, resulting in 175 potential interactors of which 167 are potential novel interactors of BubR1 following DNA damage **(Figure 4.7A)**. The 175 novel interactors are listed in Appendix **Table 7.3**.

It was key to identify the known interactors to ensure confidence within the screen. 8 known interactors of BubR1 were identified in the total list of 175 potential interactors **(Figure 4.7A).** These proteins have been mapped using the STRING database and the functions annotated **(Figure 4.7B)**, which included components of the MCC; Cdc20 and Bub3, numerous APC/C subunits and the centromeric protein; CENPE. Overall, this provides confidence in the screen results as key interactors of BubR1 were identified.

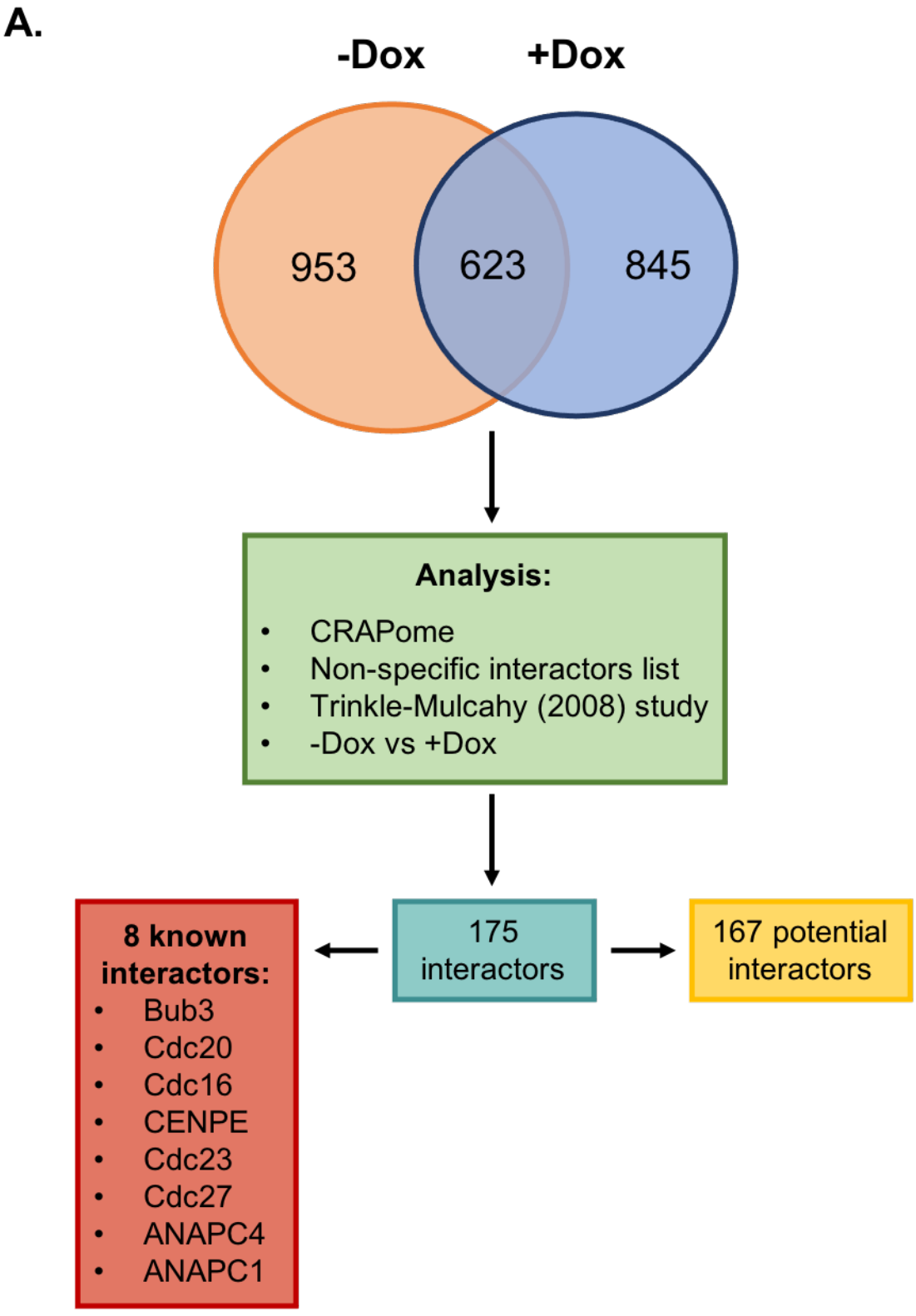

Figure 4.7: The analysis of the MS screen.

Legend on next page.

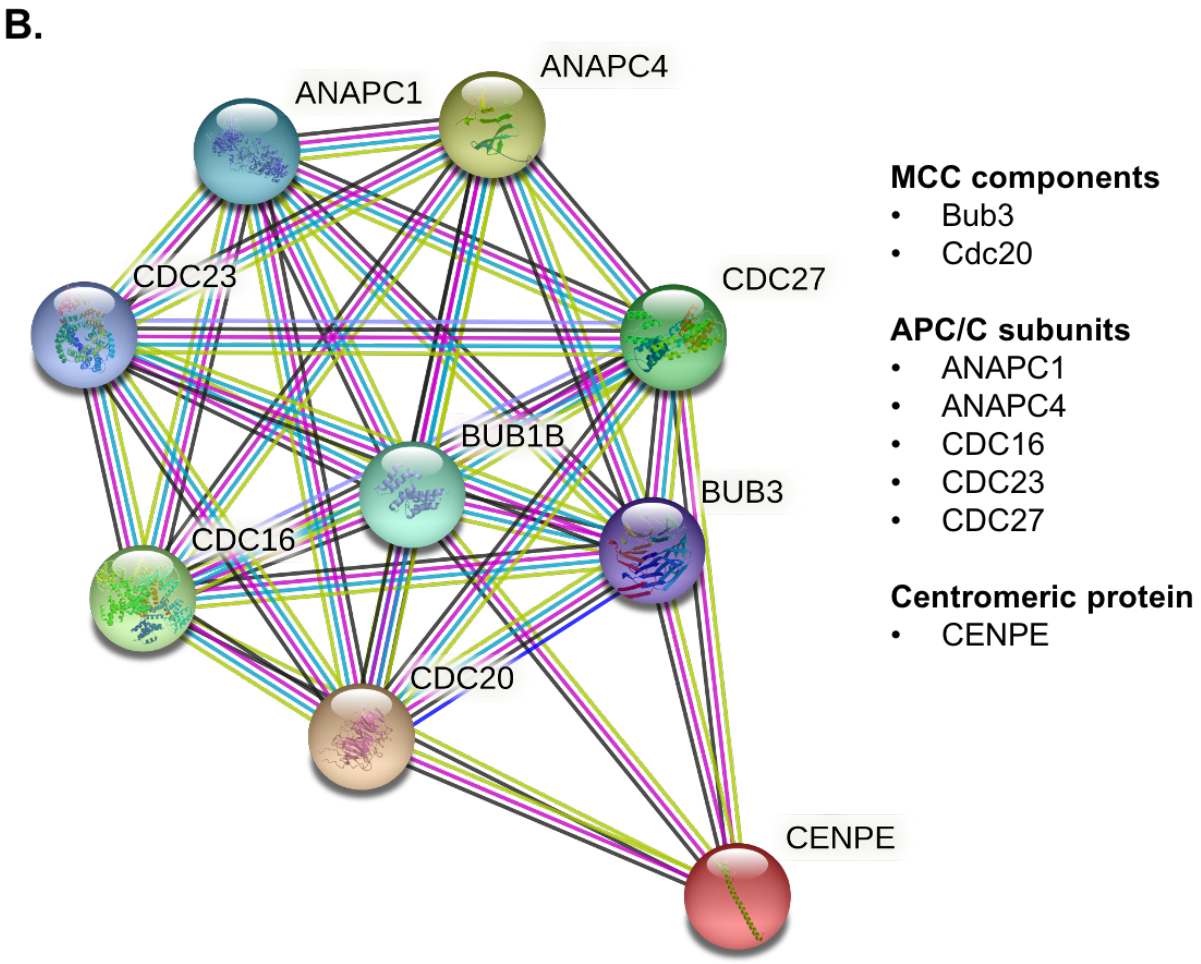

Figure 4.7: The analysis of the MS screen.

Legend on next page.

The complete list of interactors was annotated into functional pathways, using KEGG, Reactome and STRING databases **(Figure 4.7Ci)**. Multiple expected pathways were identified such as cell cycle, specifically mitosis **(Figure 4.7Cii)**, which adds further confidence to the screen. The list of interactors was in the first instance compared to the siRNA screen for proteins involved in the MDDC conducted in the Thompson laboratory **(Figure 1.9)**, aside from BubR1 there was another common protein, Upstream frameshift 1 (UPF1) **(Figure 4.7D)**.

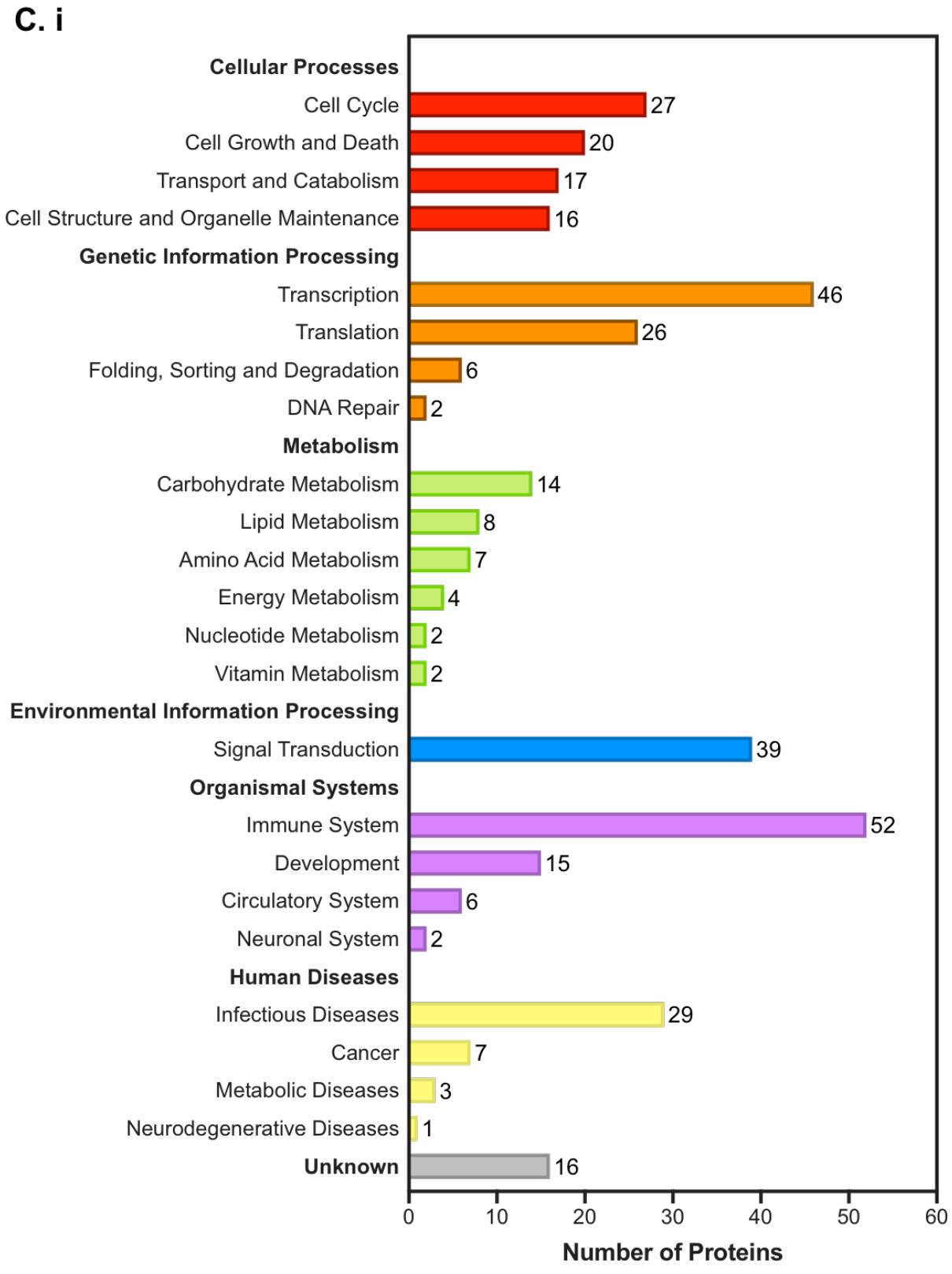

Figure 4.7: The analysis of the MS screen.

Legend on next page.

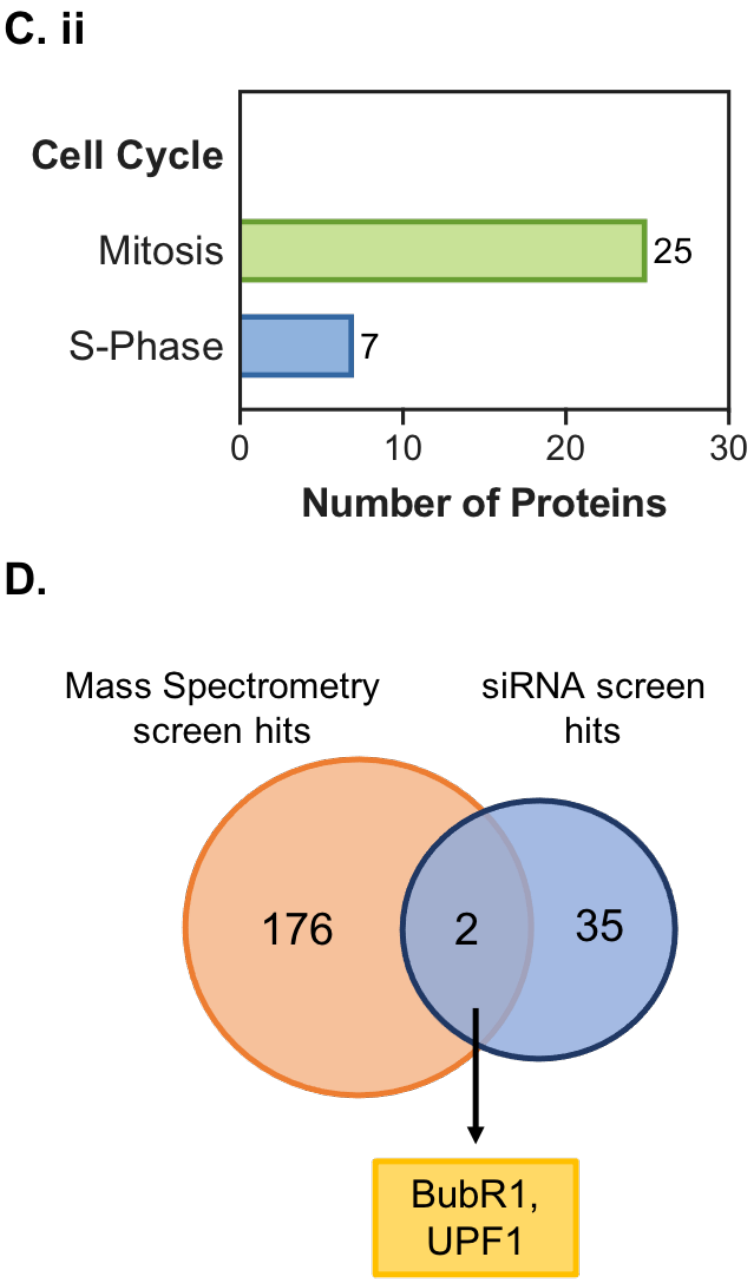

Figure 4.7: The analysis of the MS screen.

A. A comparison of the number of proteins between the MycGFP-BubR1 expressed (+Dox) and negative control (-Dox) conditions from the screen. After thorough analysis and eradication of contaminants, 175 proteins were identified as potential interactors of BubR1, 8 of which have previously been identified. **B.** The STRING analysis of the known interacting proteins of BubR1 (*BUB1B*) via gene name, with the role annotated. **Ci.** An overview and quantification of the pathways the potential interactors are involved in. This was generated using STRING, Reactome and KEGG databases. **Cii.** A breakdown of the cell cycle pathway to illustrate the number of proteins identified specifically in mitosis. **D.** A comparison of the hits of the mass spectrometry screen (including BubR1) and the hits from the siRNA DNA damage screen by the Thompson laboratory to identify commonalities.

In summary, the screen was successful in obtaining numerous potential interactors of BubR1 following DNA damage, including several known interactors providing confidence in the screen. Due to an overlap of this screen and the siRNA DNA damage screen, it was decided that UPF1 would be the first protein to be studied further.

4.2.3 The BubR1-UPF1 interaction.

UPF1 is a multifunctional enzyme involved in numerous RNA- and DNA-dependant mechanisms and is highly mobile within the cell. This enzyme is well characterised as an RNA helicase within the non-sense mediated decay (NMD) pathway, which regulates mRNA expression mainly through targeting and initiating the degradation of mRNAs containing premature termination codons (PTC) (Gupta and Li, 2018). The presence of PTC would affect the translation of the gene and produce truncated proteins, which could lead to wider detrimental effects within the cell due to potential protein functionality defects. Furthermore, independent of the NMD pathway, UPF1 is also involved in the DDR (Brumbaugh *et al.*, 2004; Azzalin and Lingner, 2006). Through the consolidation of the current findings within this chapter and the literature, it is of interest to investigate UPF1 further as a BubR1 interactor, responsible for regulating the MDDC.

4.2.3.1 The validation of the BubR1-UPF1 interaction.

Co-IP was performed to investigate the interaction between BubR1 and UPF1. This was conducted using an overexpression system, similar to the JSH601 cell line. HeLa cells manipulated by the Invitrogen Flp-In™ T-Rex™ system (Invitrogen) to feature a doxycycline-inducible expression of a Flag-tagged UPF1 protein (Flag-UPF1). These cells were gifted by Professor Carl Smythe (Department of Biomedical Science, University of Sheffield). Additionally, a Myc-BubR1 in a pCDNA3 plasmid was transfected into the cells, resulting in the overexpression of both proteins of interest. This would elucidate if these proteins interact through enhancing the protein levels, providing support of the MS screen data.

It was determined that in both untreated and IR conditions, BubR1 and UPF1 interacted **(Figure 4.8)**. There appears to be no difference in the interaction between the conditions.

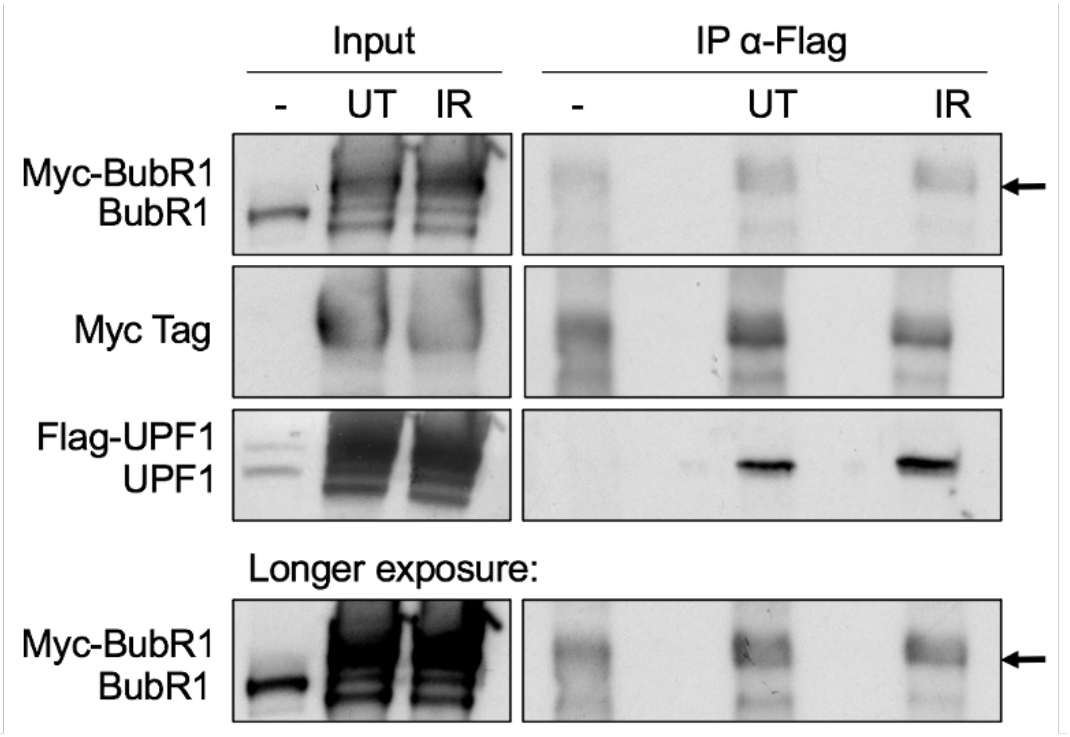

Figure 4.8: The co-immunoprecipitation (co-IP) of the BubR1-UPF1 interaction.
The co-IP results for the interaction between Flag-UPF1 and exogenous Myc-BubR1. Untreated or IR treated (16 hours post-5 Gy) Flag-UPF1 expressing HeLa cells were co-IP'ed with a Flag antibody (N= 1). The absence of doxycycline was used as a negative control. Immunoprecipitates were analysed via western blot using BubR1, Myc-Tag and UPF1 antibodies. The arrows highlight the bands of relevance.

Overall, the interaction between BubR1 and UPF1 was successfully confirmed.

4.2.3.2 The validation of the involvement of UPF1 in the MDDC.

To determine whether UPF1 plays a role within the MDDC, the effect of UPF1 knockdown was investigated on the mitotic cell population and mitotic transit following the induction of DNA damage. Firstly, the knockdown of UPF1 using siRNA was optimised through western blot analysis. This involved testing the smart pool and the four deconvoluted siRNA to determine which provided the most efficient knockdown. It was consistently found that siUPF1-1 and siUPF1-2 were most effective siRNAs **(Figure 4.9A)**.

Next cell cycle distribution analysis through pH3 and PI co-staining was conducted using all siRNAs. This will determine the effect of UPF1 depletion on the cell cycle and specifically the mitotic population in untreated and irradiated HeLa cells **(Figure 4.9B-C)**. In untreated conditions, there was no effect of UPF1 depletion on the mitotic proportion of cells. However, following IR treatment, as expected the siControl condition had a significantly enriched mitotic cell population ($p < 0.0001$) compared to the corresponding untreated condition **(Figure 4.9C)**. Each siRNA for UPF1 significantly reduced the mitotic population compared to siControl following IR treatment. The mitotic population was most reduced with siUPF1-1 and reduced the least by siUPF1-3 (both $p < 0.0001$). The degree to which each siRNA reduced the mitotic population following DNA damage, corresponds to the efficiency of the knockdown observed via western blot analysis. Hence, siUPF1-1 and siUPF1-2 were used for future experiments.

Live cell analysis was conducted to measure the role of UPF1 on mitotic transit in untreated and irradiated HeLa cells. As previously determined through FACs analysis **(Figure 4.9C)**, there was no effect of UPF1 on mitotic progression, compared to the siControl sample in untreated cells **(Figure 4.9D)**. Again, as previously shown following IR treatment, siUPF1-1 and siUPF1-2 significantly reduced the mitotic transit time (both $p = 0.0002$) **(Figure 4.9E)**. To mention, siBubR1 provided a positive control for the live cell analysis, and in untreated and irradiated cells significantly reduced the mitotic transit time compared to siControl ($p = 0.0022$ and $p < 0.0001$ respectively).

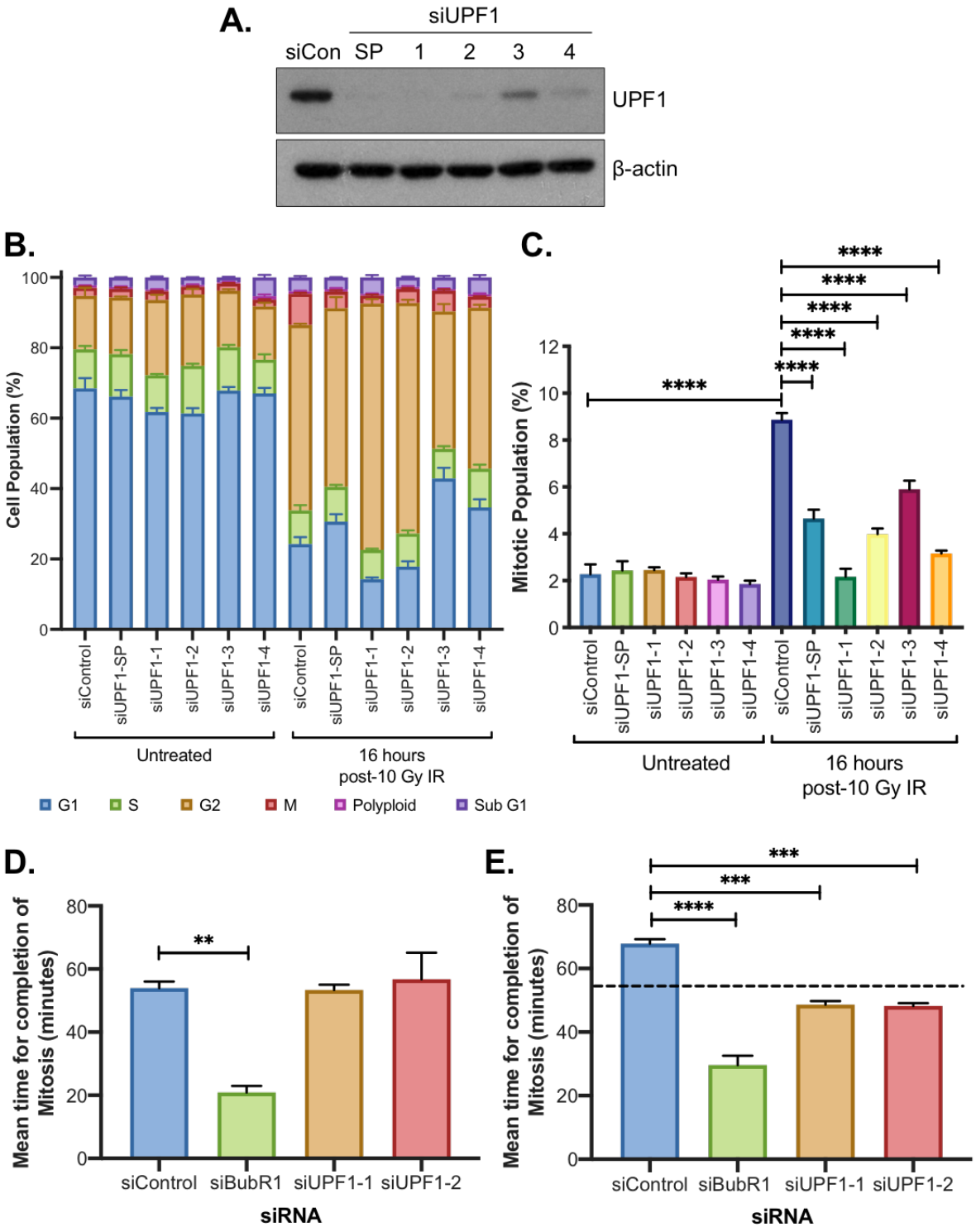

Figure 4.9: The optimisation of UPF1 siRNA's and the analysis of UPF1 depletion on the mitosis after DNA damage in HeLa cells.

Legend on next page.

Figure 4.9: The optimisation of UPF1 siRNA's and the analysis of UPF1 depletion on the mitosis after DNA damage in HeLa cells.

A. A representative western blot showing the levels of UPF1 and β-actin after transfection with each siRNA (siControl and siUPF1 smart pool (SP) and 1-4) (N= 3). **B.** Mean cell cycle phase distribution following UPF1 depletion with a control siRNA, in untreated cells or 16 hours post-10 Gy IR treatment, represented on a different scale for clarity +/- SEM (N= 3). **C.** Mean mitotic cell population following each siRNA and treatment +/- SEM (N= 3). One-way ANOVA with Dunnett's correction test for multiple comparisons was performed to determine statistical significance (**** denotes $p \leq 0.0001$). **D.** Time-lapse live cell microscopy analysis of the mean time taken to complete mitosis after BubR1 (positive control) or UPF1 depletion (siUPF1-1 and -2) in untreated HeLa cells. 50 cells for each siRNA were counted and the data represents the overall mean of each independent experiments +/- SEM (N= 3). One-way ANOVA with Dunnett's correction test for multiple comparisons was performed to determine statistical significance (** denotes $p \leq 0.01$). **E.** as in **D.** with the exception of HeLa cells were treated with 5 Gy IR (+/- SEM, N= 3). One-way ANOVA with Dunnett's correction test for multiple comparisons was performed to determine statistical significance (*** denotes $p \leq 0.001$ and **** $p \leq 0.0001$). The dotted line indicates the untreated transit time of 54 minutes from **E.**

To summarise, UPF1 was required for the prolonged mitotic transit observed following DNA damage induced by IR treatment, indicating an involvement in the MDDC.

4.3 Discussion.

In this chapter, I successfully conducted an AP-HPLC-MS/MS screen of BubR1 interactors during the MDDC. A novel interaction between BubR1 and UPF1 was established and UPF1 was confirmed to be involved in the MDDC. The mechanism behind the BubR1-UPF1 interaction and its role within the MDDC is yet to be revealed.

4.3.1 The successful AP-MS/MS screen.

To perform a successful screen of the BubR1 interactome following DNA damage, extensive optimisation of each stage of the workflow was performed. The aim of this was to enhance the quantity and quality of the BubR1 interacting proteins, to elucidate those involved in the MDDC. In summary, the screen was successfully performed, and unique interacting partners were obtained, which are involved in valuable pathways to

investigate in detail in the future. One example includes the identification of the DNA repair proteins, keratinocyte proline-rich protein (KPRP) and DNA damage-binding protein 1 (DDB1) (detailed in Appendix **Table 7.3**).

Similarly, in the study by Fang *et al.* (2006) an AP-MS/MS screen of BubR1 was conducted but in undamaged conditions, which successfully identified DDR protein PARP1 as an interactor and through subsequent testing determined a role of this interaction in response to DNA damage (Fang *et al.*, 2006). Unfortunately, PARP1 was not identified in my screen. Nevertheless, the screen conducted by Fang and colleagues had major limitations, such as the IP samples were separated on a 6 % gel and only major gel bands were excised for MS analysis. Therefore, the results obtained were restricted by protein size and the frequency of the interaction. The screen conducted in this thesis did not have these limitations, as I collected as many proteins as possible from a range of sizes under DNA damage conditions, indicating the proteins identified will be more representative of the BubR1 interactome during the response to DNA damage and more specifically, the MDDC.

4.3.2 UPF1 interacts with BubR1.

UPF1 was investigated further, as it was identified on both the MS screen conducted in this thesis and the siRNA screen previously performed in the Thompson laboratory. Additionally, this protein has been implicated within the DDR, as it was observed that in the absence of UPF1 the cell cycle was arrested in S-phase via the activation of the DDR and there was an accumulation of γH2AX. ATR phosphorylates UPF1, enabling UPF1 association with the chromatin following IR treatment, indicating UPF1 to be involved in the regulation of the DDR contributing to genome integrity. Furthermore, an interaction between UPF1 and polymerase δ was demonstrated, further supporting UPF1's role in DNA replication and repair. (Azzalin and Lingner, 2006). Finally, another paper observed an increase of phosphorylated UPF1 by ATM and NMD kinase SMG1 following 10 Gy IR treatment. It was proposed that ATM phosphorylation of UPF1 inhibited the UPF1 actions in NMD for an alternative role in the DDR. (Brumbaugh *et al.*, 2004). Therefore, the interaction between BubR1 and UPF1 was investigated in the context of the MDDC.

The BubR1-UPF1 interaction was confirmed via co-IP **(Figure 4.8)** and to my knowledge, this is a novel finding and has not been previously reported. For the co-IP, both proteins were exogenously overexpressed via Flag-UPF1 expressing HeLa cells and Myc-BubR1 transfection. This was conducted to enhance the protein levels, so the interaction would be enriched. There was no apparent difference in the level of interaction between untreated and irradiated conditions. This may indicate that the interaction is not only stimulated by DNA damage but may have a role in the unperturbed cell cycle. However, the exogenous expression of these proteins may have influenced the normal cell cycle. Therefore, further co-IP analysis of this interaction should be conducted to further confirm the BubR1-UPF1 interaction and stimulatory conditions required.

The interaction domains involved in the BubR1 and UPF1 association is undetermined. The 3D crystal structure of BubR1 is not complete, making it difficult to use modelling software to propose the interaction site. However, the 3D crystal structure of UPF1 is known and its domains are well characterised. From the literature, I deduced that the C-terminal serine-glutamine (SQ) rich domain is important for the BubR1-UPF1 interaction, as this domain is where the important activation and regulatory phosphorylation sites of UPF1 are situated (Gupta and Li, 2018). Phosphorylation of UPF1 is important for its action in NMD and the DDR. Nevertheless, the specific binding domains in which the novel association of BubR1 and UPF1 occurs is of importance for future work.

4.3.3 UPF1 is involved in the MDDC.

To study whether UPF1 has a role in mitosis and the MDDC, mitotic cell population and mitotic progression assays were performed following UPF1 knockdown and the effect on mitosis analysed. Both the mitotic population **(Figure 4.9C)** and mitotic progression **(Figure 4.9D)** assays shown there was no effect of UPF1 knockdown on mitosis in untreated HeLa cells. Yet upon the induction of DNA damage both observed a significant reduction to the mitotic population **(Figure 4.9C)** and transit time **(Figure 4.9E)** following UPF1 knockdown. Interestingly, the mitotic population assay **(Figure 4.9C)** analysed all the siRNAs examined for UPF1 (smart pool and the four deconvoluted siRNAs) and the mitotic population observed following each siRNA after

DNA damage correlated with the effectiveness of knockdown demonstrated via western blot **(Figure 4.9A)**. Taken together, these findings indicate that UPF1 is required for the MDDC.

In **Chapter 3** it was determined that SOD1 regulated the phosphatase PP2A during the MDDC **(Figure 3.21)**. Interestingly, UPF1 is a target of PP2A during NMD (Ohnishi *et al.*, 2003). Furthermore, UPF1 phosphorylation is important for its functionality and the determination of its actions, as UPF1 hyperphosphorylation is required for effective NMD (Durand, Franks and Lykke-Andersen, 2016), and DNA damage induced-ATM phosphorylation of UPF1 inhibits NMD and encourages a DDR role (Brumbaugh *et al.*, 2004). Therefore, it is conceivable that the phospho-regulation of UPF1 also influences BubR1 binding and its role within the MDDC. In the literature, it was hypothesised that mitotic kinase Plk1 and/or DDR kinase Chk1 may target multiple specific UPF1 phosphorylation motifs (Olsen *et al.*, 2010), yet these have not been confirmed experimentally. Taken together with the knowledge that ATM phosphorylates UPF1, it is suitable to theorise that all these kinases may target UPF1 for activation in the response to mitotic DNA damage and these phosphorylation events may be regulated by PP2A. Then as this thesis has found, SOD1 inactivates PP2A upon the presence of DNA damage causing the mitotic arrest, which may result in UPF1 hyperphosphorylation, stimulating BubR1 binding and activation of its role within the MDDC. In support of this, it was found that following IR treatment and the inhibition of PP2A by okadaic acid (individually and in combination), UPF1 phosphorylation increased in the SQ domain (Brumbaugh *et al.*, 2004), where I theorised BubR1 to bind. Furthermore, PP2A is a known interactor of BubR1 (Suijkerbuijk *et al.*, 2012), hence a potential UPF1-BubR1-PP2A complex may form during the MDDC. However, I hypothesise that the binding of PP2A likely occurs during checkpoint exit, as the reactivation of PP2A would be required leading to UPF1 dephosphorylation and deactivation, allowing for mitotic progression. The BubR1-PP2A interaction has been implicated in similar roles during SAC exit and mitotic progression (Espert *et al.*, 2014; Hein *et al.*, 2021). In summary, these theories provide a good basis for future experimental testing, to further comprehend the MDDC.

4.3.4 Limitations and future work.

Another level of optimisation of the co-IP that could have been examined during screen optimisation is the bead saturation level. This considers the ideal bead volume required to obtain all of the protein of interest within the total protein mixture, enabling the maximum amount of protein and interactors to be retained. In this chapter, the co-IP was scaled to a suitable degree, as the levels of protein could be seen on an SDS-PAGE gel. However, during this optimisation, the unbound and discarded fraction post-bead incubation could have been analysed via western blotting for exogenous BubR1 levels in comparison to both input (before IP) and IP samples. If there was no BubR1 in the unbound fraction, the bead volume used would be ideal. Alternatively, if the protein of interest was identified in the unbound fraction, the bead volume may be increased to maximise MycGFP-BubR1 retainment. Overall, ensuring maximum bead efficiency for enriched protein levels to input into the screen.

All cell populations were taken for analysis in the screen, which resulted in a list of interactors that were not specific for mitosis or the MDDC, despite using the 16 hours post-IR treatment time point which enriches the mitotic cell population **(Figure 4.9C)**. Therefore, the mitotic cells were substantially outnumbered by interphase cells, making it difficult to determine the mitotic/MDDC specific interactors of BubR1. To overcome this limitation, a less stringent false discovery rate (0.1 %) was applied to the final list to reduce the discrimination against potential mitotic interactors. Alternatively, cell labelling and sorting would allow mitotic cells to be isolated and input into the screen, providing BubR1 interactors specifically during the MDDC. Although a larger number of cells would be required to obtain enough mitotic cells to conduct the IP and MS analysis, with the addition of more contaminants via cell labelling techniques, adding further technical complexity to the workflow.

The interaction between BubR1 and UPF1 was confirmed using exogenous protein expression via the Invitrogen Flp-In cells that express Flag-UPF1 and further transfection of Myc-BubR1. The overexpression of both proteins would enrich the level of interaction obtained in the co-IP. However, these experimental parameters caused difficultly in determining the level of interaction occurring between the untreated and IR treated conditions, as these proteins were present in such high levels it is likely they would interact independently from the stimulatory conditions. A further investigation

into this interaction should be performed to clarify the conditions required for the interaction via co-IP of endogenous BubR1 and UPF1, and even using the JSH601 and Flag-UPF1 HeLa cells for co-IP with the endogenous counterpart. Overall, strengthening the evidence towards the interaction and examining of the association in mitosis and during the MDDC.

In addition to the co-IP of the endogenous proteins, further work can now be conducted to determine the specific role of UPF1 in the MDDC. Firstly, co-IP using truncated BubR1 and UPF1 proteins expressed within the cell will aid in the identification of the regions in which these proteins associate. Following this, a UPF1 complementation experiment should be performed to confirm UPF1's involvement in the MDDC to be true. This would involve the use of a siRNA that targets the 3'UTR (non-coding region) of UPF1 and the overexpression of a UPF1 construct, under the stimulatory conditions for the MDDC. If the complementation of UPF1 back into the cell rescued the effects observed by knockdown alone the observation would be true. Alternatively, like SOD1 in **Figure 3.6**, a standard UPF1 siRNA and a codon optimised UPF1 construct may be used to conduct this rescue experiment. Furthermore, it would be beneficial to test my proposed theory of UPF1 hyperphosphorylation stimulated by SOD1 repression of PP2A activity during the MDDC and the UPF1-BubR1-PP2A complex for checkpoint recovery. Overall, this information would determine the future direction of the work conducted to uncover the MDDC pathway.

The functional annotation of the screen hits identified numerous valuable pathways, which should be examined further. In addition to the DNA repair proteins mentioned earlier, another example includes 12 proteins identified in this screen that are involved in the spliceosome (detailed in Appendix **Table 7.3**). The spliceosome is a large protein complex (approximately 145 different proteins) (Zhou *et al.*, 2002), which is involved in pre-mRNA processing by excising (splicing) introns through a multistep reaction, a vital process during gene expression (Matera and Wang, 2014). Interestingly, a selection of the proteins obtained has been determined to influence mitosis, as the knockdown of these proteins resulted in mitotic delay and chromosome misalignment during metaphase (Hofmann, Husedzinovic and Gruss, 2010; Neumann *et al.*, 2010). Therefore, the BubR1-spliceosome association would be beneficial to investigate further within the context of mitosis and the MDDC.

4.4 Summary.

This chapter successfully conducted an MS screen of the BubR1 interactome following DNA damage. A list of potential and unique BubR1 interactors were identified. Amongst these proteins, UPF1 was confirmed to associate with BubR1 and to be involved in the MDDC. Further work is now required to investigate this interaction and its role within the MDDC.

Chapter 5: Investigating an interaction between BubR1 and MDC1 in mitosis.

5.1 Introduction, aims and hypothesis.

This thesis has demonstrated that following the induction of DNA damage, cells exhibit slower mitotic transit, which indicates the existence of a novel DNA damage response (DDR) checkpoint in mitosis, termed the mitotic DNA damage checkpoint (MDDC). Throughout this thesis, different proteins associated with the DDR and/or mitosis to establish the pathway of this checkpoint have been investigated. In addition to the current findings, there is evidence to suggest that the versatile DDR protein, MDC1 (DDR roles explained in section **1.1.4.4**) and spindle assembly checkpoint (SAC) effector, BubR1 interact during mitosis (Eliezer *et al.*, 2014). MDC1 has been found to regulate anaphase and hence mitotic progression under undamaged conditions (Townsend *et al.*, 2009; Eliezer *et al.*, 2014), whereas BubR1 has been identified to function in response to mitotic DNA damage (Nitta *et al.*, 2004; Royou, Macias and Sullivan, 2005; Fang *et al.*, 2006; Choi and Lee, 2008). Finally, preliminary data from the Thompson laboratory **(Figure 1.9A)** and the findings of this thesis **(Chapter 4)** has linked BubR1 with the MDDC. Therefore, the BubR1-MDC1 interaction was investigated in this thesis, to determine if this interaction was involved in the MDDC.

The physical interaction between BubR1 and MDC1 was found in the study by Eliezer *et al.* (2014) **(Figure 5.1)**. The experimental parameters involved the treatment of Hek293 cells with 10 Gy ionising radiation (IR) (harvested 1-hour post-treatment) and nocodazole, and it was concluded that the interaction was enhanced following nocodazole treatment due to an increased mitotic cell population (Eliezer *et al.*, 2014). However, this interaction has not been further investigated by this group or within other literature.

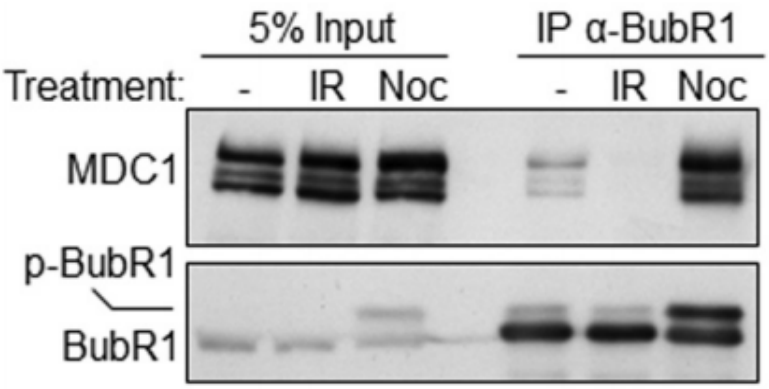

Figure 5.1: The co-immunoprecipitation of MDC1 and BubR1 conducted by Eliezer and colleagues.

It was shown that these proteins had an increased interaction after nocodazole treatment, compared to untreated or treatment 1 hour after 10 Gy ionising radiation (IR). They concluded that this was due to the increased number of cells in mitosis, hence the interaction was specific to this cell cycle phase. (Taken with permission of American Society for Biochemistry and Molecular Biology from Eliezer *et al.*, 2014).

The study by Eliezer *et al.* (2014) also found that MDC1 is involved in unperturbed mitotic progression, through regulating the localisation of Cdc20-C-Mad2 during SAC protein configuration to form the mitotic checkpoint complex (MCC) for metaphase arrest (Eliezer *et al.*, 2014). However, the role of MDC1 in mitosis is unclear as conversely, MDC1 has also been shown to be involved in mitotic progression through regulating Cdc20 activation of APC/C, to promote entry into anaphase and subsequently mitotic exit (Townsend *et al.*, 2009). Then, another study proposed that MDC1 was phosphorylated by mitotic kinase Plk1, to contribute to pro-metaphase-metaphase transition and chromosome integrity (Z. Li *et al.*, 2017). Interestingly, BubR1 is associated with all these mitotic mechanisms MDC1 has been implicated in, as BubR1 is part of the MCC and its main function is to bind to Cdc20-C-Mad2 (Lischetti *et al.*, 2014), then BubR1 also interacts with Cdc20-APC/C (Lara-Gonzalez *et al.*, 2011; Izawa and Pines, 2015) and Plk1 (Izumi *et al.*, 2009). Overall, MDC1 is involved in mitotic progression and it is logical to hypothesise that the mechanisms are dependent on an interaction with BubR1.

This results chapter will investigate the interaction between BubR1 and MDC1, as these proteins connect the SAC and DDR pathways and have been previously reported to interact. This chapter will assess the conditions which are required for this protein association and determine if this interaction is specific to mitosis. Then will establish the role of the protein association in mitosis, and more specifically its importance within the MDDC.

The hypothesis of this chapter is:

The interaction between BubR1 and MDC1 is required for the mitotic delay in response to DNA damage. The association between the proteins will increase following mitotic DNA damage compared to undamaged conditions.

The aims of this chapter are:

1. To confirm the BubR1-MDC1 interaction first established in the study by Eliezer and colleagues.
2. To investigate if the BubR1-MDC1 interaction is stimulated and required for the MDDC.

The objectives of this chapter are:

1. To quantify the effect of various treatments on the mitotic cell population.
2. To investigate the potential effects of those treatments on the BubR1-MDC1 interaction.
3. To confirm the findings of the study by Eliezer and colleagues in my own model.
4. To determine the involvement of MDC1 in mitotic transit in unperturbed or DNA damaged cells.

5.2 Results.

5.2.1 Cell cycle analysis of varying treatments to increase the mitotic cell population.

5.2.1.1 The mitotic cell population was altered in response to IR and nocodazole treatments.

Given that the focus of this thesis is to establish the interactions occurring in mitosis following DNA damage, and as the study by Eliezer *et al.* (2014) determined the BubR1-MDC1 association was enhanced in mitosis, I investigated the effect of the different treatments used by both groups on the mitotic cell population. The treatments included 10 Gy ionizing radiation (IR) and nocodazole. The Thompson laboratory has previously identified an enrichment in mitotic cells 16 hours post-IR treatment, which was further supported in this thesis with 5 Gy and 10 Gy IR doses **(Figure 3.1)**. IR treatment is known to induce DNA double strand breaks (DSBs) (International Atomic Energy Agency, 2010), resulting in the activation of the DDR. Then Eliezer and colleagues found the BubR1-MDC1 interaction was diminished by 1 hour post-10 Gy IR and enriched by nocodazole (microtubule toxin and SAC activating agent) treatments.

Cancer cell lines HeLa and MCF7, and non-cancer cells Hek293 were analysed by pHistone 3 (pH3) (serine 10) staining in combination with propidium iodide (PI) to determine the cell cycle distribution, specifically the mitotic population following each treatment **(Figure 5.2)**. A substantial increase in the mitotic proportion of cells after nocodazole treatment was observed in all cell lines when compared to untreated control conditions (HeLa and MCF7; $p < 0.0001$ and Hek293; $p = 0.0002$). Then a reduction of mitotic cells 1-hour post-IR was observed in all cell lines compared to the corresponding untreated condition. Whereas 16 hours post-IR significantly enhanced the mitotic population compared to the untreated condition in HeLa cells ($p = 0.0003$) **(Figure 5.2A)** and the same trend was observed in MCF7 cells **(Figure 5.2B)**. The Hek293 cells did not exhibit an increased mitotic cell population 16 hours post-IR like the established cancer cell lines, but it is important to highlight that the G2 population of Hek293 cells dramatically increased following these treatments when compared to the control conditions and the other cell lines **(Figure 5.2C)**.

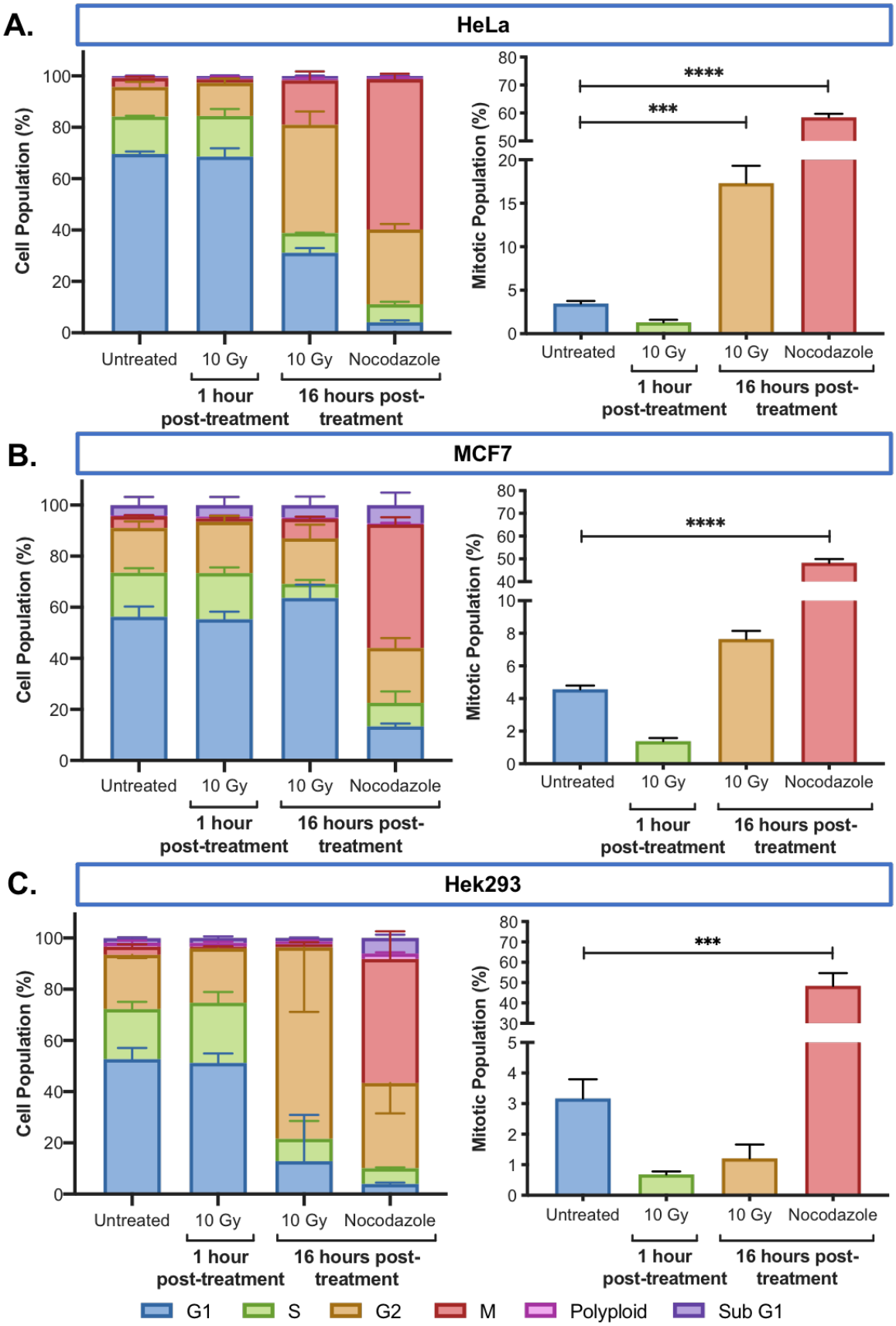

Figure 5.2: HeLa, MCF7 and Hek293 cell cycle analysis following treatment with IR and nocodazole.

Legend on next page.

Figure 5.2: HeLa, MCF7 and Hek293 cell cycle analysis following treatment with IR and nocodazole.

A. HeLa, **B.** MCF7 and **C.** Hek293 cell lines. Mean cell cycle phase distribution following each treatment; 1 hour and 16 hours post-IR (10 Gy) and 16 hours post-nocodazole (200 ng/mL) +/- SEM (N ≥ 2). Mean mitotic cell population following each treatment +/- SEM, represented on a different scale for clarity (N ≥ 2). One-way ANOVA with Dunnett's correction test for multiple comparisons was performed to determine statistical significance (*** denotes $p \leq 0.001$ and **** $p \leq 0.0001$).

In summary, nocodazole had a uniform increase in the mitotic population in all cell lines examined, which was expected as this agent stimulates SAC-induced metaphase arrest (Atassi, Schaus and Tagnon, 1975). There was also a reduction in the mitotic cell population 1-hour post-IR treatment in all cell lines. Therefore, these findings correspond to the study by Eliezer *et al.* (2014), which proposed the BubR1-MDC1 interaction occurred specifically in mitosis following enrichment of mitotic cells by nocodazole treatment but was lost following 1-hour post-IR treatment when there were fewer mitotic cells (Eliezer *et al.*, 2014). Then as expected, in the cancerous cell lines (HeLa and MCF7), 16 hours post-IR treatment exhibited an enhanced mitotic population compared to the non-cancerous Hek293 cells, indicating a mitotic arrest in response to DNA damage. I have obtained similar results via mitotic progression assays with HeLa, MCF7 and non-cancer MRC5VA cells **(Figure 3.2)**, which was proposed to be due to partially defective interphase DDR checkpoints in the cancerous cell lines, allowing progression of cells with unrepaired damage into mitosis, activating the MDDC. Overall, the BubR1-MDC1 interaction should be observed 16 hours post-IR treatment.

5.2.1.2 Cells are viable after 10 Gy IR.

From the treatments assessed in section **5.2.1.1**, there was concern that the effects on mitosis observed were due to cell death following the high dose of IR administered, rather than the MDDC. IR is a well-known and widely used anti-cancer treatment, which causes a large amount of DNA damage (International Atomic Energy Agency, 2010), including the most toxic DSBs (Jackson and Bartek, 2009). To assess the cellular fate at the 16-hour time point, a range of cell viability assays were conducted.

16 hours post-10 Gy IR was found to cause little cell death through both trypan blue staining and annexin V and PI staining. Trypan blue is a cellular stain that only enters compromised cells, 95.20 % of the cell population were considered viable 16 hours post 10 Gy IR and viability were not impacted when compared to the untreated condition (96.39 % viable) **(Figure 5.3A)**. Cellular fate was analysed through annexin V and PI staining, which more specifically stains cells that are undergoing apoptosis. It was determined that 88.95 % of the cell population was viable (Annexin V^-/PI^-) at 16 hours following IR treatment, and not significantly impacted when compared to the untreated condition (92.47 %). However, IR did cause a small increase in Annexin V^+/PI^+ or apoptotic cells (6.64 %) compared to the untreated condition (4.73 %), but this was deemed non-significant and to a lesser extent than the camptothecin positive control (9.81 %) **(Figure 5.3B-C)**.

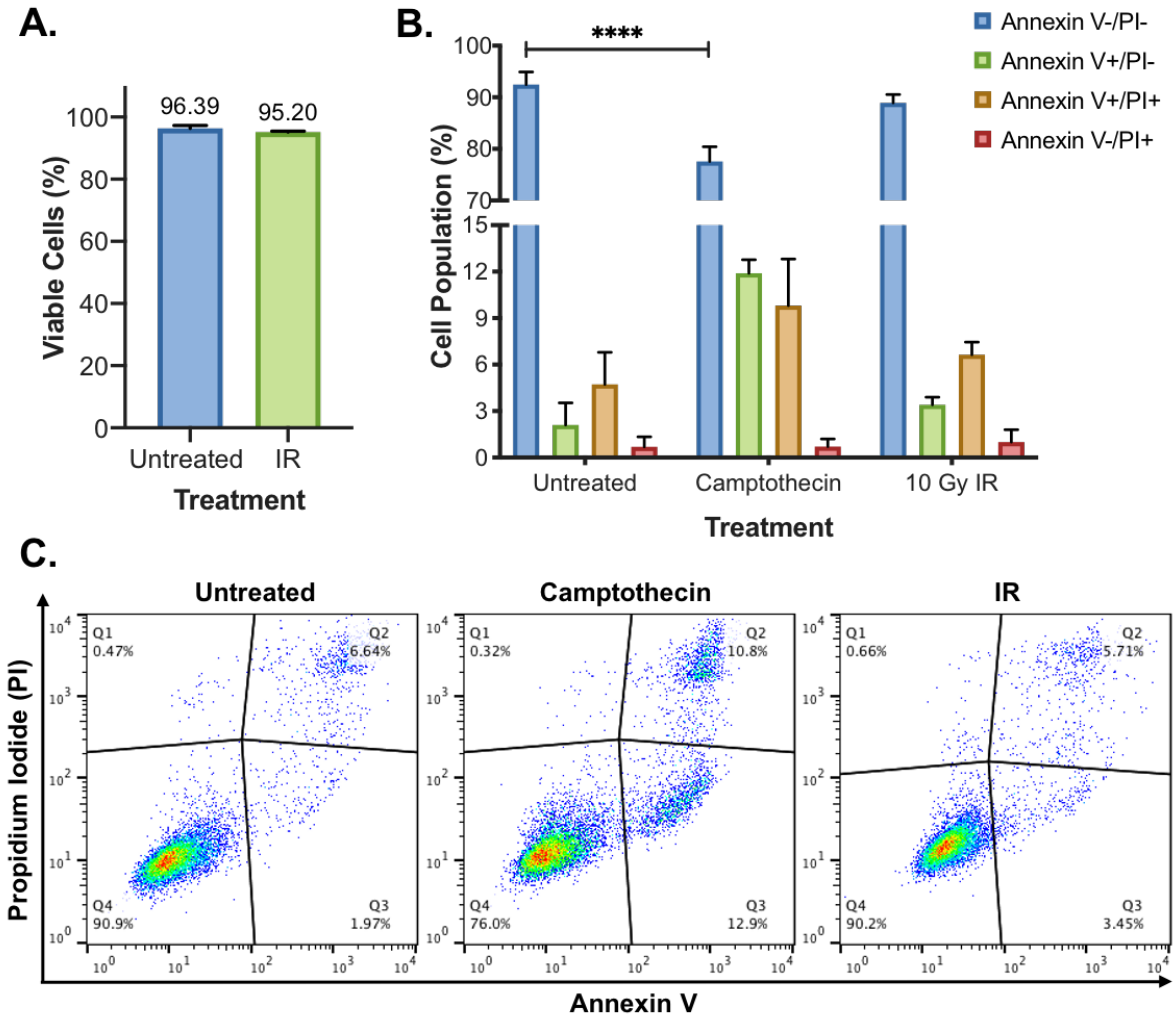

Figure 5.3: Cell viability analysis of HeLa cells following treatment with 10 Gy IR.
Legend on next page.

Figure 5.3: Cell viability analysis of HeLa cells following treatment with 10 Gy IR.
A. Mean cell viability via trypan blue assay 16 hours post-10 Gy IR -/+ SEM (N= 3). The viability percentage is represented above each bar. **B.** Mean annexin V and Propidium iodide (PI) dual stained cell populations -/+ SD (N= 3) following treatment. Cells viability was measured 16 hours post-10 Gy IR and 8 hours post-camptothecin (1 μM) treatment as a positive control. One-way ANOVA with Dunnett's correction test for multiple comparisons was performed to determine statistical significance (**** denotes $p \leq 0.0001$). **C.** A panel of example images representing the gating was applied to measure the percentage of cells within each parameter. Each treatment assessed is presented.

Overall, it was deduced that this treatment did not affect the cellular viability of HeLa cells at the 16-hour time point, so the phenotype observed was not influenced by cellular death or apoptosis pathways. Therefore, 16 hours post-IR was used with the treatments used in the Eliezer *et al.* (2014) study (1-hour post-IR and nocodazole) to further test and replicate the BubR1-MDC1 interaction.

5.2.2 The interaction between BubR1 and MDC1.

5.2.2.1 The BubR1-MDC1 association in untreated cells.

The interaction between BubR1 and MDC1 was initially established in untreated cells through co-immunoprecipitation (co-IP) and visualised using western blot **(Figure 5.4)**. The untreated co-IPs were conducted using HeLa cells for endogenous BubR1 and JSH601 cells for the exogenous expression of doxycycline-inducible Myc and green fluorescent protein (GFP) tagged BubR1 (MycGFP-BubR1) (further explanation in section **4.2.1.2**).

The interaction between endogenous BubR1 and MDC1 was verified in HeLa cells through a BubR1 pull-down for IP **(Figure 5.4Ai)**, but not successfully obtained following an MDC1 pull-down **(Figure 5.4Aii)**. Whereas in the JSH601 cells, the association with MDC1 was obtained between both endogenous and exogenous (MycGFP-BubR1) BubR1 proteins, following an MDC1 IP **(Figure 5.4Bii)**, but was not obtained following a Myc-tag pull-down **(Figure 5.4Bi)**.

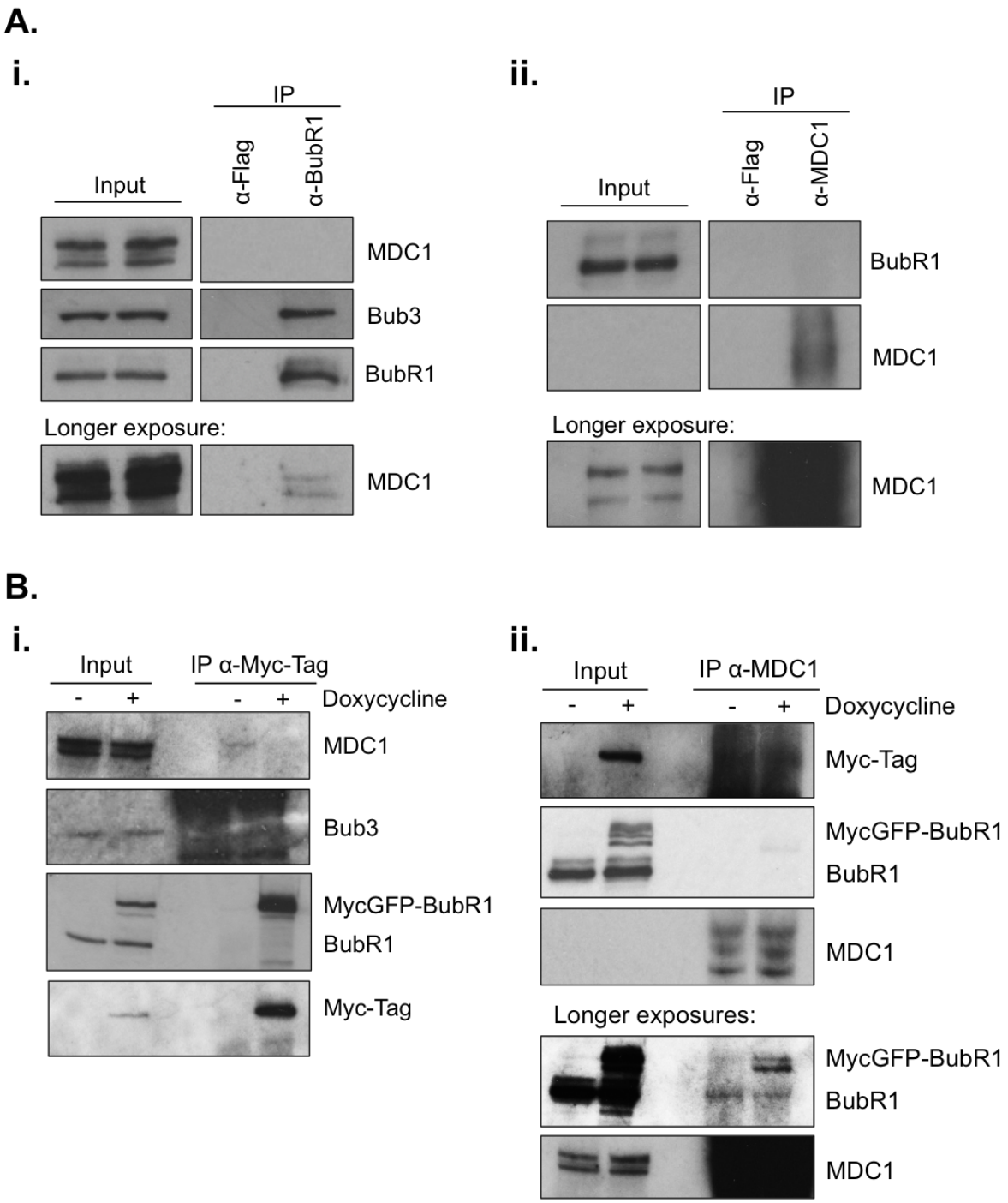

Figure 5.4: Untreated co-IP results for the interaction between MDC1 and BubR1.

Legend on next page.

Figure 5.4: Untreated co-IP results for the interaction between MDC1 and BubR1.
A. Western blot showing the interaction between MDC1 and endogenous BubR1 in HeLa cells. **i.** Untreated HeLa cells were harvested for co-IP with antibodies against Flag (negative control) or BubR1 (N= 1). Immunoprecipitates were probed for BubR1, MDC1 and Bub3 (positive control). A longer exposure was presented to highlight the protein-protein interaction. **ii.** as in **i.** with the exception, a MDC1 antibody was used for IP pull-down (N= 1). **B.** Western blot showing the interaction between MDC1 and endogenous BubR1 and exogenous MycGFP-BubR1 in JSH601 cells. **i.** Doxycycline (1 µg/mL) was administered to JSH601 cells for 48 hours and harvested for co-IP with Myc-Tag antibody (N= 1). The absence of doxycycline was used as a negative control. Immunoprecipitates were probed for Myc-Tag, BubR1, MDC1 and Bub3 (positive control). **ii.** as in **i.** with the exception, a MDC1 antibody was used for IP pull-down (N= 2). Longer exposures were presented to highlight the interaction.

Overall, it is noticeable that this interaction was weak in untreated cells, indicating the association may be transient under this condition.

5.2.2.2 The BubR1-MDC1 interaction following IR treatment.

Given that the interaction is weak in untreated cells and that untreated HeLa cells have an average of 3.46 % of cells in mitosis **(Figure 5.2A)**, I hypothesised that increasing the mitotic cell fraction using IR treatment would heighten the interaction, as Eliezer *et al.* (2014) had proposed this association specifically occurs in mitosis. Furthermore, there would also be an increase in the association if this interaction was involved in the MDDC. Both BubR1 and MDC1 co-IPs (pull-downs) of HeLa cells were conducted, following treatment with 10 Gy IR and harvested at the 16 hour time point for visualisation using western blot **(Figure 5.5)**.

The data obtained from the BubR1 co-IPs were inconsistent, as there was differing responses to IR treatment throughout experimental repeats **(Figure 5.5Ai-iv)**, as well as technical difficulties acquiring the data; MDC1 presence in the negative control **(Figure 5.5Aiii)** and the requirement of long exposures to visualise the interaction. Yet it was clear that there was an increase in the overall amount of BubR1 and phosphorylated BubR1 after IR, which could account for the increase in mitosis.

Nevertheless, the MDC1 co-IPs consistently featured BubR1 in untreated and IR treated conditions **(Figure 5.5Bi-iv)**.

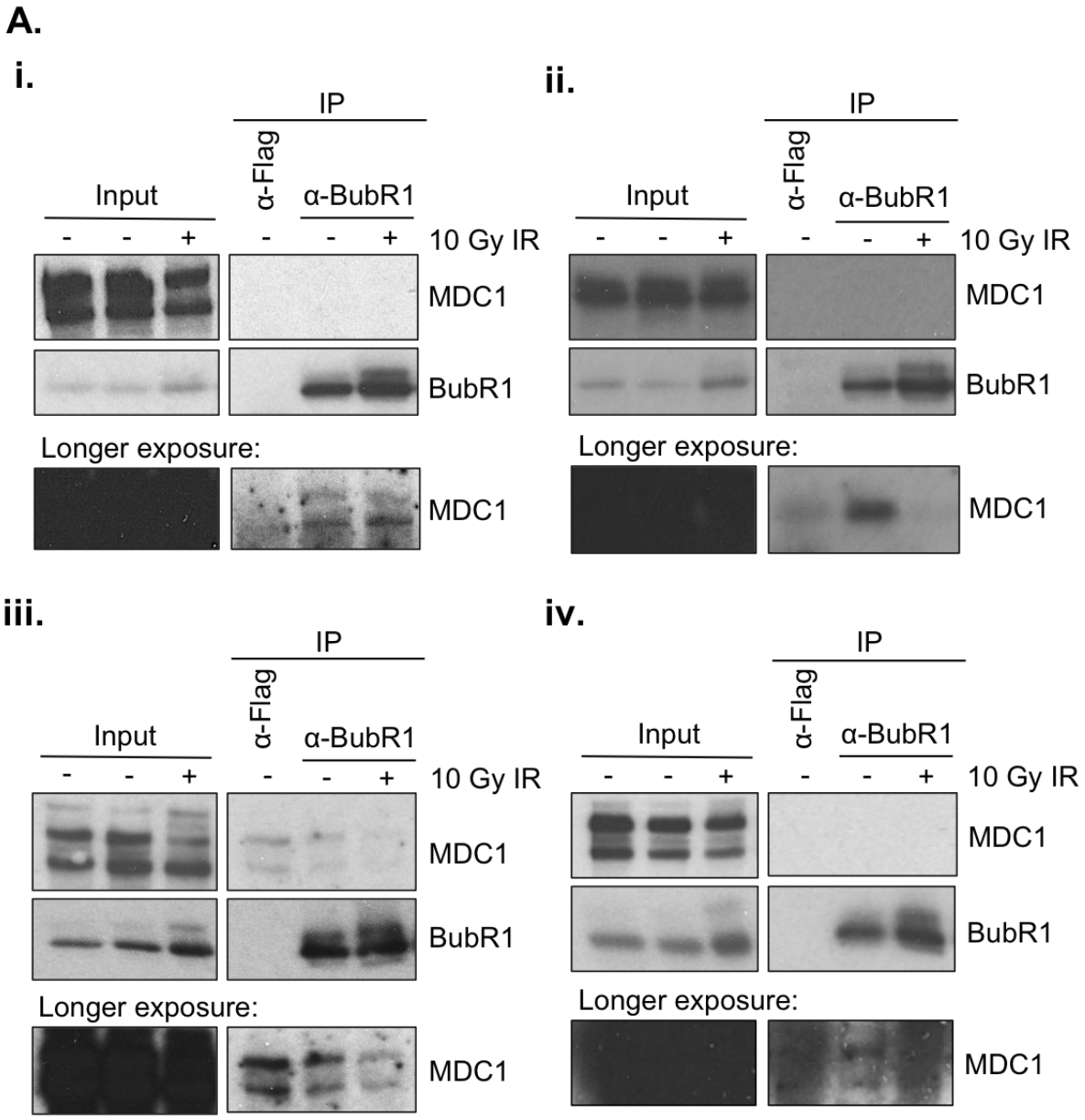

Figure 5.5: The co-IP results for the interaction between BubR1 and MDC1 following 10 Gy IR treatment.

Legend on next page.

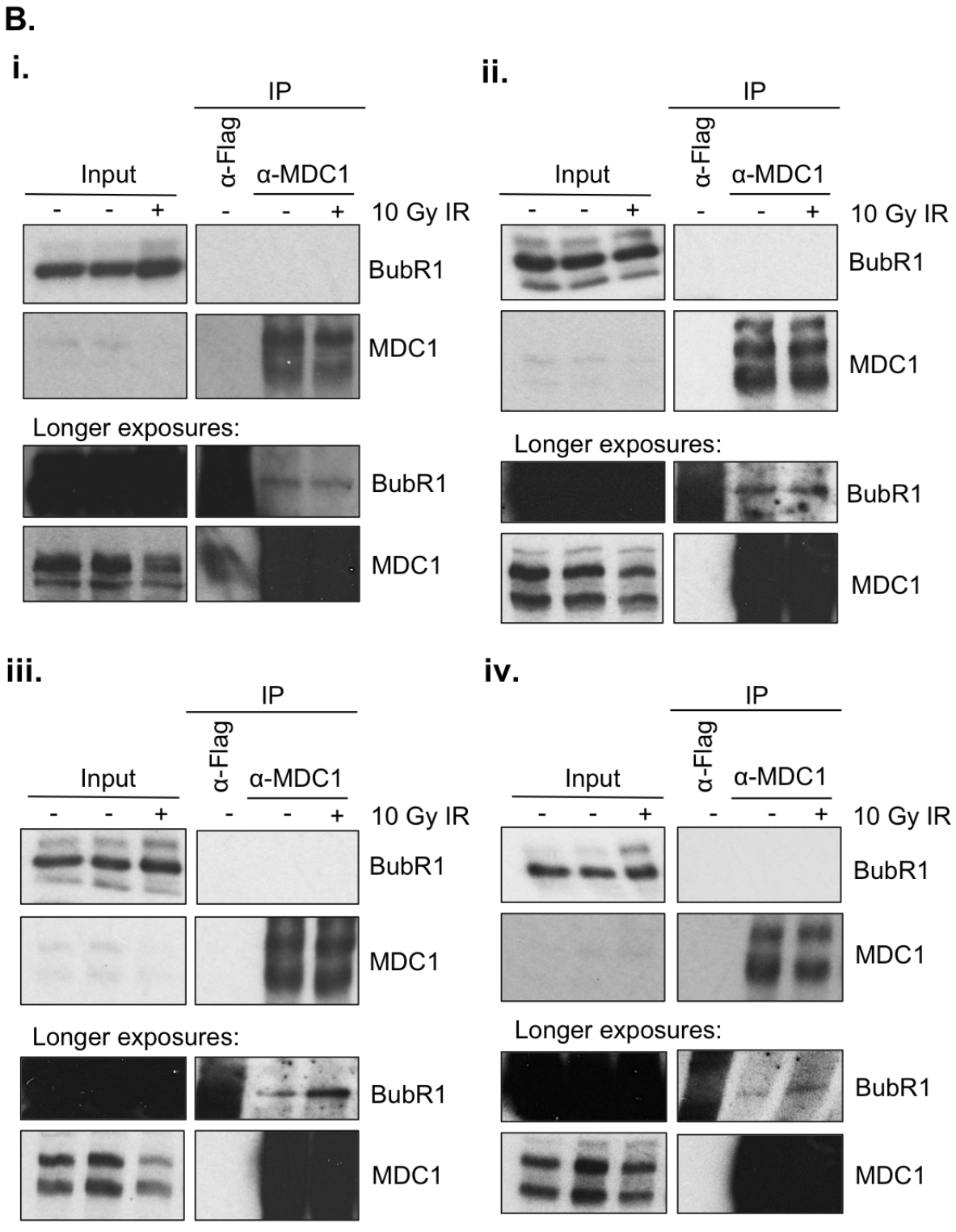

Figure 5.5: The co-IP results for the interaction between BubR1 and MDC1 following 10 Gy IR treatment.

Legend on next page.

Figure 5.5: The co-IP results for the interaction between BubR1 and MDC1 following 10 Gy IR treatment.

A. HeLa cells were treated with 10 Gy IR and harvested 16 hours post-treatment for co-IP via a BubR1 pull-down (N= 4). Immunoprecipitates were probed for BubR1 and MDC1. Each experimental repeat is shown, and the longer exposures were included to highlight the interaction. **B.** as in **A.** with the exception each MDC1 co-IP are shown (N= 4). Longer exposures were included to illustrate the interaction.

Overall, there was no clear effect of IR treatment on the interaction, yet the association between the proteins was maintained in low amounts, similarly to the untreated condition.

5.2.2.3 The BubR1-MDC1 interaction following treatment with IR and nocodazole.

Given that an increase in the interaction following IR treatment had not been found, despite the enhanced mitotic population, I repeated the experiment on which the figure from the study by Eliezer *et al.* (2014) is based **(Figure 5.6A)**, to replicate their results and compare within the context of this research. 10 Gy IR (1 hour and 16 hours post-treatment) and 200 ng/mL nocodazole were administered to the cells and different experimental conditions were examined to replicate the findings of the study by Eliezer and colleagues.

The Abcam BubR1 and Bethyl MDC1 antibodies have been used in the previous co-IPs in this chapter. Firstly, co-IP was conducted using the Abcam BubR1 antibody, however, the interaction between BubR1-MDC1 was not ascertained (data not shown). Then using the same conditions but the Bethyl MDC1 antibody for pull-down, the interaction was obtained yet shown little difference between the treatments **(Figure 5.6B)**. Furthermore, longer exposures were required to visualise the proteins, indicating low levels of interaction across all conditions, unlike the findings of Eliezer *et al.* (2014) **(Figure 5.6A)**.

To better replicate the study by Eliezer *et al.* (2014), the same experimental parameters were implemented, including the same cell line; Hek293 cells and the

same antibodies; MDC1 (Sigma) and BubR1 (SBR1.1: antibody gifted from Professor Stephen Taylor, University of Manchester). The BubR1-MDC1 interaction was successfully obtained via co-IP using a BubR1 pull-down but did not emulate the data found by Eliezer and colleagues **(Figure 5.6C)**. There was no enhanced interaction following nocodazole treatment, but the interaction may have been reduced following both IR treatments compared to the untreated condition.

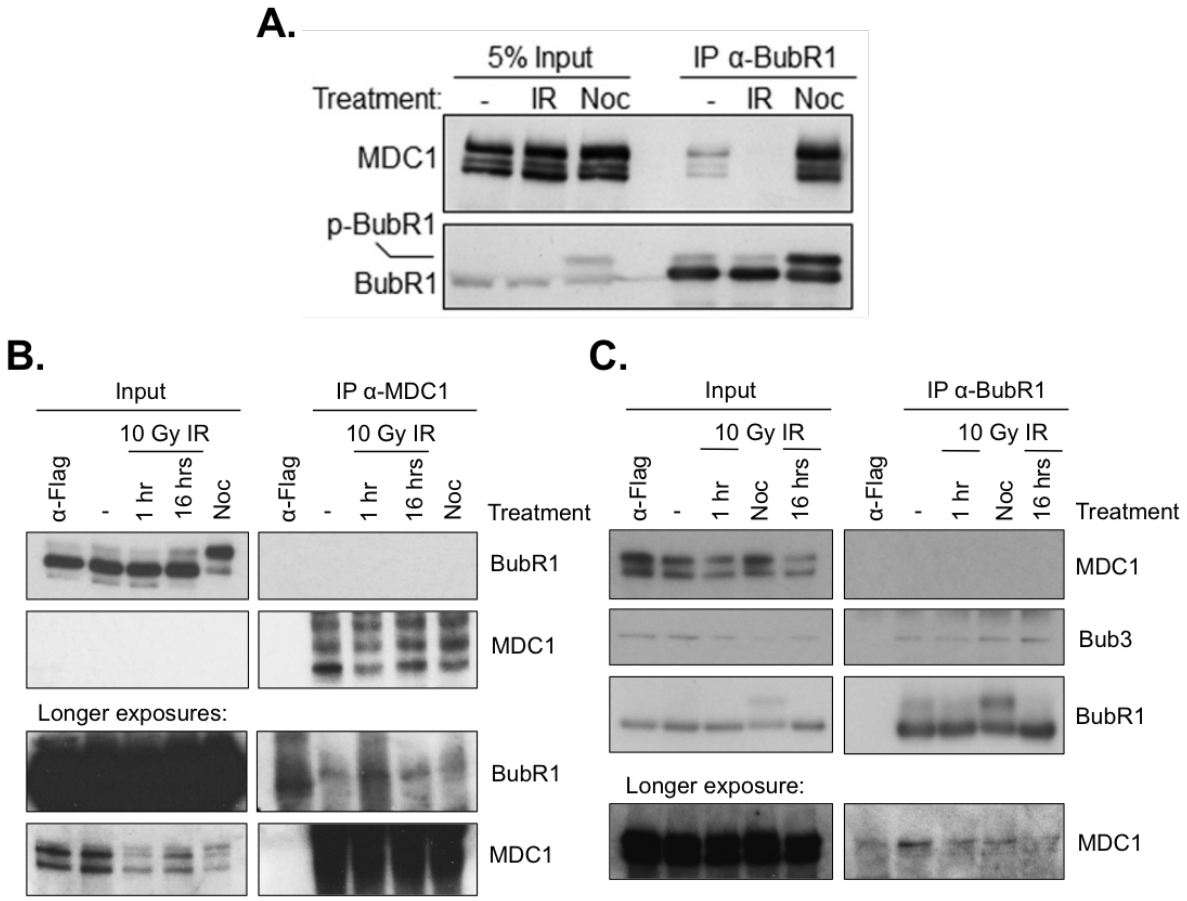

Figure 5.6: The replication of the Eliezer *et al.* (2014) study co-IP.

A. The co-IP of MDC1 and BubR1 by the Eliezer *et al.* (2014) for reference. It was shown that these proteins had an increased interaction after nocodazole (Noc) treatment, compared to untreated or treatment 1 hour after 10 Gy ionising radiation (IR) (Taken with permission of American Society for Biochemistry and Molecular Biology from Eliezer *et al.,* 2014). **B.** HeLa cells were treated with 200 ng/mL nocodazole for 16 hours and 10 Gy IR for 1- or 16 hours and harvested for co-IP with Flag and MDC1 (Bethyl) antibodies (N=1). Immunoprecipitates were probed with BubR1 and MDC1. Longer exposures were presented to highlight the interaction. **C.** Hek293 cells were treated as in **B.** with the exception Flag and BubR1 (SBR1.1) antibodies were used for pull-down during co-IP the BubR1-MDC1 interaction (N=1). Immunoprecipitates were probed with BubR1, Bub3 and MDC1. Longer exposures were presented to illustrate the interaction.

In summary, the findings obtained in the study by Eliezer *et al.* (2014) were not confirmed in this thesis.

5.2.3 MDC1 is not required for the MDDC.

The data obtained so far did not fully replicate the finding that BubR1 and MDC1 specifically interact in mitosis, as observed in the Eliezer *et al.* (2014) study. Therefore, it was of importance to replicate their data on the effect of MDC1 on mitotic progression, as well as determine if this protein is involved in the MDDC via the mitotic population and mitotic progression assays. The study by Eliezer and colleagues found that upon depletion of MDC1, the total duration of mitosis in unperturbed HeLa and U2OS cells was reduced (Eliezer *et al.*, 2014). This supported their other finding that MDC1 was required for mitotic progression through regulation of SAC-induced mitotic arrest (Eliezer *et al.*, 2014). However, in the literature, there is also data to support the opposite effect on mitosis when MDC1 was depleted. In the paper by Townsend *et al.* (2009), it was found that after MDC1 depletion there was an increase in the duration of mitosis, compared to a control in undamaged HeLa cells (Townsend *et al.*, 2009). This supported their overall finding that MDC1 was required for metaphase-anaphase transition through regulation of Cdc20 activation of APC/C (Townsend *et al.*, 2009). The findings of Townsend *et al.* (2009) are supported by the study by Li *et al.* (2017), which also found an increase in mitotic transit time following MDC1 depletion in undamaged conditions, yet the reasoning for this differed (Z. Li *et al.*, 2017). To determine the role of MDC1 on unperturbed mitotic progression and its involvement in MDDC, HeLa cells were depleted of MDC1 using the same siRNA's as in the study by Eliezer *et al.* (2014) and subjected to IR treatment.

Firstly, cell cycle distribution analysis was performed through pH3 and PI co-staining, to specifically determine the effect of MDC1 depletion on the mitotic population in untreated and irradiated HeLa cells **(Figure 5.7A-B)**. A BubR1 positive control was included to allow the comparison of the effect. In untreated conditions, there was no effect of MDC1 depletion on the mitotic proportion of cells. However, as expected when cells were treated with IR, the siControl condition had a significantly enriched mitotic cell population ($p < 0.0001$), compared to the corresponding untreated condition. But that increase was not observed following depletion of BubR1, which was

significantly reduced ($p < 0.0001$) compared to the irradiated siControl condition **(Figure 5.7B)**. The knockdown of MDC1 did not produce a consistent response following IR treatment **(Figure 5.7B)**, as siMDC1-1 significantly reduced the mitotic cell population ($p = 0.0004$) compared to the irradiated siControl condition. Whereas siMDC1-2 had no effect.

To further test the role of MDC1 on mitosis, live cell time-lapse microscopy analysis was conducted to analyse the effect on mitotic progression. Again, in untreated conditions, there was no effect of MDC1 knockdown on mitotic transit when compared to the siControl condition **(Figure 5.7C)**. Following IR treatment, the duration of mitosis in control cells (siControl) was significantly increased ($p = 0.0085$), when compared to the untreated control cells, as expected. Similarly, to the mitotic population data obtained siMDC1-2 did not affect mitotic progression. However, the cells exposed to siMDC1-1 and IR had a significant increase in mitotic transit time ($p = 0.0135$), compared to the irradiated control condition **(Figure 5.7C)**. Finally, alongside both mitotic population and mitotic progression assays, cells were harvested for western blot analysis to determine the effectiveness of MDC1 knockdown. The depletion of each protein was confirmed across all repeats for each experiment, illustrated with a representative image **(Figure 5.7D)**.

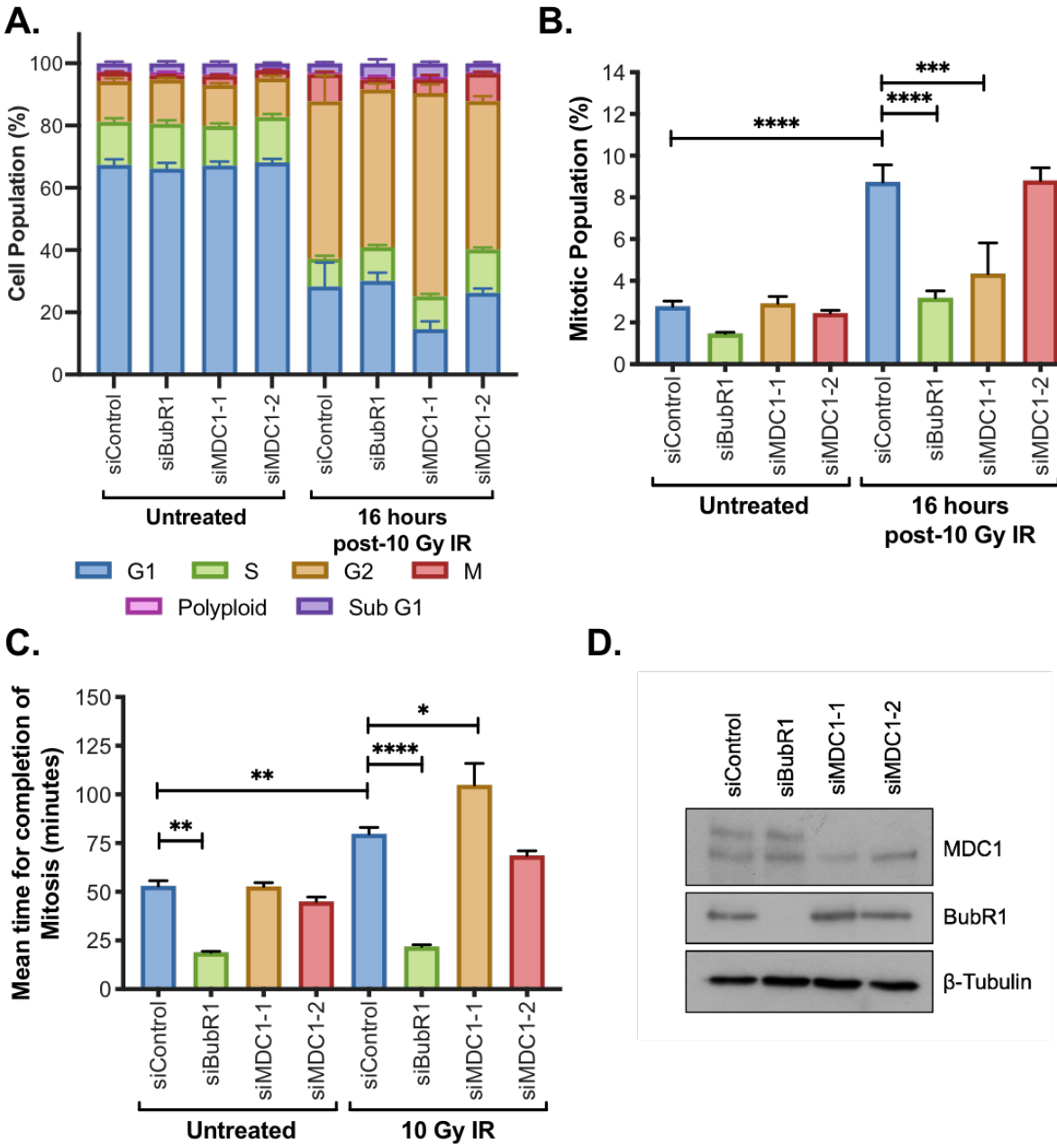

Figure 5.7: The analysis of MDC1 depletion on the mitosis after DNA damage in HeLa cells.

Legend on next page.

Figure 5.7: The analysis of MDC1 depletion on the mitosis after DNA damage in HeLa cells.

A. Mean cell cycle phase distribution following BubR1 or MDC1 depletion and 16 hours post-10 Gy IR treatment +/- SEM (N= 4). **B.** Mean mitotic cell population following each treatment +/- SEM (N= 4). One-way ANOVA with Dunnett's correction test for multiple comparisons was performed to determine statistical significance (*** denotes $p \leq 0.001$ and **** $p \leq 0.0001$). **C.** Time-lapse live cell microscopy analysis of the mean time taken to complete mitosis after BubR1 or MDC1 depletion and 10 Gy IR treatment. A maximum 50 of cells per condition were counted and the data represents the overall mean of each independent experiments +/- SEM ($N \geq 2$). One-way ANOVA with Dunnett's correction test for multiple comparisons was performed to determine statistical significance (* denotes $p \leq 0.05$, ** $p \leq 0.01$ and **** $p \leq 0.0001$). **D.** A representative western blot showing the levels of MDC1, BubR1 and β-Tubulin after transfection with each siRNA. This was conducted alongside and for the duration of the mitotic population and progression assays (N= 4).

Overall, it was determined that in my hands MDC1 knockdown has no consistent effect on unperturbed mitotic progression or mitosis following DNA damage**.** Despite the clear reduction in MDC1 expression post-transfection with both siRNA's. Therefore, the results from the studies by Eliezer, Townsend and Li and colleagues could not be reproduced.

5.3 Discussion.

In this chapter, I sought to replicate the interaction between BubR1 and MDC1 found in the literature to occur specifically in mitosis (Eliezer *et al.*, 2014), to ultimately determine if this association occurred following mitotic DNA damage. The interaction was successfully obtained, but in this thesis, the findings from Eliezer *et al.* (2014) could not be reproduced. The effect of MDC1 depletion on the mitotic population and mitotic progression in the presence of DNA damage was also analysed. I concluded from this data that MDC1 does not affect unperturbed or damaged mitotic cells in either assay tested. Overall, it was determined MDC1 is not involved in the MDDC.

5.3.1 BubR1 interacts with MDC1.

The BubR1-MDC1 association was confirmed using endogenous and exogenous BubR1 in untreated HeLa and JSH601 cells, but at low levels **(Figure 5.4)**. This supported the findings that these proteins interact as determined in the Eliezer *et al.* (2014) study, which also observed low levels of the interaction in the untreated cells **(Figure 5.1)**. Similarly, low levels of the BubR1-MDC1 interaction were found 16 hours post-IR treatment in HeLa cells **(Figure 5.5)**. This was unexpected, as it was hypothesised that due to the increase in the mitotic cell population 16 hours post-IR treatment **(Figure 5.2)**, there would be an enhanced association of these proteins as Eliezer *et al.* (2014) proposed the BubR1-MDC1 interaction is specific to mitosis. Furthermore, there were also inconsistent responses observed between the four individual co-IP experiments in both BubR1 **(Figure 5.5A)** and MDC1 pull-downs **(Figure 5.5B)** following IR treatment. These findings could be explained by the comparison of the mitotic population from an average of 3.46 % in untreated cells, to an average of 17.31 % or 58.48 % following IR and nocodazole treatments respectively **(Figure 5.2)**, as this indicates the enhanced mitotic population by IR treatment may have been insufficient to show an observable effect on the interaction. Despite extensive efforts, the BubR1-MDC1 interaction was found at low and inconsistent levels following IR treatment, indicating the interaction may not be specific to mitosis and was not required for the MDDC.

As these results were unexpected based on the data from the Eliezer *et al.* (2014) study, I sought to reproduce their experiments. Firstly, HeLa cells were used with the same treatment conditions as the Eliezer *et al.* (2014) paper, but with the addition of a 16 hours post-IR time point for comparison. The findings obtained did not show an increase in the interaction following any treatment, as the association between the proteins remained at low levels **(Figure 5.6B)**. In another attempt to replicate the Eliezer *et al.* (2014) paper's findings the same cell line, treatment conditions and antibodies were used. However, the data obtained again contradicted the findings of Eliezer *et al.* (2014) study, as the interaction was again found at low levels in all conditions tested including nocodazole treatment **(Figure 5.6C)**. Despite an average of 58.48 % of cells in mitosis after this treatment and compared to the major increase attained in the findings of Eliezer and colleagues **(Figure 5.6A)**. Therefore, the conclusions made in the study by Eliezer *et al.* (2014) were not confirmed in this thesis.

Furthermore, the hypothesis of this chapter was found not to hold true in my hands, as the association was not influenced by mitotic DNA damage, again indicating that the interaction between BubR1-MDC1 is not vital for the MDDC.

The study by Eliezer *et al.* (2014) had also determined that MDC1 interacts with Mad2 and Cdc20 and was required for the localisation of these proteins to the kinetochores and formation of the MCC (Eliezer *et al.*, 2014). Therefore, there is the possibility that the interaction found between BubR1 and MDC1 occurred indirectly via both proteins associating with a mutual protein and not directly with each other. Alternatively, yet in support of an indirect interaction, MDC1 has also been found to interact with APC/C (Townsend *et al.*, 2009) and Plk1 (Z. Li *et al.*, 2017). Despite these paper's opposing conclusions, they provide another alternative mechanism for MDC1's interaction with BubR1, as this protein also associates to Mad2, Cdc20 (Lischetti *et al.*, 2014), APC/C (Lara-Gonzalez *et al.*, 2011; Izawa and Pines, 2015) and Plk1 (Izumi *et al.*, 2009).

In a recent paper, it was determined that the interaction between MDC1 and another DDR protein TOPBP1 was responsible for ensuring chromosome stability in mitosis (Leimbacher *et al.*, 2019). This paper found that in response to the induction of DSBs via IR treatment in mitotic cells, MDC1 accumulates at the damage lesions, recruiting TOPBP1 to form filamentous structures between the MDC1 foci. These structures tether the chromatid breaks together to facilitate segregation and subsequent repair in G1 (Leimbacher *et al.*, 2019). Interestingly, BubR1 also possesses a similar role in *Drosophilia* cells following DNA damage, as along with other mitotic proteins Plk1 and Aurora B, BubR1 accumulates and forms tether structures at DNA breaks in mitosis. This was also proposed to ensure the chromatids were intact for segregation, protecting against genomic instability. (Royou *et al.*, 2010). As BubR1 and Plk1 have been found to interact in human cells (Izumi *et al.*, 2009), these findings could be applied to higher organisms. Furthermore, as previously stated MDC1 is activated by Plk1 in mitosis (Z. Li *et al.*, 2017). Therefore, the MDC1-TOPBP1 complex may also associate with BubR1 and Plk1 forming a multi-protein tethering structure at DNA damage induced chromosomal breaks (Thompson, Gatenby and Sidi, 2019). This indirect association of BubR1 and MDC1 also supports the weak interaction found in this research.

5.3.2 MDC1 is not required for unperturbed mitotic progression or the MDDC.

To further study whether MDC1 is an essential protein for mitosis and has a role in the MDDC, mitotic population and progression assays were performed following MDC1 knockdown and the effect on mitosis analysed. Both the mitotic population **(Figure 5.7B)** and mitotic progression **(Figure 5.7C)** assays shown there was no effect of MDC1 knockdown on mitosis in untreated HeLa cells. These findings suggest that MDC1 does not affect unperturbed mitosis, contradictory of the studies by Eliezer *et al.* (2014), Townsend *et al.* (2009) and Li *et al.* (2017). However, following the induction of DNA damage, siMDC1-1 significantly reduced the mitotic cell population but also significantly enhanced the mitotic transit time. This may indicate a potential involvement of MDC1 in the MDDC-mediated mitotic arrest, yet opposing effects were observed between each assay and the effects would be expected to be seen in both siRNA's examined. It was consistently observed that siMDC1-2 did not affect the mitotic population or mitotic transit time. Effective MDC1 knockdown was confirmed to be in both siRNA's through western blot analysis **(Figure 5.7D)**, so the effects of siMDC1-1 on mitosis may be due to siRNA off-target effects and the reduction in cell viability following knockdown. Taken together, the inconsistency following MDC1 depletion suggests this protein is not essential for the activation of the MDDC.

These findings yet again contradict the work conducted by Eliezer *et al.* (2014), as this paper concluded that the depletion of MDC1 lead to shorter mitotic transit compared to the control in unstressed conditions. Eliezer *et al.* (2014) investigated MDC1 knockdown in HeLa and U2OS cell lines using both siRNAs used in this thesis, and the knockdown effects were ensured via MDC1 complementation (Eliezer *et al.*, 2014). This paper conducted a thorough analysis using a minimum of 100 cells for each condition in three independent experiments, compared with a total of 27-150 cells scored across the conditions throughout three repeats in this thesis, due to poor viability particularly in the condition treated with siMDC1-1 in combination with IR. Whereas Townsend *et al.* (2009) only scored 10 mitotic cells per condition (suggesting 1 repeat), which does not seem sufficient enough to conclude that the depletion of MDC1 greatly lengthened mitotic transit in HeLa cells, compared to the control (averages of 5 hours 48 min compared to 50 min, respectively) (Townsend *et al.*, 2009). Similar results were obtained with siMDC1-1 in damaged conditions in this thesis, yet the study by Townsend *et al.* (2009) used unstressed conditions. Hence

the findings in the Townsend *et al.* (2009) paper could not be replicated either. Finally, another study also characterised the effect of MDC1 depletion on mitosis and found that there was an increase in transit time compared to the control in undamaged conditions (Z. Li *et al.*, 2017). Although, this paper only measured from nuclear envelope breakdown to anaphase, not until the completion of mitosis like this thesis and the other studies evaluated making comparison difficult. Additionally, this paper used short hairpin RNA (shRNA), which involved the transfection of HeLa cells with a recombinant retrovirus for MDC1, which was approximately 50 % efficient in MDC1 knockdown, reducing the reliability of the findings (Z. Li *et al.*, 2017). Overall, the effect of MDC1 in mitosis remains elusive, but based on the findings of this research MDC1 does not appear to be involved in mitotic progression or the MDDC.

5.3.3 Limitations.

Despite using the same MDC1 siRNAs as the study by Eliezer *et al.* (2014) the findings could not be replicated in this research. Eliezer and colleagues conducted a thorough analysis of the knockdown of MDC1, using two siRNAs and even performing a complementation experiment to show the rescue of the effect found. From the analysis conducted, this research seemed to be more credible compared to the Townsend *et al.* (2009) and Li *et al.* (2017) studies. In this research, only one siRNA (siMDC1-1) indicated an effect on mitosis, which was proposed to be due to toxicity and off-target effects and this finding opposed the data obtained by Eliezer *et al.* (2014). It may be useful to select a siRNA used by Townsend *et al.* (2009) and an independent one to determine a true effect or strengthen findings of this thesis.

As the interaction between BubR1 and MDC1 was observed to be weak in this research, I propose that it was due to an indirect association. The literature describes various potential proteins which may provide a platform for MDC1 and BubR1 binding such as Mad2, Cdc20 (Lischetti *et al.*, 2014), APC/C (Lara-Gonzalez *et al.*, 2011; Izawa and Pines, 2015), Plk1 (Izumi *et al.*, 2009) or TOPBP1 (Leimbacher *et al.*, 2019). Therefore, further depletion assays of those proteins could be performed and the maintenance of the MDC1-BubR1 interaction examined via co-IP. However, due to the inconsistency of the findings in this research, it would be difficult to obtain and

clearly determine the effect of other depleted proteins on the BubR1-MDC1 interaction.

As mentioned throughout, the detection of the BubR1-MDC1 interaction was inconsistent and weak. A strong ECL detection regent (SuperSignal™ West Pico PLUS; Thermo Fisher Scientific) was required to visualise the proteins through western blot analysis. An issue with using this reagent meant that the background was often overexposed leading to unclear bands, which were difficult to interpret. To overcome this in the future the composition of the cell lysis buffer should be considered to obtain optimum protein yield and maintain protein-protein interactions. This could be achieved by using a less stringent buffer by decreasing the salt concentrations, as high salt concentrations can negatively affect protein solubility, structure and its interactions (Arakawa and Timasheff, 1991; Voet and Voet, 2011). As the BubR1-MDC1 interaction is weak an alteration in the buffer composition may help maintain the association during the IP process. The study by Eliezer *et al.* (2014) did use different buffers compared to buffers used in this thesis, so it may be a good starting point to test the interaction again using those buffers.

5.4 Summary.

Here I have shown that the SAC kinase BubR1 and DDR protein MDC1 interact transiently or at low levels. This interaction was not affected by mitosis or DNA damage, so is probably not required for the MDDC. This was further supported by Chapter 4, as MDC1 was not found to be an interactor of BubR1 following DNA damage **(Figure 4.7Ci)**. Overall, I propose the BubR1-MDC1 interaction occurs indirectly.

Chapter 6: Discussion

6.1 Validation of the mitotic DNA damage checkpoint.

In this thesis, a delay in mitosis following DNA damage which is dependent on the antioxidant enzyme superoxide dismutase 1 (SOD1) was confirmed. This supports the existence of a mitotic DNA damage checkpoint (MDDC) and the initial investigation into the proteins involved in the pathway was conducted in this thesis. The MDDC was identified in asynchronous cancer cells, which following DNA damage, a subset of cells escaped the interphase DNA damage response (DDR) checkpoints to enter mitosis with damage lesions. This damage activates the MDDC and arrests the cell in mitosis, I theorise that damage containment and initiation of repair occurs during the MDDC, before the continuation of the cell cycle. This novel checkpoint highlights a mechanism of tumour cell evasion from current anti-cancer therapeutics, which involve the induction of DNA damage in combination with interphase DDR proteins inhibitors to impair the DDR and enhance cell death. Therefore, it is important to elucidate the pathway responsible for the MDDC to then target with therapeutics to further enhance tumour cell death. Preliminary data including a siRNA DNA damage screen conducted in the Thompson laboratory **(Figure 1.9)**, in addition to the literature, determined the potential targets to investigate in this thesis.

SOD1 was initially identified in the siRNA DNA damage screen **(Figure 1.9)**. In this thesis, a role of SOD1 in the DDR response was deduced, as cells with a reduction in SOD1 exhibited an enhanced and prolonged DDR **(Figure 3.11 and 3.12)**. It was concluded that this was due to a role of SOD1 in the homologous recombination (HR) repair pathway via the regulation of RAD51 loading to DNA lesions **(Figure 3.13)**. It is feasible to hypothesise this occurs during the MDDC, as DNA repair such as HR has been shown to be performed in mitosis following DNA damage (Godinez *et al.*, 2020). Furthermore, I report a novel role of SOD1 in mitosis, specifically within the MDDC, as the attenuation of SOD1 dysregulated mitotic arrest following DNA damage **(Figure 3.2, 3.3 and 3.4)**. The DNA damage experienced was induced by DNA damaging agents such as IR, chemotherapeutics and oxidative stress inducing agent; H_2O_2. The role of SOD1 within the MDDC was determined to be via the regulation of protein

phosphatase 2A (PP2A) **(Figure 3.21)**. Furthermore, I deduced that SOD1 acts via its enzymatic capabilities to stimulate the MDDC, with a potential supporting role of a phosphorylation site at S99 **(Figure 3.19)**. I hypothesise SOD1 exhibits pro-oxidant activity to regulate PP2A, which may occur via SOD1 directly oxidising cysteine residues leading to phosphatase inactivity, or SOD1 oxidising PP2A via the localised production of H_2O_2. These mechanisms would also allow SOD1 to maintain the cysteine oxidation state of PP2A over long time periods. The oxidation of PP2A by SOD1 is yet to be confirmed through oxidation mapping mass spectrometry (MS) analysis **(Figure 3.22)**. In support of this, SOD1 has been previously determined to possess the ability to catalyse thiol oxidation, with specificity for cysteine residues (Winterbourn, Peskin and Parsons-Mair, 2002; Bakavayev *et al.*, 2019) and regulates phosphatases by the production of H_2O_2 (Juarez *et al.*, 2008). In this thesis, the elevation of this phosphatase activity upon SOD1 knockdown or PP2A complementation encouraged mitotic progression despite the damage encountered. This supported that PP2A inactivation is required for the MDDC. In addition to PP2A, it is hypothesised that SOD1 may be a master regulator of phosphorylation events by targeting numerous other phosphatases, influencing other cellular pathways, which will be investigated in the future. The specific mechanism influenced by SOD1, in which PP2A inactivity induced mitotic arrest is currently unknown, as many phosphatases are involved in numerous pathways with various targets. Yet, this thesis identifies a specific target of SOD1 in the MDDC, providing the initial establishment of the checkpoint pathway for future work.

The mitotic effector benzimidazole (Bub)-related 1 (BubR1) is involved in the regulatory spindle assembly checkpoint (SAC) during the metaphase-anaphase transition, ensuring the proper attachment of the microtubules to the chromosomes (Musacchio and Salmon, 2007). BubR1 has been found to engage in a mitotic DNA damage response in the literature (described in section **1.3.2.6**) (Nitta *et al.*, 2004; Royou, Macias and Sullivan, 2005; Fang *et al.*, 2006; Choi and Lee, 2008; Royou *et al.*, 2010) and was found to be vital for the MDDC in the Thompson laboratory's preliminary data **(Figure 1.9)**. In this thesis, a MS screen was designed, optimised and conducted to determine the BubR1 interactome following DNA damage and to identify other proteins within the MDDC pathway. The screen hits were consolidated with the

siRNA DNA damage screen and determined Upstream frameshift 1 (UPF1) to be a potential BubR1 interactor during the MDDC **(Figure 4.7)**.

UPF1 is a multi-functional enzyme primarily involved in the non-sense mediated decay (NMD) pathway (Gupta and Li, 2018). Although this enzyme has been implicated in the DDR, such as in the S-phase checkpoint regulation and DNA repair (Azzalin and Lingner, 2006). Then, ATM targets UPF1 for phosphorylation which stimulates DDR activity and prevents NMD actions (Brumbaugh *et al.*, 2004). Considering this role, UPF1 was highlighted as a suitable protein of interest for further investigation into the MDDC. The novel BubR1-UPF1 interaction was validated **(Figure 4.8)** and the involvement of UPF1 in the MDDC was established in this thesis **(Figure 4.9)**. The specific role this interaction imposes within the MDDC is yet to be examined. However, both UPF1 and BubR1 have been implicated with PP2A. The phosphorylation of UPF1 is key to influence and activate certain roles of the enzyme, PP2A regulates UPF1 activity through dephosphorylation (Ohnishi *et al.*, 2003). Whereas the B56 subunit of PP2A directly binds to BubR1 to stimulate the SAC (Suijkerbuijk *et al.*, 2012) and mitotic progression (Espert *et al.*, 2014; Hein *et al.*, 2021). Overall, these findings support and contribute to the initial MDDC pathway establishment.

Finally, the literature recognised the DDR protein mediator of DNA damage checkpoint 1 (MDC1) as an interactor of BubR1 in mitosis (Eliezer *et al.*, 2014), hence was a conceivable interaction to investigate within the MDDC. In this thesis the interaction between BubR1 and MDC1 was ascertained at low levels **(Figure 5.4)** but was not influenced by mitosis or DNA damage **(Figure 5.5 and 5.6)**, so was independent of the MDDC **(Figure 5.7)**. In the conclusion of this chapter, I proposed the BubR1-MDC1 interaction occurs indirectly via association within a multi-protein complex at chromosomal breaks independent or downstream of the MDDC (Royou *et al.*, 2010; Leimbacher *et al.*, 2019; Thompson, Gatenby and Sidi, 2019). This may be investigated following further MDDC pathway elucidation.

6.2 The potential mechanism behind the MDDC.

Through consideration of the findings from the initial investigation into the MDDC in this thesis and deductions made from the literature, the hypothetical pathway behind the MDDC is described **(Figure 6.1)**.

It is proposed that upon the induction of DNA damage, SOD1 is phosphorylated instigating a switch from antioxidant activity to pro-oxidant activity. This is potentially stimulated by the ATM DDR pathway, specifically via Chk2 phosphorylation (described in Tsang *et al.* 2014) or Plk1 (proposed in MS screen by Olsen *et al.* 2010), for DDR repair and the MDDC activation respectively. The specific phosphorylation sites are currently unknown, yet I determined S99 to possess a supporting role within the MDDC and as this motif was proposed to be targeted by Plk1 (Olsen *et al.*, 2010), this implies the importance of this site in the potential activation of pro-oxidant SOD1 activity. Pro-oxidant SOD1 then oxidises phosphatases, which regulate HR, to prevent dephosphorylation of RAD51, enabling DNA binding and functionality for repair. HR may occur in both interphase DDR checkpoints and the MDDC. Then in mitotic cells, SOD1 inactivates PP2A via oxidation, to induce mitotic arrest. One mechanism in which PP2A inactivity stimulates mitotic cell arrest may be due to stimulation of the BubR1-UPF1 interaction. It is hypothesised that UPF1 is hyperphosphorylated by ATM and potentially by Plk1 and Chk1 (proposed in an MS screen by Olsen *et al.* 2010), in the absence of PP2A activity, which then enables BubR1 binding. This complex may then act to induce mitotic arrest and initiate repair. Finally, pro-oxidant SOD1 may also regulate other phosphatases during the MDDC and also those involved in other pathways.

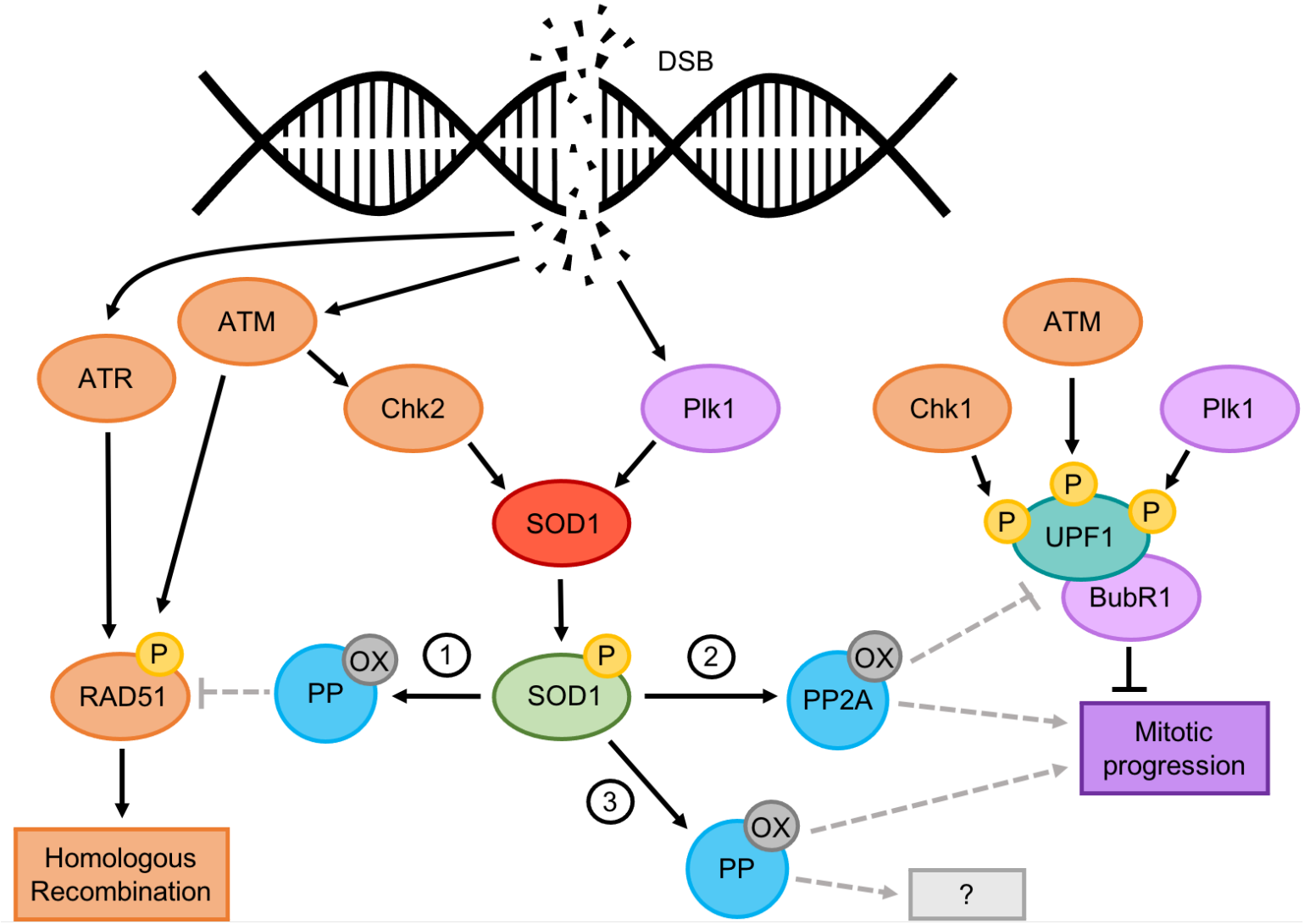

Figure 6.1: The initial proposal of the pathway involved in the MDDC.

Legend on next page.

Figure 6.1: The initial proposal of the pathway involved in the MDDC.
DNA damage such as double strand breaks (DSB), activates the ATM axis of the DNA damage response (orange) and Plk1. Chk2 and Plk1 mediate the switch of SOD1 activity from the antioxidant enzyme (red) to the pro-oxidant enzyme (green) via phosphorylation (P). **(1)** In turn, the pro-oxidant SOD1 oxidises (OX) phosphatases which mediate homologous recombination, preventing RAD51 dephosphorylation (grey dashed blunt arrow) enabling DNA repair. **(2)** Pro-oxidant SOD1 also inactivates PP2A via oxidation, which then inhibits mitotic progression (grey dashed arrow) and induces mitotic arrest (MDDC) through UPF1 hyperphosphorylation by ATM, Chk1 and Plk1 stimulating BubR1 binding. **(3)** Furthermore, pro-oxidant SOD1 may target other phosphatases contributing to the MDDC and inhibition of mitotic progression, as well as influencing other pathways.

Upon checkpoint recovery and progression of mitosis and the cell cycle, SOD1 regulated phosphatases are reduced by oxidative stress factors such as reduced glutathione (GSH). Reactivated PP2A and other phosphatases will dephosphorylate the affected factors, such as RAD51 for completion of repair, UPF1 enabling BubR1 dissociation for mitotic progression and even SOD1 to stimulate the switch back to its antioxidant role.

Overall, further experimentation will be conducted to establish evidence for this theoretical pathway.

6.3 Future impact on cancer therapy.

As the MDDC provides a mechanism of cancer cell survival from current treatments, it is of importance to establish the pathway involved and identify novel therapeutic targets to disable the checkpoint. It is thought that cancer types that heavily rely on the MDDC and in tumours that overexpress MDDC proteins, will indicate a poorer prognostic outcome which will be overcome by intervening with MDDC inhibiting agents.

Currently, it is known that numerous cancers types, such as non-small cell lung cancer (NSCLC) (Liu *et al.*, 2020), lung adenocarcinoma (Somwar *et al.*, 2011), breast cancer

(Papa *et al.*, 2014) and nasopharyngeal carcinoma (Li *et al.*, 2018) overexpress SOD1, compared to comparative normal tissues. The consequences of this include the promotion of tumour proliferation and metastasis, (Somwar *et al.*, 2011; X. Li, Chen, *et al.*, 2019; Li *et al.*, 2020; Liu *et al.*, 2020), which has been attributed to various mechanisms within each tumour type (Somwar *et al.*, 2011; Glasauer *et al.*, 2014; Li *et al.*, 2018; X. Li, Chen, *et al.*, 2019; Liu *et al.*, 2020). Therefore, the up-regulation of SOD1 in tumours indicates a poor patient prognosis (Li *et al.*, 2018; Liu *et al.*, 2020). SOD1 inhibitors such as ATN-224 has demonstrated an antitumorigenic effect (Glasauer *et al.*, 2014), leading to the implementation of this inhibitor into clinical trial testing (Lin *et al.*, 2013). Although, neither the oncogenic role of SOD1 nor the mechanism of the inhibitor has been consistently established in the literature. This highlights a limitation of the clinical applications and the current therapeutic value of SOD1 inhibitors, emphasising the importance of understanding the role of SOD1 in cancer. Overall, it is likely that the cancers which overexpress SOD1 will utilise the MDDC for survival and so inhibition of this checkpoint would be beneficial in future therapy and patient prognosis.

The impairment of phosphoregulation can lead to malignancies due to the aberrant kinase activity, most likely through downregulation of phosphatase activity (Perrotti and Neviani, 2013). PP2A has been proposed to be a tumour suppressor (Cohen and Cohen, 1989), as this phosphatase exhibits a vast number of functions within cell signalling (Kalev and Sablina, 2012). PP2A suppresses the activity of oncogenic kinases such as those involved in cell proliferation (Kalev and Sablina, 2012; Perrotti and Neviani, 2013). Dysregulation of PP2A subunits leads to phosphatase inactivity, which has been identified in many cancer types, including lung (Ruediger, Pham and Walter, 2001a) and breast (Ruediger, Pham and Walter, 2001b). As expected, the loss of PP2A activity is an indicative factor of poor prognosis (Cristóbal *et al.*, 2014). In this thesis, SOD1 was shown to regulate PP2A during the MDDC, which may indicate one mechanism in which PP2A suppresses tumorigenesis, further highlighting the beneficial clinical applications of MDDC inhibitors.

Following the further investigation into the role of the BubR1-UPF1 association in the MDDC, it may be desirable to inhibit this interaction to impair the MDDC pathway and enhance tumour cell death. Currently, UPF1 has been described as a potential tumour

suppressor, as it is frequently downregulated which correlates with poor prognosis in a variety of cancers such as gastric (L. Li *et al.*, 2017), pancreatic (Liu *et al.*, 2014) and liver (Chang *et al.*, 2016). Furthermore, the UPF1 gene attains unique somatic mutations in pancreatic adenosquamous carcinomas, impairing UPF1 functionality (Liu *et al.*, 2014). However, high levels of UPF1 expression has been reported in lung cancer which also correlates to poor prognosis (Győrffy *et al.*, 2013). Hence, it is unlikely that the majority of these cancer types, with the exception of lung cancer, will utilise the MDDC. Then BubR1 is overexpressed in chemo-radiation resistant bladder cancer (Komura *et al.*, 2021) and high-grade breast cancer, and is associated with low patient survival (Yuan *et al.*, 2006; Maciejczyk *et al.*, 2013). Therefore, BubR1 upregulation may cause an enrichment in the BubR1-UPF1 interaction, in turn promoting the MDDC and increased susceptibility to MDDC inhibitors.

In summary, the inhibition of the MDDC may be most beneficial in the treatment of breast and lung cancers.

Chapter 7: Appendix.

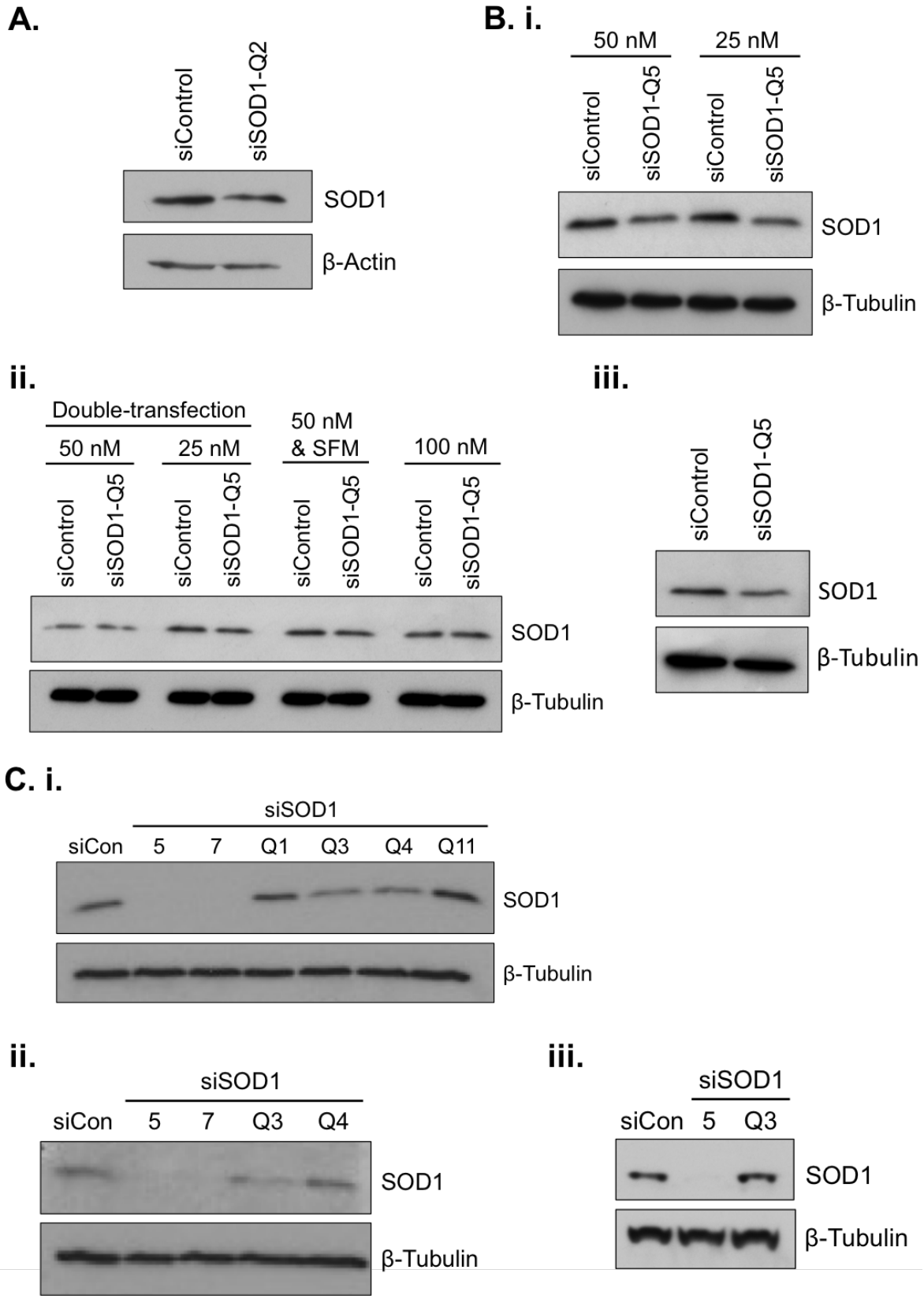

Figure 7.1: The examination into endogenous SOD1 knockdown.

Legend on next page.

Figure 7.1: The examination into endogenous SOD1 knockdown by 3'untranslated region targeting siRNAs.

Western blots showing the effectiveness of SOD1 knockdown using various Qiagen siRNAs (siSOD1-Q), which target the 3'untranslated region (UTR). All extracts were probed for SOD1 and β-Tubulin. **A.** The reverse transfection of siSOD1-Q2 compared to the siControl (N= 1). **B.** siSOD1-Q5 compared to the siControl following optimisation by **i.** differing siRNA concentration via reverse transfection (N= 1), **ii.** differing siRNA concentration via repeated knockdown (double-transfection) and serum starving for 8 hours with serum-free media (SFM) prior to reverse transfection (N= 1), and **ii.** 50 nM siRNA via forward transfection (N= 1). **C. i.** The reverse transfection of siSOD1-Q1, siSOD1-Q3, siSOD1-Q4 and siSOD1-Q11 compared to the siControl and siSOD1-5 and siSOD1-7 (N= 1). **ii.** The forward transfection of the most effective siRNAs from **i. (**siSOD1-Q3 and siSOD1-Q4) compared to the siControl and siSOD1-5 and siSOD1-7 (N= 1). **iii.** The most effective siRNA from **ii.** siSOD1-Q3 compared to the siControl and siSOD1-5 optimised via serum starving before forward transfection.

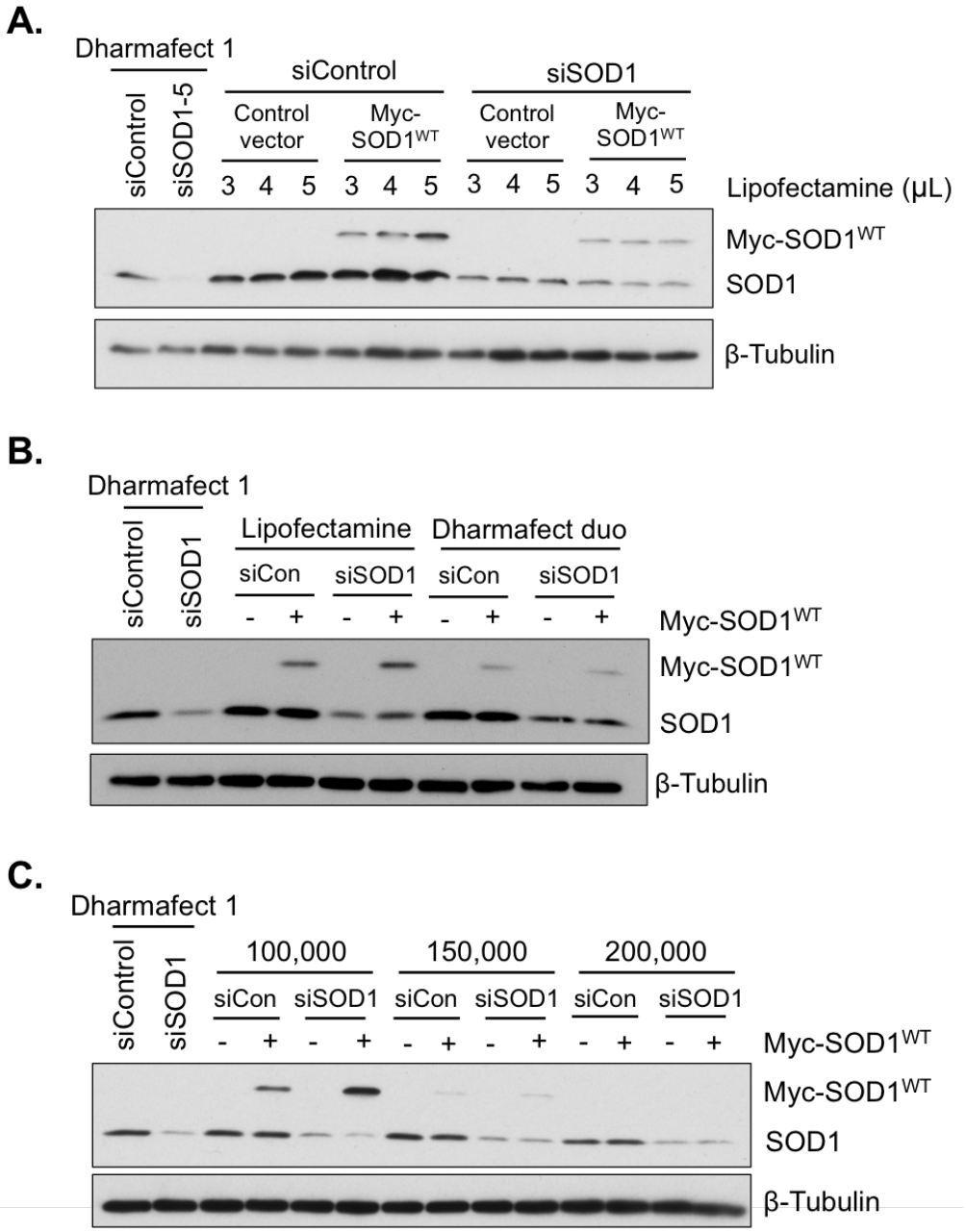

Figure 7.2: The optimisation of SOD1 knockdown and overexpression for the complementation experiments.

A. Western blot showing the knockdown and overexpression of SOD1 using siSOD1-5 and Myc-SOD1^{WT} using different concentrations of lipofectamine compared to standard transfection agent Dharmafect 1 (N= 1). Extracts were probed for SOD1 and β-Tubulin. **B.** Western blot showing the comparison of the effectiveness of lipofectamine and Dharmafect duo transfection reagents on the knockdown and overexpression of SOD1 using siSOD1-5 and Myc-SOD1^{WT} (N= 1). Extracts were probed for SOD1 and β-Tubulin. **C.** Western blot showing the knockdown and overexpression of SOD1 using siSOD1-5 and Myc-SOD1^{WT} in different cell densities transfected by Dharmafect duo (N= 1). Extracts were probed for SOD1 and β-Tubulin.

Treatment	Sequence Coverage	PP2A Residue	Observed Modification	Indication
None	60 %	C196	Carbamidomethyl	Reduced
		C266	Carbamidomethyl	Reduced
		C269	Carbamidomethyl	Reduced
SOD1	29 %	C196	N/A	Not detected
		C266	N/A	Not detected
		C269	Carbamidomethyl D4	Reduced
H_2O_2 10 mins	66 %	C196	Carbamidomethyl D4	Reduced
		C266	None	Potential oxidation
		C269	None	Potential oxidation

Table 7.1: Preliminary data for the mapping of PP2A oxidation in the presence of SOD1 and H_2O_2.

For each reaction, the sequence coverage of PP2A and the details indicating if the PP2A cysteine residues of interest were modified in the error tolerance search are displayed.

Gene name	Protein name	iBAQ intensity	UniProt protein ID
EDF1	Endothelial differentiation-related factor 1	5255000	O60869
HIST1H2BN	Histone H2B type 1-N	3574800	Q99877
HIST1H4A	Histone H4	3374900	P62805
HIST1H2AC	Histone H2A type 1-C	993750	Q93077
CCDC124	Coiled-coil domain-containing protein 124	880800	Q96CT7
HIST1H3A	Histone H3.1	788380	P68431
RPS7	40S ribosomal protein S7	663260	P62081
RPS27	40S ribosomal protein S27	598250	P42677
SRP14	Signal recognition particle 14 kDa protein	591740	P37108
RPL37A	60S ribosomal protein L37a	569200	P61513
SBDS	Ribosome maturation protein SBDS	566250	Q9Y3A5
RPL38	60S ribosomal protein L38	557860	P63173
ENO1	Alpha-enolase	410550	P06733
RPL35A	60S ribosomal protein L35a	404030	P18077
MIF	Macrophage migration inhibitory factor	332690	P14174
FAU	40S ribosomal protein S30	286560	P62861
RPS19	40S ribosomal protein S19	246900	P39019
SFPQ	Splicing factor, proline- and glutamine-rich	236250	P23246
CFL1	Cofilin-1	233580	P23528
HNRNPA2B1	Heterogeneous nuclear ribonucleoproteins A2/B1	203790	P22626
RPS12	40S ribosomal protein S12	179840	P25398
RPL12	60S ribosomal protein L12	174320	P30050
MATR3	Matrin-3	155980	P43243
NONO	Non-POU domain-containing octamer-binding protein	148840	Q15233
HNRNPA1	Heterogeneous nuclear ribonucleoprotein A1	147350	P09651
HIST1H1C	Histone H1.2	146570	P16403
PDAP1	28 kDa heat- and acid-stable phosphoprotein	140760	Q13442
RPL13	60S ribosomal protein L13	124900	P26373
STMN1	Stathmin	116270	P16949
NPM1	Nucleophosmin	92514	P06748
SLC25A5	ADP/ATP translocase 2	82394	P05141
RBM14	RNA-binding protein 14	80114	Q96PK6
TOMM34	Mitochondrial import receptor subunit TOM34	69899	Q15785
RPL23	60S ribosomal protein L23	68690	P62829
HSPA8	Heat shock cognate 71 kDa protein	62629	P11142
HSPD1	60 kDa heat shock protein	47681	P10809
PPIB	Peptidyl-prolyl cis-trans isomerase B	32967	P23284
EEF1A1	Elongation factor 1-alpha 1	28157	P68104
RPL28	60S ribosomal protein L28	23058	P46779
RPS17	40S ribosomal protein S17	19440	P08708

Table 7.2: The non-specific interactors list obtained from the on-bead digestion.

Legend on next page.

Table 7.2: The non-specific interactors list obtained from the on-bead digestion.

A list of non-specific proteins was generated during the optimisation of the on-bead digestion method performed on an untreated control sample, with a unique razor peptide number of ≥ 2 and ordered by the iBAQ intensity.

Gene name	Protein name	iBAQ intensity difference	Functional annotation	UniProt protein ID
BUB1B	Mitotic checkpoint serine/threonine-protein kinase BUB1 beta, BubR1	33267173	CC(M), ST	O60566
PPIB	Peptidyl-prolyl cis-trans isomerase B	26634000	CS	P23284
BUB3	Mitotic checkpoint protein BUB3	13617680	CC(M), ST	O43684
EDF1	Endothelial differentiation-related factor 1	6571400	TL, TC, ST, DEV	O60869
S100A9	Protein S100-A9	4861600	IS	P06702
SLC25A6	ADP/ATP translocase 3	3736300	TRANS, IF	P12236
NDUFAF3	NADH dehydrogenase [ubiquinone] 1 alpha subcomplex assembly factor 3	3138120	CARB	Q9BU61
CALML5	Calmodulin-like protein 5	2235400	IS	Q9NZT1
NDUFS7	NADH dehydrogenase [ubiquinone] iron-sulfur protein	2107200	CARB	O75251
ARGLU1	Arginine and glutamate-rich protein 1	2007350	UNKNOWN	Q9NWB6
CSTA	Cystatin-A	1498300	DEV	P01040
S100A8	Protein S100-A8	1255660	IS	P05109
POLDIP2	Polymerase delta-interacting protein 2	1242350	UNKNOWN	Q9Y2S7
NDUFAF4	NADH dehydrogenase [ubiquinone] 1 alpha subcomplex assembly factor 4	1218400	CARB	Q9P032
KCTD3	BTB/POZ domain-containing protein KCTD3	1077100	ST	Q9Y597
PYGL	Glycogen phosphorylase, liver form	1050168	CARB, IS	P06737
POLR1D	DNA-directed RNA polymerases I and III subunit RPAC2	822190	TC, IS	P0DPB6
SNRPD2	Small nuclear ribonucleoprotein Sm D2	795610	IF, TC	P62316
TOMM20	Mitochondrial import receptor subunit TOM20 homolog	725600	TRANS, TL	Q15388
YLPM1	YLP motif-containing protein 1	712760	ST	P49750
FABP5	Fatty acid-binding protein, epidermal	613800	LP, ST, IS	Q01469
SNRNP27	U4/U6.U5 small nuclear ribonucleoprotein 27 kDa protein	604620	TC	Q8WVK2
PLOD3	Procollagen-lysine,2-oxoglutarate 5-dioxygenase 3	559830	CS	O60568
LUC7L3	Luc7-like protein 3	503900	UNKNOWN	O95232
DIP2B	Disco-interacting protein 2 homolog B	458240	UNKNOWN	Q9P265
SIRT5	NAD-dependent protein deacylase sirtuin-5	446690	IS, CS	Q9NXA8
ZMAT2	Zinc finger matrin-type protein 2	419920	CS	Q96NC0
BUD31	Protein BUD31 homolog	405200	TC	P41223
SART1	U4/U6.U5 tri-snRNP-associated protein 1	381600	TC	O43290
LRRC16A	Leucine-rich repeat-containing protein 16A	379620	CRS	Q5VZK9
TMA16	Translation machinery-associated protein 16	360460	TC, F	Q96EY4
LOXL2	Lysyl oxidase homolog 2	315500	CS	Q9Y4K0
RBM12B	RNA-binding protein 12B	311190	UNKNOWN	Q8IXT5
TFG	Protein TFG	297250	TL	Q92734
RANGAP1	Ran GTPase-activating protein 1	285620	CC(M), TL, ST, IF	P46060

Table 7.3: The list of BubR1 interactors following DNA damage.

Legend on next page.

Continued…				
Gene name	**Protein name**	**iBAQ intensity difference**	**Functional annotation**	**UniProt protein ID**
NHP2	H/ACA ribonucleoprotein complex subunit 2	280390	CC(M), TC	Q9NX24
ICT1	Peptidyl-tRNA hydrolase ICT1	276740	TL	Q14197
SSBP1	Single-stranded DNA-binding protein	273420	CS	Q04837
SERPINB12	Serpin B12	273390	IS	Q96P63
NUFIP2	Nuclear fragile X mental retardation-interacting protein 2	271260	TRANS, TC, F, ST, DEV, NEU, CS	Q7Z417
SRSF5	Serine/arginine-rich splicing factor 5	261710	CC(S), TC	Q13243
ARHGAP35	Rho GTPase-activating protein 35	256530	ST, DEV	Q9NRY4
AGO2	Protein argonaute-2	245093	TC, ST, IF	Q9UKV8
JUP	Junction plakoglobin	244709.5	IS	P14923
ZNF593	Zinc finger protein 593	233550	CRS, NEU	O00488
CDC20	Cell division cycle protein 20 homolog	229564	CC(M), TL, ST, IS	Q12834
ARG1	Arginase-1	220180	AA, IS	P05089
PLOD1	Procollagen-lysine,2-oxoglutarate 5-dioxygenase 1	205390	CS	Q02809
ADAR	Double-stranded RNA-specific adenosine deaminase	201260	IS, TC	P55265
TFRC	Transferrin receptor protein 1	196690	TRANS, ST	P02786
CTNND1	Catenin delta-1	195700	IF	O60716
TOP1	DNA topoisomerase 1	189940	TL	P11387
DHX30	Putative ATP-dependent RNA helicase DHX30	180600	TL, TC, ST, IS, IF	Q7L2E3
CASP14	Caspase-14	179230	DEV	P31944
VWA8	von Willebrand factor A domain-containing protein 8	178921	UNKNOWN	A3KMH1
AGRN	Agrin	176417	MET, CS	O00468
U2SURP	U2 snRNP-associated SURP motif-containing protein	170749	TC	O15042
HSPG2	Basement membrane-specific heparan sulfate proteoglycan core protein	168650	MET, CS	P98160
GTF2F1	General transcription factor IIF subunit 1	162560	TC, ST, DEV, IF, C	P35269
TNRC6B	Trinucleotide repeat-containing gene 6B protein	157031	TC, ST	Q9UPQ9
DDX21	Nucleolar RNA helicase 2	156520	TC	Q9NR30
FXR2	Fragile X mental retardation syndrome-related protein 2	151301	CC(M), TC, ST, IS, CRS, IF, C	P51116
NUP88	Nuclear pore complex protein Nup88	151111	CC(M)(S), CGD, TL, TC, CARB, IS, IF	Q99567
CHERP	Calcium homeostasis endoplasmic reticulum protein	149388	TC	Q8IWX8
MANF	Mesencephalic astrocyte-derived neurotrophic factor	148800	CS	P55145
RBM3	RNA-binding protein 3	147310	TL, ST, IF, TC	P98179

Table 7.3: The list of BubR1 interactors following DNA damage.

Legend on next page.

Continued…

Gene name	Protein name	iBAQ intensity difference	Functional annotation	UniProt protein ID
HSPH1	Heat shock protein 105 kDa	144550	CC(M), CGD	Q92598
CDC16	Cell division cycle protein 16 homolog	143740	CC(M), CGD, IS	Q13042
KPRP	Keratinocyte proline-rich protein	140620	CC(S), TRANS, TC, DR, LP, ST, IS, DEV, C	Q5T749
AP2B1	AP-2 complex subunit beta	140430	TRANS, CARB, AA, EN, ST, IS, IF	P63010
DDX42	ATP-dependent RNA helicase DDX42	136510	IF, TC	Q86XP3
CENPE	Centromere-associated protein E	136420	CC(M), ST, IS	Q02224
IARS	Isoleucine--tRNA ligase	132778	AA	P41252
MVB12A	Multivesicular body subunit 12A	131470	IF	Q96EY5
MISP	Mitotic interactor and substrate of PLK1	130624	CC(M)	Q8IVT2
MAPK1	Mitogen-activated protein kinase 1	129480	CC(M), CGD, ST, IS, IF, C	P28482
HNRNPUL1	Heterogeneous nuclear ribonucleoprotein U-like protein 1	127800	TC	Q9BUJ2
CNN2	Calponin-2	126660	IS	Q99439
CDC23	Cell division cycle protein 23 homolog	124690	CC(M), CGD, IS	Q9UJX2
NOLC1	Nucleolar and coiled-body phosphoprotein 1	123610	TRANS, ST, IS, CRS, TC	Q14978
PAN2	PAB-dependent poly(A)-specific ribonuclease subunit PAN2	122507	F, ST, IS	Q504Q3
AP2A1	AP-2 complex subunit alpha-1	121159	TRANS, ST, IS, IF	O95782
NUP155	Nuclear pore complex protein Nup155	120288	CC(M)(S), CGD, TL, TC, CARB, IS, IF	O75694
VPS28	Vacuolar protein sorting-associated protein 28 homolog	118890	IF	Q9UK41
PAN3	PAB-dependent poly(A)-specific ribonuclease subunit PAN3	118171	F	Q58A45
PPIL4	Peptidyl-prolyl cis-trans isomerase-like 4	114246	TC	Q8WUA2
GCDH	Glutaryl-CoA dehydrogenase, mitochondrial	110872	AA	Q92947
LGALS7	Galectin-7	109620	UNKNOWN	P47929
LUC7L	Putative RNA-binding protein Luc7-like 1	107930	TC	Q9NQ29
MTHFD1L	Monofunctional C1-tetrahydrofolate synthase	103163	VIT	Q6UB35
HNRNPA0	Heterogeneous nuclear ribonucleoprotein A0	99623	IF, TC	Q13151
TUBB2A	Tubulin beta-2A chain	98768	CC(M), CGD, TL, ST, IS	Q13885
GGCT	Gamma-glutamylcyclotransferase	98527	EN	O75223
DSTN	Destrin	97833	UNKNOWN	P60981
SPRR3	Small proline-rich protein 3	96020	DEV	Q9UBC9

Table 7.3: The list of BubR1 interactors following DNA damage.

Legend on next page.

Continued…				
Gene name	**Protein name**	**iBAQ intensity difference**	**Functional annotation**	**UniProt protein ID**
RANBP2	E3 SUMO-protein ligase RanBP2	94840	CC(M)(S), CGD, TL, TC, CARB, ST, IS, IF	P49792
CACTIN	Cactin	91415	IS	Q8WUQ7
CTSD	Cathepsin D	90384	ST, IS, CS	P07339
DNAJA2	DnaJ homolog subfamily A member 2	88945	CGD	O60884
HADHA	Trifunctional enzyme subunit alpha	88510	LP	P40939
DNAJC10	DnaJ homolog subfamily C member 10	88485	UNKNOWN	Q8IXB1
RBM25	RNA-binding protein 25	88080	TRANS	P49756
CS	Citrate synthase	87075	TRANS, CARB	O75390
ATP1A1	Sodium/potassium-transporting ATPase subunit alpha-1	84188	TRANS, IF	P05023
PDCD6	Programmed cell death protein 6	83213	CGD, F, ST, IS, IF, CS	O75340
ATP2A2	Sarcoplasmic/endoplasmic reticulum calcium ATPase 2	81672	ST	P16615
ANAPC5	Anaphase-promoting complex subunit 5	80587	CC(M), CGD, IS	Q9UJX4
CDC27	Cell division cycle protein 27 homolog	79024	CC(M), CGD, IS	P30260
CAPZA2	F-actin-capping protein subunit alpha-2	78834	CGD, IS	P47755
S100A7	Protein S100-A7	78730	IS	P31151
ANAPC4	Anaphase-promoting complex subunit 4	78717	CC(M), CGD, IS	Q9UJX5
PDCD2L	Programmed cell death protein 2-like	78133	UNKNOWN	Q9BRP1
TCEB3	Transcription elongation factor B polypeptide 3	76609	TC, DEV, IF	Q14241
CYLD	Ubiquitin carboxyl-terminal hydrolase CYLD	76284	TL, IS	Q9NQC7
PRPF6	Pre-mRNA-processing factor 6	76020	IF, TC	O94906
FBXO3	F-box only protein 3	74562	CC(M), TRANS, IF	Q9UK99
CDSN	Corneodesmosin	74461	DEV	Q15517
MTHFD1	C-1-tetrahydrofolate synthase	73309	VIT	P11586
SERPINB4	Serpin B4	73149	TC	P48594
DHX36	ATP-dependent RNA helicase DHX36	72421	IS	Q9H2U1
ALDH1A2	Retinal dehydrogenase 2	71623	ST	O94788
LENG1	Leukocyte receptor cluster member 1	71302	TL, TC, LP, ST, IS, IF, C	Q96BZ8
NUP93	Nuclear pore complex protein Nup93	70326	CC(M)(S), CGD, TL, TC, CARB, IS, IF	Q8N1F7
WDR48	WD repeat-containing protein 48	69305	TL	Q8TAF3
CSTF3	Cleavage stimulation factor subunit 3	69220	TC	Q12996
SUPT16H	FACT complex subunit SPT16	68107	TC, DEV, IF	Q9Y5B9
SIAH2	E3 ubiquitin-protein ligase SIAH2	67794	TL, IS	O43255

Table 7.3: The list of BubR1 interactors following DNA damage.

Legend on next page.

Continued…

Gene name	Protein name	iBAQ intensity difference	Functional annotation	UniProt protein ID
ZC3H14	Zinc finger CCCH domain-containing protein 14	67670	CRS	Q6PJT7
CTPS1	CTP synthase 1	67240	NT	P17812
PRPF38A	Pre-mRNA-splicing factor 38A	67096	TC	Q8NAV1
DDB1	DNA damage-binding protein 1	66228	TL, DR	Q16531
UPF1	Regulator of nonsense transcripts 1	66200	F	Q92900
CAT	Catalase	64880	CGD, TRANS, IS	P04040
ANAPC1	Anaphase-promoting complex subunit 1	63846	CC(M), CGD, IS	Q9H1A4
LSM12	Protein LSM12 homolog	61786	UNKNOWN	Q3MHD2
SEC23A	Protein transport protein Sec23A	61697	TL, LP, IS	Q15436
IMMT	MICOS complex subunit MIC60	60013	CS	Q16891
LSG1	Large subunit GTPase 1 homolog	58880	UNKNOWN	Q9H089
RSRC2	Arginine/serine-rich coiled-coil protein 2	58656	ND	Q7L4I2
LEPREL1	Prolyl 3-hydroxylase 2	57464	CS	Q8IVL5
RBM6	RNA-binding protein 6	56857	UNKNOWN	P78332
TWISTNB	DNA-directed RNA polymerase I subunit RPA43	55480	TC	Q3B726
TIMM23B	Mitochondrial import inner membrane translocase subunit Tim23B	54974	UNKNOWN	Q5SRD1
GANAB	Neutral alpha-glucosidase AB	54634	TL	Q14697
TK1	Thymidine kinase	54200	CC(M), NT	P04183
PTPMT1	Phosphatidylglycerophosphatase and protein-tyrosine phosphatase 1	52406	LP	Q8WUK0
SEC24C	Protein transport protein Sec24C	52344	TL, LP, IS	P53992
CPT1A	Carnitine O-palmitoyltransferase 1, liver isoform	50107	LP, ST	P50416
MIB2	E3 ubiquitin-protein ligase MIB2	49458	IS, C	Q96AX9
NUP214	Nuclear pore complex protein Nup214	48196	CC(M)(S), CGD, TL, TC, CARB, IS, IF	P35658
CHCHD3	MICOS complex subunit MIC19	47356	TRANS	Q9NX63
PRPS1	Ribose-phosphate pyrophosphokinase 1	46149	CARB	P60891
QPCTL	Glutaminyl-peptide cyclotransferase-like protein	46084	UNKNOWN	Q9NXS2
NAT10	N-acetyltransferase 10	45810	TC	Q9H0A0
SND1	Staphylococcal nuclease domain-containing protein 1	45730	C	Q7KZF4
AFG3L2	AFG3-like protein 2	45514	TRANS	Q9Y4W6
DPM1	Dolichol-phosphate mannosyltransferase subunit 1	42670	TL, MET	O60762
STAT3	Signal transducer and activator of transcription 3	42519	CGD, ST, IS	P40763
KIAA0930	Uncharacterized protein KIAA0930	42177	ST	Q6ICG6
PDHA1	Pyruvate dehydrogenase E1 component subunit alpha, somatic form	40860	CARB, AA, ST	P08559

Table 7.3: The list of BubR1 interactors following DNA damage.

Legend on next page.

Continued…

Gene name	Protein name	iBAQ intensity difference	Functional annotation	UniProt protein ID
CFAP20	Cilia- and flagella-associated protein 20	40467	CC(M), TRANS, TC, ST	Q9Y6A4
VTI1B	Vesicle transport through interaction with t-SNAREs homolog 1B	38680	CRS	Q9UEU0
MARS	Methionine--tRNA ligase, cytoplasmic	38439	AA	P56192
CPSF2	Cleavage and polyadenylation specificity factor subunit 2	38280	TC	Q9P2I0
RHOG	Rho-related GTP-binding protein RhoG	38181	ST, IS	P84095
ACLY	ATP-citrate synthase	37489	EN, IS	P53396
SSRP1	FACT complex subunit SSRP1	37306	TC, DEV, IF	Q08945
NNT	NAD(P) transhydrogenase	37076.6	CARB	Q13423
USP15	Ubiquitin carboxyl-terminal hydrolase 15	36703	TL	Q9Y4E8
PKP1	Plakophilin-1	36349	IS, DEV	Q13835
MYO1E	Unconventional myosin-Ie	36146	TRANS, EN, ST	Q12965
SEC23B	Protein transport protein Sec23B	35748	TL, TC, IS, DEV	Q15437
SFSWAP	Splicing factor, suppressor of white-apricot homolog	35406	UNKNOWN	Q12872
FAM120B	Constitutive coactivator of peroxisome proliferator-activated receptor gamma	35142	DEV	Q96EK7
MOV10	Putative helicase MOV-10	34259	CGD, TC, ST	Q9HCE1
QARS	Glutamine--tRNA ligase	33377	AA	P47897

Functional annotation key

Cellular processes		Metabolism (continued)	
CC	Cell cycle	NT	Nucleotide metabolism
M	Mitosis	VIT	Vitamin metabolism
CGD	Cell growth and death	Environmental information processing	
TRANS	Transport and catabolism	ST	Signal transduction
CS	Cell structure and organelle maintenance	Organismal systems	
Genetic information processing		IS	Immune system
TC	Transcription	DEV	Development
TL	Translation	CRS	Circulatory system
F	Folding, sorting and degradation	NEU	Neuronal system
DR	DNA repair	Human diseases	
Metabolism		IF	Infectious diseases
CARB	Carbohydrate metabolism	C	Cancer
LP	Lipid metabolism	MET	Metabolic diseases
AA	Amino acid metabolism	ND	Neurodegenerative diseases
EN	Energy metabolism	Unknown	

Table 7.3: The list of BubR1 interactors following DNA damage.

Legend on next page.

Table 7.3: The list of BubR1 interactors following DNA damage.

The final list of proteins that potentially interact with BubR1 following DNA damage. BubR1 is the top hit (green) and the list is ordered by the difference in iBAQ intensity between the presence (+) and absence (-) of doxycycline, which was used to determine if the interaction was true and also provided the 0.1 % false discovery rate. Known interactors of BubR1 and the spliceosome factors are highlighted (blue and yellow respectively). The functional annotation is also detailed for each protein with the key at the bottom of the table.

Bibliography

Abbas, T. *et al.* (2008) 'PCNA-dependent regulation of p21 ubiquitylation and degradation via the CRL4Cdt2 ubiquitin ligase complex', *Genes & Development*, 22(18), pp. 2496–2506. doi: 10.1101/gad.1676108.

Abbotts, R. and Wilson, D. M. (2017) 'Coordination of DNA Single Strand Break Repair', *Free Radical Biology and Medicine*, 107, pp. 228–244. doi: 10.1016/J.FREERADBIOMED.2016.11.039.

Abcam (2021) *Protein Tyrosine Phosphatase Assay Kit (ab241032)*. Available at: https://www.abcam.com/protein-tyrosine-phosphatase-assay-kit-ab241032.html (Accessed: 21 July 2021).

Acilan, C., Potter, D. M. and Saunders, W. S. (2007) 'DNA repair pathways involved in anaphase bridge formation', *Genes Chromosomes and Cancer*, 46(6), pp. 522–531. doi: 10.1002/gcc.20425.

Adam, K. *et al.* (2018) 'A PIM-CHK1 signaling pathway regulates PLK1 phosphorylation and function during mitosis', *Journal of Cell Science*, 131(15). doi: 10.1242/JCS.213116.

Aebi, H. (1984) 'Catalase in vitro', *Methods in Enzymology*, 105, pp. 121–126. doi: 10.1016/S0076-6879(84)05016-3.

Ahn, J.-Y. *et al.* (2000) 'Threonine 68 Phosphorylation by Ataxia Telangiectasia Mutated Is Required for Efficient Activation of Chk2 in Response to Ionizing Radiation', *Cancer Research*, 60(21), pp. 5934–5936.

Ahn, J. H. *et al.* (2019) 'Inhibition of PP2A activity by H2O2 during mitosis disrupts nuclear envelope reassembly and alters nuclear shape', *Experimental and Molecular Medicine*, 51(6), pp. 1–18. doi: 10.1038/s12276-019-0260-0.

Alam, Z. I. *et al.* (1997) 'A generalised increase in protein carbonyls in the brain in Parkinson's but not incidental Lewy body disease', *Journal of Neurochemistry*, 69(3), pp. 1326–1329. doi: 10.1046/J.1471-4159.1997.69031326.X.

De Antoni, A. *et al.* (2005) 'The Mad1/Mad2 Complex as a Template for Mad2 Activation in the Spindle Assembly Checkpoint', *Current Biology*, 15(3), pp. 214–225. doi: 10.1016/J.CUB.2005.01.038.

Aprioku, J. S. (2013) 'Pharmacology of free radicals and the impact of reactive oxygen species on the testis', *Journal of Reproduction and Infertility*, pp. 158–172.

Arakawa, T. and Timasheff, S. N. (1991) 'The Interactions of Proteins with Salts, Amino Acids, and Sugars at High Concentration', in Gilles, R., Hoffmann, E. K., and Bolis, L. (eds) *Advances in Comparative and Environmental Physiology: Volume and Osmolality Control in Animal Cells*. Springer, pp. 226–245. doi: 10.1007/978-3-642-76226-0_8.

Atalay, P. B. *et al.* (2017) 'Hydrogen Peroxide Prolongs Mitotic Arrest in a Dose Dependent Manner and Independently of the Spindle Assembly Checkpoint Activity in Saccharomyces cerevisiae', *Acta Biologica Hungarica 2017 68:4*, 68(4), pp. 477–489. doi: 10.1556/018.68.2017.4.12.

Atassi, G., Schaus, C. and Tagnon, H. J. (1975) 'R17934-NSC238159: A new antitumor drug-II. Effect on mitotic cycle of L1210 leukemia cells in vivo and synergism with cytosine arabinoside (NSC 63878)', *European Journal of Cancer*, 11(9), pp. 609–614. doi: 10.1016/0014-2964(75)90093-6.

Awada, A. *et al.* (2015) 'Phase I trial of volasertib, a Polo-like kinase inhibitor, plus platinum agents in solid tumors: safety, pharmacokinetics and activity.', *Investigational*

New Drugs, 33(3), pp. 611–620. doi: 10.1007/s10637-015-0223-9.
Azzalin, C. M. and Lingner, J. (2006) 'The Human RNA Surveillance Factor UPF1 Is Required for S Phase Progression and Genome Stability', *Current Biology*. Cell Press, 16(4), pp. 433–439. doi: 10.1016/J.CUB.2006.01.018.
Bae, I. *et al.* (2004) 'BRCA1 induces antioxidant gene expression and resistance to oxidative stress', *Cancer Research*, 64(21), pp. 7893–7909. doi: 10.1158/0008-5472.CAN-04-1119.
Bakavayev, S. *et al.* (2019) 'Cu/Zn-superoxide dismutase and wild-type like fALS SOD1 mutants produce cytotoxic quantities of H2O2 via cysteine-dependent redox short-circuit', *Scientific Reports*, 9(1). doi: 10.1038/S41598-019-47326-X.
Bakkenist, C. J. and Kastan, M. B. (2003) 'DNA damage activates ATM through intermolecular autophosphorylation and dimer dissociation', *Nature*, 421(6922), pp. 499–506. doi: 10.1038/nature01368.
Benada, J. *et al.* (2015) 'Polo-like kinase 1 inhibits DNA damage response during mitosis', *Cell Cycle*, 14(2), pp. 219–231. doi: 10.4161/15384101.2014.977067.
Bhowmick, D. and Mugesh, G. (2015) 'Insights into the catalytic mechanism of synthetic glutathione peroxidase mimetics', *Organic and Biomolecular Chemistry*, pp. 10262–10272. doi: 10.1039/c5ob01665g.
BioTek (2021) *An Introduction to Reactive Oxygen Species - Measurement of ROS in Cells*. Available at: https://www.biotek.com/resources/white-papers/an-introduction-to-reactive-oxygen-species-measurement-of-ros-in-cells/ (Accessed: 9 July 2021).
Bordoni, M. *et al.* (2019) 'Nuclear Phospho-SOD1 Protects DNA from Oxidative Stress Damage in Amyotrophic Lateral Sclerosis', *Journal of Clinical Medicine*, 8(5), p. 729. doi: 10.3390/jcm8050729.
Boyd, S. D. *et al.* (2020) 'Mutations in superoxide dismutase 1 (SOD1) linked to familial amyotrophic lateral sclerosis can disrupt high-affinity zinc-binding promoted by the copper chaperone for SOD1 (CCS)', *Molecules*, 25(5). doi: 10.3390/molecules25051086.
Brumbaugh, K. M. *et al.* (2004) 'The mRNA surveillance protein hSMG-1 functions in genotoxic stress response pathways in mammalian cells', *Molecular Cell*, 14(5), pp. 585–598. doi: 10.1016/j.molcel.2004.05.005.
Bucher, N. and Britten, C. D. (2008) 'G2 checkpoint abrogation and checkpoint kinase-1 targeting in the treatment of cancer', *British Journal of Cancer*, 98(3), pp. 523–528. doi: 10.1038/sj.bjc.6604208.
Buffin, E. *et al.* (2005) 'Recruitment of Mad2 to the Kinetochore Requires the Rod/Zw10 Complex', *Current Biology*, 15(9), pp. 856–861. doi: 10.1016/J.CUB.2005.03.052.
Bunz, F. *et al.* (1998) 'Requirement for p53 and p21 to Sustain G2 Arrest After DNA Damage', *Science*, 282(5393), pp. 1497–1501. doi: 10.1126/SCIENCE.282.5393.1497.
Burgess, A. *et al.* (2017) 'SnapShot: Phosphoregulation of Mitosis', *Cell*, 169, p. 1358. doi: 10.1016/j.cell.2017.06.003.
Burton, J. L. and Solomon, M. J. (2007) 'Mad3p, a pseudosubstrate inhibitor of APCCdc20 in the spindle assembly checkpoint.', *Genes & development*, 21(6), pp. 655–667. doi: 10.1101/gad.1511107.
Byrne, D. P. *et al.* (2020) 'Aurora A regulation by reversible cysteine oxidation reveals evolutionarily conserved redox control of Ser/Thr protein kinase activity', *Science Signaling*, 13(639), p. 2713. doi: 10.1126/SCISIGNAL.AAX2713.
Carter, C. D. *et al.* (2005) 'Loss of SOD1 and LYS7 sensitizes Saccharomyces cerevisiae to hydroxyurea and DNA damage agents and downregulates MEC1 pathway effectors.', *Molecular and Cellular Biology*, 25(23), pp. 10273–10285. doi:

10.1128/MCB.25.23.10273-10285.2005.
Cassou, C. A. and Williams, E. R. (2014) 'Desalting protein ions in native mass spectrometry using supercharging reagents', *Analyst*, 139(19), pp. 4810–4819. doi: 10.1039/c4an01085j.
Castro, A. *et al.* (2005) 'The anaphase-promoting complex: a key factor in the regulation of cell cycle', *Oncogene*, 24(3), pp. 314–325. doi: 10.1038/sj.onc.1207973.
Chang, L. *et al.* (2016) 'The human RNA surveillance factor UPF1 regulates tumorigenesis by targeting Smad7 in hepatocellular carcinoma', *Journal of Experimental & Clinical Cancer Research*, 35(1), pp. 1–12. doi: 10.1186/S13046-016-0286-2.
Chang, T. S. *et al.* (2004) 'The RING-H2–finger protein APC11 as a target of hydrogen peroxide', *Free Radical Biology and Medicine*, 37(4), pp. 521–530. doi: 10.1016/J.FREERADBIOMED.2004.05.006.
Chatterjee, A. *et al.* (2006) 'Targeting of mutant hogg1 in mammalian mitochondria and nucleus: effect on cellular survival upon oxidative stress', *BMC Cancer*, 6(235). doi: 10.1186/1471-2407-6-235.
Chatterjee, N. and Walker, G. C. (2017) 'Mechanisms of DNA damage, repair and mutagenesis', *Environmental and Molecular Mutagenesis*, 58(5), pp. 235–263. doi: 10.1002/EM.22087.
Che, M. *et al.* (2016) 'Expanding roles of superoxide dismutases in cell regulation and cancer.', *Drug Discovery Today*, 21(1), pp. 143–149. doi: 10.1016/j.drudis.2015.10.001.
Chilà, R. *et al.* (2013) 'Chk1-Mad2 interaction: A crosslink between the DNA damage checkpoint and the mitotic spindle checkpoint', *Cell Cycle*, 12(7), pp. 1083–1090. doi: 10.4161/CC.24090.
Choi, E. and Lee, H. (2008) 'Chromosome damage in mitosis induces BubR1 activation and prometaphase arrest', *FEBS Letters*, 582(12), pp. 1700–1706. doi: 10.1016/j.febslet.2008.04.028.
ChromoTek (2020) *GFP-Trap Magnetic Agarose*. Available at: https://www.chromotek.com/fileadmin/content/PDFs/Protocols/gtma_Manual_GFP-Trap_Magnetic_Agarose.pdf (Accessed: 15 June 2021).
Chung, A. S. and Maines, M. D. (1981) 'Effect of selenium on glutathione metabolism: Induction of γ-glutamylcysteine synthetase and glutathione reductase in the rat liver', *Biochemical Pharmacology*, 30(23), pp. 3217–3223. doi: 10.1016/0006-2952(81)90521-9.
Ciccia, A. and Elledge, S. J. (2010) 'The DNA damage response: making it safe to play with knives.', *Molecular Cell*, 40(2), pp. 179–204. doi: 10.1016/j.molcel.2010.09.019.
ClinicalTrials.gov (2016) *Cytarabine With or Without SCH 900776 in Treating Adult Patients With Relapsed Acute Myeloid Leukemia*. Available at: https://www.clinicaltrials.gov/ct2/show/NCT01870596?term=chk1+inhibitor%2C+chemotherapy&cond=Cancer&rank=1 (Accessed: 30 June 2018).
ClinicalTrials.gov (2021a) *A Study to Assess the Safety and Tolerability of AZD1390 Given With Radiation Therapy in Patients With Brain Cancer*. Available at: https://www.clinicaltrials.gov/ct2/show/NCT03423628?term=irradiation%2C+atm+inhibitor&cond=Cancer&rank=1 (Accessed: 1 September 2021).
ClinicalTrials.gov (2021b) *Phase I/IIa Study of Concomitant Radiotherapy With Olaparib and Temozolomide in Unresectable High Grade Gliomas Patients*. Available at:
https://clinicaltrials.gov/ct2/show/NCT03212742?term=PARP%2C+radiotherapy&rank=1 (Accessed: 1 September 2021).

Cohen-Fix, O. and Koshland, D. (1997) 'The anaphase inhibitor of Saccharomyces cerevisiae Pds1p is a target of the DNA damage checkpoint pathway.', *Proceedings of the National Academy of Sciences of the United States of America*, 94(26), pp. 14361–14366.
Cohen-Jonathan, E., Bernhard, E. J. and McKenna, W. G. (1999) 'How does radiation kill cells?', *Current Opinion in Chemical Biology*, 3(1), pp. 77–83. doi: 10.1016/S1367-5931(99)80014-3.
Cohen, P. and Cohen, P. T. W. (1989) 'Protein Phosphatases Come of Age', *Journal of Biological Chemistry*, 264(36), pp. 21435–21438. doi: 10.1016/S0021-9258(20)88197-6.
Collura, A. *et al.* (2005) 'The fission yeast Crb2/Chk1 pathway coordinates the DNA damage and spindle checkpoint in response to replication stress induced by topoisomerase I inhibitor.', *Molecular and Cellular Biology*, 25(17), pp. 7889–7899. doi: 10.1128/MCB.25.17.7889-7899.2005.
Corcoran, N. M. *et al.* (2010) 'Sodium selenate specifically activates PP2A phosphatase, dephosphorylates tau and reverses memory deficits in an Alzheimer's disease model', *Journal of Clinical Neuroscience*, 17(8), pp. 1025–1033. doi: 10.1016/j.jocn.2010.04.020.
Coster, G. *et al.* (2007) 'The DNA damage response mediator MDC1 directly interacts with the anaphase-promoting complex/cyclosome.', *The Journal of Biological Chemistry*, 282(44), pp. 32053–32064. doi: 10.1074/jbc.M705890200.
Cristóbal, I. *et al.* (2014) 'Phosphorylated protein phosphatase 2A determines poor outcome in patients with metastatic colorectal cancer', *British Journal of Cancer*, 111(4), pp. 756–762. doi: 10.1038/bjc.2014.376.
CRUK (2011) *CRUK Survival*. Available at: https://www.cancerresearchuk.org/health-professional/cancer-statistics/survival#heading-Zero (Accessed: 3 August 2021).
CRUK (2017) *CRUK Cancer Incidence*. Available at: https://www.cancerresearchuk.org/health-professional/cancer-statistics/incidence (Accessed: 3 August 2021).
D'Angiolella, V. *et al.* (2003) 'The spindle checkpoint requires cyclin-dependent kinase activity', *Genes & Development*, 17(20), pp. 2520–2525. doi: 10.1101/GAD.267603.
D'Angiolella, V., Santarpia, C. and Grieco, D. (2007) 'Cell Cycle Oxidative Stress Overrides the Spindle Checkpoint', *Cell Cycle*, 6, pp. 576–579. doi: 10.4161/cc.6.5.3934.
Davalli, P. *et al.* (2018) 'Targeting Oxidatively Induced DNA Damage Response in Cancer: Opportunities for Novel Cancer Therapies', *Oxidative Medicine and Cellular Longevity*, 2018. doi: 10.1155/2018/2389523.
David, S. S., O'Shea, V. L. and Kundu, S. (2007) 'Base Excision Repair of Oxidative DNA Damage', *Nature*, 447(7147), pp. 941–950. doi: 10.1038/NATURE05978.
Delacroix, S. *et al.* (2007) 'The Rad9–Hus1–Rad1 (9–1–1) clamp activates checkpoint signaling via TopBP1', *Genes & Development*, 21(12), pp. 1472–1477. doi: 10.1101/GAD.1547007.
Delphin, C. *et al.* (1994) 'Characterization of baculovirus recombinant wild-type p53: Dimerization of p53 is required for high-affinity DNA binding and cysteine oxidation inhibits p53 DNA binding', *European Journal of Biochemistry*, 223(2), pp. 683–692. doi: 10.1111/J.1432-1033.1994.TB19041.X.
Denu, J. M. and Tanner, K. G. (1998) 'Specific and Reversible Inactivation of Protein Tyrosine Phosphatases by Hydrogen Peroxide: Evidence for a Sulfenic Acid Intermediate and Implications for Redox Regulation', *Biochemistry*, 37(16), pp. 5633–5642. doi: 10.1021/BI973035T.

Dephoure, N. *et al.* (2008) 'A quantitative atlas of mitotic phosphorylation', *Proceedings of the National Academy of Sciences of the United States of America*, 105(31), pp. 10762–10767. doi: 10.1073/pnas.0805139105.
Ditchfield, C. *et al.* (2003) 'Aurora B couples chromosome alignment with anaphase by targeting BubR1, Mad2, and Cenp-E to kinetochores', *The Journal of Cell Biology*, 26714(2), pp. 9521–9525. doi: 10.1083/jcb.200208091.
Doil, C. *et al.* (2009) 'RNF168 Binds and Amplifies Ubiquitin Conjugates on Damaged Chromosomes to Allow Accumulation of Repair Proteins', *Cell*, 136(3), pp. 435–446. doi: 10.1016/J.CELL.2008.12.041.
Dumetz, A. C. *et al.* (2007) 'Patterns of protein-protein interactions in salt solutions and implications for protein crystallization', *Protein Science*, 16, pp. 1867–1877. doi: 10.1110/ps.072957907.
Durand, S., Franks, T. M. and Lykke-Andersen, J. (2016) 'Hyperphosphorylation amplifies UPF1 activity to resolve stalls in nonsense-mediated mRNA decay', *Nature Communications*, 7(1), pp. 1–12. doi: 10.1038/ncomms12434.
Ehlen, A. *et al.* (2020) 'Proper chromosome alignment depends on BRCA2 phosphorylation by PLK1', *Nature Communications*, 11(1), pp. 1819–1830. doi: 10.1038/s41467-020-15689-9.
Eliezer, Y. *et al.* (2014) 'Interplay between the DNA damage proteins MDC1 and ATM in the regulation of the spindle assembly checkpoint', *Journal of Biological Chemistry*, 289(12), pp. 8182–8193. doi: 10.1074/jbc.M113.532739.
Elowe, S. *et al.* (2007) 'Tension-sensitive Plk1 phosphorylation on BubR1 regulates the stability of kinetochore–microtubule interactions', *Genes & Development*, 21(17), pp. 2205–2219. doi: 10.1101/GAD.436007.
Erasimus, H. *et al.* (2016) 'DNA repair mechanisms and their clinical impact in glioblastoma', *Mutation Research/Reviews in Mutation Research*, 769, pp. 19–35. doi: 10.1016/J.MRREV.2016.05.005.
Espert, A. *et al.* (2014) 'PP2A-B56 opposes Mps1 phosphorylation of Knl1 and thereby promotes spindle assembly checkpoint silencing', *Journal of Cell Biology*, 206(7), pp. 833–842. doi: 10.1083/JCB.201406109.
Esteller, M. *et al.* (1999) 'Inactivation of the DNA repair gene O6-methylguanine-DNA methyltransferase by promoter hypermethylation is a common event in primary human neoplasia', *Cancer Research*, 59(4), pp. 793–797.
Falchook, G. *et al.* (2018) 'Alisertib in Combination With Weekly Paclitaxel in Patients With Advanced Breast Cancer or Recurrent Ovarian Cancer', *JAMA Oncology*, 5(1), p. e183773. doi: 10.1001/jamaoncol.2018.3773.
Falck, J. *et al.* (2001) 'The ATM–Chk2–Cdc25A checkpoint pathway guards against radioresistant DNA synthesis', *Nature*, 410(6830), pp. 842–847. doi: 10.1038/35071124.
Fang, Y. *et al.* (2006) 'BubR1 is involved in regulation of DNA damage responses', *Oncogene*, 25, pp. 3598–3605. doi: 10.1038/sj.onc.1209392.
Farr, K. A. and Cohen-Fix, O. (1999) 'The metaphase to anaphase transition: A case of productive destruction', *European Journal of Biochemistry*, 263(1), pp. 14–19. doi: 10.1046/j.1432-1327.1999.00510.x.
Fiser, B. *et al.* (2013) 'Glutathione – Hydroxyl Radical Interaction: A Theoretical Study on Radical Recognition Process', *PLoS ONE*, 8(9), p. e73652. doi: 10.1371/journal.pone.0073652.
Flott, S. *et al.* (2011) 'Regulation of Rad51 function by phosphorylation', *EMBO Reports*, 12(8), pp. 833–839. doi: 10.1038/EMBOR.2011.127.
Foley, E. A. and Kapoor, T. M. (2012) 'Microtubule attachment and spindle assembly

checkpoint signalling at the kinetochore', *Nature Reviews Molecular Cell Biology*, 14(1), pp. 25–37. doi: 10.1038/nrm3494.
Foley, E. A., Maldonado, M. and Kapoor, T. M. (2011) 'Formation of stable attachments between kinetochores and microtubules depends on the B56-PP2A phosphatase', *Nature Cell Biology*, 13(10), pp. 1265–1271. doi: 10.1038/ncb2327.
Foley, T. D. *et al.* (2007) 'Oxidative Inhibition of Protein Phosphatase 2A Activity: Role of Catalytic Subunit Disulfides', *Neurochemical Research*, 32(11), pp. 1957–1964. doi: 10.1007/S11064-007-9394-X.
Forester, C. M. *et al.* (2007) 'Control of mitotic exit by PP2A regulation of Cdc25C and Cdk1', *Proceedings of the National Academy of Sciences*, 104(50), pp. 19867–19872. doi: 10.1073/PNAS.0709879104.
Forman, H. J. and Fridovich, I. (1973) 'Superoxide dismutase: A comparison of rate constants', *Archives of Biochemistry and Biophysics*, 158(1), pp. 396–400. doi: 10.1016/0003-9861(73)90636-X.
Gad, H. *et al.* (2019) 'MTH1 promotes mitotic progression to avoid oxidative DNA damage in cancer cells', *bioRxiv*, p. 575290. doi: 10.1101/575290.
Galluzzi, L. *et al.* (2014) 'Systems biology of cisplatin resistance: past, present and future', *Cell Death & Disease*, 5(5), p. e1257. doi: 10.1038/CDDIS.2013.428.
Ganem, N. J. and Pellman, D. (2012) 'Linking abnormal mitosis to the acquisition of DNA damage', *Journal of Cell Biology*, 199(6), pp. 871–881. doi: 10.1083/jcb.201210040.
Giles, N., Forrest, A. and Gabrielli, B. (2003) '14-3-3 Acts as an Intramolecular Bridge to Regulate cdc25B Localization and Activity', *Journal of Biological Chemistry*, 278(31), pp. 28580–28587. doi: 10.1074/JBC.M304027200.
Giunta, S., Belotserkovskaya, R. and Jackson, S. (2010) 'DNA damage signaling in response to double-strand breaks during mitosis', *Journal of Cell Biology*, 190(2), pp. 197–207. doi: 10.1083.
Glasauer, A. *et al.* (2014) 'Targeting SOD1 reduces experimental non-small-cell lung cancer', *The Journal of Clinical Investigation*, 124(1), pp. 117–128. doi: 10.1172/JCI71714.
Glorieux, C. *et al.* (2015) 'Regulation of catalase expression in healthy and cancerous cells', *Free Radical Biology and Medicine*, 87, pp. 84–97. doi: 10.1016/j.freeradbiomed.2015.06.017.
Godinez, V. G. *et al.* (2020) 'DNA damage induced during mitosis undergoes DNA repair synthesis', *PLoS ONE*, 15(4), pp. 1–27. doi: 10.1371/journal.pone.0227849.
Grabsch, H. *et al.* (2003) 'Overexpression of the mitotic checkpoint genesBUB1, BUBR1, andBUB3 in gastric cancer-association with tumour cell proliferation', *The Journal of Pathology*, 200(1), pp. 16–22. doi: 10.1002/path.1324.
Guo, Z., Deshpande, R. and Paull, T. T. (2010) 'ATM activation in the presence of oxidative stress', *Cell Cycle*, 9(24), pp. 4805–4811. doi: 10.4161/cc.9.24.14323.
Gupta, P. and Li, Y. R. (2018) 'Upf proteins: highly conserved factors involved in nonsense mRNA mediated decay', *Molecular Biology Reports*, pp. 39–55. doi: 10.1007/s11033-017-4139-7.
Győrffy, B. *et al.* (2013) 'Online survival analysis software to assess the prognostic value of biomarkers using transcriptomic data in non-small-cell lung cancer', *PloS One*, 8(12), p. e82241. doi: 10.1371/JOURNAL.PONE.0082241.
Han, D. *et al.* (2012) 'Polo-like kinase 1 is overexpressed in colorectal cancer and participates in the migration and invasion of colorectal cancer cells', *Medical Science Monitor: International Medical Journal of Experimental and Clinical Research*, 18(6), pp. 237–246. doi: 10.12659/MSM.882900.

Hanahan, D. and Weinberg, R. A. (2011) 'Hallmarks of Cancer: The Next Generation', *Cell*, 144(5), pp. 646–674. doi: 10.1016/J.CELL.2011.02.013.
Harris, I. S. and Denicola, G. M. (2020) 'The Complex Interplay between Antioxidants and ROS in Cancer', *Trends in Cell Biology*, 30(6), pp. 440–451. doi: 10.1016/j.tcb.2020.03.002.
Hayashi, M. T. *et al.* (2012) 'A telomere dependent DNA damage checkpoint induced by prolonged mitotic arrest', *Nature Structural & Molecular Biology*, 19(4), pp. 387–395. doi: 10.1038/NSMB.2245.
Hayward, L. J. *et al.* (2002) 'Decreased metallation and activity in subsets of mutant superoxide dismutases associated with familial amyotrophic lateral sclerosis', *Journal of Biological Chemistry*, 277(18), pp. 15923–15931. doi: 10.1074/jbc.M112087200.
He, G. *et al.* (2005) 'Induction of p21 by p53 following DNA damage inhibits both Cdk4 and Cdk2 activities', *Oncogene*, 24, pp. 2929–2943. doi: 10.1038/sj.onc.1208474.
He, P. J. *et al.* (2018) 'Oxidative stress induced by carboplatin promotes apoptosis and inhibits migration of HN-3 cells', *Oncology Letters*, 16(6), pp. 7131–7138. doi: 10.3892/OL.2018.9563.
Hegi, M. E. *et al.* (2009) 'MGMT Gene Silencing and Benefit from Temozolomide in Glioblastoma', *The New England Journal of Medicine*, 352(10), pp. 997–1003. doi: 10.1056/NEJMOA043331.
Hein, J. . *et al.* (2021) 'Coupling of Cdc20 inhibition and activation by BubR1', *The Journal of Cell Biology*, 220(5), p. e202012081. doi: 10.1083/JCB.202012081.
Hensley, K. *et al.* (1994) 'A model for beta-amyloid aggregation and neurotoxicity based on free radical generation by the peptide: relevance to Alzheimer disease.', *Proceedings of the National Academy of Sciences of the United States of America*, 91(8), pp. 3270–3274. doi: 10.1073/PNAS.91.8.3270.
Hewitt, L. *et al.* (2010) 'Sustained Mps1 activity is required in mitosis to recruit O-Mad2 to the Mad1-C-Mad2 core complex.', *The Journal of Cell Biology*, 190(1), pp. 25–34. doi: 10.1083/jcb.201002133.
Hirao, A. *et al.* (2000) 'DNA damage-induced activation of p53 by the checkpoint kinase Chk2', *Science*, 287(5459), pp. 1824–1827.
Hirose, Y., Berger, M. S. and Pieper, R. O. (2001) 'p53 effects both the duration of G2/M arrest and the fate of temozolomide-treated human glioblastoma cells', *Cancer Research*, 61(5), pp. 1957–1963.
Hirota, T. *et al.* (2003) 'Aurora-A and an Interacting Activator, the LIM Protein Ajuba, Are Required for Mitotic Commitment in Human Cells', *Cell*, 114(5), pp. 585–598. doi: 10.1016/S0092-8674(03)00642-1.
Hoebeke, J., Van Nijen, G. and De Brabander, M. (1976) 'Interaction of oncodazole (R 17934), a new anti-tumoral drug, with rat brain tubulin', *Biochemical and Biophysical Research Communications*, 69(2), pp. 319–324. doi: 10.1016/0006-291X(76)90524-6.
Hoeijmakers, J. H. J. (2001) 'Genome maintenance mechanisms for preventing cancer', *Nature*, 411(6835), pp. 366–374. doi: 10.1038/35077232.
Hofmann, J. C., Husedzinovic, A. and Gruss, O. J. (2010) 'The function of spliceosome components in open mitosis', *Nucleus*, 1(6), pp. 447–459. doi: 10.4161/NUCL.1.6.13328.
Hornig, N. C. . *et al.* (2002) 'The Dual Mechanism of Separase Regulation by Securin', *Current Biology*, 12(12), pp. 973–982. doi: 10.1016/S0960-9822(02)00847-3.
Hosoya, N. and Miyagawa, K. (2014) 'Targeting DNA damage response in cancer therapy.', *Cancer Science*, 105(4), pp. 370–388. doi: 10.1111/cas.12366.
Hughes, B. T. *et al.* (2013) 'Essential role for Cdk2 inhibitory phosphorylation during replication stress revealed by a human Cdk2 knockin mutation', *Proceedings of the*

National Academy of Sciences, 110(22), pp. 8954–8959. doi: 10.1073/pnas.1302927110.
Hyun, S. Y. and Jang, Y. J. (2015) 'p53 activates G_1 checkpoint following DNA damage by doxorubicin during transient mitotic arrest.', *Oncotarget*, 6(7), pp. 4804–4815. doi: 10.18632/oncotarget.3103.
Ikawa-Yoshida, A. *et al.* (2013) 'Contribution of BubR1 to oxidative stress-induced aneuploidy in p53-deficient cells', *Cancer Medicine*, 2(4), pp. 447–456. doi: 10.1002/cam4.101.
Ikeda, M. and Tanaka, K. (2017) 'Plk1 bound to Bub1 contributes to spindle assembly checkpoint activity during mitosis', *Scientific Reports*, 7(1), pp. 8794–8809. doi: 10.1038/s41598-017-09114-3.
Inoue, E. *et al.* (2010) 'SOD1 is essential for the viability of DT40 cells and nuclear SOD1 functions as a guardian of genomic DNA', *Journal of Nucleic Acids*, 2010. doi: 10.4061/2010/795946.
International Atomic Energy Agency (2010) *Radiation Biology: A Handbook for Teachers and Students*, *Training Course Series No. 42*. Available at: https://www-pub.iaea.org/MTCD/Publications/PDF/TCS-42_web.pdf (Accessed: 31 August 2021).
Itoh, K. *et al.* (1997) 'An Nrf2/Small Maf Heterodimer Mediates the Induction of Phase II Detoxifying Enzyme Genes through Antioxidant Response Elements', *Biochemical and Biophysical Research Communications*, 236(2), pp. 313–322. doi: 10.1006/bbrc.1997.6943.
Itoh, K. *et al.* (1999) 'Keap1 represses nuclear activation of antioxidant responsive elements by Nrf2 through binding to the amino-terminal Neh2 domain', *Genes & Development*, 13(1), pp. 76–86. doi: 10.1101/GAD.13.1.76.
Izawa, D. and Pines, J. (2012) 'Mad2 and the APC/C compete for the same site on Cdc20 to ensure proper chromosome segregation', *Journal of Cell Biology*, 199(1), pp. 27–37. doi: 10.1083/JCB.201205170.
Izawa, D. and Pines, J. (2015) 'The mitotic checkpoint complex binds a second CDC20 to inhibit active APC/C.', *Nature*, 517(7536), pp. 631–634. doi: 10.1038/nature13911.
Izumi, H. *et al.* (2009) 'BubR1 localizes to centrosomes and suppresses centrosome amplification via regulating Plk1 activity in interphase cells', *Oncogene*, 28(31), pp. 2806–2820. doi: 10.1038/onc.2009.141.
Jackson, S. P. and Bartek, J. (2009) 'The DNA-damage response in human biology and disease.', *Nature*, 461(7267), pp. 1071–1078. doi: 10.1038/nature08467.
Jang, Y. J. *et al.* (2007) 'Regulation of Polo-like Kinase 1 by DNA damage in mitosis. Inhibition of mitotic PLK-1 by protein phosphatase 2A.', *Journal of Biological Chemistry*, 282(4), pp. 2473–2482. doi: 10.1074/jbc.M605480200.
Jayakumar, S., Pal, D. and Sandur, S. K. (2015) 'Nrf2 facilitates repair of radiation induced DNA damage through homologous recombination repair pathway in a ROS independent manner in cancer cells', *Mutation Research - Fundamental and Molecular Mechanisms of Mutagenesis*, 779, pp. 33–45. doi: 10.1016/j.mrfmmm.2015.06.007.
Jelluma, N. *et al.* (2010) 'Release of Mps1 from kinetochores is crucial for timely anaphase onset', *The Journal of Cell Biology*, 191(2), pp. 281–290. doi: 10.1083/JCB.201003038.
Jeng, Y. M. *et al.* (2004) 'Overexpression and amplification of Aurora-A in hepatocellular carcinoma', *Clinical Cancer Research*, 10(6), pp. 2065–2071. doi: 10.1158/1078-0432.CCR-1057-03.
Jerome-Morais, A. *et al.* (2013) 'The effects of selenium and the GPx-1 selenoprotein on the phosphorylation of H2AX', *Biochimica et Biophysica Acta*, 1830(6), pp. 3399–3406. doi: 10.1016/j.bbagen.2013.03.010.

Jia, L., Li, B. and Yu, H. (2016) 'The Bub1–Plk1 kinase complex promotes spindle checkpoint signalling through Cdc20 phosphorylation', *Nature Communications*, 7, p. 10818. doi: 10.1038/ncomms10818.
Juarez, J. C. *et al.* (2008) 'Superoxide dismutase 1 (SOD1) is essential for H2O 2-mediated oxidation and inactivation of phosphatases in growth factor signaling', *Proceedings of the National Academy of Sciences of the United States of America*, 105(20), pp. 7147–7152. doi: 10.1073/pnas.0709451105.
Kalev, P. *et al.* (2012) 'Loss of PPP2R2A Inhibits Homologous Recombination DNA Repair and Predicts Tumor Sensitivity to PARP Inhibition', *Cancer Research*, 72(24), pp. 6414–6424. doi: 10.1158/0008-5472.CAN-12-1667.
Kalev, P. and Sablina, A. (2012) 'Protein Phosphatase 2A as a Potential Target for Anticancer Therapy', *Anti-Cancer Agents in Medicinal Chemistry*, 11(1), pp. 38–46. doi: 10.2174/187152011794941172.
Kasai, H. (1997) 'Analysis of a form of oxidative DNA damage, 8-hydroxy-2′-deoxyguanosine, as a marker of cellular oxidative stress during carcinogenesis', *Mutation Research/Reviews in Mutation Research*, 387(3), pp. 147–163. doi: 10.1016/S1383-5742(97)00035-5.
Kim, E. M. and Burke, D. J. (2008) 'DNA damage activates the SAC in an ATM/ATR-dependent manner, independently of the kinetochore.', *PLoS Genetics*, 4(2), p. e1000015. doi: 10.1371/journal.pgen.1000015.
Kim, K. Y. *et al.* (2001) 'N-Acetylcysteine Induces Cell Cycle Arrest in Hepatic Stellate Cells through Its Reducing Activity', *Journal of Biological Chemistry*, 276(44), pp. 40591–40598. doi: 10.1074/JBC.M100975200.
Kim, S. Y., Hyun, S. Y. and Jang, Y. J. (2019) 'Dephosphorylation of Plk1 occurs through PP2A-B55/ENSA/Greatwall pathway during mitotic DNA damage recovery', *Cell Cycle*, 18(10), pp. 1154–1167. doi: 10.1080/15384101.2019.1617003.
Kim, Y., Starostina, N. G. and Kipreos, E. T. (2008) 'The CRL4 Cdt2 ubiquitin ligase targets the degradation of p21 Cip1 to control replication licensing', *Genes & Development*, 22(18), pp. 2507–2519. doi: 10.1101/gad.1703708.
Kobayashi, A. *et al.* (2004) 'Oxidative Stress Sensor Keap1 Functions as an Adaptor for Cul3-Based E3 Ligase To Regulate Proteasomal Degradation of Nrf2', *Molecular and Cellular Biology*, 24(16), pp. 7130–7139. doi: 10.1128/MCB.24.16.7130-7139.2004.
Kolas, N. K. *et al.* (2007) 'Orchestration of the DNA-damage response by the RNF8 ubiquitin ligase', *Science*, 318(5856), pp. 1637–1640. doi: 10.1126/SCIENCE.1150034.
Komura, K. *et al.* (2021) 'Increased BUB1B/BUBR1 expression contributes to aberrant DNA repair activity leading to resistance to DNA-damaging agents', *Oncogene*, 40, pp. 6210–6222. doi: 10.1038/s41388-021-02021-y.
Krajewska, M. *et al.* (2015) 'Regulators of homologous recombination repair as novel targets for cancer treatment', *Frontiers in Genetics*. Frontiers, 6(96). doi: 10.3389/FGENE.2015.00096.
Kumari, S. *et al.* (2018) 'Reactive Oxygen Species: A Key Constituent in Cancer Survival', *Biomarker Insights*, 13, pp. 1–9. doi: 10.1177/1177271918755391.
Lan, W. *et al.* (2004) 'Aurora B Phosphorylates Centromeric MCAK and Regulates Its Localization and Microtubule Depolymerization Activity', *Current Biology*, 14(4), pp. 273–286. doi: 10.1016/J.CUB.2004.01.055.
Lane, S. I. R. *et al.* (2017) 'DNA damage induces a kinetochore-based ATM/ATR-independent SAC arrest unique to the first meiotic division in mouse oocytes.', *Development*, 144(19), pp. 3475–3486. doi: 10.1242/dev.153965.

Lara-Gonzalez, P. *et al.* (2011) 'BubR1 blocks substrate recruitment to the APC/C in a KEN-box-dependent manner.', *Journal of Cell Science*, 124(24), pp. 4332–4345. doi: 10.1242/jcs.094763.
Lauterburg, B. H., Corcoran, G. B. and Mitchell, J. R. (1983) 'Mechanism of action of N-acetylcysteine in the protection against the hepatotoxicity of acetaminophen in rats in vivo', *Journal of Clinical Investigation*, 71(4), pp. 980–991. doi: 10.1172/JCI110853.
Lee, J., Kumagai, A. and Dunphy, W. G. (2001) 'Positive Regulation of Wee1 by Chk1 and 14-3-3 Proteins', *Molecular Biology of the Cell*, 12(3), pp. 551–563. doi: 10.1091/MBC.12.3.551.
Lee, J. M. *et al.* (2018) 'Prexasertib, a cell cycle checkpoint kinase 1 and 2 inhibitor, in BRCA wild-type recurrent high-grade serous ovarian cancer: a first-in-class proof-of-concept phase 2 study', *The Lancet Oncology*, 19(2), pp. 207–215. doi: 10.1016/S1470-2045(18)30009-3.
Lee, J. Y. *et al.* (2007) 'Glycogen Synthase Kinase 3β Phosphorylates p21 WAF1/CIP1 for Proteasomal Degradation after UV Irradiation', *Molecular and Cellular Biology*, 27(8), pp. 3187–3198. doi: 10.1128/MCB.01461-06.
Lee, S. *et al.* (2012) 'An effective strategy for increasing the radiosensitivity of Human lung Cancer cells by blocking Nrf2-dependent antioxidant responses', *Free Radical Biology and Medicine*, 53(4), pp. 807–816. doi: 10.1016/j.freeradbiomed.2012.05.038.
Leimbacher, P. A. *et al.* (2019) 'MDC1 Interacts with TOPBP1 to Maintain Chromosomal Stability during Mitosis', *Molecular Cell*, 74(3), pp. 571–583. doi: 10.1016/J.MOLCEL.2019.02.014.
Li, J. *et al.* (2019) 'Cytoplasmic Restriction of Mutated SOD1 Impairs the DNA Repair Process in Spinal Cord Neurons', *Cells*, 8(12), pp. 1502–1522. doi: 10.3390/CELLS8121502.
Li, K. *et al.* (2020) 'Survivin in breast cancer–derived exosomes activates fibroblasts by up-regulating SOD1, whose feedback promotes cancer proliferation and metastasis', *Journal of Biological Chemistry*, 295(40), pp. 13737–13752. doi: 10.1074/JBC.RA120.013805.
Li, L. *et al.* (2017) 'The Human RNA Surveillance Factor UPF1 Modulates Gastric Cancer Progression by Targeting Long Non-Coding RNA MALAT1', *Cellular Physiology and Biochemistry*, 42(6), pp. 2194–2206. doi: 10.1159/000479994.
Li, M. *et al.* (2009) 'Hydrogen Peroxide Induces G2 Cell Cycle Arrest and Inhibits Cell Proliferation in Osteoblasts', *The Anatomical Record: Advances in Integrative Anatomy and Evolutionary Biology*, 292(8), pp. 1107–1113. doi: 10.1002/AR.20925.
Li, S. *et al.* (2018) 'Disrupting SOD1 activity inhibits cell growth and enhances lipid accumulation in nasopharyngeal carcinoma', *Cell Communication and Signaling*, 16(1), pp. 1–13. doi: 10.1186/S12964-018-0240-3.
Li, X. *et al.* (2015) 'PP2A–B56ϵ complex is involved in dephosphorylation of γ-H2AX in the repair process of CPT-induced DNA double-strand breaks', *Toxicology*, 331, pp. 57–65. doi: 10.1016/J.TOX.2015.03.007.
Li, X., Qiu, S., *et al.* (2019) 'A new function of copper zinc superoxide dismutase: As a regulatory DNA-binding protein in gene expression in response to intracellular hydrogen peroxide', *Nucleic Acids Research*, 47(10), pp. 5074–5085. doi: 10.1093/nar/gkz256.
Li, X., Chen, Y., *et al.* (2019) 'The Specific Inhibition of SOD1 Selectively Promotes Apoptosis of Cancer Cells via Regulation of the ROS Signaling Network', *Oxidative Medicine and Cellular Longevity*, 2019, pp. 1–21. doi: 10.1155/2019/9706792.
Li, Z. *et al.* (2017) 'DNA Damage Response-Independent Role for MDC1 in Maintaining Genomic Stability', *Molecular and Cellular Biology*, 37(9), pp. 1–17.

Lim, D. C. *et al.* (2020) 'Redox priming promotes Aurora A activation during mitosis', *Science Signaling*, 13(641), pp. 6707–6722. doi: 10.1126/SCISIGNAL.ABB6707.
Lim, J. M. *et al.* (2015) 'Control of the pericentrosomal H2O2 level by peroxiredoxin I is critical for mitotic progression', *The Journal of Cell Biology*, 210(1), pp. 23–33. doi: 10.1083/jcb.201412068.
Lin, J. *et al.* (2013) 'A non-comparative randomized phase II study of two doses of ATN-224, a copper/zinc superoxide dismutase inhibitor, in patients with biochemically recurrent hormone-naïve prostate cancer', *Urologic Oncology*, 31(5), pp. 581–588. doi: 10.1016/J.UROLONC.2011.04.009.
Lischetti, T. *et al.* (2014) 'The internal Cdc20 binding site in BubR1 facilitates both spindle assembly checkpoint signalling and silencing', *Nature Communications*, 5, pp. 5563–5575. doi: 10.1038/ncomms6563.
Liu, C. *et al.* (2014) 'The UPF1 RNA surveillance gene is commonly mutated in pancreatic adenosquamous carcinoma', *Nature Medicine*, 20(6), pp. 596–598. doi: 10.1038/nm.3548.
Liu, M., Wikonkal, N. M. and Brash, D. E. (1999) 'Induction of cyclin-dependent kinase inhibitors and G 1 prolongation by the chemopreventive agent N-acetylcysteine', *Carcinogenesis*, 20(9), pp. 1869–1872.
Liu, S. *et al.* (2020) 'SOD1 Promotes Cell Proliferation and Metastasis in Non-small Cell Lung Cancer via an miR-409-3p/SOD1/SETDB1 Epigenetic Regulatory Feedforward Loop', *Frontiers in Cell and Developmental Biology*, 8, pp. 213–227. doi: 10.3389/FCELL.2020.00213.
Lou, Z. *et al.* (2003) 'MDC1 is coupled to activated CHK2 in mammalian DNA damage response pathways', *Nature*, 421(6926), pp. 957–961. doi: 10.1038/nature01447.
Lou, Z. *et al.* (2006) 'MDC1 Maintains Genomic Stability by Participating in the Amplification of ATM-Dependent DNA Damage Signals', *Molecular Cell*, 21(2), pp. 187–200. doi: 10.1016/J.MOLCEL.2005.11.025.
Lu, R., Nash, H. M. and Verdine, G. L. (1997) 'A mammalian DNA repair enzyme that excises oxidatively damaged guanines maps to a locus frequently lost in lung cancer', *Current Biology*, 7(6), pp. 397–407. doi: 10.1016/S0960-9822(06)00187-4.
Luo, K., Yuan, J. and Lou, Z. (2011) 'Oligomerization of MDC1 protein is important for proper DNA damage response.', *The Journal of Biological Chemistry*, 286(32), pp. 28192–28199. doi: 10.1074/jbc.M111.258087.
Ma, N. *et al.* (2011) 'The nuclear scaffold protein SAF-A is required for kinetochore–microtubule attachment and contributes to the targeting of Aurora-A to mitotic spindles', *Journal of Cell Science*, 124(3), pp. 394–404. doi: 10.1242/JCS.063347.
Maciejczyk, A. *et al.* (2013) 'Elevated BUBR1 Expression Is Associated with Poor Survival in Early Breast Cancer Patients: 15-Year Follow-up Analysis', *Journal of Histochemistry and Cytochemistry*, 61(5), pp. 330–339. doi: 10.1369/0022155413480148.
Macůrek, L. *et al.* (2008) 'Polo-like kinase-1 is activated by aurora A to promote checkpoint recovery', *Nature*, 455(7209), pp. 119–123. doi: 10.1038/nature07185.
Mailand, N. *et al.* (2007) 'RNF8 Ubiquitylates Histones at DNA Double-Strand Breaks and Promotes Assembly of Repair Proteins', *Cell*, 131(5), pp. 887–900. doi: 10.1016/J.CELL.2007.09.040.
Mamely, I. *et al.* (2006) 'Polo-like Kinase-1 Controls Proteasome-Dependent Degradation of Claspin during Checkpoint Recovery', *Current Biology*, 16(19), pp. 1950–1955. doi: 10.1016/J.CUB.2006.08.026.
Marklund, S. L., Holme, E. and Hellner, L. (1982) 'Superoxide dismutase in extracellular fluids', *Clinica Chimica Acta*, 126(1), pp. 41–51. doi: 10.1016/0009-

8981(82)90360-6.
Marumoto, T. *et al.* (2003) 'Aurora-A Kinase Maintains the Fidelity of Early and Late Mitotic Events in HeLa Cells', *Journal of Biological Chemistry*, 278(51), pp. 51786–51795. doi: 10.1074/JBC.M306275200.
Matera, A. G. and Wang, Z. (2014) 'A day in the life of the spliceosome', *Nature Reviews Molecular Cell Biology*, 15(2), pp. 108–121. doi: 10.1038/nrm3742.
Matsuoka, S., Huang, M. and Elledge, S. J. (1998) 'Linkage of ATM to Cell Cycle Regulation by the Chk2 Protein Kinase', *Science*, 282(5395), pp. 1893–1897.
McCord, J. M. and Fridovich, I. (1969) 'Superoxide Dismutase. An Enzymic Function for Erythrocuprein (Hemocuprein)', *The Journal of Biological Chemistry*, 244(22), pp. 6049–6055.
Mcpherson, A. (2001) 'A comparison of salts for the crystallization of macromolecules', *Protein Science : A Publication of the Protein Society*, 10(2), pp. 418–422. doi: 10.1110/PS.32001.
Mikhailov, A., Cole, R. W. and Rieder, C. L. (2002) 'DNA damage during mitosis in human cells delays the metaphase/anaphase transition via the spindle-assembly checkpoint', *Current Biology*, 12, pp. 1797–1806. doi: 10.1016/S0960-9822(02)01226-5.
Minocherhomji, S. *et al.* (2015) 'Replication stress activates DNA repair synthesis in mitosis', *Nature*, 528(7581), pp. 286–290. doi: 10.1038/nature16139.
Moens, S. *et al.* (2021) 'The mitotic checkpoint is a targetable vulnerability of carboplatin-resistant triple negative breast cancers', *Scientific Reports*, 11(1), pp. 1–13. doi: 10.1038/s41598-021-82780-6.
Mondal, G. *et al.* (2007) 'Overexpression of Cdc20 leads to impairment of the spindle assembly checkpoint and aneuploidization in oral cancer', *Carcinogenesis*, 28(1), pp. 81–92. doi: 10.1093/carcin/bgl100.
Morris, J. H. *et al.* (2014) 'Affinity purification–mass spectrometry and network analysis to understand protein-protein interactions', *Nature Protocols*, 9(11), pp. 2539–2554. doi: 10.1038/NPROT.2014.164.
Moussa, Z., Judeh, Z. M. A. and Ahmed, S. A. (2020) 'Nonenzymatic Exogenous and Endogenous Antioxidants', in *Free Radical Medicine and Biology*. IntechOpen, pp. 1–22. doi: 10.5772/intechopen.87778.
Munk, S. *et al.* (2017) 'Proteomics Reveals Global Regulation of Protein SUMOylation by ATM and ATR Kinases during Replication Stress', *Cell Reports*, 21(2), pp. 546–558. doi: 10.1016/J.CELREP.2017.09.059.
Musacchio, A. and Salmon, E. D. (2007) 'The spindle-assembly checkpoint in space and time', *Nature Reviews Molecular Cell Biology*, 8(5), pp. 379–393. doi: 10.1038/nrm2163.
Nadler, Y. *et al.* (2008) 'Expression of Aurora A (but Not Aurora B) Is Predictive of Survival in Breast Cancer', *Clinical Cancer Research*, 14(14), pp. 4455–4462. doi: 10.1158/1078-0432.CCR-07-5268.
Nagaraj, A. B. *et al.* (2018) 'Mitotic Exit dysfunction through the deregulation of APC/C characterizes cisplatin resistant state in epithelial ovarian cancer', *Clinical Cancer Research*, 24(18), pp. 4588–4601. doi: 10.1158/1078-0432.CCR-17-2885.
National Cancer Institute (2020) *BRCA Gene Mutations: Cancer Risk and Genetic Testing* , *NIH Genetic Fact Sheet*. Available at: https://www.cancer.gov/about-cancer/causes-prevention/genetics/brca-fact-sheet (Accessed: 1 September 2021).
Neganova, I. *et al.* (2011) 'An Important Role for CDK2 in G1 to S Checkpoint Activation and DNA Damage Response in Human Embryonic Stem Cells', *Stem Cells*, 29(4), pp. 651–659. doi: 10.1002/stem.620.

Neumann, B. *et al.* (2010) 'Phenotypic profiling of the human genome by time-lapse microscopy reveals cell division genes', *Nature*, 464(7289), pp. 721–727. doi: 10.1038/NATURE08869.
Nguyen-Powanda, P. and Robaire, B. (2021) 'Aging and oxidative stress alter DNA repair mechanisms in male germ cells of superoxide dismutase-1 null mice', *Biology of Reproduction*, 105(4), pp. 944–957. doi: 10.1093/BIOLRE/IOAB114.
Nitta, M. *et al.* (2004) 'Spindle checkpoint function is required for mitotic catastrophe induced by DNA-damaging agents', *Oncogene*, 23(39), pp. 6548–6558. doi: 10.1038/sj.onc.1207873.
O'Connell, M. J. *et al.* (1997) 'Chk1 is a wee1 kinase in the G 2 DNA damage checkpoint inhibiting cdc2 by Y15 phosphorylation genomic integrity and prevent changes in ploidy; i.e. S-phase onset is dependent on the completion of the', *The EMBO Journal*, 16(3), pp. 545–554.
O'Malley, Y. Q. *et al.* (2003) 'The Pseudomonas secretory product pyocyanin inhibits catalase activity in human lung epithelial cells', *American Journal of Physiology: Lung Cellular and Molecular Physiology*, 285(5), pp. 1077–1086. doi: 10.1152/AJPLUNG.00198.2003.
Ohnishi, T. *et al.* (2003) 'Phosphorylation of hUPF1 induces formation of mRNA surveillance complexes containing hSMG-5 and hSMG-7', *Molecular Cell*, 12(5), pp. 1187–1200. doi: 10.1016/S1097-2765(03)00443-X.
Olsen, J. V. *et al.* (2010) 'Quantitative phosphoproteomics revealswidespread full phosphorylation site occupancy during mitosis', *Science Signaling*, 3(104). doi: 10.1126/scisignal.2000475.
Orthwein, A. *et al.* (2014) 'Mitosis inhibits DNA double-strand break repair to guard against telomere fusions.', *Science*, 344(6180), pp. 189–193. doi: 10.1126/science.1218498.
Overlack, K. *et al.* (2015) 'A molecular basis for the differential roles of Bub1 and BubR1 in the spindle assembly checkpoint', *eLife*, 4(4). doi: 10.7554/ELIFE.05269.
Pansarasa, O. *et al.* (2018) 'SOD1 in Amyotrophic Lateral Sclerosis: "Ambivalent" Behavior Connected to the Disease', *International Journal of Molecular Sciences*, 19(5), pp. 1345–1358. doi: 10.3390/IJMS19051345.
Papa, L. *et al.* (2014) 'SOD2 to SOD1 switch in breast cancer.', *The Journal of Biological Chemistry*, 289(9), pp. 5412–5416. doi: 10.1074/jbc.C113.526475.
Parrilla-Castellar, E. R., Arlander, S. J. H. and Karnitz, L. (2004) 'Dial 9–1–1 for DNA damage: the Rad9–Hus1–Rad1 (9–1–1) clamp complex', *DNA Repair*, 3(8–9), pp. 1009–1014. doi: 10.1016/J.DNAREP.2004.03.032.
Patterson, J. C. *et al.* (2019) 'ROS and Oxidative Stress Are Elevated in Mitosis during Asynchronous Cell Cycle Progression and Are Exacerbated by Mitotic Arrest', *Cell Systems*, 8(2), pp. 163–167. doi: 10.1016/J.CELS.2019.01.005.
Peng, C.-Y. *et al.* (1997) 'Mitotic and G2 Checkpoint Control: Regulation of 14-3-3 Protein Binding by Phosphorylation of Cdc25C on Serine-216', *Science*. American Association for the Advancement of Science, 277(5331), pp. 1501–1505. doi: 10.1126/SCIENCE.277.5331.1501.
Perillo, B. *et al.* (2020) 'ROS in cancer therapy: the bright side of the moon', *Experimental & Molecular Medicine*, 52(2), pp. 192–203. doi: 10.1038/s12276-020-0384-2.
Perrotti, D. and Neviani, P. (2013) 'Targeting A Tumor Suppressor To Suppress Tumor Growth: News and Views on Protein Phosphatase 2A (PP2A) as a Target for Anti-cancer Therapy', *The Lancet Oncology*, 14(6), pp. 229–238. doi: 10.1016/S1470-2045(12)70558-2.

Pizzino, G. *et al.* (2017) 'Oxidative Stress: Harms and Benefits for Human Health', *Oxidative Medicine and Cellular Longevity*, 2017, pp. 1–13. doi: 10.1155/2017/8416763.
Pontano, L. L. *et al.* (2008) 'Genotoxic stress-induced cyclin D1 phosphorylation and proteolysis are required for genomic stability.', *Molecular and Cellular Biology*, 28(23), pp. 7245–7258. doi: 10.1128/MCB.01085-08.
Prescher, N. *et al.* (2021) 'The migration behavior of human glioblastoma cells is influenced by the redox-sensitive human macrophage capping protein CAPG', *Free Radical Biology and Medicine*, 167, pp. 81–93. doi: 10.1016/J.FREERADBIOMED.2021.02.038.
Primorac, I. *et al.* (2013) 'Bub3 reads phosphorylated MELT repeats to promote spindle assembly checkpoint signaling', *eLife*, 2(2), pp. 1030–1050. doi: 10.7554/ELIFE.01030.
Raman, D. and Pervaiz, S. (2019) 'Redox inhibition of protein phosphatase PP2A: Potential implications in oncogenesis and its progression', *Redox Biology*, 27, p. 101105. doi: 10.1016/J.REDOX.2019.101105.
Rao, R. K. and Clayton, L. W. (2002) 'Regulation of protein phosphatase 2A by hydrogen peroxide and glutathionylation', *Biochemical and Biophysical Research Communications*, 293(1), pp. 610–616. doi: 10.1016/S0006-291X(02)00268-1.
Reichmann, D., Voth, W. and Jakob, U. (2018) 'Maintaining a Healthy Proteome during Oxidative Stress', *Molecular Cell*, 69(2), pp. 203–213. doi: 10.1016/j.molcel.2017.12.021.
Ren, B. J. *et al.* (2015) 'Alisertib Induces Cell Cycle Arrest, Apoptosis, Autophagy and Suppresses EMT in HT29 and Caco-2 Cells.', *International journal of molecular sciences*, 17(1), pp. 41–75. doi: 10.3390/ijms17010041.
Riley, P. A. (1994) 'Free radicals in biology : oxidative stress and the effects of ionizing radiation', *International Journal of Radiation Biology*, 65(1), pp. 27–33.
Rogakou, E. P. *et al.* (1998) 'DNA double-stranded breaks induce histone H2AX phosphorylation on serine 139', *Journal of Biological Chemistry*, 273(10), pp. 5858–5868. doi: 10.1074/jbc.273.10.5858.
Rogakou, E. P. *et al.* (1999) 'Megabase Chromatin Domains Involved in DNA Double-Strand Breaks in Vivo', *The Journal of Cell Biology*, 146(5), pp. 905–915. doi: 10.1083/JCB.146.5.905.
Rotruck, J. T. *et al.* (1973) 'Selenium: Biochemical Role as a Component of Glutathione Peroxidase', *Science*, 179(4073), pp. 588–590. doi: 10.1126/SCIENCE.179.4073.588.
Royou, A. *et al.* (2010) 'BubR1- and Polo-coated DNA tethers facilitate poleward segregation of acentric chromatids.', *Cell*, 140(2), pp. 235–245. doi: 10.1016/j.cell.2009.12.043.
Royou, A., Macias, H. and Sullivan, W. (2005) 'The Drosophila Grp/Chk1 DNA damage checkpoint controls entry into anaphase.', *Current Biology*, 15(4), pp. 334–339. doi: 10.1016/j.cub.2005.02.026.
Ruediger, R., Pham, H. T. and Walter, G. (2001a) 'Alterations in protein phosphatase 2A subunit interaction in human carcinomas of the lung and colon with mutations in the Aβ subunit gene', *Oncogene*, 20(15), pp. 1892–1899. doi: 10.1038/sj.onc.1204279.
Ruediger, R., Pham, H. T. and Walter, G. (2001b) 'Disruption of protein phosphatase 2A subunit interaction in human cancers with mutations in the Aα subunit gene', *Oncogene*, 20(1), pp. 10–15. doi: 10.1038/sj.onc.1204059.
Sajesh, B. V. *et al.* (2013) 'Synthetic lethal targeting of superoxide dismutase 1 selectively kills RAD54B-deficient colorectal cancer cells', *Genetics*. Genetics Society of America, 195(3), pp. 757–767. doi: 10.1534/genetics.113.156836.

Sau, D. *et al.* (2007) 'Mutation of SOD1 in ALS: a gain of a loss of function', *Human Molecular Genetics*, 16(13), pp. 1604–1618. doi: 10.1093/HMG/DDM110.
Saurin, A. T. *et al.* (2011) 'Aurora B potentiates Mps1 activation to ensure rapid checkpoint establishment at the onset of mitosis', *Nature Communications*, 2(1), pp. 316–325. doi: 10.1038/NCOMMS1319.
Savitsky, P. A. and Finkel, T. (2002) 'Redox Regulation of Cdc25C', *Journal of Biological Chemistry*, 277(23), pp. 20535–20540. doi: 10.1074/JBC.M201589200.
Schipler, A. and Iliakis, G. (2013) 'DNA double-strand–break complexity levels and their possible contributions to the probability for error-prone processing and repair pathway choice', *Nucleic Acids Research*, 41(16), pp. 7589–7605. doi: 10.1093/NAR/GKT556.
Schmitt, E. *et al.* (2007) 'DNA-damage response network at the crossroads of cell-cycle checkpoints, cellular senescence and apoptosis.', *Journal of Zhejiang University*, 8(6), pp. 377–397. doi: 10.1631/jzus.2007.B0377.
Shaltiel, I. A. *et al.* (2015) 'The same, only different - DNA damage checkpoints and their reversal throughout the cell cycle', *Journal of Cell Science*, 128, pp. 607–620. doi: 10.1242/jcs.163766.
Sjoberg, L., Eriksen, T. E. and Revesz, L. (1982) 'The reaction of the hydroxyl radical with glutathione in neutral and alkaline aqueous solution', *Radiation Research*, 89(2), pp. 255–263. doi: 10.2307/3575771.
Slot, J. W. *et al.* (1986) 'Intracellular Localization of the Copper-Zinc and Manganese Superoxide Dismutases in Rat Liver Parenchymal Cells', *Laboratory Investigation*, 55(3), pp. 363–371.
Smith, M. A. *et al.* (1998) 'Cytochemical Demonstration of Oxidative Damage in Alzheimer Disease by Immunochemical Enhancement of the Carbonyl Reaction with 2,4-Dinitrophenylhydrazine':, *The Journal of Histochemistry & Cytochemistry*, 46(6), pp. 731–735. doi: 10.1177/002215549804600605.
Smits, V. A. J. *et al.* (2000) 'Polo-like kinase-1 is a target of the DNA damage checkpoint', *Nature Cell Biology*, 2(9), pp. 672–676. doi: 10.1038/35023629.
Snezhkina, A. V. *et al.* (2019) 'ROS Generation and Antioxidant Defense Systems in Normal and Malignant Cells', *Oxidative Medicine and Cellular Longevity*, 2019. doi: 10.1155/2019/6175804.
Sohn, J. and Rudolph, J. (2003) 'Catalytic and Chemical Competence of Regulation of Cdc25 Phosphatase by Oxidation/Reduction', *Biochemistry*, 42(34), pp. 10060–10070. doi: 10.1021/BI0345081.
Solis, L. M. *et al.* (2010) 'Nrf2 and Keap1 abnormalities in non-small cell lung carcinoma and association with clinicopathologic features', *Clinical Cancer Research*, 16(14), pp. 3743–3753. doi: 10.1158/1078-0432.CCR-09-3352.
Somwar, R. *et al.* (2011) 'Superoxide dismutase 1 (SOD1) is a target for a small molecule identified in a screen for inhibitors of the growth of lung adenocarcinoma cell lines', *PNAS*, 108(39), pp. 16375–16380. doi: 10.1073/pnas.1113554108.
Sørensen, C. . *et al.* (2005) 'The cell-cycle checkpoint kinase Chk1 is required for mammalian homologous recombination repair', *Nature Cell Biology*, 7(2), pp. 195–201. doi: 10.1038/NCB1212.
Sørensen, C. S. *et al.* (2003) 'Chk1 regulates the S phase checkpoint by coupling the physiological turnover and ionizing radiation-induced accelerated proteolysis of Cdc25A.', *Cancer Cell*, 3(3), pp. 247–258. doi: 10.1016/S1535-6108(03)00048-5.
Speier, C., Baker, S. S. and Newburger, P. E. (1985) 'Relationships between in vitro selenium supply, glutathione peroxidase activity, and phagocytic function in the HL-60 human myeloid cell line', *Journal of Biological Chemistry*, 260(15), pp. 8951–8955. doi:

10.1016/s0021-9258(17)39441-3.
Stadtman, E. R. and Levine, R. L. (2000) 'Protein oxidation', *Annals of the New York Academy of Sciences*, 899, pp. 191–208. doi: 10.1111/J.1749-6632.2000.TB06187.X.
Stolz, A. *et al.* (2010) 'The CHK2-BRCA1 tumour suppressor pathway ensures chromosomal stability in human somatic cells', *Nature Cell Biology*, 12(5), pp. 492–499. doi: 10.1038/ncb2051.
Strasser-Wozak, E. M. C. *et al.* (1998) 'Irradiation induces G2/M cell cycle arrest and apoptosis in p53-decient lymphoblastic leukemia cells without affecting Bcl-2 and Bax expression', *Cell Death and Differentiation*, 5(8), pp. 687–693.
Sturtz, L. A. *et al.* (2001) 'A fraction of yeast Cu,Zn-superoxide dismutase and its metallochaperone, CCS, localize to the intermembrane space of mitochondria.', *Journal of Biological Chemistry*, 276(41), pp. 38084–38089. doi: 10.1074/jbc.M105296200.
Suijkerbuijk, S. J. E. *et al.* (2012) 'Integration of Kinase and Phosphatase Activities by BUBR1 Ensures Formation of Stable Kinetochore-Microtubule Attachments', *Developmental Cell*, 23(4), pp. 745–755. doi: 10.1016/j.devcel.2012.09.005.
Sullivan, S. G. *et al.* (1994) 'Effects of H2O2 on protein tyrosine phosphatase activity in HER14 cells', *Free Radical Biology and Medicine*, 16(3), pp. 399–403. doi: 10.1016/0891-5849(94)90042-6.
Sun, X. *et al.* (2020) 'NRF2 preserves genomic integrity by facilitating ATR activation and G2 cell cycle arrest', *Nucleic Acids Research*, 48(16), pp. 9109–9123. doi: 10.1093/nar/gkaa631.
Sun, X. Z. *et al.* (2003) 'Formation of Disulfide Bond in p53 Correlates with Inhibition of DNA Binding and Tetramerization', *Antioxidants and Redox Signaling*, 5(5), pp. 655–665. doi: 10.1089/152308603770310338.
Svilar, D. *et al.* (2012) 'Alkylation sensitivity screens reveal a conserved cross-species functionome', *Molecular Cancer Research*, 10(12), pp. 1580–1596. doi: 10.1158/1541-7786.MCR-12-0168.
Terasawa, M., Shinohara, A. and Shinohara, M. (2014) 'Canonical non-homologous end joining in mitosis induces genome instability and is suppressed by M-phase-specific phosphorylation of XRCC4.', *PLoS Genetics*, 10(8), p. e1004563. doi: 10.1371/journal.pgen.1004563.
ThermoFisher (2021) *Detergents for Cell Lysis and Protein Extraction*. Available at: https://www.thermofisher.com/uk/en/home/life-science/protein-biology/protein-biology-learning-center/protein-biology-resource-library/pierce-protein-methods/detergents-cell-lysis-protein-extraction.html (Accessed: 15 June 2021).
Thimmulappa, R. K. *et al.* (2002) 'Identification of Nrf2-regulated genes induced by the chemopreventive agent sulforaphane by oligonucleotide microarray', *Cancer Research*, 62(18), pp. 5196–5203.
Thompson, R. *et al.* (2015) 'An Inhibitor of PIDDosome Formation', *Molecular Cell*, 58(5), pp. 767–779. doi: 10.1016/j.molcel.2015.03.034.
Thompson, R., Gatenby, R. and Sidi, S. (2019) 'How Cells Handle DNA Breaks during Mitosis: Detection, Signaling, Repair, and Fate Choice', *Cells*, 8(9), pp. 1049–1060. doi: 10.3390/cells8091049.
Tibbetts, R. S. *et al.* (1999) 'A role for ATR in the DNA damage-induced phosphorylation of p53', *Genes & Development*, 13(2), pp. 152–157. doi: 10.1101/GAD.13.2.152.
Townsend, K. *et al.* (2009) 'Mediator of DNA damage checkpoint 1 (MDC1) regulates mitotic progression.', *The Journal of Biological Chemistry*, 284(49), pp. 33939–33948. doi: 10.1074/jbc.M109.009191.

Trinkle-Mulcahy, L. *et al.* (2008) 'Identifying specific protein interaction partners using quantitative mass spectrometry and bead proteomes.', *The Journal of Cell Biology*, 183(2), pp. 223–239. doi: 10.1083/jcb.200805092.
Tsang, C. K. *et al.* (2014) 'Superoxide dismutase 1 acts as a nuclear transcription factor to regulate oxidative stress resistance.', *Nature Communications*, 5, pp. 3446–3472. doi: 10.1038/ncomms4446.
Tsuchiya, Y. *et al.* (2020) 'Covalent Aurora A regulation by the metabolic integrator coenzyme A', *Redox Biology*, 28. doi: 10.1016/J.REDOX.2019.101318.
Uhlmann, F. *et al.* (2000) 'Cleavage of Cohesin by the CD Clan Protease Separin Triggers Anaphase in Yeast', *Cell*, 103(3), pp. 375–386. doi: 10.1016/S0092-8674(00)00130-6.
Unger, T. *et al.* (1999) 'Critical role for Ser20 of human p53 in the negative regulation of p53 by Mdm2.', *The EMBO Journal*, 18(7), pp. 1805–1814. doi: 10.1093/EMBOJ/18.7.1805.
Uziel, T. *et al.* (2003) 'Requirement of the MRN complex for ATM activation by DNA damage', *EMBO Journal*, 22(20), pp. 5612–5621. doi: 10.1093/emboj/cdg274.
Vandre, D. D. and Wills, V. L. (1992) 'Inhibition of mitosis by okadaic acid: possible involvement of a protein phosphatase 2A in the transition from metaphase to anaphase', *Journal of Cell Science*, 101(1), pp. 79–91. doi: 10.1242/JCS.101.1.79.
Vasquez, R. J. *et al.* (1997) 'Nanornolar Concentrations of Nocodazole Alter Microtubule Dynamic Instability In Vivo and In Vitro', *Molecular Biology of the Cell*, 8, pp. 973–985.
Vignard, J., Mirey, G. and Salles, B. (2013) 'Ionizing-radiation induced DNA double-strand breaks: A direct and indirect lighting up', *Radiotherapy and Oncology*, 108(3), pp. 362–369. doi: 10.1016/J.RADONC.2013.06.013.
Villeneuve, N. F. *et al.* (2009) 'Nrf2 and p21 regulate the fine balance between life and death by controlling ROS levels', *Cell Cycle*, pp. 3255–3256. doi: 10.4161/cc.8.20.9565.
Voet, D. and Voet, J. . (2011) *Biochemistry*. 4th edn. Wiley.
van Vugt, M. A. T. M. *et al.* (2010) 'A Mitotic Phosphorylation Feedback Network Connects Cdk1, Plk1, 53BP1, and Chk2 to Inactivate the G2/M DNA Damage Checkpoint', *PLoS Biology*, 8(1), p. e1000287. doi: 10.1371/journal.pbio.1000287.
Walczak, C. E., Cai, S. and Khodjakov, A. (2010) 'Mechanisms of chromosome behaviour during mitosis', *Nature Reviews Molecular Cell Biology*, 11(2), pp. 91–102. doi: 10.1038/nrm2832.
Wanders, R. J. A. *et al.* (1987) 'Catalase in cultured skin fibroblasts from patients with the cerebro-hepato-renal (Zellweger) syndrome: normal maturation in peroxisome-deficient cells', *Biochim Biophys Acta*, 923(3), pp. 478–482. doi: 10.1016/0304-4165(87)90057-2.
Wang, G. and Cole, R. B. (1994) 'Effect of Solution Ionic Strength on Analyte Charge State Distributions in Positive and Negative Ion Electrospray Mass Spectrometry', *Analytical Chemistry*, 66(21), pp. 3702–3708. doi: 10.1021/AC00093A026.
Wang, G. F. *et al.* (2017) 'Oxidative stress induces mitotic arrest by inhibiting Aurora A-involved mitotic spindle formation', *Free Radical Biology and Medicine*, 103, pp. 177–187. doi: 10.1016/J.FREERADBIOMED.2016.12.031.
Wang, H. *et al.* (2001) 'Pds1 phosphorylation in response to DNA damage is essential for its DNA damage checkpoint function.', *Genes & Development*, 15(11), pp. 1361–1372. doi: 10.1101/gad.893201.
Wang, J., Gong, Z. and Chen, J. (2011) 'MDC1 collaborates with TopBP1 in DNA replication checkpoint control', *The Journal of Cell Biology*, 193(2), pp. 267–273. doi:

10.1083/jcb.201010026.
Wang, Q. *et al.* (2013) 'Nrf2 is associated with the regulation of basal transcription activity of the BRCA1 gene', *Acta Biochimica et Biophysica Sinica*, 45(3), pp. 179–187. doi: 10.1093/abbs/gmt001.
Wang, S. *et al.* (2010) 'Analysis of the Cytotoxic Activity of the Carboplatin and Gemcitabine Combination', *Anticancer Research*, 30(11), pp. 4573–4578.
Wang, Y. *et al.* (2018) 'Superoxide dismutases: Dual roles in controlling ROS damage and regulating ROS signaling', *Journal of Cell Biology*, pp. 1915–1928. doi: 10.1083/jcb.201708007.
Wang, Z. X. *et al.* (2012) 'Overexpression of polo-like kinase 1 and its clinical significance in human non-small cell lung cancer', *The International Journal of Biochemistry & Cell Biology*, 44(1), pp. 200–210. doi: 10.1016/J.BIOCEL.2011.10.017.
Wassing, I. E. *et al.* (2021) 'The RAD51 recombinase protects mitotic chromatin in human cells', *Nature Communications*, 12(1), pp. 5380–5397. doi: 10.1038/s41467-021-25643-y.
Watanabe, N., Broome, M. and Hunter, T. (1995) 'Regulation of the human WEE1Hu CDK tyrosine 15-kinase during the cell cycle', *The EMBO Journal*, 14(9), pp. 1878–1891.
Weinberg, R. A. (2014) *The biology of Cancer*. 2nd editio. WW Norton & Co.
Winterbourn, C. C. (1995) 'Toxicity of iron and hydrogen peroxide: the Fenton reaction', *Toxicology Letters*, 82–83, pp. 969–974. doi: 10.1016/0378-4274(95)03532-X.
Winterbourn, C. C., Peskin, A. V. and Parsons-Mair, H. N. (2002) 'Thiol oxidase activity of copper,zinc superoxide dismutase', *Journal of Biological Chemistry*, 277(3), pp. 1906–1911. doi: 10.1074/jbc.M107256200.
World Health Organisation (2021) *WHO Cancer*. Available at: https://www.who.int/news-room/fact-sheets/detail/cancer (Accessed: 3 August 2021).
Wu, T. *et al.* (2014) 'Poly(ADP-ribose) polymerase-1 modulates Nrf2-dependent transcription', *Free Radical Biology and Medicine*, 67, pp. 69–80. doi: 10.1016/j.freeradbiomed.2013.10.806.
Xu, R. *et al.* (2018) 'Mitosis-specific MRN complex promotes a mitotic signaling cascade to regulate spindle dynamics and chromosome segregation.', *Proceedings of the National Academy of Sciences of the United States of America*, 115(43), pp. 10079–10088. doi: 10.1073/pnas.1806665115.
Yamagishi, Y. *et al.* (2012) 'MPS1/Mph1 phosphorylates the kinetochore protein KNL1/Spc7 to recruit SAC components', *Nature Cell Biology*, 14(7), pp. 746–752. doi: 10.1038/ncb2515.
Yamamoto, T. *et al.* (2008) 'Physiological Significance of Reactive Cysteine Residues of Keap1 in Determining Nrf2 Activity', *Molecular and Cellular Biology*, 28(8), pp. 2758–2770. doi: 10.1128/mcb.01704-07.
Yang, C. *et al.* (2011) 'Aurora-B mediated ATM serine 1403 phosphorylation is required for mitotic ATM activation and the spindle checkpoint.', *Molecular Cell*, 44(4), pp. 597–608. doi: 10.1016/j.molcel.2011.09.016.
Yang, C. *et al.* (2012) 'The kinetochore protein Bub1 participates in the DNA damage response.', *DNA Repair*, 11(2), pp. 185–191. doi: 10.1016/j.dnarep.2011.10.018.
Yang, C. *et al.* (2014) 'ATM-mediated Mad1 Serine 214 phosphorylation regulates Mad1 dimerization and the spindle assembly checkpoint.', *Carcinogenesis*, 35(9), pp. 2007–2013. doi: 10.1093/carcin/bgu087.
Yuan, B. *et al.* (2006) 'Increased Expression of Mitotic Checkpoint Genes in Breast Cancer Cells with Chromosomal Instability', *Clinical Cancer Research*, 12(2), pp. 405–410. doi: 10.1158/1078-0432.CCR-05-0903.

Yudkovsky, Y. *et al.* (2000) 'Phosphorylation of Cdc20/Fizzy Negatively Regulates the Mammalian Cyclosome/APC in the Mitotic Checkpoint', *Biochemical and Biophysical Research Communications*, 271(2), pp. 299–304. doi: 10.1006/BBRC.2000.2622.
Zachos, G. *et al.* (2007) 'Chk1 Is Required for Spindle Checkpoint Function', *Developmental Cell*, 12(2), pp. 247–260. doi: 10.1016/j.devcel.2007.01.003.
Zhang, J. *et al.* (2016) 'ROS and ROS-Mediated Cellular Signaling', *Oxidative Medicine and Cellular Longevity*, 2016. doi: 10.1155/2016/4350965.
Zhao, H. and Piwnica-Worms, H. (2001) 'ATR-mediated checkpoint pathways regulate phosphorylation and activation of human Chk1.', *Molecular and Cellular Biology*, 21(13), pp. 4129–4139. doi: 10.1128/MCB.21.13.4129-4139.2001.
Zhou, Z. *et al.* (2002) 'Comprehensive proteomic analysis of the human spliceosome', *Nature*, 419(6903), pp. 182–185. doi: 10.1038/nature01031.
Zou, L. and Elledge, S. J. (2003) 'Sensing DNA damage through ATRIP recognition of RPA-ssDNA complexes.', *Science*, 300(5625), pp. 1542–1548. doi: 10.1126/science.1083430.